UNIVERSIDAD DE CÓRDOBA

PROGRAMA DE DOCTORADO DE COMPUTACIÓN AVANZADA, ENERGÍA Y PLASMAS

ESTUDIO TEÓRICO Y EXPERIMENTAL DE LA VAINA IÓNICA FORMADA ALREDEDOR DE UNA SONDA CILÍNDRICA DE LANGMUIR INMERSA EN PLASMAS

THEORETICAL AND EXPERIMENTAL STUDY OF THE ION SHEATH SURROUNDING A CYLINDRICAL LANGMUIR PROBE IMMERSED IN PLASMAS

DIRECTORES:

JOSÉ IGNACIO FERNÁNDEZ PALOP

JUAN MANUEL DÍAZ CABRERA

AUTOR:

GUILLERMO FERNANDO REGODÓN HARKNESS

FECHA DE DEPÓSITO:

10 DE MARZO DE 2021

TITULO: *ESTUDIO TEÓRICO Y EXPERIMENTAL DE LA VAINA IÓNICA FORMADA ALREDEDOR DE UNA SONDA CILÍNDRICA DE LANGMUIR INMERSA EN PLASMAS*

AUTOR: *Guillermo Fernando Regodón Harkness*

© Edita: UCOPress. 2021
Campus de Rabanales
Ctra. Nacional IV, Km. 396 A
14071 Córdoba

https://www.uco.es/ucopress/index.php/es/
ucopress@uco.es

TÍTULO DE LA TESIS:

Estudio teórico y experimental de la vaina iónica formada alrededor de una sonda cilíndrica de Langmuir inmersa en plasmas

DOCTORANDO/A:

Guillermo Fernando Regodón Harkness

INFORME RAZONADO DEL/DE LOS DIRECTOR/ES DE LA TESIS

(se hará mención a la evolución y desarrollo de la tesis, así como a trabajos y publicaciones derivados de la misma).

La tesis presentada es de alta calidad, tanto por el desarrollo como por los resultados que presenta. Hay de destacar que las publicaciones que han dado lugar a que se pueda presentar como compendio de artículos, de acuerdo con la normativa, pertenecen a revistas de gran impacto, encontrándose entre las primeras dentro del área de Física del plasma, en la que se encuadra el contenido de la tesis.

El primer resultado importante que se muestra es la resolución completa de un modelo teórico para describir el contacto plasma-superficie, incluyendo el movimiento térmico de los iones positivos presentes en el plasma. Al incluir el movimiento térmico, aparece una singularidad en las ecuaciones cuando los iones alcanzan la velocidad del sonido que impide obtener una solución completa, desde el plasma hasta la superficie, de forma directa. La resolución de este problema desarrollada en la tesis abre nuevas puertas en la investigación, ya que la técnica presentada permite elaborar modelos más complejos. Dicha resolución ha sido publicada en la revista Physics of Plasmas (Physics of Plasmas **24**, 103516 (2017); DOI: 10.1063/1.4997844).

Como primera aplicación de la técnica anterior, se ha obtenido el potencial flotante para sondas cilíndricas y esféricas en un plasma electronegativo en función, entre otros parámetros, del grado de electronegatividad. Este tipo de plasmas son muy utilizados en las técnicas de tratamiento de superficie en atmósfera de plasma. El potencial flotante es una magnitud que se puede medir con cierta facilidad mediante sondas electrostáticas de Langmuir, de modo que proporciona un método de diagnosis en plasmas electronegativos. Los resultados relativos al potencial flotante se han publicado en la revista Plasma Sources, Science and Technology, que es la más importante dedicada a la Física del Plasma, que aparece dentro de área Physics, Fluids & Plasmas del Journal Citation Report (Plasma Sources Sci. Technol. **27** (2018) 025014; DOI: 10.1088/1361-6595/aaac58).

Para poder validar los resultados obtenidos de forma teórica, se han realizado medidas experimentales en un plasma generado mediante una descarga DC, en un dispositivo bien conocido dentro del grupo de investigación en el que se ha desarrollado la tesis. Dependiendo de las condiciones de la descarga, se pueden producir plasmas en los que aparecen dos poblaciones de electrones con dos temperaturas distintas. El plasma así generado es similar a un plasma electronegativo,

ya que aparecen dos poblaciones de partículas con carga negativa. La ventaja es que el grupo ha desarrollado ya herramientas para separar las dos poblaciones de electrones. De hecho, el desarrollo de dichas herramientas, constituyeron el Trabajo Fin de Grado que presentó en su momento el doctorando dentro del Grado de Física. Los resultados encontrados sobre la medida del potencial flotante son muy concluyentes ya que los valores encontrados para dicho potencial sólo se pueden justificar considerando las dos poblaciones. El potencial flotante es, por tanto, una magnitud significativa para medir el grado de electronegatividad de un plasma electronegativo. Los resultados experimentales y la comparación con el modelo teórico se han publicado en la revista Plasma Physics and Controlled Fusion (Plasma Phys. Control. Fusion, **61** (2019) 095015; DOI: 10.1088/1361-6587/ab3483).

Como ya se ha mencionado, la técnica desarrollada para evitar la singularidad que aparece al incluir el movimiento térmico de los iones positivos abre nuevas puertas en la investigación. Esta técnica ha sido muy bien aprovechada por el doctorando para elaborar modelos más complejos para describir el contacto plasma-superficie. Un resultado singular encontrado dentro del grupo de investigación ha sido la transición de los valores experimentales de la corriente de saturación iónica recogida por una sonda cilíndrica, desde los valores que predicen los modelos radiales a los correspondientes a modelos orbitales. Esta transición aparece en plasmas generados en Helio y no había sido observada con anterioridad. Una posible justificación de dicha transición podía ser achacada a las colisiones ion-neutro que se producen dentro de la vaina que se forma alrededor de la sonda. Esto motivó al doctorando a incluir las colisiones en el modelo. Este modelo es mucho más complejo, pero permite analizar con detalle el efecto que provocan tanto las colisiones como el movimiento térmico de los iones positivos en la corriente de saturación iónica. Los resultados se publicaron en la revista Plasma Sources, Science and Technology (Plasma Sources Sci. Technol. **28** (2019) 115017; DOI: 10.1088/1361-6595/ab515e).

Finalmente, los modelos teóricos desarrollados han permitido analizar las causas que producen la transición antes mencionada de la corriente de saturación iónica en plasmas de Helio. Tanto el grado de colisionalidad como la temperatura de iones positivos influyen significativamente en la corriente de saturación iónica. Se ha concluido que no se puede achacar únicamente a la presencia de colisiones la aparición de dicha transición, sino también a la menor masa que tienen los iones de helio en comparación con la del resto de plasmas estudiados dentro del grupo de investigación. Estos resultados experimentales fueron publicados en la revista Applied Sciences (Appl. Sci. **10** (2020) 5727; DOI: 10.3390/app10175727).

Por último, hay que destacar la gran capacidad de trabajo y autonomía del doctorando. Tal como se ha comentado, comenzó su formación dentro del grupo en el último curso del Grado de Física. Durante los primeros años, fue aprendiendo todas las técnicas, tanto teóricas como experimentales, que se utilizan en el grupo para estudiar el contacto plasma-superficie. El grado de asimilación fue tan alto, que ha permitido al doctorando desarrollar sus propias técnicas y modelos de forma autónoma. Durante los años de desarrollo de la tesis ha continuado con su formación. Ha participado de forma activa en una gran cantidad de actividades del Plan de Formación y ha presentado los resultados parciales de su investigación en los congresos internacionales más prestigiosos, dentro de área de Física del Plasma. Su forma trabajar, de abordar todos los problemas con los que se ha enfrentado, su actitud y, en resumen, su forma de ser, han enriquecido de forma significativa nuestro grupo de investigación.

Por todo ello, se autoriza la presentación de la tesis doctoral.

Córdoba, 22 de mayo de 2021

Firma del/de los director/es

Fdo.: José Ignacio Fernández Palop

Fdo.: Juan Manuel Díaz Cabrera

Agradecimientos

Siempre me he considerado una persona afortunada. Y el final de este trayecto es una confirmación más de esta observación personal. Empezar a estudiar una segunda carrera con 31 años, en este caso mi sueño de adolescente de estudiar Física, y un doctorado con 35 años, es imposible sin el apoyo de tu entorno. Empezando por el apoyo moral que comenzó con mi madre, Jennifer, la primera en ver en mi la oportunidad de convertirme en profesor de universidad e investigador y animarme a ello, y desarrollado incondicionalmente a lo largo de todos estos años por mi esposa, Maggie, a la que conocí prácticamente al comienzo de esta aventura. También por el apoyo académico, tanto en forma de guía como de estímulo, de mis referentes intelectuales dentro del grupo de investigación, José Ignacio, Juanma y Jerónimo. Los dos primeros como director y subdirector de esta tesis, y el tercero, mi paisano, como el investigador senior del grupo. La calidad intelectual y personal de los tres es un ejemplo en el que inspirarse. Sin embargo, todos ellos, y otros que no he mencionado, me disculparán si en este momento me acuerdo especialmente de las personas que no han podido ver el final de este trayecto.

Mi familia siempre fue un poco pequeña, porque la familia de mi madre vivía y vive muy lejos, y por que la mayoría de mis abuelos murieron cuando yo era muy pequeño o no había nacido. Solo mi abuela Angelina vivió para verme estudiar en la universidad. Mi abuela y mi padre, Fernando, fallecieron antes de que terminara mis estudios de Ingeniería de Telecomunicación. Mi abuela vivió una vida larga y vio a sus hijos y nietos prosperar, pero mi padre apenas convivió un mes con su primera nieta, mi sobrina Ana. La tranquila vida de jubilado le fue negada, así como ver que sus hijos y nieta alcanzaban los logros personales que hacen enorgullecer a sus progenitores. Fue su duro trabajo como médico y la situación familiar que nos dejó a mi, a mi madre Jennifer y a mis dos hermanos Andy y Micky lo que nos ha ayudado tanto a afrontar la vida. Su actitud como médico cercano le granjeó el afecto de sus pacientes, y todavía a día de hoy, 14 años después, me encuentro con personas, a veces en situaciones completamente inesperadas, que se acuerdan con cariño de él. Fue el entorno familiar que crearon mis padres, intencionada o inintencionadamente, el que nos permitió a mis hermanos y a mi evolucionar personal e intelectualmente con libertad e independencia, y convertirnos en lo que somos. Mi madre ya me ha dicho que está orgullosa de cómo los tres hermanos hemos crecido. Mi padre nunca, probablemente pensando que tendría tiempo de decirlo algún día. Por eso voy a ser yo el que se lo diga: tuviste una vida de la que estar orgulloso y espero estar a la altura de tu orgullo.

Pienso que soy una persona afortunada. He tenido la oportunidad de cometer errores y tomar malas decisiones, y aprender de ello. He disfrutado de la guía de personas que, al menos parcialmente y es algo por lo que les estaré eternamente agradecido, han ocupado el hueco que dejó mi padre. He podido viajar y conocer a mis familiares y amigos que viven en la otra punta del mundo. Además de mi familia, tengo a mi familia extendida, tanto mis amigos como los primos lejanos de mi madre y la gran familia de mi esposa. Incluso el país en el que vivo, España, que me ha financiado el doctorado a través del programa FPU, y la universidad en la que trabajo, la Universidad de Córdoba, son motivos de agradecimiento. A todos, gracias.

Guillermo, 25 de mayo de 2021

Índice

II

Índice de figuras

Índice de tablas

1 Introducción al plasma y objetivo de la tesis

El plasma, conocido también como el cuarto estado de la materia, es el estado en el que podemos observar la mayor parte de la materia del Universo, siendo una estimación prudente que el plasma constituye un porcentaje superior al 99% del total de la materia conocida. El plasma es fácilmente visible: esta constituido por iones positivos y negativos, así como por electrones, por lo que las recombinaciones en las que se libera energía en forma de fotones son frecuentes. La luz que proviene de las estrellas nace mediante este mecanismo. Más aún, la mayor parte de la luz que viaja por el Universo y aquí en la Tierra tiene su origen en alguna forma de plasma.

En la Tierra, el plasma constituye una minoría de la materia del planeta. Tenemos algunos ejemplos de plasmas naturales, como los relámpagos y las auroras boreales. Pero tenemos muchos más ejemplos de plasmas artificiales, que han demostrado tener importantes aplicaciones tecnológicas:

- Iluminación en fluorescentes y lámparas de neón.
- Fabricación de microprocesadores.
- Fabricación de dispositivos optoelectrónicos.
- Fabricación de superficies fotovoltaicas.
- Esterilización de herramientas médicas.
- Fabricación de biosensores.
- Tratamiento de la superficie de prótesis médicas para bio-compatibilidad.
- Tratamiento de cáncer con plasma.
- Esterilización de semillas en agricultura.
- Tratamiento de superficies.

Es especialmente importante el tratamiento de superficies en la industria para modificar las propiedades de los componentes de productos y funcionalización de superficies, conocido como PACVD o Plasma Assisted Chemical Vapour Deposition: obtención de superficies bio-activas y de superficies biocidas, modificación de propiedades de adherencia, tribológicas y de mojado, para aplicaciones ópticas o decorativas, tratamientos de difusión superficial, nitruración,

boronización, tratamientos de resistencia al desgaste, corrosión u oxidación en temperaturas extremas, tratamiento para optimización de las propiedades mecánicas, creación de estructuras nanotecnológicas de superficie, limpieza de superficies, polímeros…

Las aplicaciones mencionadas tienen como denominador común que se benefician del entorno químicamente activo que ofrece el plasma, con especies químicas que no se pueden encontrar mediante otros medios. Por ejemplo, en un plasma de oxígeno, usado en esterilización, pueden aparecer especies químicas como O_2^-, O^-, O^{--}, o incluso O^+, O^{++} o O_3 [1,2]. Aún en plasmas que son creados en el mismo gas de fondo, los porcentajes de cada especie química del plasma pueden tener efectos dramáticos en el comportamiento del mismo cuando interacciona con una superficie que se desea tratar.

Sin embargo, uno de los problemas que se encuentra con la utilización del plasma en aplicaciones tecnológicas es que las propiedades del mismo pueden variar de forma importante cuando se modifica la presión o la temperatura del gas de fondo. Asimismo, el plasma puede ser influenciado por los campos eléctricos que se le aplican. Dado que el plasma está formado por partículas libres con carga que tienen la capacidad de desplazarse rápidamente, el plasma tiene la tendencia a apantallar los campos eléctricos. La presencia de superficies metálicas a su vez también influye en el plasma, pudiendo recolectar y perder electrones, cuando los electrones e iones negativos por una parte y los iones positivos, por otra parte, colisionan con la superficie. Por lo tanto, el plasma se adapta rápidamente a las perturbaciones externas, de forma que resulta difícil establecer una relación entre el plasma antes y después de ser perturbado. Es por esto que el control de las propiedades del plasma es un problema esencial en física de plasma*. El control de las propiedades del plasma es un problema complejo.* Por ello se debe establecer un sistema de realimentación en el que se miden los parámetros que caracterizan al plasma y se monitoriza cómo responden a las perturbaciones, de forma que sea posible utilizar la información para conseguir el plasma con las propiedades deseadas bajo las condiciones en las que es necesario. El primer paso de este proceso de control, la caracterización del plasma, se conoce como *diagnosis de plasmas*.

Existen dos estrategias principales para diagnosticar el plasma: el primer método se basa en la espectrografía, o el estudio del espectro de luz que emite el plasma. Mediante el estudio de la intensidad lumínica en cada frecuencia y conociendo la luz que emite cada proceso físico, es posible conocer la composición del plasma. El segundo método, diseñado por Irving Langmuir, uno de los primeros científicos que trabajaron con gases ionizados y el primero en llamarlos plasmas, es la sonda electrostática de Langmuir. Se trata de un conductor con simetría

esférica, cilíndrica o plana cuyo comportamiento eléctrico cuando se sumerge en un plasma es conocido. Para estudiar dicho comportamiento eléctrico, que depende de la capacidad de las partículas del plasma para alcanzar la sonda cuando está polarizada a un determinado potencial, es necesario predecir teóricamente el comportamiento del plasma en la región que rodea la sonda, denominada *vaina*. El propio Irving Langmuir, junto con Harold M. Mott-Smith, propuso el primer modelo de vaina alrededor de una sonda electrostática de Langmuir [3]. Irving Langmuir se convirtió por méritos propios en uno de los científicos más importantes del siglo XX, llegando a ganar el premio Nobel de Química en su edición de 1932.

Desde su invención hace más de 80 años, la sonda electrostática de Langmuir se ha utilizado ininterrumpidamente para diagnosticar plasmas. Pese a que supone la introducción de un objeto en el plasma con la perturbación que ello supone, tiene algunas ventajas:

- Ha sido muy estudiado desde su invención, por lo que su comportamiento es muy conocido [4,5].
- La sonda electrostática de Langmuir cilíndrica de muy pequeñas dimensiones es relativamente fácil de construir.
- A diferencia de los métodos de espectrometría que agregan la información de la región del plasma desde donde se recoge la luz, la sonda electrostática de Langmuir provee información local del plasma en el entorno donde se coloca (como ejemplo muy elaborado de este principio, véase [6]).
- Se han diseñado sondas de Langmuir modificadas para conseguir medidas mejoradas (en plasmas fríos y calientes, respectivamente, [7,8]).

A pesar de haber sido ampliamente estudiadas, las sondas electrostáticas de Langmuir aún no se comprenden completamente. Existen dos tipos de teoría para estudiar las características de la vaina que se forma alrededor de la sonda electrostática de Langmuir inmersa en un plasma: las teorías radiales cuyo primer exponente es el modelo radial para sondas electrostáticas de Langmuir esféricas de John E. Allen, Robert L. F. Boyd y P. Reynolds de 1957 y extendido a sondas cilíndricas por Francis Chen [9–11]; y las teorías orbitales cuyo primer ejemplo sería el antes mencionado trabajo de Harold Mott-Smith y de Irving Langmuir de 1926, y cuyos trabajos más completos e influyentes son los trabajos de Ira B. Bernstein e Irving N. Rabinowitz de 1959 y el importante informe de James G. Laframboise para la University of Toronto Institute for Aerospace Studies de 1966 [3,12,13]. Los resultados de las dos teorías son contradictorios y las premisas bajo las que cada modelo es aplicable no están claramente

diferenciadas, dejando además un gran rango de condiciones del plasma en el que no está claro cuál de los dos modelos debería usarse. Cuando la sonda está polarizada positivamente con respecto al plasma y, por lo tanto, las partículas que recoge la sonda son exclusivamente electrones, las teorías orbitales demuestran ser válidas, incluso siendo suficiente con el modelo de Harold M. Mott-Smith y de Irving Langmuir [3] en muchos casos. Sin embargo, cuando se aplica a una sonda polarizada negativamente con respecto al plasma, de forma que la mayor parte de las partículas que recoge la sonda son iones positivos, los resultados experimentales demuestran que ambas teorías son válidas en distintas situaciones. Los resultados de las medidas de los parámetros del plasma que se obtienen con ambas teorías pueden diferenciarse hasta en un orden de magnitud. Una posible estrategia para relacionar ambas teorías es extender la validez de las teorías, y comprobar cómo se relacionan.

El problema principal que se ha estudiado durante el desarrollo de esta tesis es la extensión del modelo radial para la corriente de iones recogida por una sonda electrostática de Langmuir cilíndrica polarizada negativamente con respecto al plasma de Allen, Boyd y Reynolds y Chen [9,10]*, que fue modificado por Fernández Palop et al.* [11] *para incluir el efecto de la temperatura de los iones positivos cuando es mucho menor que la temperatura de los electrones y cuya validez ha sido comprobada en medidas experimentales en el laboratorio en plasmas de argón y neón* [14–17]*. En este trabajo se ha extendido la teoría de Fernández Palop et al. para incluir la posibilidad de que la temperatura de iones tenga cualquier valor* [18]*, para que incluya iones negativos* [19] *y para que considere las posibles colisiones de los iones positivos con los átomos neutros del gas de fondo* [20]*, y se han realizado medidas experimentales para comprobar la validez de estas extensiones del modelo aplicándolo a un caso de plasma con dos poblaciones de electrones* [21] *y para estudiar los límites de aplicabilidad del modelo radial en función de los parámetros característicos del plasma* [22]*.*

El trabajo desarrollado en esta tesis se enmarca en el objetivo de investigación a medio plazo del grupo de investigación TEP-230 Contacto plasma-superficie de estudiar la transición en el comportamiento de la corriente de iones recogida por una sonda electrostática de Langmuir cilíndrica de comportamiento radial (o compatible con la teoría radial de Allen, Boyd y Reynolds y de Chen [9–11]) a comportamiento orbital (o compatible con la teoría orbital de Mott-Smith y Langmuir, de Bernstein y Rabinowitz y de Laframboise [3,12,13]), mediante el estudio teórico de los modelos [11,18–20,23–26], mediante medidas experimentales [14–17,21,27,28] y utilizando simulaciones Particle-In-Cell por ordenador [29,30].

2 Antecedentes

2.1 Plasmas en física

La *física de plasma* estudia la materia cuando tiene una serie de características que permiten definir el estado en el que la materia se encuentra como *plasma*. La materia en el estado de plasma cumple las siguientes condiciones:

- *Cuasi-neutralidad:* La carga neta de la sustancia es prácticamente nula, salvo en las fronteras o en las regiones donde algún elemento externo pueda romper el equilibrio de carga, como por ejemplo las vainas que se forman alrededor de los objetos metálicos.
- *Contiene cargas positivas y negativas libres:* De esta forma, las partículas se pueden desplazar por el efecto de los campos electromagnéticos a los que se les someta.
- *Tiene comportamiento colectivo:* El movimiento de las partículas individuales no puede ser conocido, y por tanto el plasma como conjunto debe ser estudiado mediante técnicas de la física estadística y de la termodinámica, usando conceptos como la temperatura, la densidad y la presión.

Por lo tanto, una definición simplificada y útil de plasma podría ser [31]: *El plasma es un gas cuasi-neutro de partículas cargadas y partículas neutras que muestran comportamiento colectivo.*

La primera condición, la cuasi-neutralidad, puede parecer una restricción fuerte, pero la propia existencia de cargas positivas y negativas libres, la segunda condición, salvo en el caso que estén en una proporción muy desequilibrada, obliga a que se cumpla. Las partículas deben tener un grado de aleatoriedad en su movimiento, por lo que podemos suponer que, en ocasiones, se puede formar una región de carga neta no nula en una región del plasma. Dado que la fuerza de Coulomb es muy intensa, inmediatamente se formará en torno a dicha región un campo eléctrico intenso que atrae las cargas opuestas hacia la región con carga neta recién formada, cancelando la carga neta que se pudiera acumular espontáneamente.

La tercera condición, el comportamiento colectivo, permite utilizar los principios de la física estadística y de la termodinámica. Se puede definir la temperatura, la densidad y la presión y, en algunas ocasiones en las que es útil, utilizar la ecuación de los gases ideales.

$$p = nk_B T. \tag{2.1}$$

En esta expresión, p es la presión, n es la densidad de partículas, T es la temperatura y k_B es la constante de Boltzmann. También se puede relacionar la energía interna con temperatura mediante la expresión conocida,

$$E = \frac{3}{2} k_B T, \tag{2.2}$$

donde E es la energía interna de las partículas de la componente del plasma que se encuentran a temperatura T. Esta relación permite identificar la temperatura T con la energía interna E hasta el punto de que la temperatura T se suele expresar en unidades de energía. La relación entre la temperatura en grados kelvin K y la energía en electronvoltios eV es:

$$\frac{T(\mathrm{K})}{T(\mathrm{eV})} = \frac{e}{k_B} \cong 11600 \frac{\mathrm{K}}{\mathrm{eV}}, \tag{2.3}$$

siendo e la carga elemental.

En la frontera del plasma con una superficie metálica en la que se forma la vaina, la condición de cuasi-neutralidad se lleva al límite de validez, siendo necesario utilizar la ecuación de Poisson para obtener el perfil de potencial en la región. Asimismo, en muchos casos, el comportamiento colectivo debe ser estudiado de forma más detallada ya que, al existir campos intensos, la función de distribución de velocidad pierde su simetría y no puede ser considerada como una campana de Gauss. De esta forma, puede ser necesario estudiar la componente del plasma utilizando la función de distribución de velocidad y contabilizar el movimiento de las partículas de forma más detallada.

2.1.1 Cuasi-neutralidad

Con el objetivo de estimar en qué grado la condición de cuasi-neutralidad impone la igualdad entre densidad de cargas positivas y negativas y en qué grado la densidad de partículas se

puede considerar suficientemente grande, consideremos la ecuación de Poisson en una dimensión:

$$\frac{\mathrm{d}^2\phi}{\mathrm{d}x^2} = -\frac{e}{\varepsilon_0}(n_+ - n_-). \qquad 2.4$$

En esta ecuación, ϕ es el potencial a lo largo de la dimensión x, e es la carga elemental, ε_0 es la permitividad del vacío, y n_+ y n_- son las densidades de carga positiva y negativa, respectivamente. Consideremos la situación en la que la cuasi-neutralidad se empieza a romper. Respecto a las cargas positivas, asumimos, dado que son partículas masivas cuya movilidad es mucho menor que la movilidad de los electrones, que la densidad de carga positiva no varía y vale n_∞. Respecto a la carga negativa, asumimos que se debe enteramente a electrones que están en equilibrio termodinámico, por lo que su densidad se puede expresar a partir de la función de distribución que maximiza la entropía, y que deriva de la probabilidad de la colectividad canónica de la física estadística que sigue la expresión de la distribución de Boltzmann, obteniéndose el siguiente factor de Boltzmann:

$$n_- = n_\infty e^{\frac{e\phi}{k_B T_e}}, \qquad 2.5$$

donde T_e es la temperatura de los electrones y n_∞ es la densidad de electrones en la región del plasma donde se establece la referencia de potencial, que debe coincidir con la densidad de cargas positivas para que en esa región exista cuasi-neutralidad. Sustituyendo ambas densidades en (2.4) obtenemos:

$$\frac{\mathrm{d}^2\phi}{\mathrm{d}x^2} = \frac{e}{\varepsilon_0} n_\infty \left(e^{\frac{e\phi}{k_B T_e}} - 1 \right). \qquad 2.6$$

Cuando la perturbación en torno a la situación de cuasi-neutralidad no es muy grande, de modo que $|e\phi| \ll k_B T_e$, la exponencial se puede expandir en serie de Taylor, obteniendo la siguiente aproximación de orden 1 para la ecuación (2.6):

$$\frac{\mathrm{d}^2\phi}{\mathrm{d}x^2} = \frac{e^2 n_\infty \phi}{\varepsilon_0 k_B T_e}. \qquad 2.7$$

La solución para esta ecuación es la suma de dos exponenciales, una creciente y otra decreciente, que con sus respectivos coeficientes permiten cumplir las condiciones de contorno. En el caso en el que las condiciones de contorno impongan que el potencial es finito y que en un determinado punto el potencial vale ϕ_0, punto que se puede colocar en $x = 0$ sin pérdida de generalidad, la solución es:

$$\phi = \phi_0 e^{-\frac{|x|}{\lambda_D}}. \qquad 2.8$$

En esta última expresión se ha definido un parámetro importante que define la escala espacial del plasma, *la longitud de Debye* λ_D,

$$\lambda_D = \sqrt{\frac{\varepsilon_0 k_B T_e}{e^2 n_\infty}}. \qquad 2.9$$

La solución (2.8) demuestra que un plasma es capaz de atenuar el potencial en un punto del espacio y que a una distancia de unos pocos λ_D, la perturbación ha desaparecido. La longitud de Debye λ_D depende inversamente de la raíz cuadrada de la densidad de partículas cargadas libres, conocida como densidad del plasma, lo que permite tener una idea de si el plasma es demasiado tenue para la escala del problema que se estudie. Según esta solución, el campo eléctrico también se atenúa exponencialmente, pero en los plasmas reales, los electrones tienen un movimiento térmico aleatorio que provoca desequilibrios locales. Si los desequilibrios son importantes, la cuasi-neutralidad lo compensa rápidamente, pero si los desequilibrios son muy pequeños, el movimiento térmico de los electrones impide que se compense, dejando un campo eléctrico residual. Consideremos un desequilibrio de orden Δn_e a lo largo de una distancia de orden L en la densidad de electrones n_e en el seno de un plasma. Entre los puntos extremos del desequilibrio se establece un campo eléctrico de valor [32]:

$$E = \frac{e\Delta n_e L}{\varepsilon_0}, \tag{2.10}$$

de forma que la energía necesaria para que un electrón llegue desde un punto a otro del desequilibrio es:

$$U = \int_0^L eE \, \mathrm{d}x = eEL = \frac{e^2 \Delta n_e L^2}{2\varepsilon_0}. \tag{2.11}$$

Dado que la energía disponible para los electrones para realizar el desplazamiento desde un punto a otro es la energía térmica de los mismos en la dirección del desequilibrio,

$$U = \frac{1}{2} k_B T_e, \tag{2.12}$$

llegamos a la conclusión de que si el campo eléctrico es mayor, entonces es capaz de arrastrar a los electrones para compensar el desequilibrio, mientras que si el campo es menor, el movimiento térmico de los electrones impide la cancelación del campo eléctrico. Igualando (2.11) y (2.12), y usando la definición de longitud de Debye (2.9), se obtiene:

$$\frac{e^2 \Delta n_e L^2}{2\varepsilon_0} = \frac{1}{2} k_B T_e, \tag{2.13}$$

$$\frac{\Delta n_e}{n_e} = \left(\frac{\lambda_D}{L}\right)^2, \tag{2.14}$$

de forma que se comprueba que la condición de cuasi-neutralidad $\Delta n_e / n_e$ está relacionada con la relación de escala entre la longitud de Debye λ_D y la escala espacial del problema L. En general, la condición de cuasi-neutralidad es muy útil para evitar tener que resolver la ecuación de Poisson, *aunque esto no siempre es posible, como en los problemas de interfaz entre plasma y superficie*.

Dado que la escala espacial de las ecuaciones del plasma es del orden de la longitud de Debye λ_D, el plasma debe mostrar comportamiento colectivo en dicha escala espacial para

poder ser estudiado según las técnicas de la física de plasma. Consideremos la cantidad de partículas en una esfera de Debye, es decir, una esfera cuyo radio es la longitud de Debye λ_D, en un plasma con densidades de partículas n_j, con j el subíndice que distingue cada tipo de partícula presente en el plasma. El número de partículas $N_{D,j}$ en la esfera de Debye es:

$$N_{D,j} = \frac{4}{3}\pi\lambda_D^3 n_j. \qquad 2.15$$

Para que sea posible considerar el estudio del comportamiento colectivo de las distintas especies de partículas presentes en el plasma, es necesario que este número de partículas $N_{D,j}$ sea mucho mayor que 1. Por lo tanto, se puede concluir que las condiciones que un gas parcialmente ionizado debe cumplir para poder ser considerado plasma están definidas en función de la relación entre la longitud de Debye λ_D con respecto a la escala espacial del plasma L que establece la validez de la condición de cuasi-neutralidad, y en función de la cantidad de partículas en una esfera de Debye, que permite estudiar el plasma con técnicas de la física estadística y de la termodinámica,

$$\lambda_D \ll L, \qquad 2.16$$

$$N_{D,j} \gg 1 \quad \forall j. \qquad 2.17$$

Los principios básicos de la física de plasma son aplicables si se cumplen estas condiciones (2.16) y (2.17). Para poder tener una idea más clara de cómo de restrictivas son estas condiciones, véase la **Error! Reference source not found.** en la que se comparan algunos plasmas que podemos encontrar en la naturaleza o en los laboratorios de plasma.

Como se puede observar en la **Error! Reference source not found.**, algunos parámetros pueden variar en unos rangos que abarcan muchos órdenes de magnitud. No deja de resultar interesante que se puedan aplicar los principios básicos del plasma en condiciones tan dispares y alejadas, lo que sin duda es un éxito de la física de plasma. En la última fila de la **Error! Reference source not found.** se muestra el experimento del grupo TEP-230 Contacto plasma-superficie en el que esta tesis se ha realizado, mostrando que resulta ser una descarga particularmente fría y poco densa, *lo que hace que sea posible estudiar la interfaz entre plasma y superficie metálica en condiciones únicas*.

Tipo	n_e	T_e	λ_D	$N_{D,e}$
Reactor de Fusión (toroide)	$10^{19}\ \mathrm{m}^{-3}$	100 eV	24 μm	5.4×10^5
Reactor de Fusión (pinza)	$10^{23}\ \mathrm{m}^{-3}$	1000 eV	0.74 μm	1.7×10^5
Ionosfera	$10^{11}\ \mathrm{m}^{-3}$	0.05 eV	5.3 mm	6.1×10^4
Descarga luminiscente RF	$10^{15}\ \mathrm{m}^{-3}$	2 eV	330 μm	1.5×10^5
Llama	$10^{13}\ \mathrm{m}^{-3}$	0.1 eV	740 μm	1.7×10^4
Espacio interestelar	$10^{6}\ \mathrm{m}^{-3}$	0.01 eV	74 cm	1.7×10^6
Descarga DC del grupo TEP-230	$10^{16}\ \mathrm{m}^{-3}$	0.2 eV	33 μm	1.5×10^3

Tabla 1: Ejemplos de parámetros típicos en distintos tipos de plasmas

2.1.2 Descargas de plasma: Plasma y Vaina

Una descarga de plasma es un experimento en el que se genera un plasma cuando, mediante algún mecanismo, se ioniza parcialmente el gas, de forma que aparece una población de iones y electrones suficientemente importante como para que el comportamiento colectivo de las cargas sea predominante. Siempre hay una probabilidad importante de que los iones positivos se recombinen con electrones o iones negativos y emitan un fotón de una determinada energía. Es decir, el plasma está permanente perdiendo energía, al menos, mediante emisión de fotones. El plasma existe en tanto que el mecanismo que lo genera siga manteniéndose.

Considérense dos electrodos separados por una distancia L en una cámara de vacío con una determinada diferencia de potencial V entre ambos. Si no hay partículas con carga libres en la cámara, el potencial que se forma entre ambos electrodos es, por la ecuación de Poisson en una dimensión (2.4) para $n_+ = n_- = 0$, una línea recta. Estableciendo la referencia de potencial en el cátodo donde también establecemos la referencia del eje x,

$$\phi(x) = \frac{x}{L}V. \qquad 2.18$$

Si del cátodo consiguen salir electrones, por ejemplo, mediante termo-ionización, se forma una nube de electrones que se desplazan hasta el ánodo. El movimiento de los electrones, si el potencial creado entre los electrodos es predominante frente al posible efecto colectivo de

los demás electrones de la nube, debe conservar la energía del electrón. Asumiendo que los electrones salen prácticamente desde el reposo, se cumple:

$$\frac{1}{2}m_e\big(v_e(x)\big)^2 = \phi(x). \qquad 2.19$$

En esta expresión, m_e es la masa del electrón y $v_e(x)$ es la velocidad del electrón en la región con potencial $\phi(x)$. Además, dado que no se acumulan cargas en el espacio interelectródico la densidad de corriente eléctrica j_e debe conservarse.

$$-en_e(x)v_e(x) = j_e = \text{cte}. \qquad 2.20$$

Esta expresión, junto con la ecuación de Poisson en una dimensión (2.4) con $n_+ = 0$ y la densidad de cargas negativas igual a la densidad de carga de los electrones $n_- = n_e$, permite obtener la siguiente ecuación:

$$\frac{\mathrm{d}^2\phi}{\mathrm{d}x^2} = \frac{e}{\varepsilon_0}n_e = -\frac{j_e}{\varepsilon_0 v_e(x)} = -\frac{j_e}{\varepsilon_0}\sqrt{\frac{m_e}{2e\phi(x)}}. \qquad 2.21$$

Esta ecuación se puede resolver, por ejemplo, probando una potencia para el perfil $\phi(x) = \phi_0 x^c$, e imponiendo las condiciones de contorno de potencial y campo eléctrico nulos en el cátodo y potencial V en el ánodo. El resultado es que la corriente es proporcional al potencial elevado a $3/2$. Esta solución se llama ley de Child-Langmuir. El perfil de potencial que se obtiene es [33]:

$$\phi(x) = \left(\frac{-9j_e}{4\varepsilon_0}\right)^{\frac{2}{3}}\left(\frac{m_e}{2e}\right)^{\frac{1}{3}}x^{\frac{4}{3}} = \left(\frac{x}{L}\right)^{\frac{4}{3}}V. \qquad 2.22$$

El perfil del potencial ha dejado de ser una línea recta por el efecto de la carga de los electrones que constituyen la corriente.

Los electrones que son arrancados por termo-ionización pueden alcanzar energías que típicamente están en el rango de los $50\ \mathrm{eV}$, más que suficiente para superar la energía de

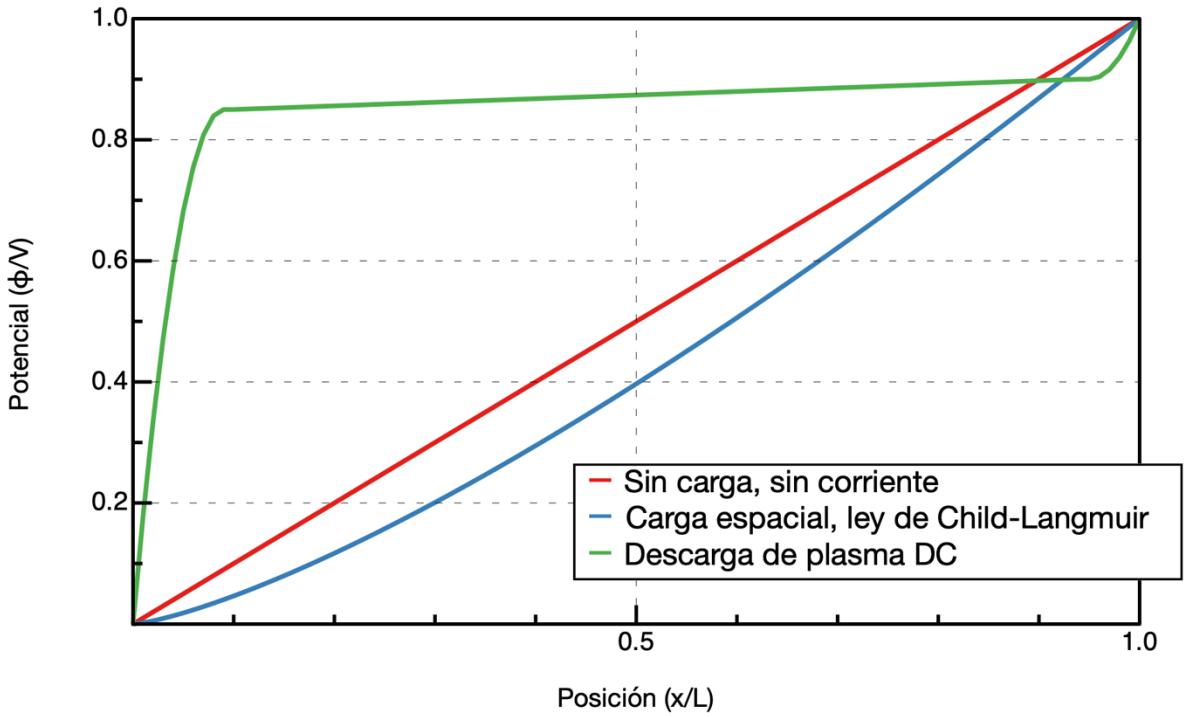

Figura 1: Perfiles de potencial en una campana de vacío entre dos electrodos a una distancia L con una diferencia de potencial V en los casos en que no se crea carga espacial (rojo), en que el efecto de carga espacial es predominante (Ley de Child-Langmuir, azul) y en una descarga DC típica como la que se usa en el grupo de investigación TEP-230 (verde).

ionización de los átomos neutros. Por ejemplo, el argón tiene una energía de ionización de $15.75\ \mathrm{eV}$. Si se introduce gas, como por ejemplo argón, en el espacio interelectródico, los electrones energéticos son capaces de arrancar los electrones de los átomos neutros y producir así más electrones e iones positivos. Estos electrones a su vez, al ser acelerados por el campo, también pueden adquirir energía suficiente para producir más ionizaciones, del mismo modo que ocasionalmente un ion puede encontrarse con un electrón y recombinarse emitiendo un fotón. Cuando se alcanza un estado de equilibrio, el plasma ha sido creado. En la región interelectródica, el plasma fuerza la cuasi-neutralidad de forma que el campo eléctrico está limitado al valor estimado usando (2.10) y (2.14) en la sección 2.1.1. Este campo no es suficiente para que la diferencia de potencial entre los electrodos alcance los valores en el rango de los miles de voltios que se encuentran en las descargas de plasmas de corriente continua DC, como la que se usa en el grupo de investigación TEP-230 Contacto plasma-superficie. Por lo tanto, necesariamente debe haber una región cerca de los electrodos en la que la carga no se neutraliza, una vaina. Típicamente, la mayor parte del potencial cae en la región del cátodo, de donde se

arrancan los electrones. Por ese motivo, el dispositivo de descarga DC del grupo de investigación TEP-230 Contacto plasma-superficie tiene el cátodo apantallado, salvo la superficie circular que se opone al ánodo.

El plasma DC descrito es generado mediante uno de los dos métodos principales de generación de descargas de plasma. Otro método es el plasma RF, en el que se aplica un intenso campo electromagnético variable en una región de gas enrarecido que es capaz de ionizar los átomos del gas. Pese a que la descarga se genera de forma completamente diferente, las vainas que se forman alrededor de los objetos metálicos son similares. Existen dos tipos de descargas RF, las capacitivas y las inductivas. En las descargas RF capacitivas, la referencia de potencial está en uno de los dos electrodos capacitivos, y algunas magnitudes físicas del plasma sufren una oscilación periódica con la frecuencia de la fuente de alimentación de la descarga [6]. En las descargas RF inductivas no existe una referencia de potencial, por lo que el potencial al que se encuentra el plasma puede desplazarse incluso aunque se introduzca una pequeña perturbación, ya sea una sonda o un campo externo, o incluso cambios en la temperatura o presión [34]. Esto puede tener importancia a la hora de utilizar la sonda electrostática de Langmuir polarizada positiva o negativamente con respecto al potencial del plasma. En el laboratorio del grupo de investigación TEP-230 Contacto plasma-superficie también se dispone un dispositivo para generar una descarga RF inductiva. Sin embargo, siendo el objetivo principal de esta tesis el estudio de la región de saturación iónica en que la corriente es casi exclusivamente de iones positivos, y siendo para ello necesario conocer el grado de polarización negativa de la sonda con respecto al plasma, es importante tener la referencia de potencial bien establecida, por lo que para este trabajo se ha utilizado solo la descarga DC.

La vaina, realmente, no puede ser considerada como plasma, ya que no cumple la condición de cuasi-neutralidad. Sin embargo, pese a que su estudio es complejo debido a la necesidad de resolver la ecuación de Poisson acoplada con las ecuaciones de fluidos o de partículas, la cantidad de aplicaciones industriales que existen gracias a la interacción entre plasma y superficie metálica (fabricación de microprocesadores, dispositivos fotovoltaicos, esterilización, PACVD o Plasma Assisted Chemical Vapour Deposition) hacen que sea un área de investigación activa desde que surgió la física de plasma como un cuerpo teórico unificado.

2.2 Descripción teórica de un plasma y conceptos esenciales

Como en cualquier problema de física, para estudiar el plasma es posible utilizar distintos conjuntos de ecuaciones y premisas dependiendo del grado de complejidad o simplicidad que se desee obtener, lo que a su vez va a influir en los resultados que se obtendrán a partir de los modelos construidos. La elección del modelo es esencial, ya que, como resulta obvio, un modelo demasiado simple puede no ser capaz de conseguir resultados interesantes o suficientemente detallados. Por ejemplo, si un modelo asume en las ecuaciones simetría de algún tipo, como podría ser simetría esférica, cilíndrica o de traslación en alguna dirección, por la propia definición de simetría el modelo no será capaz de distinguir ninguna estructura en la dimensión simétrica.

Por otro lado, un modelo demasiado complejo tiene dos problemas fundamentales: la física del problema puede quedar oscurecida por la complejidad matemática no resultando claro qué premisa del modelo provoca qué consecuencias en los resultados, lo que dificulta la aplicación de las premisas del modelo a otras situaciones; además, los elementos matemáticos adicionales pueden convertir el modelo en un sistema matemático sin solución analítica y con solución numérica compleja, inestable o incluso caótica.

Por lo tanto, uno de los objetivos fundamentales de la física como ciencia es encontrar siempre el modelo matemático más sencillo que describe los fenómenos observados en la naturaleza. En el caso de los modelos de plasma podemos encontrar tres descripciones diferentes desde el punto de vista matemático que se aplican a la interfaz de un plasma con una superficie metálica, cada uno con su rango de aplicabilidad.

- *Modelo de fluidos:* Estudia el plasma como si fuera un fluido ideal, por lo que la ecuación de los gases ideales se cumple para cada una de las componentes del plasma. Las componentes gaseosas tienen cada una su presión parcial. La relación entre las componentes gaseosas del plasma se define, por una parte, mediante la condición de cuasi-neutralidad entre las componentes cargadas en la región del plasma donde sea aplicable, o mediante la ecuación de Poisson en las regiones donde podamos argumentar que la cuasi-neutralidad se puede romper [9–11]. La frecuencia de colisión entre las distintas especies nos puede permitir identificar variables termodinámicas en algunos casos, o establecer relaciones entre las mismas en otros casos [35]. Como ejemplo de las consideraciones anteriores, por la condición de cuasi-neutralidad, la suma de las densidades de las especies positivas $n_{+,i}$ multiplicadas por su carga $q_{+,i}$ es igual a la suma de las densidades de las especies negativas $n_{-,j}$ por su carga $q_{-,j}$,

$$\sum_i q_{+,i} n_{+,i} - \sum_j q_{-,j} n_{-,j} = 0. \qquad 2.23$$

En el caso típico de un plasma electropositivo mono-componente tendríamos que, en la región del plasma, la densidad de iones positivos y la densidad de electrones coinciden, y de hecho se les suele denotar como densidad del plasma:

$$n_+ = n_e = n_p. \qquad 2.24$$

Por otra parte, típicamente la densidad de átomos neutros n_n es varios ordenes de magnitud superior a la densidad del plasma n_p, por lo que la probabilidad de que ocurra una colisión entre un electrón y un ion es mucho menor que la probabilidad de que ocurra una colisión entre un neutro y un ion. Por esto, típicamente podemos identificar la temperatura de las componentes iónicas del plasma con la temperatura del gas neutro T_n, mientras que los electrones tienen su propio valor de temperatura T_e [36].

- *Modelo de partículas:* Cuando las componentes del plasma no pueden considerarse como fluidos ideales, es necesario seguir el movimiento de las partículas individuales [12,13]. Como es razonable imaginar, esta descripción es mucho más compleja, pero permite obtener resultados cuando las componentes gaseosas del plasma dejan de estar termalizadas y están en condiciones de no equilibrio termodinámico local. Este tipo de modelos tiene una dificultad intrínseca en la definición de las condiciones de contorno en la frontera con otras regiones del plasma. En teoría de vainas, se asume que la función de distribución de velocidades de las partículas en la frontera con el plasma es una función de distribución de Maxwell-Boltzmann. Sin embargo, existen argumentos para decir que la función de distribución en la frontera con el plasma es otra, como por ejemplo una función de distribución de Maxwell-Boltzmann desplazada [30], la función de distribución calculada por Riemann para el caso de un plasma en el que dominan las colisiones [37] o la función de distribución calculada por Tonks y Langmuir para el caso de un plasma en el que domina la ionización [38]. También es difícil definir unívocamente y de forma útil la distancia a la que se debe colocar la frontera con el plasma [39].
- *Ecuación de Boltzmann:* En las situaciones en las que se desea incluir los efectos de colisiones e ionización en el propio modelo de la vaina o en la región previa a la vaina que la conecta con el plasma, llamada *pre-vaina*, y no solo considerarlos para calcular la función de distribución en la frontera, es necesario recurrir a la ecuación de Boltzmann,

$$\frac{\partial f(\boldsymbol{x},\boldsymbol{v})}{\partial t} + \boldsymbol{v}\cdot\frac{\partial f(\boldsymbol{x},\boldsymbol{v})}{\partial \boldsymbol{x}} + \frac{\boldsymbol{F}}{m}\cdot\frac{\partial f(\boldsymbol{x},\boldsymbol{v})}{\partial \boldsymbol{v}} = \left.\frac{\partial f(\boldsymbol{x},\boldsymbol{v})}{\partial t}\right]_C, \qquad 2.25$$

expresión en la que $f(\boldsymbol{x},\boldsymbol{v})$ es la función de distribución de velocidades en la región del espacio $\boldsymbol{x}$ para una determinada especie química de masa m sometida a una fuerza neta $\boldsymbol{F}$. Las variables $\boldsymbol{x}$ y $\boldsymbol{v}$ podrían ser vectores, por lo que denotan a x y v de un sistema unidimensional o a los vectores $\vec{x}$ y $\vec{v}$ de un espacio vectorial de dimensión mayor, en cuyo caso las derivadas parciales debemos entenderlas como gradientes en los espacios de posición y de velocidades, respectivamente. El término que permite considerar los efectos de colisiones e ionización es el término del miembro derecho que tiene el subíndice C, gracias al que es posible quitar y añadir partículas en la región espacial $\boldsymbol{x}$. Las colisiones se modelan quitando partículas con una velocidad y añadiendo partículas con otra velocidad distinta, mientras que la ionización se modela añadiendo partículas según una función de distribución deseada (para una revisión completa de posibles particularizaciones del término de colisiones, véase el trabajo de Nanbu [40]). En realidad el modelo completo debe incluir tantas ecuaciones como especies químicas, que interaccionan mediante el término de fuerza y el término de colisiones.

Cada una de las descripciones que se han introducido se utiliza en distintas situaciones, o incluso se pueden usar distintas descripciones para distintos tipos de partículas dentro del mismo modelo. Algunos resultados teóricos importantes se obtienen con alguno de los tipos de modelos y son aplicables en otras situaciones, y de hecho se utilizan como premisas en otros modelos más complejos. Ejemplos de ello son los conceptos de cuasi-neutralidad y de longitud de Debye, que se utilizan siempre que sea posible para evitar la necesidad de resolver la ecuación de Poisson y para establecer la escala del problema para intuir qué modelo es aplicable, respectivamente. La longitud de Debye λ_D permite también establecer una relación de escala para obtener casos límite en los casos en que alguna variable espacial, como puede ser el radio de la sonda electrostática de Langmuir, sea mucho mayor o mucho menor que la longitud de Debye λ_D. Veamos otros resultados teóricos importantes.

2.2.1 Borde del plasma

La condición de cuasi-neutralidad proviene de la movilidad de las partículas que constituyen el plasma. Es decir, las cargas del conjunto de la descarga se reestructuran para que las

densidades de carga positiva sean iguales a las densidades de carga negativa, según se establece en (2.23). Este es un principio integral, es decir, implícitamente se utiliza el hecho de que se conserva el número de partículas de cada tipo en el conjunto de la descarga. Por otra parte, la ecuación de Poisson (2.4) es una ecuación diferencial que establece una condición en un punto, por lo que una condición global como la conservación del número total de partículas en un volumen determinado no se puede introducir de forma sencilla. Necesariamente, debemos analizar las soluciones obtenidas y comprobar su conformidad con la condición de conservación en el conjunto de la descarga.

Consideremos la ecuación de Poisson (2.4) en el caso en el que existe cuasi-neutralidad, ignorando por ahora que el movimiento térmico de los electrones impide la cuasi-neutralidad perfecta:

$$\frac{\mathrm{d}^2\phi}{\mathrm{d}x^2} = -\frac{e}{\varepsilon_0}(n_+ - n_-) = 0. \qquad 2.26$$

Esto significa que en condiciones de cuasi-neutralidad, el potencial es una línea recta. La movilidad de los electrones y los iones asegura que el campo eléctrico es nulo y, por lo tanto, el potencial es constante:

$$\phi = \phi_p. \qquad 2.27$$

Como se puede observar, en el caso de cuasi-neutralidad y considerando la ecuación como un sistema dinámico en la variable ϕ, la ecuación se encuentra en un punto fijo. Sin embargo, observemos que si existe un desequilibrio en la carga, haciéndola positiva y creciente en el sentido de la x creciente, entonces la derivada segunda del potencial es negativa, por lo que la función $\phi(x)$ es cóncava hacia abajo (∩). Esto implica necesariamente que el potencial, en el caso de un mínimo desequilibrio de carga positiva, decrece a medida que aumenta x.

$$n_+ > n_- \Rightarrow \phi(x) < \phi_p;\ \frac{\mathrm{d}^2\phi}{\mathrm{d}x^2} < 0. \qquad 2.28$$

En el caso de que el potencial se haga negativo, si suponemos que los electrones se modelan mediante un factor de Boltzmann, y por tanto mediante la ecuación (2.5), con n_p la densidad de electrones en el plasma donde el potencial es ϕ_p,

$$n_- = n_p e^{\frac{e(\phi-\phi_p)}{k_B T_e}}, \qquad 2.29$$

la densidad de electrones disminuye debido a la reducción del potencial, lo que aumenta el desequilibrio. El potencial tiene un perfil de crecimiento inicialmente exponencial, como en (2.8), pero en el momento en que la aproximación de que el potencial es suficientemente pequeño, $|e\phi| \ll k_B T_e$, deja de ser válida, el crecimiento es incluso más acusado. Habiendo comprobado que la ecuación de Poisson, considerada como un sistema dinámico en la variable ϕ tiene un punto fijo inestable en el valor del potencial del plasma, es comprensible que el valor inicial del sistema dinámico influya dramáticamente en el cálculo del perfil de potencial. Este punto inicial es lo que llamamos ***borde del plasma***, y su elección de acuerdo con los principios de cuasi-neutralidad puede ser un problema complejo. En algunos modelos de vainas, como el modelo radial de Allen, Boyd y Reynolds [9], la elección del punto donde se coloca el borde del plasma es casi irrelevante, ya que la solución es muy insensible a la elección concreta del borde del plasma (Sección 2.5.2), pero en otros modelos, como el modelo orbital de Laframboise [13] o el modelo radial de Fernández Palop *et al.* [11], la decisión es crítica. En el modelo orbital, la sensibilidad de la solución con respecto a la posición del borde del plasma hace que en la práctica se use el caso límite OML (Orbital Motion Limited) para sonda de radio muy pequeño con respecto a la longitud de Debye λ_D (Sección 2.5.3). En el modelo radial de Fernández Palop, la sensibilidad de la solución con respecto a la elección para el borde del plasma limita su validez a temperatura de los iones T_+ muy pequeña con respecto a la temperatura de los electrones T_e, y, en última instancia, ha motivado la realización del trabajo desarrollado en esta tesis.

2.2.2 Criterio de Bohm

Consideremos una superficie plana en contacto con un plasma electropositivo con una población de iones positivos, cada uno con carga e y una población de electrones, alrededor de la que se forma una vaina iónica positiva que atrae a los iones positivos y repele a los electrones, esto es, el potencial de la superficie metálica es inferior al potencial del plasma. Consideremos que la diferencia entre el potencial en el borde de la vaina x_0 y el potencial del plasma es

despreciable frente a la diferencia entre el potencial en la vaina en el punto x y en el plasma. Por tanto, coloquemos la referencia de potencial en el plasma y la referencia espacial en $x_0 = 0$. Supongamos que el sistema se encuentra en estado estacionario. Consideremos que los iones entran en la vaina con una determinada velocidad v_0 dirigida hacia la pared metálica. Luego se discutirá de dónde puede surgir esta velocidad inicial. La conservación de la energía para los iones nos permite escribir:

$$\frac{1}{2}m_+ v_+(x)^2 + e\phi(x) = \frac{1}{2}m_+ {v_0}^2, \tag{2.30}$$

donde m_+ es la masa del ion positivo, $v_+(x)$ es la velocidad del ion en el punto x y $e\phi(x)$ es la energía potencial del ion positivo en el mismo punto; obsérvese que $\phi(x) < 0$. Es posible resolver para la velocidad $v_+(x)$.

$$v_+(x) = \left({v_0}^2 - \frac{2e\phi(x)}{m_+}\right)^{\frac{1}{2}}. \tag{2.31}$$

Consideremos ahora la ecuación de continuidad para los iones en su aproximación a la superficie metálica plana. Dado que no se acumulan iones, la densidad de corriente de iones j_+ es constante.

$$j_+ = n_p v_0 = n_+(x)v_+(x), \tag{2.32}$$

con n_p la densidad del plasma. Sustituyendo (2.31) en (2.32), obtenemos:

$$n_+(x) = n_p\left(1 - \frac{2e\phi(x)}{m_+ {v_0}^2}\right)^{-\frac{1}{2}}. \tag{2.33}$$

Podemos, finalmente, escribir la ecuación de Poisson (2.4) con los electrones comportándose según la distribución de Boltzmann (2.5) y los iones según (2.33). Con ello obtenemos:

$$\frac{\mathrm{d}^2\phi}{\mathrm{d}x^2} = -\frac{e}{\varepsilon_0}\left(n_+(x) - n_-(x)\right) = -\frac{en_p}{\varepsilon_0}\left(\left(1 - \frac{2e\phi(x)}{{m_+v_0}^2}\right)^{-\frac{1}{2}} - e^{\frac{e\phi(x)}{k_BT_e}}\right). \tag{2.34}$$

Multiplicando ambos miembros de (2.34) por el campo eléctrico,

$$\xi(x) = \frac{\mathrm{d}\phi(x)}{\mathrm{d}x}, \tag{2.35}$$

es posible realizar la primera integración de esta expresión, resultando:

$$\frac{1}{2}\left(\left(\frac{\mathrm{d}\phi(x)}{\mathrm{d}x}\right)^2 - \left(\frac{\mathrm{d}\phi}{\mathrm{d}x}\Big|_{x=0}\right)^2\right) = \frac{n_p{m_+v_0}^2}{\varepsilon_0}\left(\left(1 - \frac{2e\phi(x)}{{m_+v_0}^2}\right)^{\frac{1}{2}} - 1\right) + \frac{n_pk_BT_e}{\varepsilon_0}\left(e^{\frac{e\phi(x)}{k_BT_e}} - 1\right). \tag{2.36}$$

De la expresión (2.36) recién obtenida, se concluye un resultado muy interesante, que se denomina *criterio de Bohm*. Para deducirlo, realizamos la expansión en serie de Taylor para el potencial $\phi(x)$ y utilizamos los términos hasta orden $\phi(x)^2$ en el miembro de la derecha, ya que el término cuadrático es el primero que no se cancela.

$$\left(1 - \frac{2e\phi(x)}{{m_+v_0}^2}\right)^{\frac{1}{2}} - 1 \cong -\frac{1}{2}\left(\frac{2e\phi(x)}{{m_+v_0}^2}\right) - \frac{1}{4}\left(\frac{2e\phi(x)}{{m_+v_0}^2}\right)^2, \tag{2.37}$$

$$e^{\frac{e\phi(x)}{k_BT_e}} - 1 \cong \frac{e\phi(x)}{k_BT_e} + \frac{1}{2}\left(\frac{e\phi(x)}{k_BT_e}\right)^2. \tag{2.38}$$

Sustituyendo (2.37) y (2.38) en (2.36) obtenemos la siguiente expresión:

$$\frac{1}{2}\left(\left(\frac{\mathrm{d}\phi(x)}{\mathrm{d}x}\right)^2 - \left(\frac{\mathrm{d}\phi}{\mathrm{d}x}\Big|_{x=0}\right)^2\right) = \frac{n_p}{\varepsilon_0}\left(e\phi(x)\right)^2\left(-\frac{1}{{m_+v_0}^2} + \frac{1}{2k_BT_e}\right). \tag{2.39}$$

Podemos observar en (2.39) que para que el campo eléctrico $\frac{\mathrm{d}\phi(x)}{\mathrm{d}x}$ aumente en la dirección en la que se desplazan los iones y, por tanto, para que los iones positivos sean acelerados hacia la superficie metálica plana que se encuentra a un potencial negativo, es necesario que el paréntesis del miembro derecho sea mayor que cero. Es decir, para que la vaina se pueda formar, debe cumplirse que la velocidad inicial v_0 con la que los iones entran en la vaina satisfaga la condición:

$$v_0 > v_B = \sqrt{\frac{2k_B T_e}{m_+}}. \qquad 2.40$$

Esta es la expresión del criterio de Bohm y el valor v_B es conocido como ***velocidad de Bohm***. Es la mínima velocidad con la que deben aproximarse los iones a la vaina para que ésta se pueda formar. La velocidad debe ser adquirida en la región del plasma próxima a la vaina, o pre-vaina, por un campo eléctrico residual que permita la aceleración de los iones hasta alcanzar dicha velocidad. Tanto los modelos de descargas de plasma en su frontera con superficies metálicas como muchos modelos de vainas en su conexión con el plasma utilizan este valor como condición de contorno. Sin embargo, la velocidad de Bohm es un concepto no exento de discusión en la comunidad científica de física de plasmas [39,41–43]. Es un valor mínimo de la velocidad, pero no se puede afirmar nada acerca del grado con el que se cumple la desigualdad, es decir, que conocemos el valor mínimo de la velocidad pero no conocemos su valor exacto. Por otra parte, es un valor asintótico y no es aplicable en condiciones en las que los recorridos libres medios de colisión de los iones no son muy grandes [44].

2.2.3 Fórmula de Druyvesteyn

Se ha considerado que la función de distribución de energía de los electrones o EEDF, en los análisis teóricos que se han realizado hasta ahora, sigue la función de distribución de Maxwell-Boltzmann. Esta suposición proviene principalmente de la alta movilidad de los electrones con respecto a los iones y la situación de equilibrio que tienen los electrones en una vaina electronegativa que los repele. Sin embargo, también es posible medir experimentalmente en plasmas reales la EEDF y comprobar la validez de dicha suposición. La conclusión es que en muchos casos, la EEDF es una función de distribución de Maxwell-Boltzmann. El método de medida de la función de distribución de energía de los electrones $f_E(E)$ se basa en una fórmula

conocida como *fórmula de Druyvesteyn*, que es válida para cualquier superficie metálica no cóncava inmersa en un plasma [45].

$$[f_E(E)]_{E=-eV} = \frac{-4}{Ae^2}\sqrt{\frac{-m_e V}{2e}}\frac{\mathrm{d}^2 I}{\mathrm{d}V^2}, \qquad 2.41$$

donde V es el potencial que se impone en la superficie metálica, I es la corriente que drena al plasma, A es el área de la superficie que recolecta la corriente, y e y m_e son la carga y la masa del electrón, respectivamente. Para obtener la expresión de la fórmula de Druyvesteyn es conveniente recordar antes cómo se relacionan las funciones de distribución para distintas variables. Si se sigue este esquema, establecido por Kagan Y.M. y Perel V.I. en 1964 [45,46], se obtiene una forma de la demostración de la fórmula de Druyvesteyn que es válida para cualquier sonda no cóncava, validez que el propio Druyvesteyn sugirió para los casos particulares de sonda cilíndrica y plana [45]. La función de distribución en el caso más general se da en función de las tres componentes de la velocidad y para el caso isótropo se reduce a una función de distribución del módulo de la velocidad.

$$f_{\vec{v}}(\vec{v})\mathrm{d}^3\vec{v} = f_{\vec{v}}(v,\theta,\varphi)\mathrm{d}^3\vec{v} = f_{\vec{v}}(v)v^2\sin\theta\,\mathrm{d}v\,\mathrm{d}\theta\,\mathrm{d}\varphi. \qquad 2.42$$

Mediante integración en las coordenadas angulares se obtiene:

$$f_v(v)\mathrm{d}v = 4\pi v^2 f_{\vec{v}}(v)\mathrm{d}v. \qquad 2.43$$

Esta función de distribución de las coordenadas de la velocidad se puede, al ser una distribución isótropa, poner en función de la energía. Redefinimos la función de distribución para que su argumento sea la energía por simplicidad en la notación, lo que siempre es posible gracias a la relación unívoca entre módulo de la velocidad y energía:

$$f_{\vec{v}}(v) = f_{\vec{v}}\left(\sqrt{\frac{2}{m_e}(E+eV)}\right) \rightarrow f_{\vec{v}}(E), \qquad 2.44$$

donde V es el potencial eléctrico que se impone en la superficie metálica no cóncava. De este modo, tenemos la relación entre la función de distribución de energía y la de velocidad, en esta última forma dada.

$$f_E(E)\mathrm{d}E = 4\pi v^2 f_{\vec{v}}(E)\mathrm{d}v. \qquad 2.45$$

Para calcular ahora la intensidad de corriente electrónica que recoge un diferencial de área de conductor inmerso en un plasma sobre el que se ha formado una vaina iónica positiva, considérese el número de electrones que viajan en una determinada dirección dada por los ángulos polar θ y azimutal φ:

$$f_{\vec{v}}(E)v^2 \sin\theta \,\mathrm{d}v \,\mathrm{d}\theta \,\mathrm{d}\varphi. \qquad 2.46$$

El número de electrones por unidad de tiempo que cruzan un diferencial de superficie, considerando el eje z perpendicular a dicho diferencial de superficie, se obtiene como el producto escalar del vector superficie por el flujo de electrones, siendo este el número de electrones de la ecuación anterior por la velocidad $\vec{v}$.

$$\mathrm{d}A\; v\cos\theta\, f_{\vec{v}}(E)v^2 \sin\theta \,\mathrm{d}v \,\mathrm{d}\theta \,\mathrm{d}\varphi. \qquad 2.47$$

Con esto, obtener la corriente es inmediato, sin más que multiplicar por la carga del electrón $-e$. Ésta es la corriente que cruza un elemento de superficie y desde una determinada dirección.

$$I_e(\mathrm{d}A, v, \theta, \varphi) = -e\,\mathrm{d}A f_{\vec{v}}(E)v^3 \sin\theta\cos\theta \,\mathrm{d}v \,\mathrm{d}\theta \,\mathrm{d}\varphi. \qquad 2.48$$

Para obtener la corriente total se integra en todas las direcciones permitidas. Si la superficie del conductor no es cóncava en ningún punto, para todos los elementos diferenciales de superficie del conductor se cumple que el espacio de integración corresponde con el hemisferio $z > 0$, con lo que los límites de integración quedan:

$$I_e(\mathrm{d}A) = -e\,\mathrm{d}A \int_{\varphi=0}^{\varphi=2\pi} \int_{\theta=0}^{\theta=\frac{\pi}{2}} \int_{v=0}^{v=\infty} f_{\vec{v}}(E) v^3 \sin\theta \cos\theta \,\mathrm{d}v \,\mathrm{d}\theta \,\mathrm{d}\varphi$$
$$= -e\,\mathrm{d}A\,\pi \int_{v=0}^{v=\infty} f_{\vec{v}}(E) v^3 \mathrm{d}v. \qquad 2.49$$

Integrando en toda la superficie del conductor inmerso en el plasma, asumiendo que la corriente es la misma en todos los puntos de la misma, se obtiene:

$$I_e = -e\,A\,\pi \int_{v=0}^{v=\infty} f_{\vec{v}}(E) v^3 \mathrm{d}v. \qquad 2.50$$

Si ahora realizamos el cambio de variable entre la energía y la velocidad para realizar la integral, obtenemos:

$$E = \frac{1}{2} m_e v^2 - eV, \qquad 2.51$$

$$I_e = -A\,\frac{2e\pi}{{m_e}^2} \int_{E=-V}^{E=\infty} f_{\vec{v}}(E)(E + eV)\mathrm{dE}. \qquad 2.52$$

Esta expresión se puede derivar con respecto al voltaje V en la sonda, teniendo precaución ya que el valor a derivar aparece tanto en los límites de integración como en el integrando. Se obtiene, de este modo:

$$\frac{\mathrm{d}^2 I_e}{\mathrm{d}V^2} = -A \frac{2e^3\pi}{{m_e}^2} [f_{\vec{v}}(E)]_{E=-eV}. \qquad 2.53$$

Ahora se utiliza (2.45) que relaciona la función de distribución de energía con la de velocidad. La función de distribución de energía es la misma en todo el plasma, ya sea el interior de la vaina, la superficie del conductor o el seno del plasma, por lo que está justificado utilizar $E = \frac{1}{2} m_e v^2$, donde la velocidad, por corrección debería ser una función de la posición, cuya función de distribución sí varía de región a región a causa del cambio en el potencial.

$$f_{\vec{v}}(E) = \frac{1}{4\pi v^2} f_E(E) \frac{\mathrm{d}E}{\mathrm{d}v} = \frac{m_e}{4\pi v} f_E(E) = \frac{m_e}{4\pi} \sqrt{\frac{m_e}{2E}} f_E(E), \qquad 2.54$$

$$\frac{\mathrm{d}^2 I_e}{\mathrm{d}V^2} = -A \frac{2e^3\pi}{{m_e}^2} \left[\frac{m_e}{4\pi} \sqrt{\frac{m_e}{2E}} f_E(E) \right]_{E=-eV} = -A \frac{e^3}{4m_e} \sqrt{\frac{2m_e}{-eV}} [f_E(E)]_{E=-eV} \qquad 2.55$$

Despejando la función de distribución en esta última expresión, obtenemos la forma usualmente utilizada de la fórmula de Druyvesteyn (2.41).

$$[f_E(E)]_{E=-eV} = \frac{-4}{Ae^2} \sqrt{\frac{-m_e V}{2e}} \frac{\mathrm{d}^2 I}{\mathrm{d}V^2}, \qquad 2.56$$

donde se ha sustituido la corriente electrónica I_e por la corriente total I ya la contribución de la corriente iónica es mínima. Esta fórmula tiene validez en el rango en el que los límites de integración impuestos son válidos. En particular, la velocidad $v \in [0, \infty)$, por lo que la tensión de la sonda V debe ser, por la ecuación (2.51), $V < 0$, medida con respecto al potencial del plasma. Las medidas realizadas sobre la curva característica I-V de un plasma son ruidosas, por lo que la obtención de la derivada segunda de la curva característica I-V no es fácil de conseguir. Son necesarias técnicas de suavización para filtrar el ruido de la señal medida para obtener una curva característica I-V numéricamente derivable [7,15,27,47,48]. Las medidas demuestran que si ni la potencia que genera la descarga ni la presión son demasiado bajas, la función de distribución de energía de los electrones EEDF puede considerarse de Maxwell-Boltzmann. Esto ocurre porque, aunque los electrones que generan la descarga son de alta energía, en torno a los 50 eV, al cabo de sucesivas colisiones, pierden energía al ionizar los neutros y generan nuevos electrones de más baja energía, entre 0.3 y 2 eV dependiendo del tipo de descarga. Cuando la presión es suficientemente alta, y los átomos neutros son suficientemente numerosos, los electrones procedentes de las ionizaciones sucesivas son predominantes dando lugar a una EEDF de Maxwell-Boltzmann compatible con una temperatura única de equilibrio, aunque el sistema realmente no esté en equilibrio [4,34,49,50]. Este hecho es conocido como la ***paradoja de Langmuir*** [51], y es importante, ya que las teorías de vainas electronegativas más importantes como la teoría radial de Allen, Boyd y Reynolds [9,11,52] y la teoría orbital de Bernstein y Rabinowitz, ampliada por Laframboise [3,12,13], utilizan como premisa que los electrones se pueden caracterizar mediante la distribución de Maxwell-Boltzmann en equilibrio térmico.

2.3 Paso de la ecuación de Boltzmann al modelo de fluidos

La ecuación de Boltzmann es sin duda una potente herramienta para estudiar sistemas físicos complejos, aunque la complejidad inherente a un sistema de ecuaciones integro-diferenciales limita su uso a unas pocas situaciones. Sin embargo, cuando es posible usarla, permite añadir luz a la física del sistema que se estudia.

$$\frac{\partial f_j(\boldsymbol{x},\boldsymbol{v_j})}{\partial t}+\boldsymbol{v_j}\cdot\frac{\partial f_j(\boldsymbol{x},\boldsymbol{v_j})}{\partial \boldsymbol{x}}+\frac{\boldsymbol{F_j}}{m_j}\cdot\frac{\partial f_j(\boldsymbol{x},\boldsymbol{v_j})}{\partial \boldsymbol{v_j}}=\left.\frac{\partial f_j(\boldsymbol{x},\boldsymbol{v_j})}{\partial t}\right]_C, \qquad 2.57$$

donde $f_j(\boldsymbol{x},\boldsymbol{v_j})$ es la función de distribución de partículas de la especie química j-ésima de masa m_j sometida a una fuerza externa $\boldsymbol{F_j}$ con velocidad entre $\boldsymbol{v_j}$ y $\boldsymbol{v_j}+\mathrm{d}\boldsymbol{v_j}$ en el volumen diferencial de tamaño $\mathrm{d}\boldsymbol{x}$ situado en el punto $\boldsymbol{x}$. En esta ecuación, el término de colisiones del miembro derecho es un término integro-diferencial, ya que las colisiones y la ionización que ocurren en una región del espacio $\boldsymbol{x}$ dependen, en general, de la densidad de partículas incidentes de cada tipo que hay en dicho punto con cada velocidad relativa con respecto a cada partícula. La integral del término de colisiones, aunque de gran complejidad, se puede construir como [40]:

$$\left.\frac{\partial f_j(\boldsymbol{x},\boldsymbol{v_j})}{\partial t}\right]_C=\sum_k\iint\left[f_j(\boldsymbol{x},\boldsymbol{v_j'})f_k(\boldsymbol{x},\boldsymbol{v_k'})-f_j(\boldsymbol{x},\boldsymbol{v_j})f_k(\boldsymbol{x},\boldsymbol{v_k})\right]\left|\boldsymbol{v_j}-\boldsymbol{v_k}\right|\sigma_{jk}\mathrm{d}\Omega\mathrm{d}v_\mathrm{k}, \qquad 2.58$$

donde la sumatoria en k se realiza sobre todos los tipos de partículas presentes en el plasma, $\boldsymbol{v_k}$ es la velocidad de la partícula incidente, y la integral en el ángulo sólido Ω incluye la información sobre $\boldsymbol{v_j'}$ y $\boldsymbol{v_k'}$, las velocidades de las partículas después de la colisión. La sección eficaz σ_{jk} mide la probabilidad de que una colisión entre las partículas de las especies químicas j y k con velocidades $\boldsymbol{v_j}$ y $\boldsymbol{v_k}$, terminen con velocidades $\boldsymbol{v_j'}$ y $\boldsymbol{v_k'}$ despues de la colisión, respectivamente. La deducción de esta expresión para el término de colisiones incluye la condición de caos molecular, hipótesis que tiene una implicación importante desde el punto de vista teórico: asumiendo que las velocidades de las partículas antes de la colisión no presentan correlación se rompe la simetría entre el instante anterior y posterior a la colisión, que permite a su vez escribir una ecuación que diferencia entre la evolución temporal hacia el futuro y hacia el pasado, a partir de leyes fundamentales perfectamente simétricas en el tiempo [53–55].

El fenómeno de ionización en plasmas ocurre generalmente por las colisiones que sufren los átomos neutros cuya densidad se puede considerar generalmente mucho mayor que la densidad del plasma, $n_n \gg n_p$, y, por lo tanto, apenas varía en el proceso de ionización. Dado que n_n es prácticamente constante, el término de ionización generalmente se puede integrar fácilmente. Sin embargo, el fenómeno de las colisiones de los iones con los neutros es mucho más complejo, porque la función de distribución de velocidad de los iones cambia notablemente en dicho proceso de colisiones y, por lo tanto, no se puede sacar de la integral. Por lo tanto, la función de distribución $f_j(\boldsymbol{x}, \boldsymbol{v_j})$ está tanto en las derivadas parciales en el miembro izquierdo de (2.57) como en el integrando de (2.58).

Es posible derivar las ecuaciones básicas de fluidos a partir de la ecuación de Boltzmann, ignorando el término de colisiones. Para ello, se calculan los primeros tres momentos de la ecuación de Boltzmann. El primer momento, o momento de orden cero, se obtiene integrando la ecuación de Boltzmann en el espacio de velocidades, teniendo en cuenta que la integral de $f_j(\boldsymbol{x}, \boldsymbol{v_j})$ en el espacio de velocidades es simplemente la densidad de partículas $\int f_j(\boldsymbol{x}, \boldsymbol{v_j}) \mathrm{d}^3 \boldsymbol{v_j} = n_j(\boldsymbol{x})$, y asumiendo fuerzas conservativas, se obtiene la siguiente expresión:

$$\frac{\partial n_j}{\partial t} + \frac{\partial}{\partial \boldsymbol{x}} \cdot (n_j \boldsymbol{u_j}) = 0, \qquad 2.59$$

donde $\boldsymbol{u_j}$ es la velocidad media de las partículas y $n_j \boldsymbol{u_j}$ es el flujo de masa de la especie química j-ésima. Esta es la ecuación de la conservación de la masa o número de partículas [56], también conocida como la ecuación de continuidad. El segundo momento de la ecuación de Boltzmann se obtiene multiplicando la ecuación de Boltzmann por el momento lineal $m_j \boldsymbol{v_j} = m_j(\boldsymbol{u_j} + \boldsymbol{w_j})$. En esta expresión se descompone explícitamente la velocidad instantánea de una partícula $\boldsymbol{v_j}$ en forma de suma de la velocidad media $\boldsymbol{u_j}$ más la velocidad aleatoria alrededor de la velocidad media $\boldsymbol{w_j}$. Integrando en el espacio de velocidades se obtiene la siguiente expresión:

$$\frac{\partial(n_j \boldsymbol{u_j})}{\partial t} + \frac{1}{2}\frac{\partial(n_j u_j^2)}{\partial \boldsymbol{x}} - n_j \frac{\boldsymbol{F_j}}{m_j} + \frac{1}{m_j}\frac{\partial}{\partial \boldsymbol{x}} \cdot \bar{\bar{\boldsymbol{P}}}_{\boldsymbol{j}} = \sum_k \mathrm{P}_{jk}. \qquad 2.60$$

Esta es la ecuación de balance de momento lineal para la especie química j-ésima, también conocida como la ecuación de Navier-Stokes en el caso de fluidos [56]. En esta

expresión $\overline{\overline{\boldsymbol{P}}}_{\boldsymbol{j}}$ es el tensor de esfuerzos, $\overline{\overline{\boldsymbol{P}}}_{\boldsymbol{j}} = m_j n_j \boldsymbol{w_j w_j}$, y P_{jk} es la variación en el momento de la partícula fluida por colisiones con las partículas de la especie química k-ésima. Por último, el segundo momento de la ecuación de Boltzmann se obtiene multiplicando por la energía cinética $\frac{1}{2} m_j {v_j}^2 = \frac{1}{2} m_j \left(\boldsymbol{u_j} + \boldsymbol{w_j}\right)^2$ e integrando en el espacio de velocidades.

$$\frac{\partial}{\partial t}\left(K_j + U_j\right) + \frac{\partial}{\partial \boldsymbol{x}} \cdot \boldsymbol{w_j}\left(K_j + U_j\right) = \frac{\partial}{\partial \boldsymbol{x}}\left(\boldsymbol{Q_j} - \boldsymbol{W_j}\right), \tag{2.61}$$

donde K_j es la energía cinética, U_j es la energía interna, $\boldsymbol{Q_j}$ es el flujo de calor que entra en el elemento de volumen diferencial $\boldsymbol{dx}$ y $\boldsymbol{W_j}$ es el flujo de trabajo que realizan las partículas de la especia química j-ésima del interior del elemento de volumen diferencial $\boldsymbol{dx}$ hacia el exterior.

Es suficiente con obtener los tres primeros momentos para describir un fluido. Sin embargo, es necesario entender las premisas que se utilizan de forma intrínseca al utilizar las ecuaciones de fluidos, particularmente porque las ecuaciones de fluidos normalmente se derivan a partir de principios macroscópicos y, por tanto, estas premisas no se establecen de forma explícita ni resultan obvias.

- *El tercer momento de la ecuación de Boltzmann es despreciable.* Dicho de otra manera, el fluido se puede caracterizar correctamente utilizando solo los momentos hasta segundo orden, y con conceptos como media y varianza de la distribución de velocidad, es decir, velocidad media y temperatura. Esto implica que la función de distribución de velocidades se puede modelar, para todas las especies, como una campana de Gauss.

$$f(\vec{v}) = \frac{1}{\sigma^3 (2\pi)^{3/2}} e^{\frac{(\vec{v}-\vec{\mu})^2}{2\sigma^2}}. \tag{2.62}$$

  En la región de la vaina en la que existen campos eléctricos que pueden llegar a ser importantes, las partículas con velocidades distintas en la campana de Gauss pueden comportarse de forma muy distinta. En particular, si el hecho de que una partícula intercepte una superficie metálica depende de la velocidad con la que la partícula comienza su orbita alrededor de la misma, puede ocurrir que una proporción de las partículas descritas por la función de distribución de velocidad intercepten la superficie metálica, mientras que otra parte de las partículas no lo hagan, orbitando de vuelta a su posición inicial. En los modelos de fluidos, necesariamente, o bien interceptan la superficie metálica

todas las partículas o bien ninguna partícula. Debe existir un mecanismo de colisiones entre partículas del mismo tipo lo suficientemente importante como para termalizar el fluido en una escala más rápida que la de la dinámica de las ecuaciones de fluidos [57]. Dado que las colisiones entre partículas del mismo fluido conservan la masa, el momento lineal y la energía, no suponen ningún cambio en las ecuaciones de fluidos. Los modelos de partículas no tienen este problema, ya que en estos modelos se utiliza la función de distribución de velocidades y, por lo tanto, ésta puede tener cualquier forma funcional.

- *Cada especie del plasma tiene su propia temperatura*. El ritmo al que se transfiere la energía entre partículas del mismo tipo debe ser suficientemente grande en comparación con la inversa del tiempo característico del problema como para que las partículas estén termalizadas en todo momento. Sin embargo, el ritmo de transferencia de energía entre partículas de distinto tipo debe ser suficientemente bajo como para que cada especie tenga su propia temperatura. Teniendo en cuenta que todas las frecuencias de colisión entre partículas cargadas van a ser del mismo orden de magnitud, ambas condiciones se pueden cumplir simultáneamente en el caso en el que las masas de las partículas del plasma sean muy diferentes. Este es el caso de los plasmas electropositivos de una componente en los que solo hay un tipo de anión pesado y un tipo de partícula negativa de masa mucho menor, los electrones, entre los que la transferencia de energía en una colisión es despreciable [58]. En el caso de partículas sin carga, la fuerza interviniente es de corto alcance, por lo que la sección eficaz es mucho menor. Por lo tanto, la condición también se puede cumplir en el caso en el que hay dos tipos de partículas pesadas, una con carga y otra sin carga, de forma que las colisiones entre iones y neutros sean menos frecuentes que las colisiones entre iones. Si esto no es posible, es necesario diseñar un mecanismo de transferencia de momento y energía de un tipo de partícula a otro e introducirlo en los modelos.
- *Se puede definir la partícula fluida*, es decir, en la escala espacial del problema se puede definir una distancia infinitesimal en la que cabe un número muy grande de partículas.
- *La velocidad media de las partículas no es demasiado grande*. La velocidad media de las partículas multiplicada por la escala de tiempo a la que el fluido se termaliza [57], debe ser mucho menor que la escala espacial del problema. Esto impone una restricción adicional a la velocidad máxima de las partículas fluidas en las soluciones a los modelos de fluidos.

Cuando las limitaciones impuestas por el paso de la ecuación de Boltzmann a las ecuaciones de fluidos se incumplen, la validez de los resultados de los modelos de fluidos puede

quedar en entredicho. Sin embargo, a menudo los resultados obtenidos resultan cumplirse un poco más allá del rango de validez esperado. Por ejemplo, si la velocidad del fluido es muy grande y el fluido no tiene tiempo para termalizarse, pero el cambio en la función de distribución de velocidad del fluido predicho por el modelo al desplazarse una distancia del orden de la escala del problema no es importante, el cambio predicho por el modelo no tiene influencia en los resultados, por lo que la solución obtenida es válida. En este punto, las medidas experimentales y los razonamientos heurísticos son la única manera de justificar la validez y definir la aplicabilidad de los modelos [59–61].

2.4 Fenómenos fundamentales de un plasma

En un plasma, las partículas y las superficies se encuentran sometidas a campos electromagnéticos intensos o a altas temperaturas que provocan varios efectos que en condiciones menos extremas pueden ser ignorados. En esta sección se van a describir los que tienen más relevancia en teoría de vainas electronegativas. Trataremos dos tipos importantes de efecto:

- *Colisiones*: En su movimiento en el plasma, existe la posibilidad de que las partículas se encuentren con otras presentes en el plasma. La colisión debe modelarse mediante una probabilidad asociada a la velocidad relativa de aproximación y de salida entre las partículas que participan en la colisión. Sin embargo, la recomendación estándar es que este modelo completo y complejo de las colisiones se puede simplificar a una sección eficaz isotrópica y una sección eficaz de retroceso o *backscattering*. La primera significa que una partícula puede encontrarse con otra y salir desviada en cualquier dirección con la misma probabilidad, mientras que la segunda implica que las partículas solo pueden salir de la colisión con la velocidad relativa opuesta a la inicial [62,63].
- *Emisión*: Mediante aplicación de energía sobre una superficie metálica, ya sea mediante calentamiento, impacto de partículas, diferencia de potencial o radiación electromagnética, es posible que los electrones del metal adquieran una energía superior a la función de trabajo del material, permitiendo al electrón abandonar el metal y pasar a formar parte del plasma.

2.4.1 Colisiones con los átomos neutros

En su movimiento en el seno del plasma, los iones pueden tener una colisión con los electrones, con otros iones y con los átomos neutros del gas. En las colisiones con los electrones, salvo en el caso de los pocos electrones más energéticos que tengan capacidad para ionizar doblemente al ion, la colisión es elástica con muy poca transferencia de energía debido a la gran diferencia de masas que hay entre las dos partículas. Debido a que en los plasmas fríos el ratio de ionización del gas suele estar por debajo de 10^{-6}, la probabilidad de que un ion se encuentre con un átomo neutro de su mismo elemento es muy superior a la probabilidad de que se encuentre con otro ion igual. Por lo tanto el tipo de colisión más relevante es la colisión con un neutro, tras la que pueden ocurrir varias reacciones [62–64]:

- El ion puede arrancar un electrón del neutro generando otro ion positivo.
- El ion puede entrar en un estado excitado que por decaimiento acabe liberando un fotón con la energía de dicho estado excitado.
- Puede transferir momento al neutro.
- Puede producir una molécula ionizada.
- Puede intercambiar un electrón.

De todas estas reacciones, la más frecuente en plasmas fríos es la última, la colisión de intercambio de carga (Charge-Exchange o C-E collision) [41,62,63,65]. En este caso, la proximidad entre el ion y el átomo neutro permite la superposición de la nube electrónica del último electrón del átomo con el ion, lo que a su vez provoca con una cierta probabilidad un salto del electrón desde el átomo neutro al ion. Este intercambio de carga es equivalente a un intercambio de momento: se produce un ion con el momento lineal del neutro y un neutro con el momento lineal del ion. Por lo general, los iones se desplazan por el efecto de los campos electromagnéticos en el plasma, mientras que los neutros están en equilibrio, con una velocidad media nula. Por esto, en los modelos de fluidos, se puede introducir el efecto de las colisiones de intercambio de carga como un término de pérdida de momento lineal o fricción. En los modelos de partículas, la sección eficaz isotrópica es, por lo tanto, nula y la sección eficaz de retroceso es igual a la sección eficaz total.

2.4.2 Ionización

La ionización se puede producir cuando una partícula suficientemente energética colisiona de forma inelástica con un átomo neutro del gas de fondo, de forma que se genera un nuevo ion que pasa a formar parte del plasma. Típicamente, las partículas que generan ionización son los electrones de alta energía, que en las descargas de laboratorio pueden tener hasta $50\ \mathrm{eV}$. En sucesivas colisiones, los electrones rápidos van perdiendo energía que ceden para que electrones de los átomos neutros puedan ser arrancados y se incorporen al plasma. La probabilidad de que se produzca una ionización depende de la densidad de electrones rápidos y de la densidad de átomos neutros. En muchas descargas, esta probabilidad se puede considerar como un valor constante en una región considerable del plasma. Los modelos de partículas pueden incorporar este efecto mediante un término constante de adición de electrones y de iones [38,66–69]. Sin embargo, en los modelos de fluidos se produce un efecto que no se puede modelar bien. La adición de iones con velocidad media nula en una población de iones que tiene una función de distribución de Gauss con velocidad media no nula, supondría una función de distribución conjunto que nunca va a ser una distribución de Gauss, por lo que los conceptos de fluidos, como la temperatura, serían insuficientes para modelar la población de iones. Para poder seguir usando el modelo de fluidos, debe de existir un mecanismo de termalización del fluido de iones que garantice que los nuevos iones son acelerados y que los iones previos incorporan su masa a la partícula fluida. Este mecanismo debe ser suficientemente rápido en comparación con la escala de tiempo de la ionización.

2.4.3 Emisión en sondas y en descargas

Los electrones de un metal están en un pozo de potencial cuya profundidad se conoce como función de trabajo W del material. Cuando un electrón adquiere energía suficiente, puede superar la profundidad del pozo de potencial y salir del metal. Este efecto se puede utilizar para introducir electrones en el gas y generar plasma [70,71]. Por otra parte, la corriente generada por los electrones emitidos se puede utilizar para compensar la corriente iónica en diagnosis (EEP, Electron Emitting Probe) [8]. La energía que los electrones adquieren puede tener distintos orígenes.

- *Termo-emisión*: En un metal que se calienta lo suficiente, alcanzando los varios cientos de grados centígrados, la probabilidad de que un electrón adquiera espontáneamente energía suficiente como para superar la función de trabajo del metal puede ser apreciable,

dependiendo del material metálico [72]. La función de trabajo del metal puede tener valores relativamente bajos como, por ejemplo, los $2.3\ \mathrm{eV}$ para el potasio, aunque la mayor parte de los metales están en el rango de los 3.5 o $5\ \mathrm{eV}$. El tungsteno, comúnmente utilizado en sondas electrostáticas de Langmuir por su función trabajo alta, alcanza los $4.5\ \mathrm{eV}$.

- *Extracción por colisión*: Cuando una partícula colisiona con una superficie metálica, existe una probabilidad de que un electrón de la superficie reciba parte de la energía y salga de la superficie. Por ejemplo, la descarga DC del grupo de investigación TEP-230 Contacto plasma-superficie en la que este trabajo se enmarca presenta este efecto cuando las corrientes de iones y de electrones acelerados por los campos eléctricos intensos, propios de la proximidad de los electrodos, entran en el cátodo y en el ánodo respectivamente. Incluso algunas partículas que se encuentran en estados excitados, como por ejemplo el helio meta-estable con una energía de $19.7\ \mathrm{eV}$, tiene suficiente energía como para superar la función de trabajo del metal sin necesidad de adquirir energía cinética [73].
- *Diferencia de potencial*: Un campo eléctrico intenso provoca que las cargas positivas y negativas de un átomo neutro de desplacen ligeramente provocando que el átomo pase a tener un momento dipolar eléctrico. Si se impone una diferencia de potencial importante entre dos metales, los dipolos de la superficie pueden ser lo suficientemente importantes como para arrancar un electrón. En las descargas de plasma, donde la presión del gas es baja pero aún lejos del vacío, este efecto es secundario frente a la ruptura del gas dieléctrico, en que los dipolos del gas neutro pueden disociarse en un electrón y un ion.
- *Radiación electromagnética*: Se trata del efecto fotoeléctrico, en el que un electrón de la superficie metálica captura un fotón de energía suficiente como para escapar del pozo de potencial.

2.4.4 Emisión secundaria en sondas

El intercambio de electrones entre la superficie metálica de la sonda y el plasma circundante genera la corriente que la sonda drena hacia el plasma. La corriente positiva, saliente, está generada por la recogida de electrones, mientras que la corriente negativa, entrante, proviene de la captura de electrones de la superficie metálica de la sonda por los iones positivos cuando se acercan a la misma. La corriente negativa implica, por lo tanto, colisiones de partículas pesadas contra la sonda. La energía cinética adicional de la colisión puede ser recogida inelásticamente por un segundo electrón del metal, y si la energía recogida es suficiente como

para superar la función de trabajo del metal, el electrón puede escapar del material metálico. Este efecto se conoce como *emisión secundaria* [58,74,75].

La corriente entrante producida por el escape de electrones durante la emisión secundaria es por lo general pequeña, pero en los casos en los que las medidas de corriente recogida por la sonda son muy delicadas como, por ejemplo, cuando se recoge corriente iónica con la sonda polarizada negativamente con respecto al plasma, el efecto de la emisión secundaria puede ser apreciable. Los electrones secundarios son emitidos con una energía que depende de la velocidad de los iones. La conservación de la energía en este proceso arroja:

$$K_e + W = E_+, \qquad 2.63$$

donde K_e es la energía cinética del electrón arrancado, W es la función de trabajo del material y E_+ es la energía total del ion incidente que incluye su energía cinética y la posible energía adicional, si se encuentra en un estado excitado. Como la sonda está polarizada negativamente con respecto al seno del plasma, los electrones son repelidos y se incorporan al fluido de electrones del plasma, por lo que la corriente de los electrones secundarios se debe cancelar en la corriente recogida por la sonda para poder medir la corriente iónica. Esta corriente normalmente es demasiado pequeña como para tener un efecto sobre la temperatura de los electrones del plasma.

2.5 Teorías de sondas electrostáticas de Langmuir

Una sonda electrostática de Langmuir es un conductor eléctrico, generalmente con simetría esférica, cilíndrica o plana, que se introduce en un plasma y sobre el que se puede medir la corriente eléctrica que drena hacia el plasma para cada potencial eléctrico que se impone en la sonda. A partir de esta respuesta eléctrica, se pueden deducir las propiedades del plasma, como son la densidad del plasma n_p o la temperatura de los electrones T_e. Las sondas más utilizadas son la esférica, como la que se utilizó en la sonda espacial Rosseta que la Agencia Espacial Europea lanzó para explorar en cometa 67P/Churyumov-Gerasimenko, y la cilíndrica, como las sondas comerciales ESPion de Hiden Analytical®, por su sencillez de construcción.

La diagnosis con sondas electrostáticas de Langmuir es, incluso más de 80 años después de su invención, uno de los métodos más utilizados en diagnosis de plasmas, ya que proporciona información local sobre el plasma en la región donde se coloca. Sin embargo, la explicación teórica consistente para explicar la región del plasma alrededor de la sonda, o vaina, aún no está bien establecida, a pesar del esfuerzo que se ha realizado en las últimas décadas [39,76,77] en la comunidad científica dedicada a este área. Varias teorías se han establecido para explicar la interacción entre una sonda electrostática de Langmuir y el plasma circundante. En esta sección se describe dicha interacción desde el punto de vista experimental y se describen las teorías más importantes.

2.5.1 Curva característica de corriente-tensión I-V de la sonda electrostática de Langmuir

Una sonda electrostática de Langmuir inmersa en un plasma drena una determinada corriente hacia el plasma para cada diferencia de potencial entre la sonda y el seno del plasma, dependiendo de los parámetros del plasma, como la densidad del plasma n_p o la temperatura de los electrones T_e. La corriente se considera positiva cuando es saliente de la sonda, es decir, cuando la sonda recoge electrones. Si se realiza un barrido en el potencial de la sonda y se mide la corriente eléctrica drenada por la sonda considerando positiva la corriente hacia el plasma para obtener la curva característica corriente-tensión o curva característica I-V de la sonda electrostática de Langmuir, se pueden distinguir tres regiones como se observa en la Figura 2:

- *Zona de saturación electrónica*: A la derecha de la curva característica se encuentran los puntos para los que la sonda se encuentra polarizada positivamente con respecto al plasma, por lo que los electrones y los iones negativos son atraídos hacia la sonda y los

iones positivos son repelidos. Los iones positivos no alcanzan la sonda, debido a la energía relativamente baja que tienen, en el orden de la temperatura ambiente $T_+ = 0.03\ \mathrm{eV}$. El límite inferior que define esta zona es el valor del potencial del plasma V_p donde se encuentra un punto de inflexión en la curva característica I-V. La forma funcional proporcional entre las variables I^2 y V es característica de esta zona, para el caso de sondas cilíndricas, y tiene que ver con el modelo orbital que describe correctamente la corriente electrónica en esta zona (véase la sección 2.5.3).

- *Zona de retardo electrónico*: En el centro hay una estrecha banda limitada por arriba por el potencial del plasma y por abajo por el potencial de corte V_c, para el que se anula la corriente. En esta zona, el potencial de la sonda es inferior al potencial del plasma, pero la diferencia entre ambos es del mismo orden que la temperatura electrónica T_e de forma que algunos electrones, los más energéticos, pueden alcanzar la sonda. El límite inferior no se puede definir con precisión, ya que el decaimiento en la corriente electrónica recogida es exponencial con respecto a la diferencia entre el potencial del plasma y el potencial de la sonda. El potencial flotante se define como el potencial referido con respecto al potencial del plasma para el que la corriente neta drenada por la sonda hacia el plasma es nula, es decir, la corriente iónica iguala a la corriente electrónica.

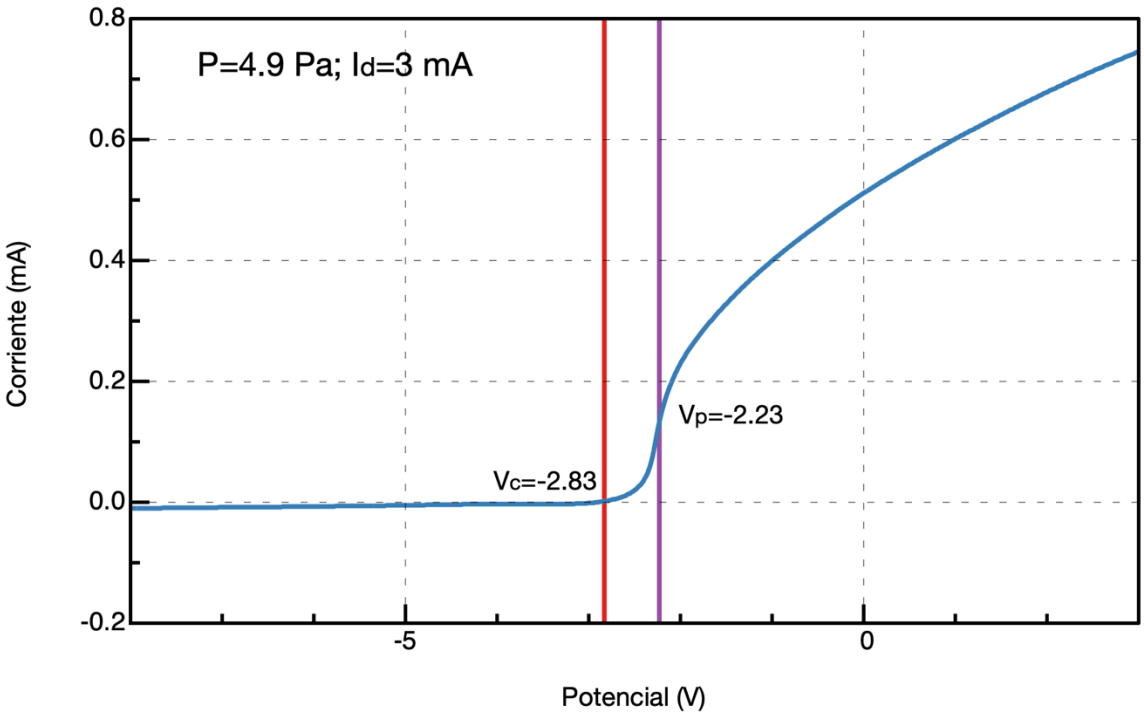

Figura 2: Curva característica corriente-tensión I-V experimental típica, plasma de argón, presión $P = 4.9\ \mathrm{Pa}$ y corriente de descarga $I_d = 3\ \mathrm{mA}$.

- *Zona de saturación iónica*: A la izquierda de la curva característica, el potencial es muy negativo con respecto al potencial del plasma, por lo que prácticamente ningún electrón es capaz de alcanzar la sonda. La corriente es debida solo a los iones positivos. Esta zona de la curva característica I-V es muy interesante: las medidas en esta zona son difíciles debido a que la corriente es muy baja, pero precisamente por eso drenan poca corriente del plasma y, por lo tanto, producen una perturbación mínima en el conjunto de la descarga, lo que puede ser crítico en descargas muy frías como la del grupo de investigación TEP-230 Contacto plasma-superficie en que el trabajo de esta tesis se enmarca.

El potencial flotante, es decir, el potencial referido al potencial del plasma para el que la corriente iónica recogida por la sonda iguala a la corriente electrónica en la zona de retardo electrónico, es muy importante, porque en muchas aplicaciones tecnológicas una superficie metálica a tratar se deja eléctricamente aislada, de forma que la corriente neta hacia o desde la superficie es nula. Se trata de una condición experimentalmente muy sencilla de conseguir, aunque la explicación teórica ha demostrado ser una tarea muy compleja. Modelar apropiadamente los iones es fundamental, porque da información clave acerca de la energía cinética con la que los iones colisionan con la superficie, y la energía cinética de la colisión es el parámetro que determina si el ion choca sin otro efecto más que arrancar un electrón o si se queda implantado o daña la superficie.

2.5.2 Modelo radial ABR (Allen, Boyd y Reynolds)

Considérese una sonda electrostática de Langmuir cilíndrica infinitamente larga de radio r_p inmersa en un plasma electropositivo, con una población de electrones con temperatura T_e y una única población de iones fríos con carga e. Todas las magnitudes físicas del problema deben ser función solo de la distancia al eje de simetría r. La velocidad de los iones fríos es prácticamente nula en el problema y se cumple, por la condición de cuasi-neutralidad, que:

$$n_{+0} = n_{e0}. \qquad 2.64$$

donde n_{+0} es la densidad de los iones positivos en el plasma y n_{e0} es la densidad de los electrones en el plasma. Consideremos el caso en el que la sonda se polariza negativamente con respecto al plasma y, por lo tanto, al moverse en un potencial retardador pueden alcanzar

el equilibrio térmico, de modo que pueden ser modelados utilizando un factor de Boltzmann (2.5):

$$n_e(r) = n_{e0} e^{\frac{e\phi(r)}{k_B T_e}}, \tag{2.65}$$

con $n_e(r)$ la densidad de electrones a una distancia r del eje de simetría, k_B la constante de Boltzmann y $\phi(r)$ el potencial referido al potencial del plasma, a una distancia r del eje de simetría. En el entorno alrededor de la sonda se forma una vaina donde se rompe la cuasi-neutralidad y permite conectar el plasma y la superficie de la sonda, que se encuentra a un potencial ϕ_p negativo con respecto al plasma. La vaina debe ser modelada utilizando la ecuación de Poisson [9,31], que en coordenadas cilíndricas con la simetría descrita, siendo $n_+(r)$ y $n_e(r)$ la densidad de iones y de electrones a una distancia r del eje de simetría y siendo ε_0 la permitividad eléctrica del vacío y e la carga elemental, es:

$$\frac{1}{r}\frac{\mathrm{d}}{\mathrm{d}r}\left(r\frac{\mathrm{d}\phi(r)}{\mathrm{d}r}\right) = -\frac{e}{\varepsilon_0}\big(n_+(r) - n_e(r)\big). \tag{2.66}$$

Los iones positivos se mueven en un potencial acelerador hacia la sonda y los que llegan a su superficie se recombinan. Por tanto, la distribución de iones positivos está muy afectada por la presencia de la sonda, de modo que no pueden alcanzar el equilibrio térmico y su distribución no puede modelarse utilizando (2.5). Asumiendo que los iones positivos se pueden modelar como un fluido, es posible obtener el perfil de potencial. Para ello, escribimos la ecuación de balance de energía en ausencia de colisiones para los iones positivos, de masa m_+, que establece la velocidad radial del fluido $v_+(r)$ a la que los iones se aceleran desde el plasma, donde su velocidad media es nula, al alcanzar una región de la vaina que se encuentra a un potencial $\phi(r)$.

$$\frac{1}{2}m_+\big(v_+(r)\big)^2 + e\phi(r) = 0. \tag{2.67}$$

Recuérdese que el potencial es negativo para recoger los iones positivos. En ausencia de ionización, la ecuación de conservación de la masa para los iones establece que el flujo de iones debe ser constante. Aplicando esta condición a una sección del conductor cilíndrico de

longitud L, se puede establecer que el número de iones positivos que atraviesan cualquier superficie cilíndrica de radio r, centrada con el eje de la sonda, por unidad de tiempo es independiente de r:

$$j_+ = 2\pi r L n_+(r) v_+(r) = cte. \tag{2.68}$$

Despejando $v_+(r)$ en (2.67) e insertándolo en (2.68),

$$n_+(r) = \frac{j_+}{2\pi r L\left(\sqrt{\frac{-2e\phi(r)}{m_+}}\right)}. \tag{2.69}$$

Este término, junto con (2.65), se puede introducir en la ecuación de Poisson (2.66) obteniendo una ecuación diferencial para el potencial $\phi(r)$ que solo depende de la distancia al eje r,

$$\frac{1}{r}\frac{\mathrm{d}}{\mathrm{d}r}\left(r\frac{\mathrm{d}\phi(r)}{\mathrm{d}r}\right) = -\frac{e}{\varepsilon_0}\left(\frac{j_+}{2\pi r L}\sqrt{\frac{m_+}{-2e\phi(r)}} - n_{e0}e^{\frac{e\phi(r)}{k_B T_e}}\right). \tag{2.70}$$

Para ver la estructura matemática de la ecuación y los grados de libertad, es conveniente utilizar variables adimensionales.

$$y = -\frac{e\phi(r)}{k_B T_e}, \qquad \lambda_D = \sqrt{\frac{\varepsilon_0 k_B T_e}{e^2 n_{e0}}},$$

$$x = \frac{r}{\lambda_D}, \qquad I_+ = \frac{i_+ r_p e}{2\pi\varepsilon_0}\sqrt{\frac{m_+}{2{k_B}^3{T_e}^3}}, \tag{2.71}$$

$$i_+ = \frac{e j_+}{L}, \qquad I_p = \frac{I_+}{r_p}\lambda_D = \frac{I_+}{x_p}.$$

En esta expresión, y es el potencial adimensional, x es la distancia adimensional con respecto al eje de simetría, λ_D es la longitud de Debye, i_+ es la corriente eléctrica por unidad de longitud recogida por la sonda, I_+ es la corriente eléctrica por unidad de longitud adimensional e I_p es el cociente entre la corriente eléctrica por unidad de longitud adimensional y el radio de la sonda adimensional x_p. Con esto, se obtiene la siguiente ecuación adimensional:

$$\frac{1}{x}\frac{\mathrm{d}}{\mathrm{d}x}\left(x\frac{\mathrm{d}y}{\mathrm{d}x}\right) = \frac{I_p}{x\sqrt{y}} - e^{-y}. \qquad 2.72$$

Como se puede observar, la solución solo depende de una variable, el cociente I_p. Para integrar esta expresión no es posible simplemente empezar en $y = 0$ para x suficientemente grande, ya que y aparece en un denominador. Para encontrar una condición de contorno en la que sea posible empezar la integración numérica, consideramos la pre-vaina en la que asumimos que aún se conserva la condición de cuasi-neutralidad (2.64) pero el potencial deja de ser nulo y, por lo tanto, permite que los iones se aceleren. Por lo tanto, utilizando (2.65) y (2.69):

$$n_+(r) = n_e(r),$$

$$\frac{j_+}{2\pi r L\left(\sqrt{\frac{-2e\phi(r)}{m_+}}\right)} = n_{e0}e^{\frac{e\phi(r)}{k_B T_e}}, \qquad 2.73$$

en su versión adimensional,

$$\frac{I_p}{x\sqrt{y}} = e^{-y}. \qquad 2.74$$

Por lo tanto, solo queda elegir un valor de $x = x_0$ suficientemente grande, y resolver la ecuación para obtener el correspondiente valor de $y = y_0$ de forma numérica para obtener una condición inicial (x_0, y_0) a partir de la que empezar a integrar la ecuación diferencial (2.72). Este método de utilizar la condición de cuasi-neutralidad para obtener la condición inicial ofrece soluciones que son muy independientes del valor de x_0 elegido, siempre que sea lo

suficientemente grande como para asegurar que partimos de la zona cuasi-neutra. Con esta solución se puede obtener el perfil de potencial que depende del cociente adimensional I_p, tal y como se muestra en la Figura 3. A partir de (2.68) y (2.69) es posible calcular también la densidad de iones positivos adimensional $N(x) = n_+(\lambda_D x)/n_{e0}$ y la velocidad adimensional de los iones $V(x) = v(\lambda_D x)\sqrt{m_+/2k_B T_e}$. El campo eléctrico adimensional también se puede obtener como el gradiente del potencial $z(x) = \mathrm{d}y(x)/\mathrm{d}x$. Un ejemplo completo se muestra en la Figura 4.

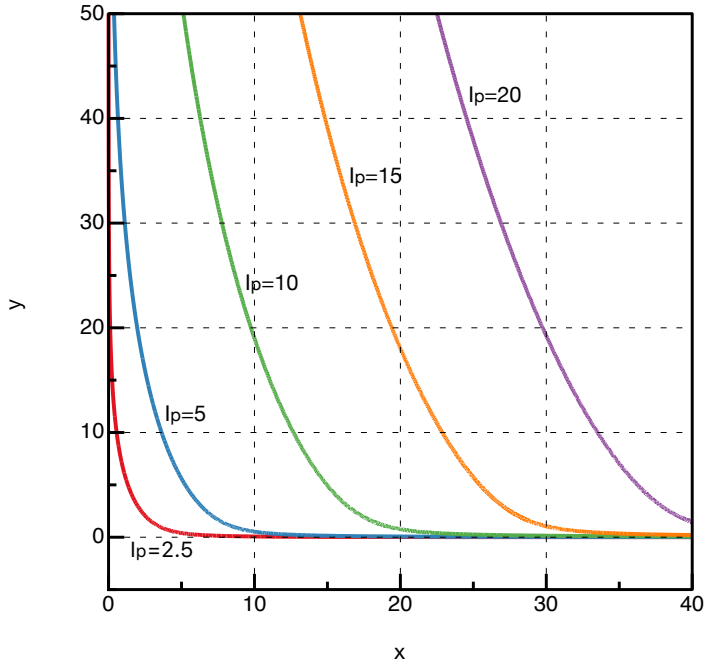

Figura 3: Perfiles de potencial según el modelo radial ABR.

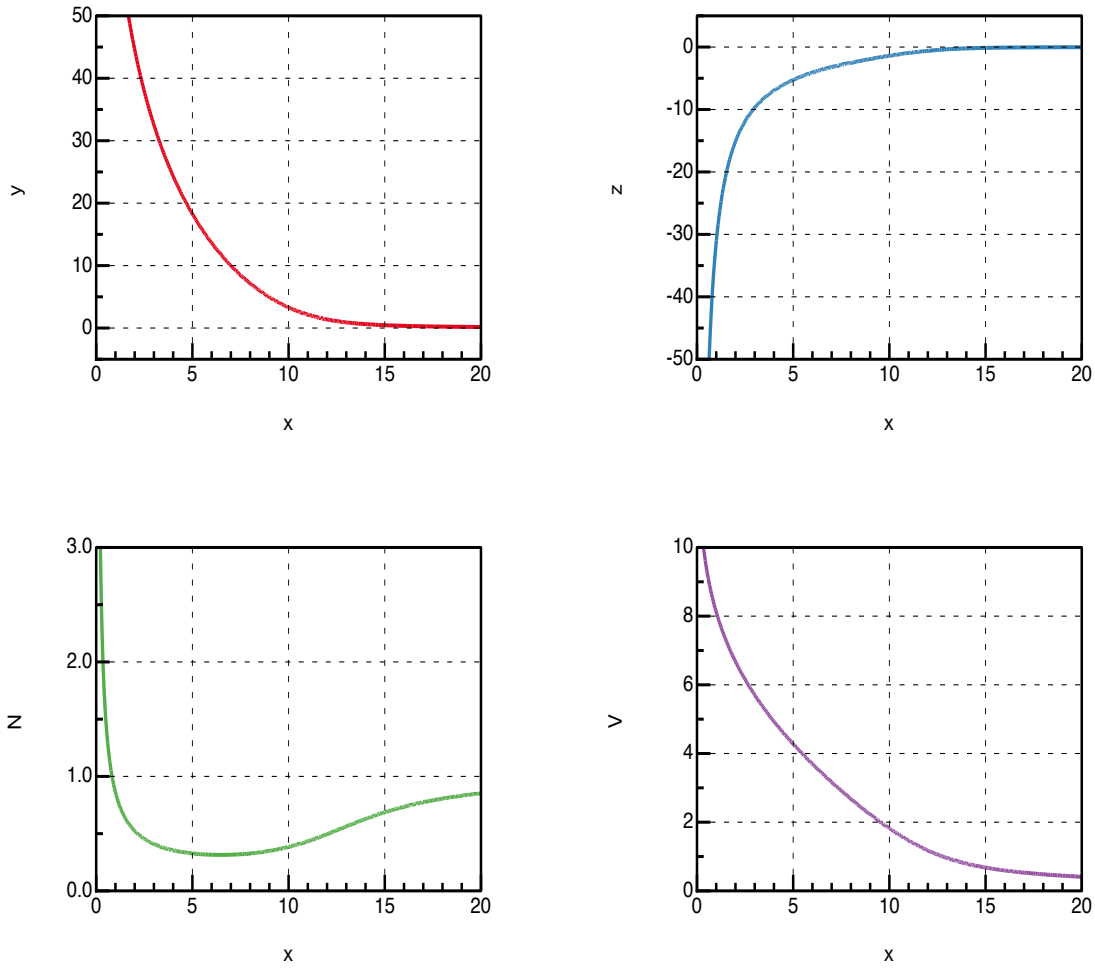

Figura 4: Ejemplo completo según el modelo radial ABR, para $I_p = 7$.

A partir de estos datos es interesante obtener, para cada radio de la sonda, la curva característica I-V del modelo ABR, que se puede comparar con las curvas características I-V experimentales, y que se muestra en la Figura 5 para distintos valores de x_p. Finalmente, de gran interés en el laboratorio de plasma, es conocer el potencial flotante, es decir, el potencial para el que la corriente iónica se iguala a la electrónica. La segunda se puede obtener con la fórmula de efusión aplicada sobre la superficie de la sonda. Por lo tanto, la corriente electrónica por unidad de longitud es:

$$i_e = e2\pi r_p \frac{1}{4} n_e(r_p)\langle v_e\rangle = e2\pi r_p n_{e0} e^{\frac{e\phi_p}{k_B T_e}} \sqrt{\frac{k_B T_e}{2\pi m_e}}. \qquad 2.75$$

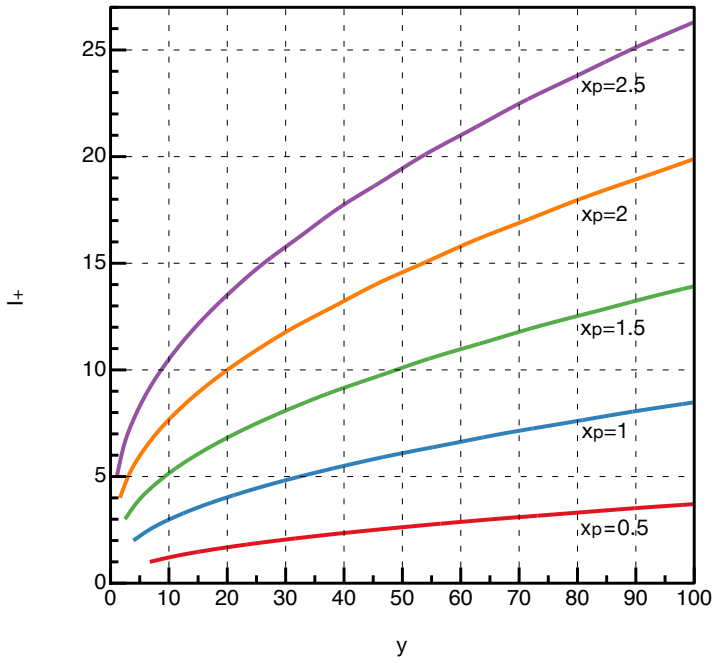

Figura 5: Curvas características I-V según el modelo radial ABR.

Igualando la corriente iónica con la electrónica, se puede realizar una búsqueda para encontrar el valor del potencial de la sonda ϕ_p que satisface la igualdad para cada radio de sonda r_p. Los resultados de los cálculos dependen del gas utilizado y un ejemplo de cálculo del potencial flotante adimensional y_f, para el gas argón se muestra en la Figura 6.

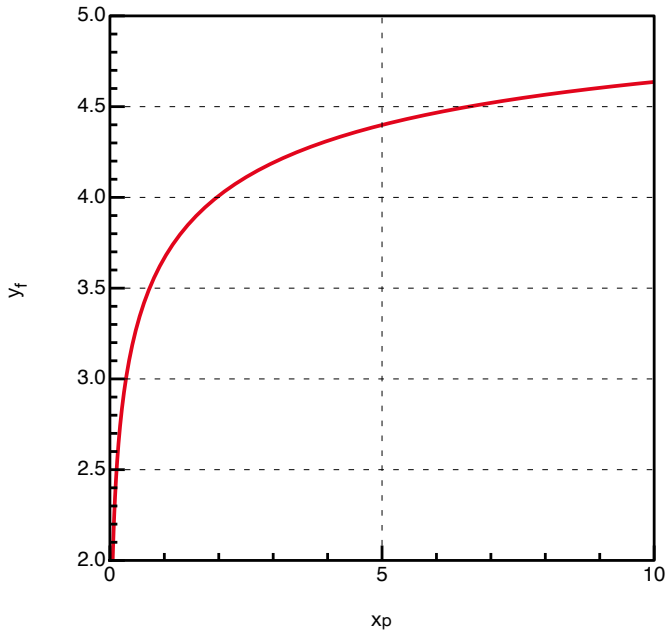

Figura 6: Potencial flotante en función del radio adimensional de la sonda para un plasma electropositivo de argón según el modelo radial ABR.

2.5.3 Modelo orbital OML (Orbital Motion Limited)

Considérese una sonda electrostática de Langmuir cilíndrica infinitamente larga de radio r_p inmersa en un plasma electropositivo, con una población de electrones con temperatura T_e y una única población de iones con carga e. Supóngase que la sonda está polarizada negativamente de forma que atrae a los iones y que estos tienen una función de distribución de equilibrio termodinámico con temperatura T_+ en el plasma, a una distancia $r \to \infty$. Se define el borde de la vaina de forma que el recorrido libre medio de los iones λ_i sea lo suficientemente largo como para que los iones puedan recorrer la vaina prácticamente sin colisiones, $\lambda_i \gtrsim r_s - r_p$ (el símbolo $\gtrsim$ quiere decir mayor pero no similar), donde r_s es la distancia desde el borde de la vaina hasta el eje de simetría. Los iones se desplazan con una velocidad $\boldsymbol{v}(r) = \big(u(r), v(r), w(r)\big)$ determinada a una distancia r, en el espacio tangente al sistema de referencia cilíndrico $\boldsymbol{x} = (r, \theta, z)$. Por lo tanto el problema se reduce a resolver la ecuación de Boltzmann para la función de distribución de velocidad $f(r, \boldsymbol{v})$ de las partículas de masa m y carga e en ausencia de ionización y colisiones [3,12,13],

$$\boldsymbol{v} \cdot \frac{\partial f(r, \boldsymbol{v})}{\partial \boldsymbol{x}} - \frac{e}{m} \frac{\partial \phi(r)}{\partial \boldsymbol{x}} \cdot \frac{\partial f(r, \boldsymbol{v})}{\partial \boldsymbol{v}} = 0, \tag{2.76}$$

y la ecuación de Poisson para el potencial $\phi(r)$ con respecto al potencial en el seno del plasma a una distancia r del eje de simetría,

$$\nabla^2 \phi(r) = -\frac{e}{\varepsilon_0}\big(n_+(r) - n_e(r)\big), \tag{2.77}$$

donde la relación entre ambas ecuaciones (2.76) y (2.77) se establece gracias a la definición de densidad de iones en función de la función de distribución.

$$n_+(r) = \int_{\mathbb{R}^3} f(r, \boldsymbol{v}) \mathrm{d}^3 \boldsymbol{v}. \tag{2.78}$$

Como se muestra en las expresiones, por el argumento de simetría cilíndrica, las variables solo pueden depender de la distancia radial r con respecto al eje de simetría, por lo

que las derivadas parciales con respecto a las coordenadas θ y z se anulan y las expresiones del gradiente y del laplaciano se simplifican.

$$\frac{\partial}{\partial \boldsymbol{x}} = \left(\frac{\partial}{\partial r}, 0,0\right),$$
$$\nabla^2 = \left(\frac{1}{r}\frac{\partial}{\partial r}\left(r\frac{\partial}{\partial r}\right), 0,0\right). \qquad 2.79$$

Consideremos el caso en el que la sonda se polariza negativamente con respecto al plasma y, por lo tanto, los electrones se encuentran en un pozo de potencial y, dado que su movilidad es mucho mayor que la de los iones, pueden ser modelados mediante un factor de Boltzmann:

$$n_e(r) = n_{e0} e^{\frac{e\phi(r)}{k_B T_e}}, \qquad 2.80$$

donde n_{e0} es la densidad de electrones en el seno del plasma, que por cuasi-neutralidad debe ser igual a la densidad de iones n_{+0} en el seno del plasma. En el interior de la vaina, las trayectorias de las partículas solo pueden depender de las constantes del movimiento, ya que en ausencia de colisiones desde el radio de la vaina r_s hasta la superficie de la sonda r_p, se deben cumplir las leyes de conservación. Las constantes del movimiento son la energía perpendicular al eje, la energía a lo largo del eje y el momento angular.

$$E_\perp = \frac{1}{2} m_+ (u^2 + v^2) + e\phi(r),$$
$$E_\parallel = \frac{1}{2} m_+ w^2, \qquad 2.81$$
$$J = m_+ r v.$$

Obsérvese que el movimiento en la dirección z está completamente desacoplado del movimiento en las otras dos direcciones. Por lo tanto, la función de distribución cumple:

$$f(r, \boldsymbol{v}) = f_1(E_\perp, J) f_2(E_\parallel). \qquad 2.82$$

La función de distribución $f_1(E_\perp, J)$ se puede dividir en dos, una para las partículas que se aproximan a la sonda, $f_{1,-}(E_\perp, J)$ y otra para las partículas que se alejan de la sonda, $f_{1,+}(E_\perp, J)$. Si a medida que la trayectoria se acerca a la sonda desde el infinito, para un determinado valor de $(E_\perp, J)$ la trayectoria tiene un punto de retorno antes de alcanzar la sonda, la función de distribución de alejamiento respecto a la superficie de la sonda es la misma que la de acercamiento a la sonda, $f_{1,+}(E_\perp, J) = f_{1,-}(E_\perp, J) = \frac{1}{2} f_1(E_\perp, J)$, mientras que si el punto de retorno está más cerca del eje que la superficie de la sonda, la relación depende de las propiedades de la superficie. Para una superficie perfectamente absorbente, $f_{1,+}(E_\perp, J) = 0$ y $f_{1,-}(E_\perp, J) = f_1(E_\perp, J)$. En la región $r > \lambda_i$ en la que las colisiones no se pueden ignorar, el término de colisiones en la ecuación de Boltzmann debe ser tenido en cuenta y las trayectorias ya no son función de las constantes del movimiento. Sin embargo, si λ_i es lo suficientemente grande como para que la proporción de partículas que alcanza la sonda no sea muy grande, la función de distribución $f_{1,-}(E_\perp, J)$ puede ser considerada de Maxwell-Boltzmann.

También es posible un tercer tipo de órbita, la órbita cerrada. Se puede comprobar más cómodamente utilizando el potencial efectivo.

$$U(r, J) = e\phi(r) + \frac{J^2}{2m_+ r^2}. \qquad 2.83$$

Suponiendo que el potencial $\phi(r)$ es siempre negativo y decreciente hacia la sonda, si el potencial diverge a $-\infty$ para $r \to 0$ más lentamente que el ritmo al que el término centrífugo diverge a $+\infty$, para valores de J^2 suficientemente bajos, puede existir un mínimo en torno al que pueden existir orbitas cerradas. Los iones que provienen desde el infinito no pueden alcanzar esa orbita cerrada, pero dado que ocasionalmente habrá una colisión que modifique la velocidad de los iones, todas las orbitas posibles necesariamente se llenan con iones en equilibrio térmico a temperatura T_+.

Las expresiones (2.81) se pueden invertir.

$$u = \pm\sqrt{\frac{2\left(E_\perp - e\phi(r)\right)}{m_+} - \frac{J^2}{{m_+}^2 r^2}},$$

$$v = \frac{J}{m_+ r}, \qquad 2.84$$

$$\mathrm{w} = \pm\sqrt{\frac{2E_\parallel}{m_+}}.$$

Por lo tanto, para resolver el problema numéricamente solo queda escribir la integral, tanto el integrando como los límites de integración, (2.78) en función de las variables $(E_\perp, J)$. Sin embargo, el problema numérico es complejo, por lo que vamos a resolverlo bajo algunas suposiciones adicionales que nos permiten obtener un caso límite de aplicación práctica, el límite OML (Orbital Motion Limited).

- La densidad de iones es conocida en el borde de la vaina.
- La función de distribución de iones en el borde de la vaina es de Maxwell-Boltzmann, con una temperatura bien definida.
- El potencial en el borde de la vaina es prácticamente igual al potencial del plasma donde se coloca la referencia.
- En el interior de la vaina no hay colisiones.
- La sonda es lo suficientemente grande como para que no haya trayectorias cerradas en la vaina.
- La sonda se encuentra a un potencial $\phi(r_p) = \phi_p$ negativo con respecto al potencial en el seno del plasma.
- La superficie de la sonda es perfectamente absorbente.
- La vaina es mucho más grande de la sonda.

Las ecuaciones de conservación permiten relacionar las velocidades en el borde de la vaina y en la superficie de la sonda.

$$\frac{1}{2}m_+\left(u(r_p)^2+v(r_p)^2\right)+e\phi_p=\frac{1}{2}m_+(u(r_s)^2+v(r_s)^2),$$

$$\frac{1}{2}m_+w(r_p)^2=\frac{1}{2}m_+w(r_s)^2, \qquad 2.85$$

$$m_+r_pv(r_p)=m_+r_sv(r_s).$$

Estas expresiones se pueden escribir de la siguiente forma:

$$v(r_p)=\frac{r_s}{r_p}v(r_s),$$

$$w(r_p)=w(r_s), \qquad 2.86$$

$$u(r_p)=u(r_s)-v(r_s)\left(\left(\frac{r_s}{r_p}\right)^2-1\right)-\frac{2e\phi_p}{m_+}.$$

Solo contribuyen a la corriente los iones que alcanzan la superficie. Los iones deben entrar en la vaina, $u(r_s)>0$, y su velocidad radial $v(r_s)$ debe ser menor que el límite para el que $u(r_p)>0$. No hay condición limitante para $w(r_s)$.

$$|v(r_s)|<\sqrt{\frac{{r_p}^2}{{r_s}^2+{r_p}^2}\left(u(r_s)^2-\frac{2e\phi_p}{m_+}\right)}=v_{lim}(u(r_s)). \qquad 2.87$$

La corriente iónica por unidad de longitud total para el potencial de la sonda determinado ϕ_p es:

$$i_+=e2\pi r_s\int_{-\infty}^{+\infty}\int_{0}^{+\infty}\int_{-v_{lim}(u(r_s))}^{+v_{lim}(u(r_s))}u(r_s)f(u(r_s),v(r_s),w(r_s))\mathrm{d}v(r_s)\mathrm{d}u(r_s)\mathrm{d}w(r_s). \qquad 2.88$$

Utilizando la premisa de que la función de distribución es de Maxwell-Boltzmann en el borde de la vaina para los iones:

$$f\big(u(r_s), v(r_s), w(r_s)\big) = n_{+0}\left(\frac{m_+}{2\pi k_B T_+}\right)^{\frac{3}{2}} e^{-\frac{m_+}{2k_B T_+}\left(u(r_s)^2+v(r_s)^2+w(r_s)^2\right)}, \tag{2.89}$$

y realizando la integración, para la corriente iónica por unidad de longitud se obtiene:

$$i_+ = e2r_p n_{+0}\sqrt{\frac{\pi k_B T_+}{2m_+}}\left[e^{-\frac{e\phi_p}{k_B T_+}}\,\mathrm{erfc}\left(\sqrt{-\frac{{r_s}^2}{{r_s}^2+{r_p}^2}\frac{2e\phi_p}{m_+}}\right)+\right.$$
$$\left.+\frac{r_s}{r_p}\left(\mathrm{erf}\left(\sqrt{-\frac{{r_p}^2}{{r_s}^2+{r_p}^2}\frac{2e\phi_p}{m_+}}\right)\right)\right], \tag{2.90}$$

con las expresiones $\mathrm{erf}(x) = \frac{2}{\sqrt{\pi}}\int_0^x e^{t^2}\mathrm{d}t$ y $\mathrm{erfc}(x) = 1 - \mathrm{erf}(x)$, que definen la función error $\mathrm{erf}(x)$ y la función complementaria del error $\mathrm{erfc}(x)$. Usando que $\mathrm{erf}(x) \sim \frac{2}{\sqrt{\pi}}x$ para $x \ll 1$, en el límite en el que $r_s \gg r_p$ se obtiene la corriente por unidad de longitud en el límite OML:

$$i_+ = e2r_p n_{+0}\sqrt{\frac{\pi k_B T_+}{2m_+}}\left[e^{-\frac{e\phi_p}{k_B T_+}}\,\mathrm{erfc}\left(\sqrt{-\frac{2e\phi_p}{m_+}}\right)+\frac{2}{\sqrt{\pi}}\sqrt{-\frac{e\phi_p}{k_B T_+}}\right]. \tag{2.91}$$

Si además la sonda se polariza de forma suficientemente negativa, la función $\mathrm{erfc}(x)$ se aproxima también a su valor límite $\mathrm{erfc}(x) \sim e^{-x^2}\frac{1}{\sqrt{\pi}x}$ para $x \to \infty$ [78]. Esto confirma que el segundo término es el dominante y, por lo tanto:

$$i_+ = e4r_p n_{+0}\sqrt{-\frac{e\phi_p}{2m_+}}. \tag{2.92}$$

Obsérvese que el límite contrario, el límite $r_s \approx r_p$, incumple la premisa de que los iones capturados sean un porcentaje poco importante para que la función de distribución en el borde

de la vaina se pueda considerar como una distribución de Maxwell-Boltzmann. En el límite OML no se puede obtener el perfil de potencial en la vaina, pero sí se puede obtener la curva característica I-V. Utilizando las mismas unidades adimensionales que en la solución ABR (2.71):

$$\mathrm{I}_{+} = \frac{{x_p}^2}{\pi}\sqrt{y}, \qquad 2.93$$

Es posible representar las curvas características I-V, como se muestra en la Figura 7, en las mismas condiciones que las obtenidas según el modelo ABR para una mejor comparación.

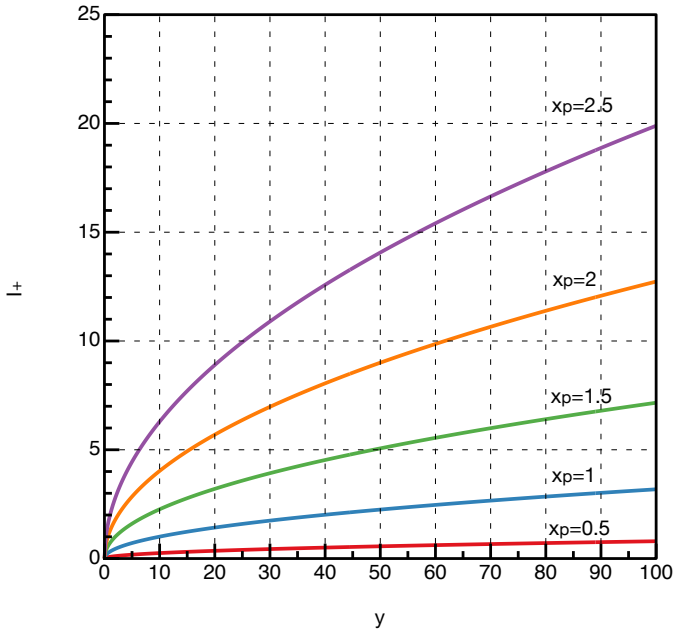

Figura 7: Curvas características I-V según el modelo orbital OML.

Como se puede observar en la Figura 7 al compararla con la Figura 5, la corriente obtenida es siempre inferior a la corriente según el modelo ABR en las mismas condiciones. En este modelo simplificado, el tratamiento de los iones positivos y de los electrones es el mismo, es decir, ambos tipos de partículas se encuentran en equilibrio termodinámico en el borde de la vaina y alcanzan la sonda según las leyes de conservación. Por lo tanto, y dado que tanto la corriente iónica y como la corriente electrónica por unidad de longitud son proporcionales al radio de la sonda, como en (2.75) y (2.92), según el modelo orbital OML el potencial flotante solo depende del gas. Para argón, el potencial flotante adimensional es $y_f = 4.7036$.

2.5.4 Sonin Plot

El Sonin Plot es un diagrama de aplicación práctica en el laboratorio de plasma, en el que representa la siguiente corriente adimensional:

$$I'(y_p) = \frac{i}{er_p n_{e0}} \sqrt{\frac{m_+}{2\pi k_B T_e}}, \tag{2.94}$$

frente a la corriente adimensional,

$$I'(y_p){x_p}^2 = \frac{ier_p}{\varepsilon_0} \sqrt{\frac{m_+}{2\pi {k_B}^3 {T_e}^3}}, \tag{2.95}$$

donde i es la corriente recogida por la sonda por unidad de longitud, e es la carga elemental, r_p y $x_p = \frac{r_p}{\lambda_D}$ son el radio de la sonda y el radio adimensional de la sonda normalizado con respecto a la longitud de Debye λ_D, n_{e0} es la densidad electrónica en el seno del plasma, m_+ es la masa del ion, T_e es la temperatura electrónica, k_B es la constante de Boltzmann y ε_0 es la permitividad del vacío. El valor de potencial de la sonda adimensional $y_p = -\frac{e\phi_p}{k_B T_e}$ es elegido *a priori* y utilizado en la obtención de las curvas del Sonin Plot teóricas. Este diagrama se puede utilizar para diagnosticar el plasma, ya que la abscisa, el término $x_s = I'(y_p){x_p}^2$, no depende de la densidad del plasma y se puede medir experimentalmente. Si se obtiene la ordenada del Sonin Plot teórico, $y_s = I'(y_p)$, para dicha abscisa x_s, se puede despejar la densidad del plasma, n_{e0} [14–16,48]. Debido a que existen distintas teorías para explicar el movimiento de los iones en su caída hacia una sonda electrostática de Langmuir cilíndrica polarizada negativamente con respecto al plasma, debería ser conocido previamente, antes de diagnosticar, qué teoría explica correctamente la caída de los iones hacia la sonda para las condiciones del plasma del experimento. Alternativamente, se puede utilizar la densidad del plasma medida por otro método y utilizar el punto (x_s, y_s) experimental para conocer qué teoría es válida para cada conjunto de condiciones [14–16,48].

En la Figura 8 se muestran los puntos teóricos del Sonin Plot según la teoría radial ABR y según la teoría orbital OML. Como se puede observar en la figura, los puntos obtenidos según la teoría radial ABR corresponden con corrientes mayores que los puntos obtenidos según la teoría orbital OML. También se puede observar cómo para sondas pequeñas, que corresponden con la zona izquierda del Sonin Plot, la corriente obtenida según la teoría OML disminuye mucho más con respecto a la corriente obtenida según la teoría ABR, que recoge todos los iones independientemente del tamaño de la sonda.

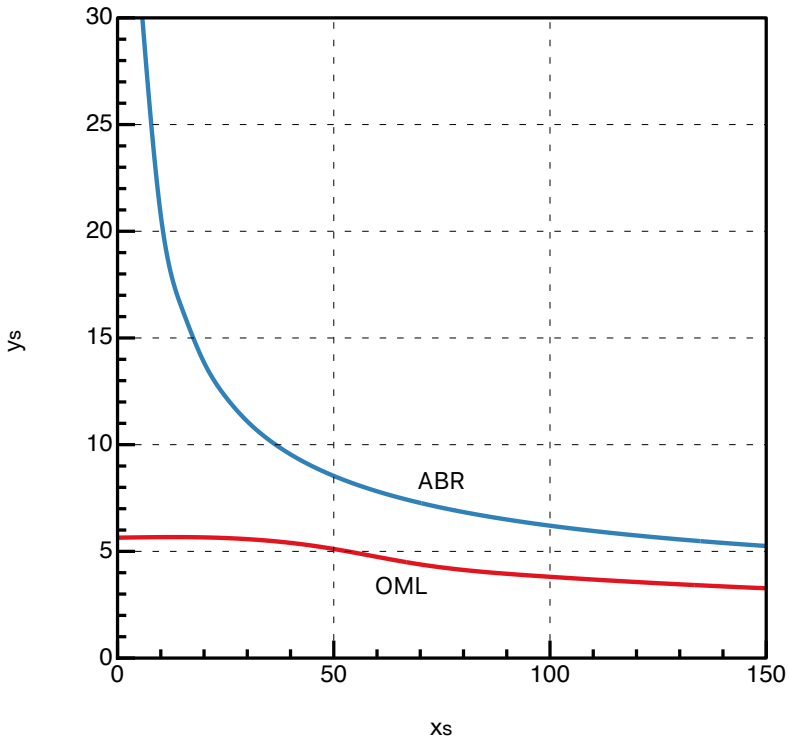

Figura 8: Sonin Plot teórico según las teorías ABR y OML.

2.6 Trabajo experimental y trabajo teórico

En física, todo esfuerzo teórico está supeditado a las medidas experimentales que finalmente confirman o rechazan los argumentos teóricos. En física de plasma, el trabajo experimental es complejo, debido a que por la naturaleza eléctrica de las partículas libres que conforman el plasma, éstas se adaptan a cualquier perturbación que se les aplique. Por lo tanto, los instrumentos de medida pueden perturbar el plasma de forma considerable. Por otra parte, el plasma es un entorno inherentemente ruidoso, por lo que la realización de medidas significativas es difícil. La necesidad de herramientas que perturban el plasma y de enfrentarse al ruido de las medidas es lo que hace que las medidas experimentales en física de plasma entrañen gran dificultad. Además, algunas aplicaciones tecnológicas requieren plasmas muy tenues y fríos, como es el caso de esterilización de herramientas quirúrgicas, algunas de las cuales pueden ser de plásticos flexibles que podrían dañarse con la aplicación de plasmas demasiado calientes [79,80]. En este sentido, la utilización de instrumentos invasivos en plasmas, como es el caso de la sonda electrostática de Langmuir, debe realizarse con cuidado. La sonda electrostática de Langmuir es la herramienta más utilizada, debido a que es muy conocida y fácil de fabricar. La sonda se puede polarizar positiva o negativamente con respecto al plasma:

- *Polarizada positivamente con respecto al plasma*: La sonda recoge casi exclusivamente electrones. Incluso los iones negativos, al tener muy baja movilidad, se recogen de forma minoritaria en la mayoría de los plasmas [81,82], con excepciones notables como los plasmas de oxígeno [7,83,84]. Sin embargo, la corriente recogida en la zona electrónica de la curva característica I-V tiene unos valores considerables, muchas veces tan solo un orden de magnitud por debajo de la corriente de descarga, por lo que la perturbación producida en el plasma puede ser importante. Por otra parte, la mayor corriente recogida tiene como consecuencia que la relación de señal-ruido es mejor. Además, los electrones siempre caen a la sonda según la teoría orbital OML, por lo que la relación lineal I^2-V permite obtener información fiable de los parámetros del plasma. Sin embargo, el hecho de que se pueda ignorar la influencia de los iones tiene como consecuencia que no se obtiene información de las especies de iones del plasma.
- *Polarizada negativamente con respecto al plasma*: La sonda recoge principalmente iones positivos, y una cierta cantidad de electrones cuando la sonda no está polarizada muy negativamente. La ventaja principal de la zona iónica de la característica I-V es que la corriente recogida es entre 10 y 100 veces menor que cuando la sonda está polarizada positivamente con respecto al potencial del plasma, por lo que la perturbación sobre el

plasma es mucho menor. Sin embargo, por este motivo, la relación de señal-ruido es mucho peor y son necesarias técnicas avanzadas de suavización de los datos para analizar los resultados de las medidas en esta zona [7,47]. Además, el comportamiento de los iones se puede describir según la teoría radial ABR o según la teoría orbital OML [16,85] dependiendo de la presión o de la potencia de la descarga, lo que dificulta la aplicación de las teorías de recolección de iones positivos en sondas electrostáticas de Langmuir en la diagnosis de plasmas en el laboratorio.

Una descarga de plasma no es perfectamente homogénea y la sonda electrostática de Langmuir es una herramienta que permite medir la variación espacial y temporal de las características de la descarga [6,86]. La sonda electrostática de Langmuir se suele utilizar para medir los parámetros del plasma como, por ejemplo:

- *Potencial del plasma*: Es el potencial al que se encuentra el plasma circundante. En el contexto de la descarga, el potencial del plasma puede cambiar de una región de la descarga a otra. Pese a que esté definido de forma inequívoca, la medición del potencial del plasma puede llegar a ser un problema complicado. El consenso actual es que se localiza en el punto de inflexión de la curva característica I-V.
- *Potencial de corte*: El potencial de corte es el potencial al que se debe imponer un objeto metálico para que la corriente neta sea nula. Debido a que un objeto metálico aislado inmerso en un plasma adquiere espontáneamente este potencial, es interesante conocer si el potencial de corte permite tratar la superficie del objeto de forma satisfactoria. El potencial flotante, es decir, la diferencia entre el potencial de corte y el potencial del plasma es muy fácil de medir, pero es difícil de calcular teóricamente.
- *Densidad del plasma*: Es la densidad de carga positiva y negativa en el seno del plasma que, por la condición de cuasi-neutralidad, deben ser iguales.
- *Temperatura de los electrones*: Pese a que un plasma frío no es un sistema en equilibrio, los electrones tienen normalmente una función de distribución de velocidades de Maxwell-Boltzmann similar a una distribución de equilibrio con una temperatura bien definida. Como se estableció en la sección 2.2.3, este hecho se le conoce como paradoja de Langmuir [51].
- *Función de distribución de energía de los electrones*: Mediante la fórmula de Druyvesteyn, es posible medir la función de distribución de energía electrónica o EEDF. De esta manera, se puede comprobar experimentalmente la conocida como paradoja de Langmuir [51]. Sin

embargo, en muchas situaciones, la función de distribución medida no coincide con una única temperatura bien definida. En algunos casos, aparecen dos poblaciones de electrones de distintas temperaturas, particularmente en plasmas poco densos en los que los electrones energéticos plasmógenos no llegan a perder toda su energía en colisiones ionizantes con los neutros. Estos electrones energéticos constituyen la población de temperatura caliente y los electrones menos energéticos que son arrancados de los neutros durante el proceso de ionización constituyen la población de temperatura fría. En otros casos, aparecen poblaciones de electrones en las que se observa un corte en la EEDF de electrones de alta energía, en situaciones en las que dichos electrones superen la energía de activación de algún proceso de excitación atómica [4,34,49,50].

Esta posibilidad de obtener tanta información a partir de la medida de la curva característica I-V de una sonda electrostática de Langmuir explica por qué es una herramienta tan utilizada desde su invención hace más de 80 años. Algunos de estos parámetros pueden ser obtenidos mediante otros medios, pero otros no y, además, la sonda electrostática de Langmuir permite obtener los parámetros de forma local, para así poder caracterizar la descarga.

2.6.1 Descarga del grupo de investigación TEP-230 Contacto plasma-superficie

Las medidas experimentales producidas como parte del trabajo de esta tesis se han realizado en un dispositivo experimental que consiste en una gran campana de vacío constituida por un gran cilindro de vidrio Pirex colocado verticalmente, de 40 cm de altura y 31 cm de diámetro interior en la que se hace el vacío y se permite la entrada de gas de forma controlada utilizando un controlador de flujo másico de gas MKS 247 [14–16]. Las tapas metálicas tienen pasamuros para realizar las conexiones eléctricas con los dos electrodos circulares de 8 cm de diámetro, separados una distancia de 15 cm y que constituyen el ánodo y el cátodo de la descarga, y con la sonda electrostática de Langmuir cilíndrica de tungsteno de 6 mm de longitud y 0.1 mm de radio, colocada entre ambos electrodos en la región en la que el plasma formado es más homogéneo, a unos 6 cm del ánodo.

La descarga es generada utilizando una fuente de alimentación de bajo ruido KEPCO BHK 2000-0.1MG que puede alcanzar hasta 2000 V, y que se configura como fuente de corriente constante para asegurar que la corriente de descarga, que es la que determina principalmente la densidad del plasma de la descarga, es constante. La sonda electrostática de Langmuir cilíndrica se polariza utilizando un generador de señales configurado para generar una

rampa, y la tensión y la corriente recogida por la sonda se calculan midiendo dos canales de forma simultanea, tal y como se muestra en la Figura 9, de un convertidor analógico-digital PCI6122 de National Instruments controlado mediante un instrumento virtual o VI (*virtual instrument*) desarrollado en el entorno LabView [15,27]. Se toman 2000 medidas de 16 bits de resolución en 4 ms, de forma que se garantiza que la sonda no cambia de temperatura durante la medida debido al efecto resistivo del tungsteno de la sonda, lo que podría modificar la función trabajo del material.

El instrumento virtual de LabView obtiene parámetros fundamentales del plasma realizando cálculos sobre la curva característica I-V de la sonda electrostática de Langmuir, como son la obtención de la función de distribución de energía electrónica o EEDF, el potencial flotante, el potencial del plasma, la densidad del plasma o la temperatura de los electrones utilizando varios métodos, en distintas zonas de la curva característica I-V, tanto la zona de saturación iónica, como la zona de saturación electrónica o la zona de retardo electrónico. También permite guardar en un fichero las medidas de los dos canales del convertidor analógico-digital para poder analizarlos con el mismo VI u otro software de análisis numérico, si es necesario.

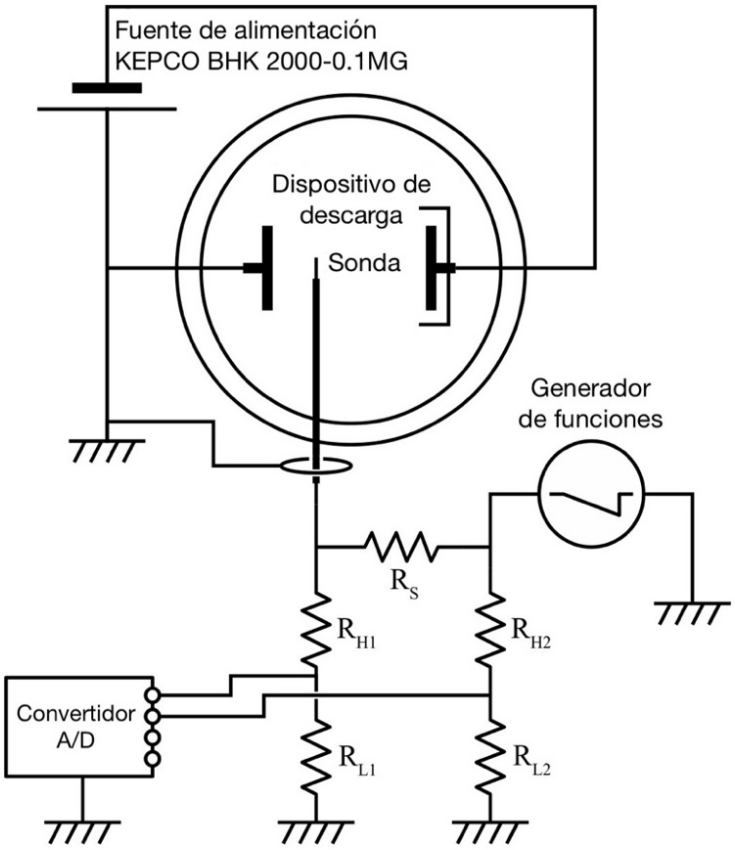

Figura 9: Esquema del dispositivo de descarga del grupo TEP-230

2.6.2 Simulaciones

Las medidas experimentales en el laboratorio son, en última instancia, el elemento que permite confirmar o invalidar una teoría. Sin embargo, y particularmente cierto en el caso de la medida de la curva característica I-V de una sonda electrostática de Langmuir, no ofrecen información detallada y es necesario manipular la señal medida de forma elaborada, tanto por la relación señal ruido como por la limitada validez de las teorías de sondas electrostáticas de Langmuir. Por ello, es muy interesante desarrollar simulaciones en ordenador para poder obtener información pormenorizada de todos los tipos de partículas presentes en el plasma. Sin embargo, para obtener información estadísticamente válida, es necesario simular muchas partículas que interaccionan entre sí. En este sentido, las simulaciones PIC (Particle-In-Cell) ofrecen una alternativa viable para obtener buenos resultados [87].

En una simulación PIC, las partículas son desplazadas mediante un algoritmo de paso temporal y la fuerza que acelera las partículas proviene del potencial que genera el conjunto de las partículas de la descarga. La carga de las partículas se acumula en función de su posición en la simulación, que está dividida en celdas para cuantificar y resolver el potencial mediante las técnicas usuales de resolución de la ecuación de Laplace. Las simulaciones PIC se han convertido en una herramienta fundamental que funciona como enlace entre el trabajo teórico y las medidas experimentales [29,30,74,88–96].

3 Hipótesis y objetivos

El trabajo desarrollado en esta tesis, titulada ***"Estudio teórico y experimental de la vaina iónica formada alrededor de una sonda cilíndrica de Langmuir inmersa en plasmas"***, ha tenido como motivación principal la búsqueda de una generalización y una extensión del modelo radial de Allen, Boyd y Reynolds (ABR) [9] para la corriente iónica entrante en una sonda electrostática de Langmuir polarizada negativamente con respecto al plasma, aplicado a sondas electrostáticas de Langmuir cilíndricas [10], para introducir la temperatura de los iones positivos y estudiar su efecto en la corriente. El efecto de la temperatura de los iones positivos en el modelo de fluidos ABR fue introducido y calculado para temperatura de iones suficientemente baja con respecto a la temperatura de los electrones por Fernández Palop *et al.* [11]. Esta tesis se ha desarrollado en el grupo de investigación TEP-230 Contacto plasma-superficie, siendo uno de sus objetivos a medio plazo encontrar una explicación teórica al cambio de régimen de validez de los modelos radiales a validez de los modelos orbitales. Se pretende relacionar el cambio con los parámetros característicos del plasma, las temperaturas de los iones y de los electrones, la densidad del plasma y los recorridos libres medios de las partículas que conforman el plasma, especialmente los iones positivos que generan la corriente iónica, en los distintos tipos de colisión que pueden sufrir.

3.1 Hipótesis de trabajo

La principal hipótesis requerida en el desarrollo de este trabajo para garantizar la aplicabilidad de los resultados obtenidos es la validez del modelo de fluidos. Esto tiene implicaciones importantes con respecto al recorrido libre medio de los iones en sus colisiones con el resto de las partículas del plasma.

3.1.1 Recorrido libre medio de colisión ion-ion.

Las colisiones entre iones conservan la energía y el momento interno del fluido de iones. Sin embargo, si el recorrido libre medio de las colisiones ion-ion es demasiado grande con respecto a la escala del problema, que viene dada por la longitud de Debye λ_D, es decir, si el número de

Knudsen es demasiado grande, las colisiones son demasiado infrecuentes y es necesario estudiar los iones como partículas. En el caso de la interacción entre iones, la fuerza de Coulomb es de largo alcance, por lo que el fluido de iones no es un gas de Boltzmann. En este caso se pueden encontrar dos tipos de colisiones entre iones [57]:

- *Colisiones frontales*: En este tipo de colisión se incluyen las que tienen un parámetro de impacto b lo suficientemente bajo como para que las partículas se desvíen mucho con respecto a su dirección original. Definimos el parámetro de impacto máximo b_0 como aquel para el que la deflexión con respecto a la trayectoria original es $\alpha_0 = \pi/2$. Analizando la colisión se obtiene [36]:

$$b_0 = \frac{e^2}{4\pi\varepsilon_0\mu v^2}, \qquad 3.1$$

  para iones de carga $+e$, donde μ es la masa reducida $\mu = 0.5m_+$ con m_+ es la masa del ion, ε_0 es la permitividad eléctrica del vacío y v es el módulo de la velocidad relativa de la colisión. Debido a que típicamente la densidad de iones es baja en los plasmas fríos, este tipo de colisiones es muy infrecuente.

- *Colisiones distantes*: En este tipo de colisiones las partículas cargadas pasan lejos pero aun así perciben el efecto de la otra partícula como una desviación pequeña en la trayectoria de la partícula. Como el rango de la fuerza de Coulomb es infinito, en general es difícil establecer un valor máximo para la distancia de interacción entre las partículas, pero en un plasma, debido a la capacidad de apantallamiento del plasma, se puede usar como distancia máxima la propia longitud de Debye, λ_D, del plasma. Por lo tanto, decimos de una colisión que es distante si su parámetro de impacto b es menor que la longitud de Debye $b < \lambda_D$ pero no es lo suficientemente pequeño como para que sea una colisión frontal, $b > b_0$.

De esta discusión, inicialmente puede parecer que las colisiones distantes entre iones apenas tienen capacidad de desviar la trayectoria de los iones. Para calcular la desviación que produce una colisión distante es suficiente con obtener la media de la desviación con respecto a todos los posibles parámetros de impacto $b \in [b_0, \lambda_D]$, obteniendo un determinado ángulo de deflexión de las colisiones distantes, $\alpha \ll 1$. El recorrido libre medio para las colisiones distantes que desvían poco las partículas se puede estimar utilizando como sección eficaz σ_α una circunferencia cuyo radio es la longitud de Debye λ_D [58]:

$$\lambda_\alpha = \frac{1}{n_+ \sigma_\alpha} = \frac{1}{\pi n_+ {\lambda_D}^2}. \qquad 3.2$$

Por lo que podemos obtener el número de Knudsen para las colisiones, para los valores típicos de la descarga DC del grupo TEP-230 Contacto plasma-superficie, tal y como se mostraron en la Error! Reference source not found. en la página Error! Bookmark not defined., es decir, para la densidad de iones $n_+ = 10^{16}\ \mathrm{cm}^3$ y para la longitud de Debye $\lambda_D = 33\ \mu\mathrm{m}$:

$$Kn_\alpha = \frac{\lambda_\alpha}{\lambda_D} = \frac{1}{\pi n_+ {\lambda_D}^3} = 9 \cdot 10^{-4}. \qquad 3.3$$

Por lo tanto, las colisiones distantes son muy frecuentes, pero apenas desvían la trayectoria de los iones. Sin embargo, el efecto acumulado de muchas colisiones distantes puede desviar mucho la trayectoria de un ion. El efecto acumulado de las colisiones distantes se realiza de forma similar al problema del caminante aleatorio en una dimensión en la variable ángulo, y obteniendo la probabilidad de que un ion se desvíe $\pi/2$. Este estudio ofrece el siguiente resultado para plasmas electropositivos con iones de carga $+e$ con temperatura T_+ [36,57,97]:

$$\lambda_{i-i} = \frac{25\pi {\varepsilon_0}^2 (k_B T_+)^2}{e^4\, \mathrm{n}_+ \ln\Lambda}, \qquad 3.4$$

donde se ha utilizado la definición del logaritmo de Coulomb,

$$\ln\Lambda = \ln\left(\frac{\lambda_D}{b_0}\right). \qquad 3.5$$

Utilizando para la velocidad relativa de la colisión distante v_+ la velocidad térmica, de tal forma que,

$$\frac{1}{2} m_+ v_+^2 = \frac{3}{2} k_B T_+, \qquad 3.6$$

se obtiene la siguiente expresión para el logaritmo de Coulomb [36],

$$\ln \Lambda = \ln\left(6\pi n_+ {\lambda_D}^3 \frac{T_+}{T_e}\right). \qquad 3.7$$

Para los valores típicos de la descarga DC del grupo TEP-230 Contacto plasma-superficie, tal y como se mostraron en la Error! Reference source not found. en la página Error! Bookmark not defined., es decir, $n_+ = 10^{16}\ \mathrm{m}^3$, $\lambda_D = 33\ \mu\mathrm{m}$ y temperatura electrónica $T_e = 0.2\ \mathrm{eV}$, el logaritmo de Coulomb vale $\ln \Lambda = 9$. Con estos datos, el recorrido libre medio de un ion para la colisión entre iones es de $\lambda_{i-i} = 1.8mm$. Por lo tanto, el número de Knudsen para las colisiones distantes entre iones vale:

$$Kn_{i-i} = \frac{\lambda_{i-i}}{\lambda_D} = 55. \qquad 3.8$$

Concluimos pues que Kn_α es muy pequeño pero Kn_{i-i} es grande. En el trabajo desarrollado en esta tesis se usa la hipótesis de que, en las condiciones del plasma utilizado en el grupo de investigación TEP-230 Contacto plasma-superficie, existen colisiones distantes frecuentes que apenas desvían la trayectoria de los mismos en la distancia característica de la escala del problema. La comparación de los números de Knudsen Kn_α y Kn_{i-i} permite afirmar que *el modelo de fluidos está justificado y, además, que las partículas no sufren una desviación importante debido a las colisiones entre iones y se pueden ignorar*.

3.1.2 Recorrido libre medio de colisión entre iones y neutros.

Dado que la densidad de los átomos neutros es mucho más grande que la densidad del plasma, hasta 10^6 veces más, las colisiones de los iones con los neutros pueden tener un efecto importante. Dado que los átomos neutros no tienen carga, la colisión entre los iones y los neutros está relacionada con el tamaño del átomo. El tipo de colisión más frecuente para plasmas fríos es la colisión de tipo intercambio de carga o C-E (Charge-Exchange) [41,62,63,65], en las que la proximidad del ion y el átomo neutro provoca la superposición de las nubes electrónicas de los átomos y en las que hay cierta probabilidad de que un electrón del átomo neutro salte al ion. El recorrido libre medio para este tipo de colisión se puede calcular utilizando las secciones medias de colisión obtenidas por Maiorov [58,98]. Utilizando estos datos se obtienen las siguientes expresiones para argón [17]:

$$\sigma_{C-E,Ar}(T_+ = 300\ \mathrm{K}) = 79.5 \cdot 10^{-16}\ \mathrm{cm}^2, \quad 3.9$$

$$\lambda_{i,Ar}(\mathrm{cm}) = \frac{1}{258.4 \cdot P(\mathrm{mTorr})}. \quad 3.10$$

Para las presiones de trabajo de la descarga DC de plasma del grupo de investigación TEP-230 Contacto plasma-superficie, en el orden de los $5\ \mathrm{Pa}$ o $37.5\ \mathrm{mTorr}$, el recorrido libre medio de colisión con los neutros tiene un valor de:

$$\lambda_{i,Ar} \approx 1\ \mu\mathrm{m}. \quad 3.11$$

Este valor implica que es del mismo orden que la longitud de Debye, por lo que el efecto de las colisiones con los neutros puede ser importante. Por lo tanto, se usa como hipótesis que, en el plasma usado en el grupo de investigación TEP-230 Contacto plasma-superficie, ***puede ocurrir que las colisiones de intercambio de carga C-E deban ser tenidas en cuenta en los modelos teóricos para modelar la vaina iónica positiva alrededor de una sonda electrostática de Langmuir inmersa en un plasma electropositivo.***

3.1.3 Pre-vainas

En el contexto de la descarga completa, la recombinación de iones con electrones y la pérdida de partículas en las paredes que envuelven el plasma implican una pérdida de partículas, que debe ser compensada por el fenómeno de ionización y de emisión de electrones que alimente la descarga para poder alcanzar un estado estacionario. Supongamos que una pared metálica plana inmersa en un plasma tiene un potencial inferior al potencial del plasma, de forma que atrae a los iones positivos del plasma. En estado estacionario, la densidad de corriente de iones debe ser constante. Suponiendo que la pared es suficientemente grande como para que la vaina formada pueda ser considerada unidimensional, la densidad de corriente j_+ es el producto de la densidad de iones n_+ por la velocidad media de los iones v_+ y es constante:

$$j_+ = n_+ v_+ = cte. \quad 3.12$$

Bajo la hipótesis de que la vaina se ha formado, el potencial es decreciente y el campo es más intenso en los puntos más próximos a la superficie. El estudio realizado en la sección 2.2.2 Criterio de Bohm, demuestra que los iones deben entrar en la vaina con una velocidad superior a la velocidad de Bohm, pero por (3.12), si la velocidad de los iones aumenta, la densidad de los iones debe disminuir, rompiendo la cuasi-neutralidad. Se llega así a la conclusión de que, en el espacio anterior a la vaina, o pre-vaina, debe existir un mecanismo que permita conectar de forma continua las magnitudes físicas entre el plasma y la vaina, a pesar de que estos iones sean acelerados hacia la sonda. Los tres mecanismos de pre-vaina que se deben tener en cuenta son:

- *Pre-vaina por colisiones*: Las colisiones permiten que los iones sean acelerados mientras algunos de ellos son frenados, de forma que es posible aumentar la velocidad media de los iones y mantener la cuasi-neutralidad. Este modelo fue resuelto para una superficie plana inmersa en un plasma electropositivo con una única especie de iones por Riemann [37,42]
- *Pre-vaina de ionización*: En el espacio de la pre-vaina se van generando iones por el efecto de las colisiones de los electrones energéticos con los átomos neutros, de forma que es posible que los iones sean acelerados y que se mantenga la cuasi-neutralidad. Este modelo, para una superficie plana, fue resuelto por Tonks y Langmuir [38].
- *Pre-vaina geométrica*: Es los casos de vaina con simetría radial, esférica o cilíndrica, la conservación de la densidad de corriente de iones se escribe usando la siguiente expresión:

$$\mathrm{j}_+ = 2D\pi r^D n_+(r) v_+(r) = cte, \qquad 3.13$$

donde r es la distancia al punto o eje de simetría para simetría esférica y cilíndrica respectivamente, D permite distinguir el tipo de simetría con $D = 1$ para simetría cilíndrica y $D = 2$ para simetría esférica, y j_+ es la corriente iónica para simetría esférica y la corriente por unidad de longitud para simetría cilíndrica. Por lo tanto, en los casos de simetría radial, ocurre que la corriente iónica puede ser constante a medida que los iones son acelerados y se acercan a la sonda debido al menor volumen disponible para los iones en las regiones más próximas a la sonda.

Debido a esto, en la vaina que se forma alrededor de una sonda electrostática de Langmuir cilíndrica inmersa en un plasma, a menudo la pre-vaina es menor y el efecto de los

mecanismos de pre-vaina por colisiones y de ionización se pueden ignorar. En la descarga del grupo de investigación TEP-230 Contacto plasma-superficie, el mecanismo de pre-vaina por colisiones debe ser tenido en cuenta en algunas condiciones del plasma, pero el mecanismo de pre-vaina de ionización puede ignorarse. Por lo tanto, se usa como hipótesis, en el trabajo desarrollado en esta tesis, que *los efectos de ionización ocurren a una escala mucho mayor que la pre-vaina geométrica y por lo tanto pueden ignorarse.*

3.2 Objetivos de la tesis

Esta tesis se enmarca dentro del grupo de investigación TEP-230 Contacto plasma-superficie del Departamento de Física de la Universidad de Córdoba. El objetivo de la investigación del grupo es realizar modelos de la vaina que se forma alrededor de una sonda electrostática de Langmuir cilíndrica y aplicarlo a las descargas DC y RF, y determinar en qué condiciones está justificado utilizar los modelos radiales o de fluidos [9–11] y en qué condiciones es necesario utilizar los modelos orbitales [3,12,13] para modelar la corriente iónica recogida por una sonda electrostática de Langmuir polarizada negativamente con respecto al plasma. Para ello, se realizan estudios teóricos, tanto modelos matemáticos resueltos de forma numérica [11,23–26] como simulaciones PIC [29,30], y se realizan medidas experimentales [14–17,27,28,47]. El proyecto de esta tesis surge de la necesidad de adaptar los modelos utilizados previamente, tanto el modelo de Fernández Palop de 1996 [11] como las publicaciones de la tesis de Morales Crespo [23–26] a plasmas electronegativos, o plasmas con dos poblaciones de especies negativas. Estos plasmas son muy importantes en la industria [58,99–102], por lo tanto, es muy interesante disponer de modelos precisos de sondas electrostáticas de Langmuir inmersas en este tipo de plasmas para realizar la diagnosis del plasma. El plan de trabajo de la tesis se detalla en las siguientes secciones, indicando en qué artículo se consigue cada objetivo.

3.2.1 Aplicación del modelo de Fernández Palop a plasmas electronegativos

En el año 1996, Fernández Palop propuso un modelo para ofrecer una posible explicación a medidas experimentales en las que la corriente iónica recogida resultaba ser mayor que las predicciones de los modelos existentes [11]. En los modelos tradicionales radiales [9,10] siempre se predice una corriente iónica superior a la de los modelos orbitales tradicionales [3,12,13], y de hecho, el modelo radial de Allen, Boyd y Reynolds (ABR) [9] era considerado como una cota

superior a la corriente predicha por el modelo orbital completo de Laframboise [13]. Efectivamente, en los modelos orbitales, algunos iones pueden orbitar y volver al plasma, mientras que en los modelos radiales todos los iones son recogidos por la sonda. Sin embargo, algunas medidas muy precisas de la corriente iónica recogida por una sonda electrostática de Langmuir arrojaban corrientes superiores a la predicha por el modelo radial ABR, por lo que Fernández Palop propuso la energía térmica de los iones como una fuente adicional de energía que justificaría que se recogiera una corriente superior. Se consideró que la temperatura de los iones es conocida, igual a la temperatura ambiente y que en el plasma muy frío del grupo de investigación TEP-230 Contacto plasma-superficie, la temperatura ambiente no es despreciable frente a las temperaturas tan bajas que alcanzan los electrones en la descarga DC del grupo, en el rango de $[1000K, 4000K]$. Este modelo solamente pudo ser resuelto usando la condición de que la temperatura de iones es suficientemente baja. Por lo tanto, el primer objetivo de esta tesis ha sido la adaptación del modelo de Fernández Palop de 1996 a plasmas electronegativos con la idea de poder aplicarlo a medidas experimentales en las que haya dos poblaciones de especies negativas.

Sin embargo, durante la adaptación de dicho modelo se descubrió el motivo de por qué no pudo ser resuelto de forma exacta para cualquier temperatura de iones. El motivo es que cuando los iones son acelerados desde el plasma hasta la superficie de la sonda, alcanzan un punto en el que la velocidad del fluido de iones es igual a la velocidad local del sonido, relacionada con la presión parcial de los iones. En dicho punto, cuya posición es desconocida *a priori*, hay una singularidad matemática [103] que se encuentra más cerca de la sonda cuanto mayor es el cociente entre la temperatura de los iones con respecto a la temperatura de los electrones, cociente que ha sido llamado $\beta = T_+/T_e$ por mucho autores y designación que se ha utilizado en este trabajo. Para una temperatura de iones nula, la singularidad diverge hacia el infinito, pero para temperatura de iones no nula, la solución numérica no puede cruzar la singularidad. Si se utiliza la misma estrategia de Allen, Boyd y Reynolds [9], tal y como se detalla en la sección 2.5.2, de empezar la integración numérica en la solución cuasi-neutra, se encuentra que para un cociente β suficientemente bajo la solución cuasi-neutra cruza la singularidad naturalmente y es posible iniciar la integración numérica más cerca de la sonda que el punto donde aparece la singularidad. Sin embargo, si el cociente β es demasiado alto, la solución cuasi-neutra deja de ser válida antes de cruzar la singularidad, por lo que si se empieza la integración numérica en la solución cuasi-neutra, los resultados numéricos invariablemente divergen.

Como parte de esta tesis se ha desarrollado una metodología para solventar esta dificultad, que se recoge un artículo publicado en la revista *Physics of Plasmas* en 2017 [18]. En dicho artículo se describe la técnica utilizada para empezar la integración en un punto de la solución que cumpla la condición de cuasi-neutralidad en el plasma. Se deriva una expresión para obtener una condición que debe cumplir el punto, inicialmente desconocido, en el que los iones cruzan la singularidad de la velocidad local del sonido, y se utiliza esta condición para buscar la posición de la singularidad que permite cumplir la condición de cuasi-neutralidad en el plasma. El problema se reduce, por lo tanto, a una solución de un sistema de ecuaciones diferenciales mediante el método de tiro, en el que el punto inicial está muy próximo a la singularidad de la que se conoce tan solo una condición pero no su posición y el punto final es el plasma cuasi-neutro. Una vez encontrada la posición de la singularidad, se puede resolver el sistema de ecuaciones diferenciales integrando hacia la superficie de la sonda.

Como aplicación de gran interés tecnológico, como parte de esta tesis, se ha aplicado el modelo resuelto para obtener el potencial flotante en plasmas electronegativos. El modelo ha sido adaptado para introducir una segunda población negativa, cuyos resultados se han publicado en un artículo en la revista *Plasma Sources Science and Technology* en 2018 [19]. En este artículo se obtiene la solución del modelo, aplicada a un plasma electronegativo con una población de iones positivos, una población de iones negativos y una población de electrones.

3.2.2 Verificación experimental del modelo teórico obtenido

El modelo de Fernández Palop [11] ha resultado exitoso en medidas de diagnosis de plasmas electropositivos en los que la corriente iónica recogida es mayor a la corriente predicha por el modelo radial de Allen, Boyd y Reynolds [9], en las medidas de Díaz-Cabrera *et al.* [14–17,27,48]. La generalización del modelo a plasmas electronegativos permite además utilizarlo en la diagnosis de plasmas con dos poblaciones de especies negativas. Sin embargo, la aplicación a experimentos con plasmas electronegativos es difícil debido a que típicamente estos plasmas son químicamente muy activos, por lo que aparecen muchos tipos de especies tanto negativas como positivas. Por ejemplo, en un plasma de oxígeno, pueden aparecer especies químicas como O_2^-, O^-, O^{--}, o incluso O^+, O^{++} o O_3 [1,2]. Por lo tanto, es un desafío experimental encontrar las condiciones para las que tan solo una especie química negativa sea predominante, que junto con los electrones y los iones positivos formarían el plasma electronegativo.

Sin embargo, es conocido que en ciertas condiciones la Función de Distribución de Energía de los Electrones, o EEDF, no se puede adscribir a una EEDF de Maxwell-Boltzmann. En algunos casos en los que la presión es suficientemente baja, dependiendo de la potencia de la descarga, los electrones energéticos plasmógenos con energías de hasta 50 eV no pierden toda su energía en colisiones ionizantes, de forma que en el plasma hay una proporción importante de dos tipos de electrones, los electrones de alta energía con una temperatura más elevada, y los electrones que son arrancados de los átomos como resultado de las colisiones ionizantes, con una temperatura menor [4,34,49,50]. A esta función de distribución se le conoce como función de distribución de energía de los electrones (EEDF) bi-maxwelliana, debido a que se puede descomponer en la suma de dos distribuciones de Maxwell-Boltzmann. Dicha función de distribución, que puede ser medida mediante la fórmula de Druyvesteyn, es compatible con dos poblaciones de electrones de distinta temperatura.

Por lo tanto, para validar el modelo de Fernández Palop, aplicado a plasmas electronegativos con dos poblaciones de especies negativas, se puede utilizar un plasma electropositivo con una única especie de iones positivos y dos especies de electrones de distinta temperatura. La generalización a plasmas con más especies negativas es trivial.

Como parte del trabajo desarrollado en esta tesis se ha realizado un conjunto de medidas experimentales con el objetivo de aplicar el modelo desarrollado en esta tesis [18] generalizado para plasmas electronegativos, cuyos resultados se han publicado en un artículo en la revista *Plasma Physics and Controlled Fusion* en 2019 [21]. En el artículo se describen las medidas realizadas en la descarga DC del grupo de investigación TEP-230 Contacto plasma-superficie en plasmas de argón y neón, en condiciones en las que hay una transición desde una función de distribución compatible con una función de Maxwell-Boltzmann a una función de distribución bi-maxwelliana. Se comprueba que el potencial flotante obtenido utilizando tan solo una población de electrones no es capaz de seguir el potencial flotante medido, mientras que el potencial flotante obtenido utilizando el modelo desarrollado en esta tesis [18] con dos poblaciones de especies negativas si puede predecir el potencial flotante medido.

3.2.3 Introducción de colisiones con los neutros en el modelo

Las colisiones de tipo intercambio de carga, o C-E, entre los iones y los neutros en su desplazamiento hacia la sonda son consideradas como un fenómeno que permite relacionar y explicar la corriente iónica medida diferente a la predicha por los modelos. En los modelos

radiales, las colisiones son similares a un término de fricción, por lo que la corriente recogida es menor que la corriente recogida en ausencia de colisiones. En los modelos orbitales, sin embargo, las colisiones modifican la trayectoria de los iones, deteniéndolos en su órbita alrededor de la sonda y permitiendo que la corriente recogida sea mayor que la predicha en ausencia de colisiones. Por lo tanto, las colisiones hacen que las corrientes de ambos modelos se aproximen a la zona intermedia entre los dos. Sin embargo, *a priori* no es posible distinguir si se trata de un comportamiento orbital con colisiones o un comportamiento radial con colisiones, que pueden ofrecer corrientes muy parecidas, desde el punto de vista cualitativo. Por lo tanto, es muy interesante realizar modelos precisos que introduzcan las colisiones para poder comparar las medidas cuantitativamente, aunque este problema es de difícil solución [31,41,43,65,67,104–106].

Normalmente las colisiones entre los iones y los neutros se introducen mediante un término que incluye una frecuencia de colisión constante [104], aunque desde el punto de vista físico es más razonable pensar que el recorrido libre medio es constante, mientras que la frecuencia de colisión depende de la velocidad [41]. El motivo por el que normalmente se prefiere utilizar una frecuencia de colisión constante es que, matemáticamente, el problema con frecuencia de colisión constante es más fácil de tratar. De hecho, el modelo radial de Allen, Boyd y Reynolds [9] no había podido ser resuelto hasta ahora con un término de colisiones con recorrido libre medio constante. Al introducir las colisiones en el modelo de Fernández Palop [11], es posible escribir sistema de ecuaciones diferenciales con dos parámetros, el cociente β entre la temperatura de los iones y la temperatura de los electrones y el cociente Λ_+ entre el recorrido libre medio de colisiones de intercambio de carga λ_+ y la longitud de Debye λ_D. Se obtiene una jerarquía de sistemas de ecuaciones diferenciales encadenadas mediante el método de perturbaciones en el parámetro adimensional $\mu = 2{\Lambda_+}^{-1}$, de forma que $\mu = 0$ en el caso sin colisiones y $\mu \lesssim 1$ en el caso en que las colisiones son poco frecuentes en la vaina. El sistema de orden 0 coincide con el modelo de Fernández Palop, resuelto de forma exacta en [18]. La solución para el sistema de orden n es utilizada para resolver el sistema de orden $n+1$, de forma que se puede encontrar, *a priori*, la solución exacta. De esta forma, todas las funciones que resuelven el sistema completo se escriben como suma de una serie de términos del método de perturbaciones:

$$y(x) = y_0(x) + \mu y_1(x) + \mu^2 y_2(x) + \mu^3 y_3(x) + \cdots, \qquad 3.14$$

con $y_n(x)$ la solución del sistema de orden n. Es interesante que, de la misma forma que el modelo de Fernández Palop converge hacia el modelo radial de Allen, Boyd y Reynolds cuando la temperatura de los iones tiende a $\beta \to 0$, la solución obtenida mediante el método que se ha descrito converge de forma natural a una solución para el modelo de Allen, Boyd y Reynolds con colisiones con recorrido libre medio constante. Dicha solución, al igual que la solución exacta [18] para el modelo de Fernández Palop, depende del tratamiento de la singularidad realizado y, dado que la singularidad se encuentra en el infinito en el modelo de Allen, Boyd y Reynolds, no se podía utilizar en el tratamiento matemático y la solución no había podido ser hallada hasta ahora.

El desarrollo teórico de la jerarquía de sistemas de ecuaciones diferenciales descrito para resolver el modelo de Fernández Palop con colisiones con recorrido libre medio constante ha sido publicado en la revista *Plasma Sources Science and Technology* en 2019 [20]. En el artículo se explica la metodología propuesta para la resolución del modelo de Fernández Palop [11] y el modelo radial de Allen, Boyd y Reynolds [9] mediante el tratamiento de la singularidad propuesto en [18], y se resuelve para los dos primeros sistemas, el de orden 0 y el de orden 1, y se estima el rango de validez de la solución en la variable μ. Es interesante que una de las conclusiones del trabajo de este artículo es que el efecto de la temperatura de los iones y el efecto de las colisiones puede llegar a cancelarse, lo que podría explicar la dificultad para realizar medidas precisas en los que se perciban la influencia de alguno de estos efectos en los plasmas para los que los modelos radiales son aplicables.

3.2.4 Estudio experimental de la influencia de las colisiones y la masa del ion en la validez de los modelos radiales

En una investigación previa del grupo de investigación TEP-230 Contacto plasma-superficie se encontraron condiciones para un plasma de Helio en que los resultados de la diagnosis del plasma son compatibles con las teorías radiales y con las teorías orbitales, y una zona intermedia en la que ninguna de las dos es válida, es decir, una zona de transición entre validez de las teorías radiales y validez de las teorías orbitales [16,17]. Como parte del objetivo del grupo de investigación de establecer los límites de validez de los modelos radiales, se planificaron una serie de medidas para estudiar la influencia de las colisiones de los iones con los neutros en la validez de la teoría radial. Para ello se realizaron una serie de medidas realizadas a presión

constante y otra a corriente de descarga constante. Debido a que es mucho más sencillo cambiar la corriente de descarga que la presión, en las investigaciones previas del grupo TEP-230 Contacto plasma-superficie siempre se realizaron series del primer tipo. Sin embargo, después de analizar las dependencias del cociente entre el recorrido libre medio de colisiones de tipo intercambio de carga o C-E con respecto a la longitud de Debye Λ_+, se concluyó que es posible determinar si las colisiones pueden provocar la transición entre la validez de las teorías orbitales y las teorías radiales. Para verlo, considérese primero una serie a presión constante: si aumenta la corriente de descarga, con las demás magnitudes físicas constantes, la densidad del plasma aumenta, por lo que la longitud de Debye disminuye y el cociente Λ_+ necesariamente debe aumentar. Por otra parte, al aumentar la densidad del plasma, las colisiones de los electrones energéticos son más frecuentes y por lo que disminuye la población de electrones energéticos y, por tanto, disminuye la temperatura de los electrones. De esta forma el cociente β entre la temperatura de iones positivos y la temperatura de los electrones debe aumentar también. Por este razonamiento, una serie a presión constante variando la corriente de descarga siempre va a presentar una relación monótona creciente entre Λ_+ y β, lo que no nos permite distinguir si la transición ocurre a causa de la variación en una u otra variable.

Considérese ahora una serie a corriente de descarga constante, en la que se varía lentamente la presión. Si aumenta la presión, la densidad del plasma aumenta por existir más átomos neutros que pueden ser ionizados por los electrones energéticos. Por el mismo razonamiento que en el caso anterior, el cociente β entre la temperatura de los iones y la temperatura de los electrones va a aumentar y la longitud de Debye va a disminuir. Sin embargo, si aumenta la presión, el recorrido libre medio de colisión debe disminuir también. Al variar ambos en el mismo sentido con un aumento de la presión, el recorrido libre medio y la longitud de Debye, no es posible predecir *a priori* cuál va a ser dominante y si el cociente entre ambos, Λ_+, aumenta o disminuye al incrementar la presión de la descarga. Al realizar series a corriente de descarga constante en una descarga de plasma de helio, se comprobó experimentalmente que la disminución del recorrido libre medio es predominante y que al aumentar β, el cociente Λ_+ disminuye. Debido a que la transición hallada en un plasma de helio ocurre al aumentar la presión [16,17], que viene acompañada de un aumento en β y una disminución en Λ_+, se concluye que el cociente entre la temperatura de los iones y la temperatura de los electrones es la magnitud que produce la transición. Sin embargo, notando que la transición solo se observa en la descarga de plasma de helio, y no se observa en las descargas de plasma de neón o de argón [16,17], para los mismos valores de β, se concluye que la masa del ion es la magnitud física que

determina la aparición de la transición entre la validez de las teorías radiales y de las teorías orbitales.

Estos resultados se han publicado en un artículo en la revista Applied Sciences [22]. En el artículo se revisa la transición entre la validez de las teorías radiales y validez de las teorías orbitales ya encontrada anteriormente, esta vez centrándose en la influencia del recorrido libre medio de colisión de tipo intercambio de carga o C-E. Se han publicado las nuevas series realizadas para determinar la influencia predominante del cociente β frente al cociente Λ_+ y se ofrecen algunas posibles explicaciones teóricas en función de la velocidad orbital de los iones después de su última colisión antes de alcanzar la sonda.

4 Artículos

4.1 Como primer autor

PHYSICS OF PLASMAS **24**, 103516 (2017)

Removal of singularity in radial Langmuir probe models for non-zero ion temperature

Guillermo Fernando Regodón,[1,a)] José Ignacio Fernández Palop,[1] Antonio Tejero-del-Caz,[2] Juan Manuel Díaz-Cabrera,[3] Rafael Carmona-Cabezas,[1] and Jerónimo Ballesteros[1]
[1]*Departamento de Física, Universidad de Córdoba, E-14071 Córdoba, Spain*
[2]*Instituto de Plasmas e Fusão Nuclear, Instituto Superior Técnico, Universidade de Lisboa, Lisboa, Portugal*
[3]*Departamento de Ingeniería Eléctrica, Universidad de Córdoba, E-14071 Córdoba, Spain*

(Received 27 July 2017; accepted 7 September 2017; published online 3 October 2017)

We solve a radial theoretical model that describes the ion sheath around a cylindrical Langmuir probe with finite non-zero ion temperature in which singularity in an *a priori* unknown point prevents direct integration. The singularity appears naturally in fluid models when the velocity of the ions reaches the local ion speed of sound. The solutions are smooth and continuous and are valid from the plasma to the probe with no need for asymptotic matching. The solutions that we present are valid for any value of the positive ion to electron temperature ratio and for any constant polytropic coefficient. The model is numerically solved to obtain the electric potential and the ion population density profiles for any given positive ion current collected by the probe. The ion-current to probe-voltage characteristic curves and the Sonin plot are calculated in order to use the results of the model in plasma diagnosis. The proposed methodology is adaptable to other geometries and in the presence of other presheath mechanisms. *Published by AIP Publishing.*
[http://dx.doi.org/10.1063/1.4997844]

I. INTRODUCTION

The theoretical structure of the boundary between a neutral plasma and a metallic surface is yet not fully understood, despite the efforts which have been made over the last decades.[1–4] There are several applications which benefit from advances in this area: in surface treatment assisted by plasma, the frequency and the energy of impact from the plasma particles are governed by the potential and ion population density profiles; in plasma diagnosis, the ion current collected by a Langmuir probe can be calculated by analyzing the plasma-surface boundary.

Diagnosis with Langmuir probes is, eighty years after its invention, still one of the most important methods of plasma diagnosis since it is one of the few methods providing local information about the plasma parameters. Several theories have been introduced to establish the relation between the plasma parameters and the current collected by the probe at any probe voltage. In the 1960s, Laframboise[5] developed his complete theory for the ion current collected by a cylindrical Langmuir probe, based on the mathematical framework of Benstein and Rabinowitz.[6] His theory considers all the possible orbits that may be described by the positive ions around the probe. However, experiments show that positive ions, especially the heavier ones, do not follow an orbital motion around the probe but are well described by radial theories instead.[7–14] Allen *et al.*[15] developed a theory taking into account this radial motion for the case of a spherical Langmuir probe, a theory which was soon after generalized by Chen[16] for cylindrical Langmuir probes. These radial motion theories are jointly known as the ABR theory (from authors Allen, Boyd and Reynolds) and were developed for the case of cold ions.

Solutions for Langmuir probe models have appeared through the years. The model by Laframboise already considered positive ion temperature when applied to ion sheaths.[5] The Tonks–Langmuir model has been solved only recently for non-zero ion temperature.[17,18] But no complete solution for ABR models for any ion temperature has yet been released. The extension of the ABR theory by Fernández Palop[19] considers the thermal motion of the ions. However, the presence of the supersonic ion singularity[20] makes the integration of Langmuir probe fluid models starting in the quasineutral plasma impossible and therefore, alternative strategies have been developed for a small enough ion to electron temperature quotient.[19,21–25] Despite the difficulties relating non-zero ion temperature, the ion current that is collected by Langmuir probes is of great interest in plasma diagnosis for theoretical knowledge,[4] for practical considerations,[26] and for technological applications.[27,28]

It has been proved that the thermal motion of the ions strongly influences many aspects of the collected ion current and the sheath structure. As has been recently reported[10,29] a helium plasma that is best described by means of radial motion for cold ions, changes its behavior to orbital motion when the ion temperature increases. In electronegative plasmas, it may attenuate and eliminate the complex multilayer that appears when the Bohm criterion is multivalued.[2] In this paper, we solve the model proposed by Fernández Palop *et al.*[19] for cylindrical Langmuir probes. The singularity that appears in the model when the ion flow reaches the ion speed of sound is treated with no approximations, for any ion temperature value, following the proposal made by Valentini to state conditions to remove the supersonic ion singularity that

[a)]Electronic mail: z62rehag@uco.es

appears in Langmuir probe sheath models.[20] The model is further numerically solved. This solution for the model allowed us to obtain electric potential profiles and ion-current to probe-voltage characteristics in the ion saturation zone, the ion density profiles, and the Sonin plot. A numerical fit for the Sonin plot is provided in order for the results of this paper to be readily usable in plasma laboratories.

II. REMOVAL OF SUPERSONIC ION SINGULARITY

Generally speaking, in a first order differential equation model we have a certain number of dependent variables and an equal number of equations. Together with the appropriate initial conditions, we should be capable of finding a solution, in theory. However, this is not always a simple task, and such is the case of radial sheath models. It is well known that there is a point in the solution that has to get across the supersonic ion singularity that appears in these models. Valentini was the first to show that the supersonic ion singularity is a regular singularity and that it may be eliminated by simply considering that the limit of all physical variables remain finite and non-zero when the solution approximates the singularity.[20]

This being correct, it has not been enough to find a global solution in these radial sheath models. The singularity certainly enables us to find two relations between the variables in an *a priori* unknown point, the singularity point, in the global solution: the condition that the variables meet to create the singularity, and the condition that the variables have to fulfill in order to allow the variables to remain finite. We can state more conditions in a different point: quasineutrality in the plasma. Only in the case of ion temperature equating zero, both conditions occur in the same known point, that is, the infinity point, and that is the reason behind this case being the only one with an exact numerical solution using standard procedures. In this paper, we prove that we can use both conditions occurring in different points to obtain a general solution. This procedure is applicable to other geometries and in the presence of ionization or collisions, with suitable adaptations.

III. HYPOTHESES AND EQUATIONS

Consider a collisionless neutral plasma consisting of positive ions and electrons. Let us also consider an infinite cylindrical conductor (*probe*) with r_p radius, negatively biased with respect to the plasma. The presence of the probe creates a zone of non-neutrality around it, which is referred to as the sheath. The electric potential around the probe will be a function only of the distance to the axis of the probe, r. We denote the potential referred to the plasma potential as $\phi(r)$, and we particularize it in the surface of the probe as $\phi(r_p) = \phi_p$. Similarly, the particle densities will be functions only of r due to the symmetry of the problem, and Poisson's equation can thus be written as follows:

$$\frac{1}{r}\frac{\mathrm{d}}{\mathrm{d}r}\left(r\frac{\mathrm{d}\phi(r)}{\mathrm{d}r}\right) = -\frac{e}{\varepsilon_0}[n_+(r) - n_e(r)], \tag{1}$$

where each ion is assumed to possess a charge e, and where the ion and electron densities at r are $n_+(r)$ and $n_e(r)$, respectively.

We assume that electrons may be described by using the Maxwellian distribution function and therefore the electron density will be

$$n_e(r) = n_{e0}\exp\left(\frac{e\phi(r)}{k_\mathrm{B}T_e}\right), \tag{2}$$

where n_{e0} is the electron density at the plasma sufficiently far from the probe and T_e is the electron temperature. For the description of ions, we will consider a fluid approximation assuming radial motion. The momentum balance equation for steady flow with the above assumption is

$$m_+ n_+ v_+(r)\frac{\mathrm{d}v_+(r)}{\mathrm{d}r} = -en_+(r)\frac{\mathrm{d}\phi(r)}{\mathrm{d}r} - \frac{\mathrm{d}p_+(r)}{\mathrm{d}r}, \tag{3}$$

where m_+ and $v_+(r)$ are the positive ion mass and velocity field, respectively, and $p_+(r)$ is the positive ion partial pressure at r. The flow is assumed to be adiabatic,[30,31] and therefore, the pressure will be related to the positive ion density as follows:

$$p_+(r) = k_\mathrm{B}T_+\frac{n_+(r)^\kappa}{n_{eo}^{\kappa-1}}, \tag{4}$$

where T_+ is the temperature of the positive ions in the unperturbed plasma, and where the neutrality condition has been considered. In (4), the constant $\kappa = 3, 2, \frac{5}{3}$ is the constant polytropic coefficient for one, two and three degrees of freedom, respectively. However, Kuhn, Riemann *et al.*,[32] from kinetic arguments, and Gyergyek and Kovacic,[33,34] from a two fluid model in a recent paper, suggest that there is some interval in which κ is not well approximated by any of these three values. On the other hand, Gyergyek and Kovacic prove, from a two fluid model, that the region of the sheath and presheath is well approximated by adiabatic ion flow, and that the basic conclusions on the ion temperature effect are little sensitive to the value of the constant polytropic coefficient. Being so, we are interested in finding a procedure that is usable for any value of κ, in order to check the sensitivity of this fluid model to its value. In numerical calculations we will solve for the constant polytropic coefficient values $\kappa = 2$ and $\kappa = 3$.

If the last expression for the pressure (4) is introduced into the momentum balance equation (3), after integrating, the following energy balance equation is obtained:

$$\frac{1}{2}m_+v_+^2(r) + e\phi(r) + \frac{\kappa}{\kappa-1}k_\mathrm{B}T_+\left(\frac{n_+(r)}{n_{eo}}\right)^{\kappa-1} = \frac{\kappa}{\kappa-1}k_\mathrm{B}T_+. \tag{5}$$

Finally, we must consider the continuity equation for the positive ion fluid which can be expressed as follows if no ionizations take place in the sheath:

$$i = e2\pi r n_+(r)v_+(r), \tag{6}$$

where i is the positive ion current per unit length collected by the probe. If this last equation (6) is introduced into (5), one may obtain

$$S(r) + e\phi(r)n_+^2(r) + \frac{\kappa}{\kappa-1}k_B T_+ n_+^2(r) \times \left[\left(\frac{n_+(r)}{n_{eo}}\right)^{\kappa-1} - 1\right] = 0, \quad (7)$$

where we have noted $S(r)$ as the independent term of the energy balance equation (7) when considered as a polynomial in $n_+(r)$

$$S(r) = \frac{1}{2}m_+\left(\frac{i}{e2\pi r}\right)^2. \quad (8)$$

Equation (7) relates the potential with the ion density, which can be used together with Poisson's equation to numerically obtain the potential profile, once given the right initial conditions. This equation is a cubic for $\kappa = 2$ and a quartic for $\kappa = 3$, both of which have two positive roots for sufficiently low $S(r)$, which is always positive. The other root or roots are negative or nonexistent; the local maximum of the polynomial, if present, always occurs at $n_+ = 0$.

As $S(r)$ is increased, these roots get closer and ultimately coalesce into one and disappear in a saddle-node bifurcation. The bifurcation is related to the sheath variables, so it creates a relation of special significance in the solution. As there are no positive solutions for n_+ for $S(r)$ values greater than the bifurcation point, the values of the sheath parameters have no meaning beyond it. Also, at the convergence point of the saddle-node bifurcation, the derivative of n_+ with respect to $S(r)$, and hence with respect to r, diverges, creating a singularity. To clarify this, let us consider the continuity equation in the differential form (the dependence on r is not explicitly written)

$$\mathrm{d}(v_+ n_+ A) = 0, \quad (9)$$

which we particularize to cylindrical surfaces with area per unit length $A/L = 2\pi r$ around the axis of the cylinder. Hence we get a relation between the relative variations in velocity, positive ion density, and distance to the axis

$$\frac{\mathrm{d}v_+}{v_+} = -\frac{\mathrm{d}n_+}{n_+} - \frac{\mathrm{d}r}{r}. \quad (10)$$

On the other hand, we can write the pressure term in the momentum balance equation (3) as follows:

$$\mathrm{d}p_+ = m_+ c_+^2 \mathrm{d}n_+, \quad (11)$$

where we made use of the definition of the speed of sound $c_+^2 = m_+^{-1}\frac{\partial p_+(r)}{\partial n_+(r)}$. Introducing (10) and (11) into the momentum balance equation (3), we obtain the relative variation in the positive ion density

$$\frac{\mathrm{d}n_+}{n_+} = \frac{v_+^2\frac{\mathrm{d}r}{r} - e\frac{\mathrm{d}\phi}{m_+}}{c_+^2(1-M^2)}, \quad (12)$$

where we have used $M = v_+/c_+$, the Mach number of the fluid particle. Thus we find that the denominator becomes null when the fluid reaches the speed of sound, and therefore

$$v_+ = c_+. \quad (13)$$

It is not physically admissible for the positive ion density to diverge, as proved by Valentini,[20] and we conclude that at the point where the fluid reaches the speed of sound the numerator must also be null, and we obtain

$$\frac{\mathrm{d}\phi}{\mathrm{d}r} = \frac{m_+ v_+^2}{er}. \quad (14)$$

Equations (13) and (14) are the conditions that the variables must meet in the regular singularity. In order for the equations to be in the dimensionless form, we introduce the following dimensionless variables and parameters, with λ_D being the Debye length:

$$I_i = \frac{ir_p e}{2\pi\varepsilon_0 k_B T_e}\left(\frac{m_+}{2k_B T_e}\right)^{\frac{1}{2}}, \quad \beta = \frac{T_+}{T_e}, \quad x = \frac{r}{\lambda_D}, \quad N_+(x) = \frac{n_+(r)}{n_{eo}}, \quad y(x) = -\frac{e\phi(r)}{k_B T_e}. \quad (15)$$

Poisson's equation can thus be expressed as

$$\frac{1}{x}\frac{\mathrm{d}y(x)}{\mathrm{d}x} + \frac{\mathrm{d}^2 y(x)}{\mathrm{d}x^2} = N_+(x) - e^{-y(x)}. \quad (16)$$

We can also write the energy balance equation for positive ions (7) using the dimensionless variables and parameters, and yields

$$\frac{I_i^2}{x^2 x_p^2} - \left(y(x) + \frac{\kappa}{\kappa-1}\beta\right)N_+^2(x) + \frac{\kappa}{\kappa-1}\beta N_+^{\kappa+1}(x) = 0, \quad (17)$$

where $x_p = r_p/\lambda_D$ is the dimensionless probe radius. This last equation can be solved to obtain the dimensionless positive ion density $N_+(x)$. For simplicity, we will not explicitly write the x dependence from now on. The ABR theory must be recovered in the limiting case $\beta \to 0$, so the following condition must be fulfilled by the positive ion density distribution:

$$N_+ \underset{\beta\to 0}{\sim} \frac{I_i}{x x_p\sqrt{y}}. \quad (18)$$

Besides this condition, at the plasma, the positive ion density must fulfil the neutrality condition, and thus

$$N_+ \underset{x\to\infty}{\sim} \mathrm{e}^{-y}. \quad (19)$$

Equation (17) is the dimensionless version of (7) and has three or four roots for $\kappa = 2$ and $\kappa = 3$, respectively, two of which are real and positive if the independent term of (17), as stated before, is sufficiently close to zero. When used in Poisson's equation (16), the lower of the positive roots can be numerically proved to converge to the ABR limit, but the greater of the positive roots converges, when

used in Poisson's equation (16) with properly chosen initial conditions, to the neutrality condition. Therefore, Eq. (17) has two roots, both valid although in different regions, the sheath and the quasi-neutral plasma.

We may write the conditions for the regular singularity, (13) and (14), in dimensionless form as well. We first turn (13) into a different form, by means of continuity equation (6) to solve v_+ and using the thermodynamical relation (4) between p_+ and n_+ in the definition of c_+

$$\frac{i}{2\pi e r n_+} = \sqrt{\kappa \frac{p_+}{m_+ n_+}} = \left(\frac{k_B T_+ n_{+0} \left(\frac{n_+}{n_+ 0} \right)^{\kappa}}{\kappa \, m_+ n_+} \right)^{\frac{1}{2}}, \tag{20}$$

from where we obtain the dimensionless equation

$$N_+^{\kappa+1} = \frac{2 I_i^2}{x^2 x_p^2 \beta \kappa}. \tag{21}$$

Moreover, from (14) we obtain

$$\frac{\mathrm{d}y}{\mathrm{d}x} = -\frac{2 I_i^2}{x^3 x_p^2 N_+^2}. \tag{22}$$

We may introduce (21) into the energy balance equation (17) to solve y as a function only of x, and yields

$$y = \frac{\kappa+1}{\kappa-1} \left(\frac{I_i}{x x_p} \right)^{2\frac{\kappa-1}{\kappa+1}} \left(\frac{\beta\kappa}{2} \right)^{\frac{2}{\kappa+1}} - \frac{\kappa}{\kappa-1} \beta. \tag{23}$$

We may also introduce the same Eq. (21) into (22) to find $\frac{\mathrm{d}y}{\mathrm{d}x}$

$$\frac{\mathrm{d}y}{\mathrm{d}x} = -\frac{2^{\frac{2\kappa}{\kappa+1}} (\beta\kappa)^{\frac{2}{\kappa+1}}}{x^{1+2\frac{\kappa-1}{\kappa+1}}} \left(\frac{I_i}{x_p} \right)^{2\frac{\kappa-1}{\kappa+1}}, \tag{24}$$

which is precisely the derivative of (23), although obtained otherwise. This means that the positive ion flow, when it reaches the speed of sound, must be tangent to the curve defined by (23), if the singularity is to be removed.[20] We now spell out the roots for the energy balance equation (17).[19] We find the smaller positive solution

$$N_{+1} = \frac{I_i}{x x_p \sqrt{y + 2\beta}} \left(\cos\frac{\theta}{3} - \frac{\sqrt{3}}{3} \sin\frac{\theta}{3} \right)^{-1}, \tag{25}$$

and the greater positive solution

$$N_{+2} = \frac{I_i}{x x_p \sqrt{y + 2\beta}} \frac{\sqrt{3}}{2} \left(\sin\frac{\theta}{3} \right)^{-1}, \tag{26}$$

for $\kappa = 2$, θ being defined as follows:

$$\theta = \arcsin\left(\frac{\beta I_i}{x x_p} \left(\frac{3}{y + 2\beta} \right)^{\frac{3}{2}} \right). \tag{27}$$

These solutions exist as long as the argument of the arcsine, being always positive or null, is lower than 1. Thus the condition for the existence of solution is

$$y \geq 3 \left(\frac{I_i \beta}{x x_p} \right)^{\frac{2}{3}} - 2\beta. \tag{28}$$

We also find both solutions for $\kappa = 3$

$$N_{+1,2} = + \left(\frac{y + \frac{3}{2}\beta \mp \sqrt{\left(y + \frac{3}{2}\beta \right)^2 - \frac{6\beta I_i^2}{x^2 x_p^2}}}{2 \frac{I_i^2}{x^2 x_p^2}} \right)^{\frac{1}{2}}, \tag{29}$$

being N_{+1} with the minus sign the smaller positive solution and N_{+2} with the plus sign the greater one. These solutions also exist on the validity of the following condition:

$$y \geq \sqrt{\beta 6} \frac{I_i}{x x_p} - \frac{3}{2}. \tag{30}$$

These expressions, (28) and (30), with the equality sign, coincide with (23) particularised for $\kappa = 2$ and $\kappa = 3$, respectively. So, we conclude that the curve defined by (23) is also the limit for which the two positive roots for (17) converge into one, the greater root of this equation being valid for $x \to \infty$ and the smaller root for $x \to 0$. This regular supersonic singularity curve is decreasing, it has a vertical asymptote in $x = 0$, and cuts the horizontal axis for finite $\beta > 0$ values. In Fig. 1, we show the qualitative graph of this limiting curve and the corresponding qualitative shape of the polynomial, cubic or quartic, in dimensionless energy balance equation (17) as small insets in the figure.

As the solution crosses the singularity and the correct solution changes from the greater positive root to the smaller positive one, the plasma parameters change according to Poisson's equation (16). A close-up of the cubic polynomial in energy balance equation (17) as the solution closes to the singularity from the plasma is shown in Fig. 2. The small triangles indicate the greater positive root which approximates quasi-neutrality $N \to 1$ for $x \to \infty$. Similarly, we show a

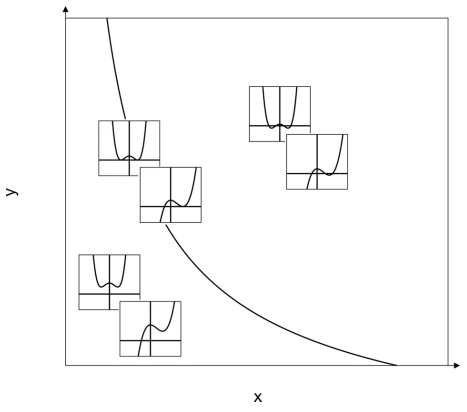

FIG. 1. Qualitative graph of the limiting curve defined by the bifurcation in the energy balance equation (17).

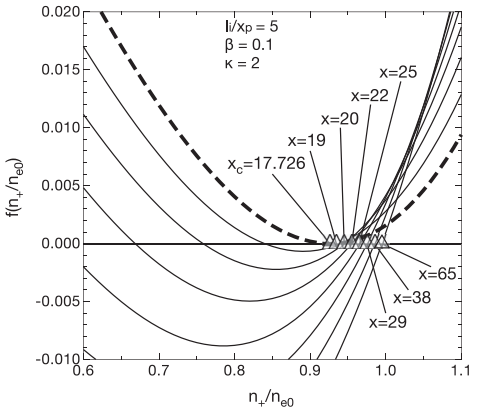

FIG. 2. Cubic polynomial in the energy balance equation for changing plasma parameters, from plasma (regular lines) to singularity (dashed bold line) for $I_i/x_p = 5$, $\beta = 0.1$ and $\kappa = 2$.

close-up of the same cubic polynomial as the solution reaches the singularity from the probe in Fig. 3 and the small triangles indicate the smaller positive root which converges to ABR for $\beta \to 0$.

Even when we have found two expressions, (23) and (24), that the singularity point must fulfill, there is still ambiguity to where it is located. With two expressions and three variables (potential, its slope, and radial coordinate) there is still one degree of freedom. We can delimit the radial coordinate of the supersonic ion singularity by the intercept of the curve defined by (23) with the x axis, for $\kappa = 2$

$$x_l = \left(\frac{3}{2}\right)^{\frac{3}{2}} \frac{I_i}{x_p\sqrt{\beta}}, \tag{31}$$

and for $\kappa = 3$

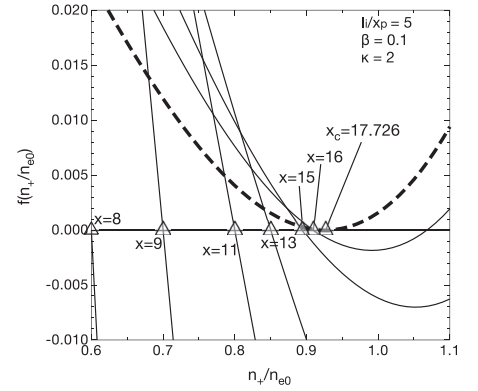

FIG. 3. Cubic polynomial in the energy balance equation for changing plasma parameters, from probe (regular lines) to singularity (dashed bold line) for $I_i/x_p = 5$, $\beta = 0.1$ and $\kappa = 2$.

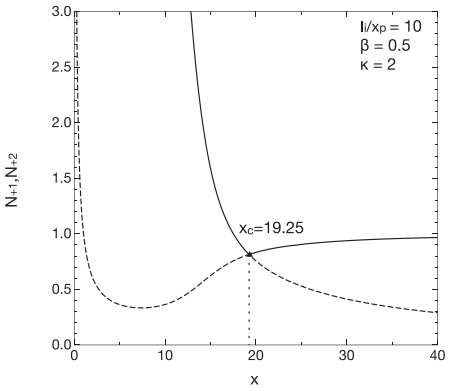

FIG. 4. Greater positive root (full line) and smaller positive root (dashed line) of the energy balance equation (17) for $I_i/x_p = 10$, $\beta = 0.5$ and $\kappa = 2$.

$$x_l = \sqrt{\frac{8}{3\beta}}\frac{I_i}{x_p}. \tag{32}$$

We can numerically search for a x_c value that generates y and $\frac{dy}{dx}$ through (23) and (24) that converges to the quasi-neutral solution for increasing x to the plasma by means of the greater root of (17), and then use this value to generate the solution for decreasing x to the sheath by means of the smaller root of (17). This is the way to obtain a smooth continuous solution for y and $\frac{dy}{dx}$ for all x, crossing through the singularity that occurs at x_c when the ions become supersonic. In Fig. 4, we show both solutions for a representative profile for $I_i/x_p = 10$, $\beta = 0.5$, and $\kappa = 2$, and illustrate how smoothness requires the aforementioned change in the used root of (17). In Fig. 5, we show a complete solution for Poisson's equation (16), for the same plasma parameters, with small insets which show that the root of (17) is being used in each part of the profile, with the small triangle indicating the point where the singularity is crossed, $x = x_c$.

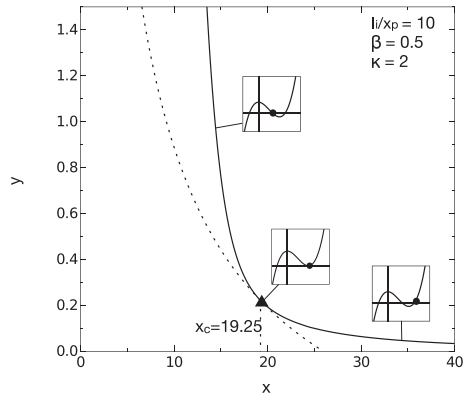

FIG. 5. Potential profile for $I_i/x_p = 10$, $\beta = 0.5$ and $\kappa = 2$ (full line) and limit curve of existence of roots of the energy balance equation (17) (dotted line).

Finally, for each pair of parameters, I_i/x_p and β, we can find the position of the resolved singularity for the solution that reaches quasi-neutrality for $x \to \infty$. It is interesting to study the position of the singularity against both parameters. Figure 6 shows how the position of the singularity moves further from the probe as the ions get colder.

IV. ANALYSIS OF THE SOLUTION

In relation to the general discussion in Sec. II, we state the following summary. The model may be written as having four dependent variables: potential, its slope, ion current, and ion density. The independent variable is the distance to the axis. If we know the value of the four variables at one point in the solution, we can solve the model. However, even if we know the conditions in the plasma, the presence of the singularity makes integration unstable and an alternative is needed. Ignoring collisions and ionizations, we have established that the ion current is a constant through the continuity equation (6) and thus we can render it as a parameter. In the conditions of this model, the momentum balance equation is integrable as in (7) and so ion density has a definite relation to the potential, reducing the model to two variables and the distance to the axis. The presence of the regular supersonic ion singularity allows us to relate both potential and its slope to the distance to the axis in the point where the singularity occurs, as in (23) and (24), and thus there is only one indeterminancy in the distance to the axis where such singularity is located. For each value of the distance to the axis we can numerically integrate the equations, and only one of these solutions fulfills the quasineutrality condition in the plasma. The solution is found by means of a modified shooting method in which the starting point of the numerical integration is searched in the range given by (31) or (32) using conditions (23) and (24).

The dynamical system has two branches that merge into one algebraic branch line. The solution moves through one of the branches and is able to change smoothly and continuously from one branch to the other only if it arrives tangent to the algebraic branch line. The solution then moves into the other branch. As the branch line corresponds to the velocity of the ions reaching the ion speed of sound, it is possible, if the total ion current is too low, that there is no solution which fulfills quasineutrality in the plasma and that reaches such velocity before the radial coordinate is null. These values of ion current are too low for the premises of sheath formation to hold. The following results have been collected using secure values for the total ion current.

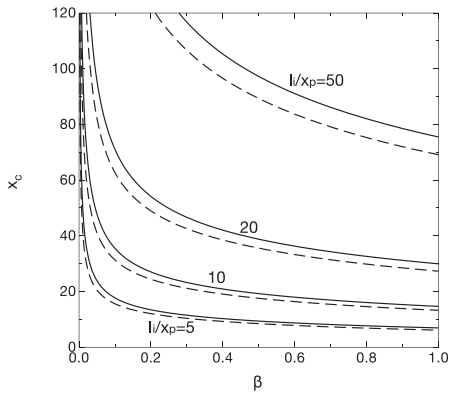

FIG. 6. Position x_c of the singularity as a function of β for different $\frac{I_i}{x_p}$ values, for $\kappa = 2$ (full lines) and $\kappa = 3$ (broken lines).

V. RESULTS

Illustrative results and plots have been obtained for $\kappa = 2, 3$, which correspond to two-dimensional and one-dimensional thermal motion, respectively. They have been chosen because, for cylindrical Langmuir probes, they correspond to both small and large probe radius limits compared to the Debye length, $r_p \ll \lambda_D$ and $r_p \gg \lambda_D$, respectively, and we may assume that in the case of intermediate probe radius values, κ would remain somewhere between these two limiting values.[19,30,32] We first show the potential profiles obtained by integrating Poisson's equation (16) using as the initial condition the point in the $\left(y, \frac{dy}{dx}\right)$ space that converges to the quasineutrality condition. Figures 7 and 8 show the profiles obtained for various I_i/x_p values for β ranging from the set $\{0, 0.1, 0.2, 0.35, 0.5, 1\}$ for $\kappa = 2$ and $\kappa = 3$, respectively. Profiles for both κ values coincide for $\beta = 0$ when the thermal motion is ignored in the ABR limit and their difference becomes more important as β increases. As can be seen in these figures, the potential increases more quickly when the thermal motion is less important. This is reasonable since thermal motion is an additional source of energy for the ions to reach the probe and, for the same current, the potential needed to obtain such current is less. We appreciate in these figures that the difference between both κ values is relatively small, proving that the constant polytropic coefficient is not very critical, although such difference increases with β.

For a constant x_p value, the dimensionless ion current collected by the probe can be obtained from curves analogous to those obtained for Figs. 7 and 8, by cross plotting. Figure 9 shows the dependence on β of the dimensionless ion-current to probe-voltage characteristic for β ranging from the previous set $\{0, 0.1, 0.2, 0.35, 0.5, 1\}$ for $\kappa = 2$ and $\kappa = 3$. As shown, the dimensionless ion current is greater if the ions have a greater temperature. This is a reasonable result, since thermal motion allows more ions to reach the probe. The increase is greater than 40% in the ion current collected for $\beta = 1$ for the same voltage at the probe, which makes the thermal motion an essential factor in the system dynamics and thus cannot be ignored in plasma diagnosis. We also notice that for $\kappa = 3$ the ion current collected is some units greater than for $\kappa = 2$, and that this difference increases with β.

We have evaluated the dimensionless ion-current to probe-voltage characteristic for a number of x_p values, which we show in Fig. 10. In this figure, we compare the ABR limit with the dimensionless ion-current to probe-voltage characteristics with our results for increasing β values up to $\beta = 1$.

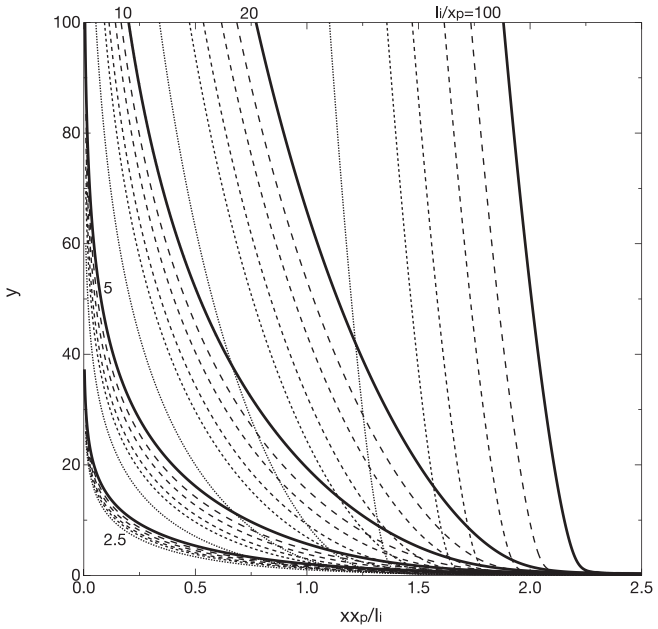

FIG. 7. Potential distribution in the surroundings of the probe at various $\frac{l_i}{x_p}$ values for $\kappa = 2$, for $\beta = 0$ (full curve), for $\beta = 0.1$, 0.2, 0.35, and 0.5 (broken lines), and for $\beta = 1$ (dotted line).

The effect of the ion thermal motion is important even for small β values for all x_p values, and so it should be taken into account in plasma diagnosis laboratories when using Langmuir probes. Again, we see that the difference between two-dimensional and one-dimensional adiabatic flow is small.

From the profiles obtained by solving Poisson's equation, we can get the ion population density by means of the energy balance equation (17). We show the ion population density profiles for several values of β in Fig. 11. As can be seen, the ion population density initially decreases as ions get closer to the axis due to the acceleration suffered, but when they reach a minimum, the ion density grows since the geometric compression reduces the volume allowed for them. The minimum is found closer to the probe and at a higher value of ion population for increasing β.

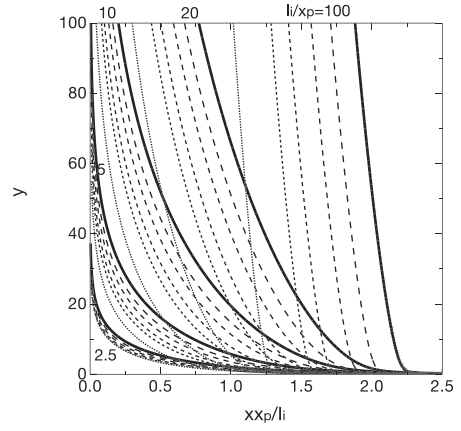

FIG. 8. Potential distribution in the surroundings of the probe at various $\frac{l_i}{x_p}$ values for $\kappa = 3$, for $\beta = 0$ (full curve), for $\beta = 0.1$, 0.2, 0.35, and 0.5 (broken lines), and for $\beta = 1$ (dotted line).

VI. EXPERIMENTAL APPLICATIONS

The results of the model can be applied in plasma diagnosis most simply by means of the Sonin plot, which is a useful representation of the ion current collected by a probe.

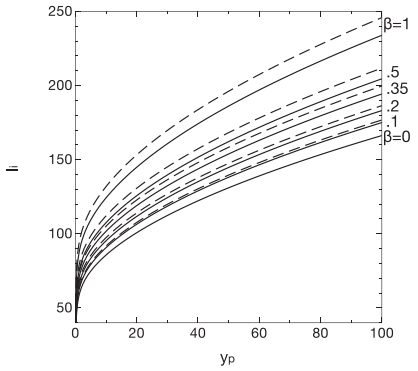

FIG. 9. Dimensionless ion-current to probe-voltage characteristic for $x_p = 10$ for $\kappa = 2$ (full lines) and for $\kappa = 3$ (broken lines), for several values of β.

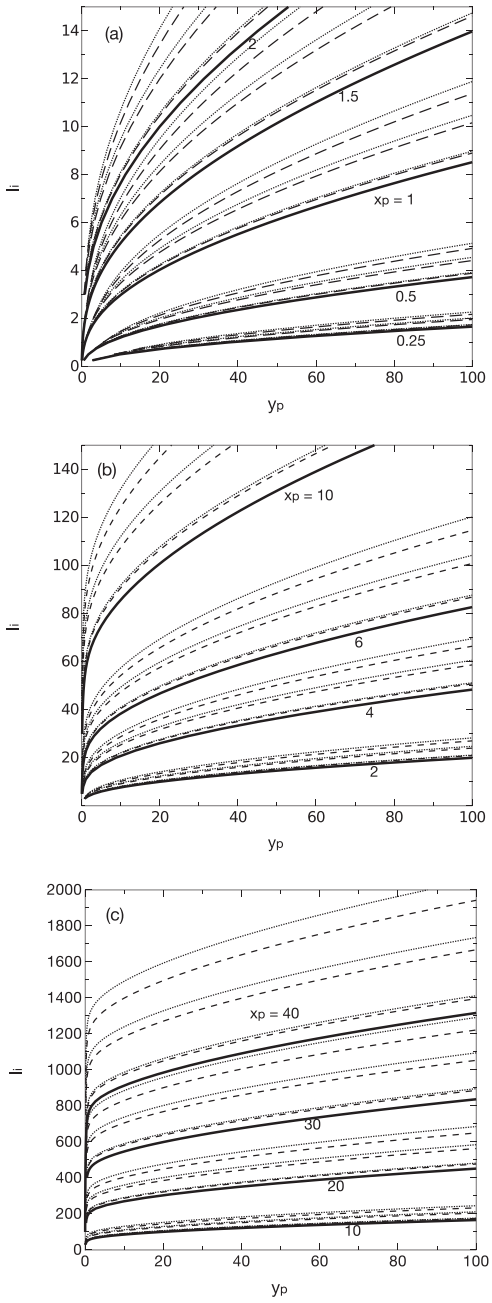

FIG. 10. Dimensionless ion-current to probe-voltage characteristic for several x_p values for ABR limit (full lines), and for $\kappa = 2$ (broken lines) and $\kappa = 3$ (dotted lines), for several values of $\beta = 0.1$, 0.5 and 1. (a) $x_p \in \{0.25, 0.5, 1, 0.5, 2\}$, (b) $x_p \in \{2, 4, 6, 10\}$, and (c) $x_p \in \{10, 20, 30, 40\}$.

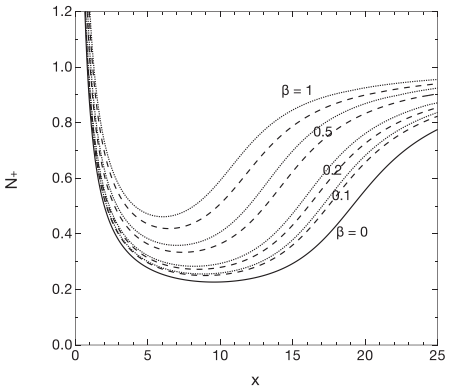

FIG. 11. Ion population density for $I_i/x_p = 10$ for the ABR limit (full line), for $\kappa = 2$ (broken lines), and for $\kappa = 3$ (dotted lines), for several values of $\beta = 0.1$, 0.2, 0.5, and 1.

In the Sonin plot, the following dimensionless current is represented

$$I_i'(25) = I_i 2\sqrt{\pi}\left(\frac{\lambda_D}{r_p}\right)^2 = \frac{i}{e r_p n_{e0}}\sqrt{\frac{m_+}{2\pi k_B T_e}}, \tag{33}$$

versus

$$I_i'(25)x_p^2 = \frac{I_i e r_p}{\varepsilon_0}\left(\frac{m_+}{2\pi k_B^3 T_e^3}\right)^{\frac{1}{2}}. \tag{34}$$

$I_i'(25)$ is used to denote this dimensionless ion current for $y_p = 25$. The abscissa in the Sonin plot does not depend on the plasma density n_e. The Sonin plot can be used to compare the experimental dimensionless ion current with the theoretical one.[8–11] Besides, the Sonin plot can also be used to diagnose the plasma density.[8–11] Figure 12 represents the Sonin plot for both kinds of adiabatic flow for β from 0 to 1.

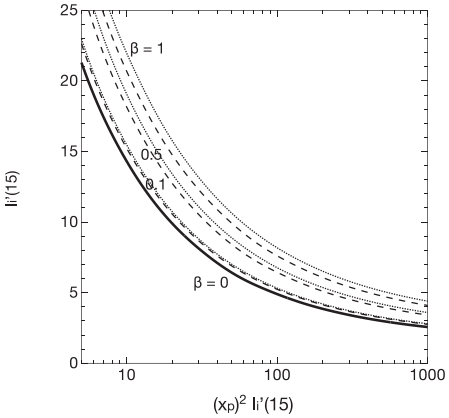

FIG. 12. Sonin plot for $I_i/x_p = 10$ for the ABR limit (full line), for $\kappa = 2$ (broken lines), and for $\kappa = 3$ (dotted lines), for several values of $\beta = 0.1$, 0.5, and 1.

In order to ease the application of this Sonin plot for experimental measurements of the plasma density, for an adimensional probe voltage $y_p = 25$, we have found a parameter-fitted function that deviates from the numerical solution less than 1.5% in terms of the ion to electron temperature quotient β, that is, with respect to the difference between the Sonin plot value for $\beta = 1$ and $\beta = 0$. This means an error smaller than 0.6% in the absolute value in the ordinate value of the Sonin plot. Such an error translates into 22.5 K for usual electron temperatures in low-temperature plasmas, $T_e = 1500$ K. The fitting function is as follows, a, b, c, d being the fitting parameters

$$I_i'(25) = a\ln\left[\left(\frac{b}{\ln(I_i'(25)x_p^2)}\right)^c + 1\right] + d. \tag{35}$$

For each of the fitting parameters, expressions relating the parameter to β have been found as third degree polynomials. For example, for the first coefficient, a

$$a(\beta) = a_3\beta^3 + a_2\beta^2 + a_1\beta + a_0. \tag{36}$$

The values of the coefficients for the fitting parameters for $\kappa = 2$ and for $\kappa = 3$ are collected in Table I.

VII. CONCLUSIONS

The proposed theoretical model for the potential distribution in the surroundings of a cylindrical probe, immersed in a plasma in the absence of ionization, has permitted us to find an exact numerical solution for the potential profile, for any value of ion temperature T_+ and any constant polytropic coefficient κ. The model includes the ABR as the limiting case of cold ions ($\beta \to 0$) and provides the complete solution from the plasma to the probe. The mathematical condition that allowed us to solve the model exactly is the regularity of the supersonic ion singularity. This condition has permitted us to state mathematical conditions that must be fulfilled in the singularity and to find a regular supersonic singularity curve to which the potential profile must be tangent at the singularity. This curve is also an algebraic branch line that permits the smooth continuation between the two branches, the subsonic, and the supersonic branches of the model.

We introduced thermal motion for both two-dimensional and one-dimensional adiabatic flow for the positive ion flow. The two-dimensional adiabatic flow may be used in the case of a small probe radius compared to the Debye length $r_p \ll \lambda_D$, while the one-dimensional flow may only be used if the probe radius is much greater than the Debye length, $r_p \gg \lambda_D$. The electric potential grows more quickly (going from the plasma to the probe) when the ion thermal motion is absent. By cross plotting many electric potential profiles, we have been able to produce several ion-current to probe-voltage characteristics for several probe radii. As has been shown, the ion current is greater when thermal motion is present, and this increase can represent more than 40% when the temperature of the ions is equal to that of the electrons. Besides, the one-dimensional adiabatic ion flow is greater than the two-dimensional adiabatic one, although the sensibility to the constant polytropic coefficient κ is much less than the sensibility to the ion temperature to the electron temperature ratio β, coinciding with the results by other authors. As an important experimental application, we have studied the Sonin plot, a useful representation to compare the theoretical ion current with the experimental measurements, which we have evaluated for $y_p = 25$. Due to the effect of the positive ion temperature, an upwards shift in the Sonin plot is obtained when the ion thermal motion is considered, and such a shift has been calculated for β up to $\beta = 1$. A useful fitting formula for the Sonin plot is given to be easily used in plasma diagnosis laboratories.

TABLE I. Values of the fitting parameters in the Sonin plot fitting function through Eqs. (35) and (36).

$\kappa = 2$		$\kappa = 3$	
Parameter	Value	Parameter	Value
a_0	11.892	a_0	11.892
a_1	7.0968	a_1	9.1383
a_2	–3.9824	a_2	–5.9789
a_2	$9.7765\text{e} \times 10^{-1}$	a_2	1.3875
b_0	3.7135	b_0	3.7133
b_1	2.1058×10^{-1}	b_1	2.1305×10^{-1}
b_2	3.3567×10^{-2}	b_2	1.1991×10^{-1}
b_3	-3.2812×10^{-3}	b_3	-1.8682×10^{-2}
c_0	2.9926	c_0	2.9928
c_1	5.2323×10^{-2}	c_1	7.8233×10^{-2}
c_2	-6.2761×10^{-3}	c_2	-2.4424×10^{-3}
c_3	5.6487×10^{-3}	c_3	1.7980×10^{-2}
d_0	1.1831	d_0	1.1834
d_1	9.5816×10^{-1}	d_1	1.1740
d_2	-2.2459×10^{-1}	d_2	-3.0330×10^{-1}
d_3	5.1919×10^{-2}	d_3	9.0467×10^{-2}

[1] J. E. Allen, Plasma Sources Sci. Technol. **18**, 014004 (2009).
[2] R. N. Franklin and J. Snell, J. Phys. D: Appl. Phys. **33**, 1990 (2000).
[3] R. N. Franklin, J. Phys. D: Appl. Phys. **37**, 1342 (2004).
[4] K.-U. Riemann, Plasma Sources Sci. Technol. **18**, 014006 (2009).
[5] J. G. Laframboise, UTIAS Report No. 100, University of Toronto Institute for Aerospace Studies, Toronto, 1966.
[6] I. B. Benstein and I. N. Rabinowitz, Phys. Fluids **2**, 112 (1959).
[7] B. M. Annaratone, M. W. Allen, and J. E. Allen, J. Phys. D: Appl. Phys. **25**, 417 (1992).
[8] J. Ballesteros, J. I. Fernández Palop, M. A. Hernández, and R. Morales Crespo, Appl. Phys. Lett. **89**, 101501 (2006).
[9] J. M. Díaz-Cabrera, M. V. Lucena-Polonio, J. I. Fernandez Palop, R. Morales Crespo, M. A. Hernández, A. Tejero-del Caz, and J. Ballesteros, J. Appl. Phys. **111**, 063303 (2012).
[10] J. M. Díaz-Cabrera, J. Ballesteros, J. I. Fernandez Palop, and A. Tejero-del Caz, Plasma Sources Sci. Technol. **24**, 025026 (2015).
[11] J. M. Díaz-Cabrera, J. I. Fernández Palop, R. Morales Crespo, M. A. Hernández, A. Tejero-del Caz, and J. Ballesteros, Measurement **55**, 66 (2014).
[12] Z. Xu and W. Lu, Plasma Sci. Technol. **15**, 764 (2013).
[13] P. Bryant, A. Dyson, and J. E. Allen, J. Phys. D: Appl. Phys. **34**, 1491 (2001).
[14] M. Klindworth, O. Arp, and A. Piel, J. Phys. D: Appl. Phys. **39**, 1095 (2006).
[15] J. E. Allen, R. L. F. Boyd, and P. Reynolds, Proc. Phys. Soc. **70**, 297 (1957).
[16] F. F. Chen, J. Nucl. Energy **7**, 47 (1965).
[17] L. Kos, D. D. Tskhakaya, and N. Jelić, Phys. Plasmas **18**, 053507 (2011).
[18] D. D. Tskhakaya, L. Kos, and N. Jelić, Phys. Plasmas **21**, 073503 (2014).

[19]J. I. Fernández Palop, J. Ballesteros, V. Colomer, and M. A. Hernández, J. Phys. D: Appl. Phys. **29**, 2832 (1996).
[20]H. B. Valentini, J. Phys. D: Appl. Phys. **21**, 311 (1988).
[21]J. I. Fernández Palop, J. Ballesteros, M. A. Hernández, R. Morales Crespo, and S. Borrego Del Pino, J. Phys. D: Appl. Phys. **37**, 863 (2004).
[22]J. I. Fernández Palop, J. Ballesteros, M. A. Hernández, R. Morales Crespo, and S. Borrego Del Pino, J. Phys. D: Appl. Phys. **38**, 868 (2005).
[23]J. I. Fernández Palop, J. Ballesteros, R. Morales Crespo, and M. A. Hernández, J. Phys. D: Appl. Phys. **41**, 235201 (2008).
[24]R. M. Crespo, J. I. F. Palop, M. A. Hernández, and J. Ballesteros, J. Appl. Phys. **95**, 2982 (2004).
[25]R. Morales Crespo, J. I. Fernandez Palop, J. Ballesteros, M. A. Hernandez, and M. V. Lucena Polonio, IEEE Trans. Plasma Sci. **37**, 1715 (2009).
[26]M. V. Lucena-Polonio, J. M. Díaz-Cabrera, J. I. F. Palop, R. M. Crespo, M. A. Hernández, and J. Ballesteros, Plasma Phys. Controlled Fusion **53**, 124024 (2011).
[27]T. Kubota, H. Ohtake, R. Araki, Y. Yanagisawa, T. Iwasaki, K. Ono, K. Miwa, and S. Samukawa, J. Phys. D: Appl. Phys. **46**, 415203 (2013).
[28]D.-C. Kwon, M.-Y. Song, and J.-S. Yoon, J. Phys. D: Appl. Phys. **46**, 025202 (2013).
[29]A. Tejero-del Caz, J. I. Fernández Palop, J. M. Díaz-Cabrera, and J. Ballesteros, Plasma Sources Sci. Technol. **25**, 01LT03 (2016).
[30]K. U. Riemann, J. Phys. D: Appl. Phys. **24**, 493 (1991).
[31]E. Zawaideh, F. Najmabadi, and R. W. Conn, Phys. Fluids **29**, 463 (1986).
[32]S. Kuhn, K.-U. Riemann, N. Jelić, D. D. Tskhakaya, D. Tskhakaya, and M. Stanojević, Phys. Plasmas **13**, 013503 (2006).
[33]T. Gyergyek and J. Kovačič, Phys. Plasmas **24**, 063505 (2017).
[34]T. Gyergyek and J. Kovačič, Phys. Plasmas **24**, 063506 (2017).

IOP Publishing Plasma Sources Science and Technology
Plasma Sources Sci. Technol. 27 (2018) 025014 (9pp) https://doi.org/10.1088/1361-6595/aaac58

Floating potential in electronegative plasmas for non-zero ion temperatures

Guillermo Fernando Regodón[1], José Ignacio Fernández Palop[1], Antonio Tejero-del-Caz[2], Juan Manuel Díaz-Cabrera[3], Rafael Carmona-Cabezas[1] and Jerónimo Ballesteros[1]

[1] Departamento de Física, Universidad de Córdoba, E-14071 Córdoba, Spain
[2] Instituto de Plasmas e Fusão Nuclear, Instituto Superior Técnico, Universidade de Lisboa, Lisboa, Portugal
[3] Departamento de Ingeniería Eléctrica, Universidad de Córdoba, E-14071 Córdoba, Spain

E-mail: z62rehag@uco.es

Received 28 November 2017, revised 17 January 2018
Accepted for publication 1 February 2018
Published 21 February 2018

Abstract

The floating potential of a Langmuir probe immersed in an electronegative plasma is studied theoretically under the assumption of radial positive ion fluid movement for non-zero positive ion temperature: both cylindrical and spherical geometries are studied. The model is solvable exactly. The special characteristics of the electronegative pre-sheath are found and the influence of the stratified electronegative pre-sheath is shown to be very small in practical applications. It is suggested that the use of the floating potential in the measurement of negative ions population density is convenient, in view of the numerical results obtained. The differences between the two radial geometries, which become very important for small probe radii of the order of magnitude of the Debye length, are studied.

Keywords: Langmuir probe, floating potential, ion saturation current, electronegative plasma

1. Introduction

The study of electronegative plasmas is important due to its applications in many areas of plasma technology. Of particular interest is their application in the microelectronic industry, in which this kind of plasma is used in etching and deposition techniques. The kind of plasma which is most often used in plasma cleaning is oxygen plasma, composed of both positive and negative species. In both examples, the interest lies in the interaction of a plasma with a metallic surface.

Oxygen plasma is also used in sterilization by plasma. In this last example, due to the plastic nature of many medical components, the use of a cold plasma is essential [1]. Thus, in diagnosing and controlling such cold plasmas, it is important to take into account the temperature of the ions. The temperature of the negative ions is usually included, with a good degree of accuracy, in a straightforward manner, as a second negative population density of constant temperature, in thermal equilibrium with the electric field distribution (together with the electron population density), even though this is not always an appropriate description. In particular, plasmas in which different ion species are created in different regions may escape this distribution and may have to be modelled as a fluid. Regarding positive ions, satisfactory treatments of the positive ion temperature have only recently started to appear in the literature. In this sense, Gyergyek makes an interesting and comprehensive review in a recent article [2].

The theory of Langmuir probes has been developed through the years due to the interest in its important applications. On the one hand, Langmuir probes provide reliable local information on the plasma parameters, and are used for all kinds of plasmas, from low temperature plasmas to fusion plasmas [3]. On the other hand, dust grains in a plasma can be considered as spherical Langmuir probes with a non-zero charge but collecting zero net current. In fact, the charge of the particle is an essential parameter to characterize the dust particle in dusty plasmas [4, 5]. In this paper, we study a radial model for a Langmuir probe. In view of the failure of the orbital motion theories for cold enough ion temperature plasmas [6], the basic radial model was introduced by Allen, Boyd and Reynolds for spherical geometry, and later modified by

Chen for cylindrical geometry, in the case of cold ions [7, 8] (which will subsequently be referenced as ABR limit). The positive ion temperature may be included in the model in several ways. It may be introduced by means of kinetic models, where the temperature does not appear explicitly as an input in the model, but can be obtained *a posteriori* [9]. It may also be introduced in a fluid model as a variable in the state equations of the plasma gas components [2, 10]. The effects of the positive ion temperature can also be studied in PIC simulations of the sheath [11, 12]. The conclusions of these studies indicate that, although the polytropic coefficient of the positive ion plasma gas component may not be constant, the sensitivity of the model to its value is small. In this sense, the calculations made by other authors using a constant polytropic coefficient are useful, especially because they are simpler and quicker to obtain [13]. The negative ion temperature may also be included as a variable, although it is usual to introduce it as a Maxwellian population density, as is done for the electrons. Even in this very simple form, the negative ion temperature may have astonishing effects on the plasma-wall interaction; in this sense, the multilayered electronegative sheath attracted much attention in the last two decades [14–23].

In this paper, we solve a model that takes into account the positive ion temperature, as well as the negative ions population, in an electronegative sheath. We solve the model for two radial geometries, cylindrical and spherical, and we explain its differences. We have studied the floating potential with respect to the plasma potential as an interesting and easily measurable physical variable [24], and how it may be used in order to estimate the negative ions population. The conclusions of this model, which has been solved with the new technique developed by the authors [25], support the already established experimental conclusion that the floating potential is a good indicator of the electronegativity of a plasma [26], and extend its range of applicability to arbitrary positive ion temperatures. The model does not require any assumption about the negative ions temperature, which is also arbitrary. The conditions in which the multilayered electronegative sheath appears are studied and the process by which it disappears, with increasing negative ion temperature or additional pre-sheath geometric mechanism, is observed.

2. Hypotheses and equations

Consider a collisionless neutral plasma consisting of positive ions, negative ions and electrons. Let us consider a probe with either spherical or cylindrical geometry, of radius r_p, negatively biased with respect to the plasma. The presence of the probe creates a zone of non neutrality around it, referred to as the ion sheath. The electric potential ϕ and all other variables will be functions only of the distance r to the centre of the sphere or to the axis of the cylinder. In particular, for the electric potential referred to the plasma, $\phi = \phi(r)$. The potential at the probe will be denoted as ϕ_p. The geometry is selected by means of a parameter, D, for which the value is $D = 1$ for cylindrical geometry and $D = 2$ for spherical geometry. Poisson's equation, when applied to the surroundings of the sheath, takes the following form

$$\frac{1}{r^D}\frac{\mathrm{d}}{\mathrm{d}r}\left(r^D\frac{\mathrm{d}\phi(r)}{\mathrm{d}r}\right) = -\frac{e}{\varepsilon_0}[n_+(r) - n_-(r) - n_e(r)], \quad (1)$$

where each ion is assumed to possess charge $\pm e$ and where the positive ion, negative ion and electron densities are $n_+(r)$, $n_-(r)$ and $n_e(r)$, respectively. We will assume that both electron and negative ions may be well described using a Maxwellian distribution function:

$$n_e(r) = n_{e,0}\exp\left(\frac{e\phi(r)}{k_\mathrm{B}T_e}\right), \quad (2)$$

$$n_-(r) = n_{-,0}\exp\left(\frac{e\phi(r)}{k_\mathrm{B}T_-}\right). \quad (3)$$

In these equations, $n_{e,0}$ and $n_{-,0}$ are the electron and negative ion densities at the plasma, T_e and T_- are their constant temperatures, and k_B is Boltzmann's constant. It follows that the quasineutrality condition requires, in the plasma, that

$$n_+(r \to \infty) = n_{e,0} + n_{-,0}. \quad (4)$$

We describe the ions by using a radial fluid approximation. Thus, for the ions we use the momentum balance equation that takes the following form

$$m_+n_+v_+(r)\frac{\mathrm{d}v_+(r)}{\mathrm{d}r} = -en_+(r)\frac{\mathrm{d}\phi(r)}{\mathrm{d}r} - \frac{\mathrm{d}p_+(r)}{\mathrm{d}r}, \quad (5)$$

where m_+, $v_+(r)$ and $p_+(r)$ are the ion mass, the ion radial velocity field and the ion gas partial pressure at r. In a collisionless sheath, the ions flow adiabatically, therefore we can relate the partial pressure to the ion density by means of the state equation for the ion gas.

$$p_+(r) = k_\mathrm{B}T_+\frac{n_+(r)^\kappa}{n_{e,0}^{\kappa-1}}. \quad (6)$$

The polytropic coefficient κ is dependent on the geometry of the system, $\kappa = 2$ for cylindrical coordinates and $\kappa = 5/3$ for spherical coordinates. However, there is still an unresolved discussion as to whether a constant polytropic coefficient approximates appropriately the fluid behaviour of the ions [2, 9, 10] or, even if it is well approximated, what the polytropic coefficient should be. For example, in both cylindrical and spherical geometries with a large probe radius, the adiabatic flow may be considered one dimensional and $\kappa = 3$ should be used [13]. The method presented in this paper is valid for any constant polytropic coefficient.

When (6) is introduced into (5), the resulting expression can be integrated using the neutrality condition at the plasma, and we obtain the following energy balance equation:

$$\frac{1}{2}m_+v_+^2(r) + e\phi(r) + \frac{\kappa}{\kappa-1}k_\mathrm{B}T_+\left(\frac{n_+(r)}{n_{e,0}}\right)^{\kappa-1} = \frac{\kappa}{\kappa-1}k_\mathrm{B}T_+. \quad (7)$$

We close the system of equations with continuity equation that allows us to relate the ion velocity field to the ion density. If i_+ is used to denote the ion current in the case of spherical geometry, $D = 2$, or the ion current per unit length for cylindrical geometry, $D = 1$:

$$i_+ = e2\pi D r^D n_+(r) v_+(r). \tag{8}$$

In order to make the equations dimensionless, we introduce dimensionless variables. The selection of the dimensionless ion current (spherical geometry) or current per unit length (cylindrical geometry) has been chosen to be consistent with the original paper by Allen [7] and with the classic textbook by Swift and Schwar [27]

$$\begin{aligned} I_i &= \frac{i_+ e r_p^{2-D}}{2\pi D \varepsilon_0 k_B T_e}\left(\frac{m_+}{2k_B T_e}\right)^{\frac{1}{2}}, & x &= \frac{r}{\lambda_D}, \\ \beta &= \frac{T_+}{T_e}, & N_+(x) &= \frac{n_+(r)}{n_{e,0}}, \\ \gamma &= \frac{T_e}{T_-}, & \alpha_0 &= \frac{n_{-,0}}{n_{e,0}}, \\ y(x) &= -\frac{e\phi(r)}{k_B T_e}, & V_+(x) &= v_+(r)\sqrt{\frac{m_+}{2k_B T_e}}, \end{aligned} \tag{9}$$

where we have used the definition of λ_D, the Debye length,

$$\lambda_D = \sqrt{\frac{\varepsilon_0 k_B T_e}{e^2 n_{e,0}}}. \tag{10}$$

With these definitions, we use x_p as the dimensionless probe radius. We further make the following definition, independent of the probe radius as can be deduced from equation (9), which will be useful in numerical calculations,

$$I_p = \frac{I_i}{x_p^{2-D}}. \tag{11}$$

We point out that, for spherical coordinates $D = 2$, I_p equals I_i. Using the relations given by (9) and (11), the system of equations takes the following form, where the probe radius does not appear and thus becomes arbitrary:

$$\frac{D}{x}\frac{dy(x)}{dx} + \frac{d^2y(x)}{dx^2} = N_+(x) - e^{-y(x)} - \alpha_0 e^{-\gamma y(x)}, \tag{12}$$

$$I_p = N_+(x) V_+(x) x^D, \tag{13}$$

$$\left(\frac{I_p}{x^D N_+(x)}\right)^2 - y(x) + \beta\frac{\kappa}{\kappa - 1}\left[\left(\frac{N_+(x)}{1 + \alpha_0}\right)^{\kappa-1} - 1\right] = 0. \tag{14}$$

The system of equations has a singularity that prevents integration starting from the plasma. Instead, we will find the position of the singularity and integrate from this initial distance to the axis to the plasma and to the probe, following the procedure first presented by Regodón *et al* [25]. In order to obtain the position of the singularity, we consider the continuity equation in differential form. From now on, we will not explicitly write the dependance on r or on x,

$$\frac{dV_+}{V_+} + \frac{dN_+}{N_+} + D\frac{dx}{x} = 0. \tag{15}$$

Let us also consider the dimensionless local speed of sound at distance r, and introduce (6) in it, to obtain

$$C_+^2 = c_+^2\frac{m_+}{2k_B T_e} = \frac{1}{m_+}\frac{\partial p_+}{\partial n_+}\frac{m_+}{2k_B T_e} = \frac{\beta\kappa}{2}N_+^{\kappa-1}. \tag{16}$$

For cold ions, there is no ion pressure, and there is no possible sound wave. Therefore, their speed of sound converges to 0, the ion fluid would always be supersonic, and the model converges to the ABR limit. We now introduce (15) and (16) into the momentum balance equation (5). Doing so, we obtain the following expression:

$$\frac{1}{N_+}\frac{dN_+}{dx} = \frac{\frac{V_+^2 D}{x} + \frac{1}{2}\frac{dy}{dx}}{C_+^2 - V_+^2}. \tag{17}$$

The denominator equals zero and the system has a singularity when the ions reach the local speed of sound. In order to force the physical quantities to stay bounded, it is necessary that, in the singularity, the numerator should become zero too, giving a second condition in the singularity. For the first condition, the one of the denominator equating zero, we may write C_+ as a function of N_+ (through its definition (16)), and substitute V_+ as a function of N_+ and x (using (13)). We then can solve N_+ as a function of x in the singularity.

$$N_+^{\kappa+1} = \frac{2}{\beta\kappa}(1 + \alpha_0)^{\kappa-1}\frac{I_p^2}{x^{2D}}. \tag{18}$$

This intermediate result can be used in the momentum balance equation (14) to solve y as a function of x in the singularity, and in the second condition, the numerator equating zero, to solve $\frac{dy}{dx}$ as a function of x.

$$y = \left(\frac{\beta\kappa}{2}\right)^{\frac{2}{\kappa+1}}\left(\frac{\kappa + 1}{\kappa - 1}\right)\left(\frac{I_p}{(1 + \alpha_0)x^D}\right)^{2\frac{\kappa-1}{\kappa+1}} - \frac{\beta\kappa}{\kappa - 1}, \tag{19}$$

$$\frac{dy}{dx} = -\frac{2D}{x^{2D\frac{\kappa-1}{\kappa+1}+1}}\left(\frac{\beta\kappa}{2}\right)^{\frac{2}{\kappa+1}}\left(\frac{I_p}{1 + \alpha_0}\right)^{2\frac{\kappa-1}{\kappa+1}}. \tag{20}$$

Equations (19) and (20) prove that the potential profile must be tangent to the curve defined by (19) in the singularity. Only one point of this curve allows integration that fulfills quasineutrality in the plasma limit. This curve is also an algebraic branch line in which the solution of the system changes from one of the two positive roots of (14) to the other. For more details, we refer the reader to previous work carried out by the authors [25].

3. Floating potential

Floating potential is defined as the potential of the probe with respect to the plasma potential that the probe attains when the total current, in or out of the probe, is null. In mathematical terms, this definition requires that the positive ion current into the probe equates the sum of the electron and the negative ion

currents out of the probe (or currents per unit length in case of cylindrical geometry),

$$i_+ = i_e + i_-. \tag{21}$$

Both the electron and the negative ion currents can be calculated as the effusion of the gases in equilibrium into the probe. The expression for the incoming electron current at distance r, where we have considered the different dimensions of variable i_e for both geometries, is

$$i_e = e\frac{A_\mathrm{p}}{L^{2-D}}n_{e,0}\frac{\langle v_e\rangle}{4} = e2\pi D r^D n_{e,0}\sqrt{\frac{k_\mathrm{B}T_e}{2\pi m_e}}\,\mathrm{e}^{\frac{e\phi}{k_\mathrm{B}T_e}}, \tag{22}$$

where A_p is the probe area and L is the length of the probe in the case of cylindrical geometry. We may write a similar expression for the negative ion current. In dimensionless units (independent of the probe radius), to be compared to I_p,

$$I_{p,e} = x^D\sqrt{\frac{m_+}{4\pi m_e}}\,\mathrm{e}^{-y}, \tag{23}$$

whilst for the dimensionless negative ion current,

$$I_{p,-} = x^D\alpha_0\sqrt{\frac{m_+}{4\pi m_-\gamma}}\,\mathrm{e}^{-\gamma y}. \tag{24}$$

For each positive ion current, the system can be integrated to obtain the potential profile. For each constant value of I_p, given β, κ, γ and α_0 values, the potential profile gives the probe potential y that the probe would reach if the probe had radius x. By means of the potential profile, given the ion masses m_+ and m_-, using (23) and (24), the electron and negative ion currents for each probe radius can also be calculated. The desired probe radius is the abscissa of the point where this curve reaches the value $I_{p,e} + I_{p,-} = I_p$, and, going back to the potential profile, the floating potential can be obtained. In figure 1(a), we show an example of a calculated potential for each probe radius and the corresponding positive ion current, and in figure 1(b), the sum of the electron and negative ion currents, for parameters $\beta = 0.5$, $\kappa = 2$, $\gamma = 2$ and $\alpha_0 = 1$, for an oxygen plasma and cylindrical geometry, $D = 1$. These plots enable the calculation of the floating potential.

Solving the model for different positive ion currents will give pairs of (x_p, y_f), and the results of the calculation are shown as an example in figure 1. For very low positive ion currents, the model cannot be solved, that is, the sheath cannot be formed. All plots in this work use values for I_p high enough in order for the premise of sheath formation to hold.

The floating potential depends on the positive and negative ion masses through (23) and (24). As a model case, we solve the system for an oxygen electronegative plasma in conditions [28, 29] in which the major positive and negative ion populations are O^+ and O^-, with masses $m_+ = 15.9989$u and $m_- = 15.9999$u. This kind of plasma is used, for example, in sterilization by plasma [30].

3.1. Results for cylindrical geometry

In this section, we gather the results of the model for a variety of plasma parameters in cylindrical geometry. We will use the

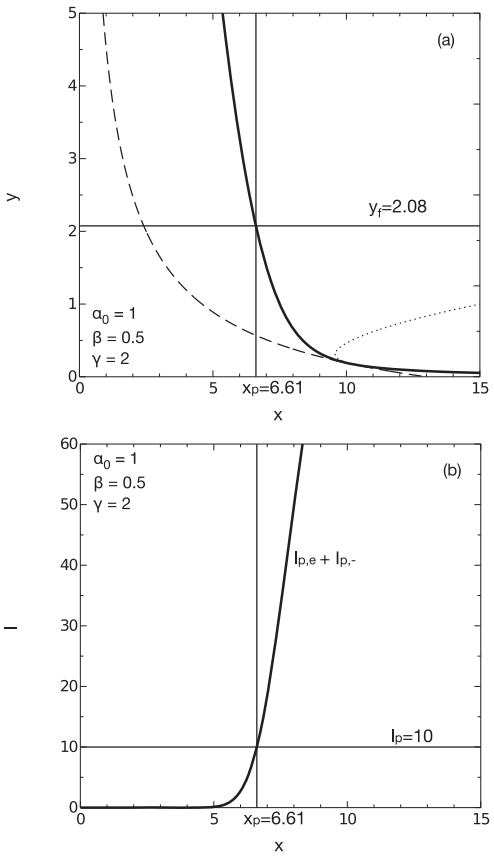

Figure 1. Example relative to the obtaining of the floating potential for $\beta = 0.5$, $\kappa = 2$, $\gamma = 2$ and $\alpha_0 = 1$ for cylindrical geometry, $D = 1$. (a) Potential profile (bold line), algebraic branch line (dashed line) and quasineutral solution (dotted line). (b) Sum of the electrons and negative ions currents (bold line).

value of $\kappa = 2$. For $\alpha_0 = 0$, the value of the negative ion temperature is meaningless, so the results are dependant only on one parameter, that is, β. In figure 2, we show the floating potential for pure ABR ($\beta = 0$) and the dependance of the floating potential on β for the present case of oxygen electronegative plasma. It is shown that the floating potential is lower in the case of warm positive ions. This is a consequence of the positive ions having more energy to reach the probe for the same potential, thus needing a less negative potential to allow more electrons to reach the probe and compensate the positive ion current. It can also be observed that, for larger probes, the effect on the floating potential is more important.

In general, for $\alpha_0 \neq 0$, the negative ion temperature influences the results. The model is equally solvable for any values of positive and negative ions temperatures. However, as the ions and the neutrals have similar masses, these species

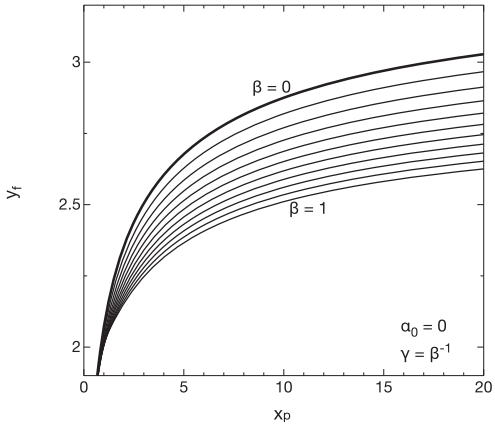

Figure 2. Floating potential y_f as a function of the probe radius x_p for cylindrical geometry for $\alpha_0 = 0$ for β from 0 (bold line) to 1 (full lines) in 0.1 β steps.

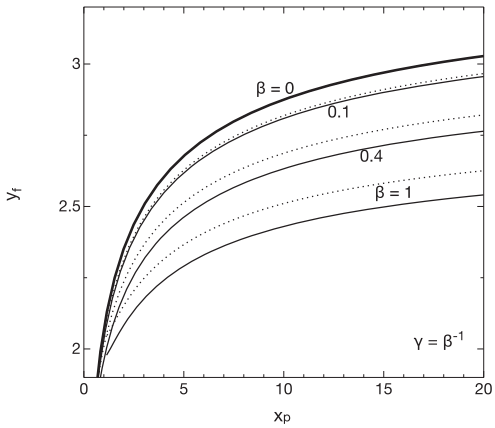

Figure 3. Floating potential as a function of the probe radius x_p for cylindrical geometry for $\alpha_0 = 0.1$ for β from 0 (bold line) to 1 (full lines). Floating potential for $\alpha_0 = 0$ (dotted lines) are plotted for comparison.

will be thermalized as long as the surrounding plasma is much larger than the probe region and is sufficiently homogeneous. The electrons, having much smaller mass, have very weak energy transfers during their collisions with the ions, and have their own temperature. This assumption is usually used in theoretical work [31] and has been verified experimentally [26, 32]. In mathematical terms, $\beta = \gamma^{-1}$, and we may speak of β as the dimensionless ion temperature, for both positive and negative ions. In the case of $\beta = 0$, the parameter α_0 disappears in (12) and (14), and the solution for arbitrary α_0 is the bold line in figure 2, the pure ABR solution.

For $\alpha_0 \neq 0$ and for increasing β, there will be more ions to reach the probe thanks to the additional thermal energy of

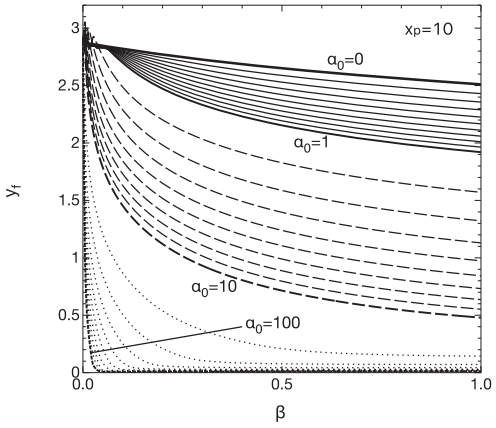

Figure 4. Floating potential as a function of the ion temperatures β for cylindrical geometry for $\gamma = \beta^{-1}$ for α_0 values of $\alpha_0 = 0$ (bold line), [0.1, 1] (full lines), [2, 10] (dashed lines), and [20, 100] (dotted lines).

the positive ions, but there will also be warmer negative ions to slow down the positive ions. We see that the influence of β is double. In figure 3, we compare the cases of $\alpha_0 = 0$ in dotted lines and $\alpha_0 = 0.1$ in full lines, and observe that the floating potential decreases for β in the range [0,1], the increased energy of the positive ions being the most important effect.

In figure 4, we show the dependance of the floating potential on β, for various α_0 values for constant $x_p = 10$. The plots for other x_p values are similar. The general trend of decreasing floating potential for increasing ion temperature is well observed. We see in figure 4 that the floating potential is very sensitive to the negative ions population density, and not so sensitive to the ion temperature. We may note in the upper left corner in figure 4, although it cannot be seen clearly, that for very low ion temperature ratios ($\beta < 0.075$) the floating potential is slightly higher for some $\alpha_0 \neq 0$ values than the floating potential for $\alpha_0 = 0$. It is clearer to plot the dependance of the floating potential on the electronegativity parameter α_0 for some selected values of ion temperature β and constant probe radius $x_p = 10$, as we show in figure 5. For very small ion temperatures, there is a range in α_0 between 1 and 6 where the floating potential oscillates with changing α_0 (dashed lines in figure 5). The nature of this oscillation is the same as that of the stratified electronegative pre-sheath, about which much has been written in the past two decades. However, the difference in the floating potential between $\beta < 0.075$ and pure ABR ($\beta = 0$) is less than 0.1, or 26 mV for $T_e = 3000$ K. Such small ion to electron temperature ratio may be unrealistic and such small difference in the floating potential is definitely difficult to measure.

For higher β values, the influence of the electronegativity is steady, decreasing the floating potential for all α_0, although with different sensitivity (full lines in figure 5). Higher electronegativity values ($\alpha_0 \gtrsim 4$) have a very strong influence for $\beta < 0.1$, and a further increase in β decreases the floating potential less abruptly.

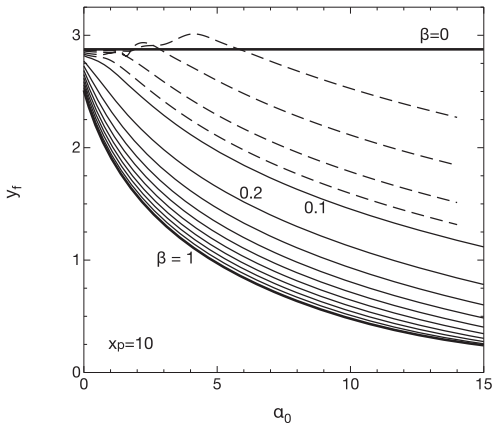

Figure 5. Floating potential as a function of the electronegativity parameter α_0 for cylindrical geometry for $\beta = 0$ (bold line), β in the range [0.1, 0.9] (full lines), and $\beta = 1$ (bold line) for $\gamma = \beta^{-1}$. Also, plotted as a reference, the oscillating solutions for $\beta = 0.01$, 0.025, 0.05, 0.075 (dashed lines).

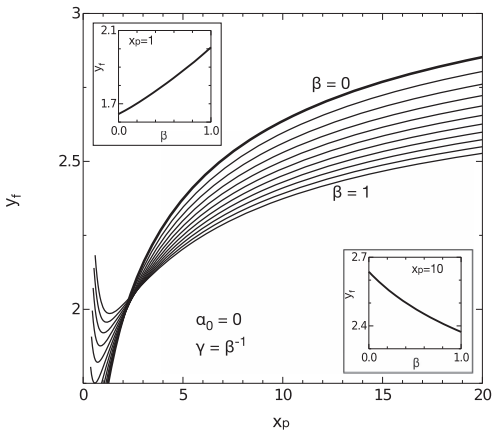

Figure 6. Floating potential as a function of the probe radius x_p for spherical geometry for $\alpha_0 = 0$ for β from 0 (bold line) to 1 (full lines). In the small inserts, the floating potential is plotted as a function of the ion temperature β for $x_p = 1$ (top left) and $x_p = 10$ (bottom right).

3.2. Asymptotic limit cases

In this section we will discuss two limit cases for the electronegativity value α_0:

- In the lower limit, still considering $\alpha_0 \neq 0$, the electron current is predominant over the negative ion current collected by the probe. Thus, an increase in the electronegativity has the effect of increasing the positive ion population density and, as a consequence, the positive ion current. For the electron current to compensate the increase in positive ion current, the floating potential must decrease through the negative exponential in (23).
- In the higher limit, the negative ion current is predominant due to the α_0 factor multiplying in (24), except for $\beta \to 0$. In this case, the y_f against β plot converges to a line. This is the only possible behaviour, as we see that for one single negative species, the floating potential is a value that depends only on the relative temperature. If the single negative species is negative ions, under the assumption $\beta = \gamma^{-1}$, the relation between the positive ion temperature and the negative ion temperature is one, and therefore, there is a single y_f' value, relative to the negative ion temperature. Thus, the floating potential relative to the electron temperature is

$$y_f = -\frac{e\phi}{k_B T_e} = -\frac{e\phi}{k_B T_-}\frac{T_-}{T_e} = \beta y_f' \tag{25}$$

giving a straight line that crosses the origin. For very low β values, the negative ions disappear from the sheath, whatever the α_0 value is, leaving the electrons to rule the behaviour of the positive ions in the sheath. In the case of the oxygen plasma that we study in this paper, the positive and negative ion masses are the same, and the value of y_f', having both ions the same mobility, should be $y_f' = 0$. However, as the negative ions mobility is not much higher than that of the positive ions, the Maxwellian approximation to the behaviour of the negative ions is inappropriate. We deduce that, in the case of the negative ion current being greater than the electron current (giving a very small floating potential), the results of this model would not be applicable. In order to make the calculations for this case, the same treatment should be applied to both ion species [2, 10].

In the solutions obtained with the model studied in the present paper, the linear asymptotic limit is found for $\alpha_0 = 10^5$, giving $y_f' = 1.72 \times 10^{-3}$ (for that α_0 value) which is below the range of measurability and beyond the range of the applicability of this model. Although not appreciable in the case under study, there could be an intermediate α_0 range where the behaviour of the floating potential is ruled by the electron current for low β values, but not for higher β values. We can see that parameter γ in (24) may increase the negative ion current enough to make it comparable to the electron current, and thus for higher β values the floating potential is modified by the presence of negative ions.

3.3. Results for spherical geometry

We now show the results of the model for a variety of plasma parameters in spherical geometry. We will use the value of $\kappa = \frac{5}{3}$. In this case, the geometrical compression is a stronger pre-sheath mechanism, and a smaller electric field is needed to accelerate the positive ions in order to create the sheath. A less intense electric field implies a flatter potential in the pre-sheath, which is consequently longer and requires a longer distance from the axis to reach the quasineutral solution.

In figure 6, we show the floating potential for $\alpha_0 = 0$ depending on the positive ion temperature. The behaviour of

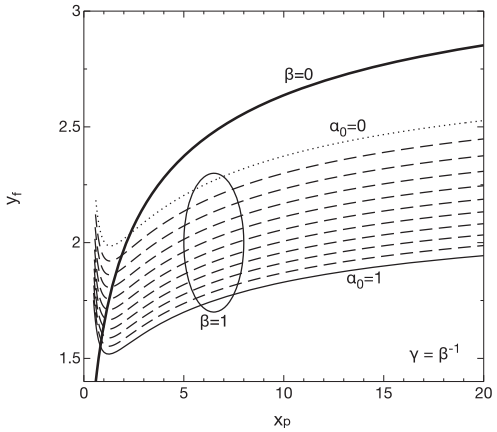

Figure 7. Floating potential as a function of the probe radius x_p for spherical geometry for $\beta = 0$ (bold line), and for $\beta = 1$, $\alpha_0 = 0$ (dotted line), α_0 in the range [0.1, 0.9] (dashed lines) and $\alpha_0 = 1$ (full line).

the floating potential for large spherical probes, with the probe radius x_p greater than approximately 2.5, is the same as for cylindrical probes, that is, the thermal motion of the positive ions is an additional source of energy for them to reach the probe, and therefore the floating potential is reduced, allowing more electrons to compensate the increase in positive ion current. In contrast, for smaller spherical probes, with the probe radius x_p lower than approximately 2.2, the floating potential may increase for higher positive ion temperatures. This anomalous behaviour can only occur in a very special set of circumstances, which will be studied in the next section.

For increasing α_0 values, we again see that the most important effect of the inclusion of negative ions is an increase in the positive ion population density in the plasma, and therefore in the positive ion current. The floating potential decreases, as shown in figure 7 for the particular case of ion temperature $\beta = 1$ (we again study the case of equal positive and negative ion temperatures, $\beta = \gamma^{-1}$).

In figure 8, we show analogous plots to figures 4 and 5, in this case solved for spherical geometry. We show that the behaviour of the floating potential is very similar for this probe radius. The same features can be found in this plot, especially the oscillations for very low ion temperature. In figure 9, we show the same plots again, in this case for the probe radius x_p equating 1. We see in this figure that the floating potential behaviour changes, unlike in cylindrical geometry where all probe radii give similar plots. The floating potential, for low electronegativity parameter values α_0, increases with the ion temperature, following the anomalous behaviour already shown in 6. It is remarkable though that for higher electronegativity parameter values, the results of the model are almost insensitive to the ion temperature for β greater than 0.3. The oscillations due to the stratified pre-sheath appear again for very low, unrealistic ion temperature values.

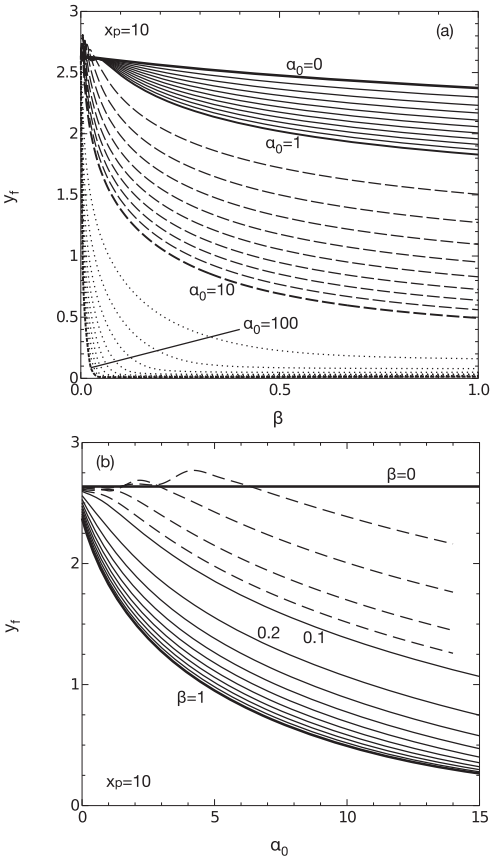

Figure 8. Floating potential for $x_p = 10$ as a function of the ion temperature β for spherical geometry for $\gamma = \beta^{-1}$ for several α_0 values (a), and as a function of the electronegativity parameter α_0 for various β values (b).

3.4. Anomalous floating potential behaviour for small probe radii in spherical geometry

As shown in figure 9, the floating potential increases with increasing ion temperature β, for small probe radii in a range of α_0 values. We analyse this trend by analysing the positive ion density profiles for different plasma conditions. This plot can be obtained by simply solving the energy balance equation (14) for each point of the potential profile. We show the positive ion density profiles in figure 10. We see that the positive ion density initially decreases as the positive ions accelerate in their fall into the probe. After the minimum of the positive ion density profile, the geometric compression increases the positive ion density. This decrease in the positive ion density due to the acceleration of the ions is less important for smaller dimensionless positive ion currents, or conversely the geometric compression is more important. In

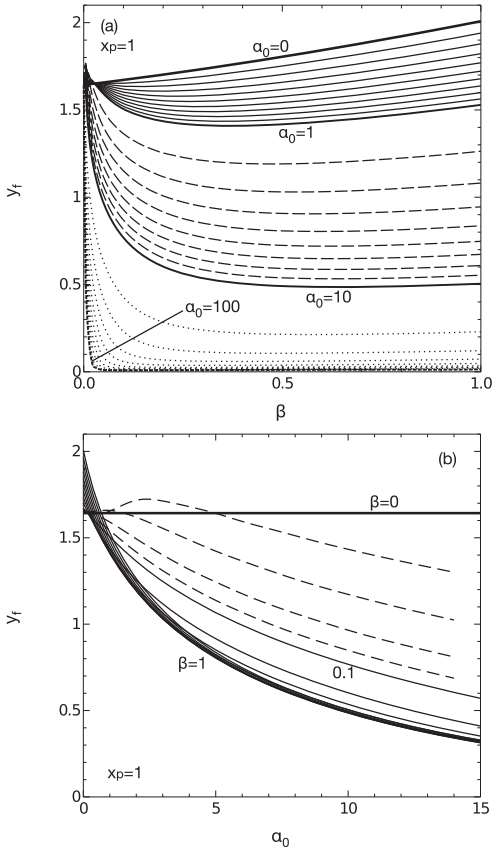

Figure 9. Floating potential for $x_p = 1$ as a function of the ion temperature β for spherical geometry for $\gamma = \beta^{-1}$ for several α_0 values (a), and as a function of the electronegativity parameter α_0 for various β values (b).

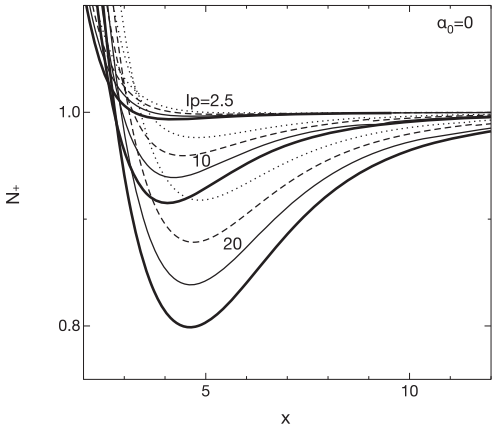

Figure 10. Positive ion density profile for several dimensionless positive ion current for spherical geometry for $\beta = 0$ (bold lines), for $\beta = 0.2$ (full lines), $\beta = 0.5$ (dashed lines) and $\beta = 1$ (dotted lines), for $\gamma = \beta^{-1}$.

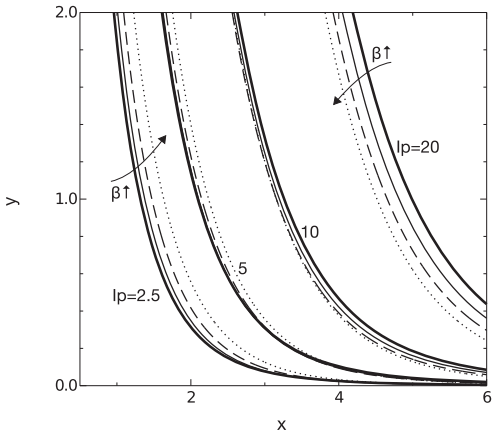

Figure 11. Potential profile for several dimensionless positive ion currents for spherical geometry for $\beta = 0$ (bold lines), for $\beta = 0.2$ (full lines), $\beta = 0.5$ (dashed lines) and $\beta = 1$ (dotted lines), for $\gamma = \beta^{-1}$.

all cases, the increase of the ion temperature increases the positive ion density and raises the minimum. Except for smaller positive ion currents, the positive ion density is ever increasing and does not have a minimum. This plot shows that the geometrical compression is stronger than the acceleration of the ions due to the free fall for lower positive ion currents.

When the floating potential is calculated, smaller positive ion currents correspond to smaller probe radii: in the case of small probe radius, an increase of the ion temperature causes the pressure of the positive ion gas to increase, exerting a force away from the probe, thus making it more difficult for the ions to reach the probe. We show in figure 11 the potential profiles for increasing ion temperature β for several positive dimensionless ion currents. In this figure, it is clear that, for higher positive ion currents, the pressure of the positive ion gas helps the ions to reach the probe (requiring a lower potential to get the same positive ion current), and that, for smaller positive ion currents, this pressure hinders the free fall of the ions into the probe (forcing a higher potential to maintain the same positive ion current). As a conclusion, for this latter case, an increase in the positive ion temperature translates into an increase of the outward pressure and an increase of the potential profile, and hence an increase in the floating potential.

4. Conclusions

In this paper, we have solved the radial fluid model for a Langmuir probe in the presence of both positive and negative

ions for non-zero ion temperatures. We have applied this solution to the obtention of the floating potential for an electronegative oxygen plasma. We have shown that the influence of the negative ions is restricted to the modification of the positive ions population density in the plasma, due to the high mass of negative ions compared to the mass of electrons. This greater positive ion population density in the plasma increases the floating potential as a consequence of the higher positive ion current value collected by the probe.

We have found the consequences of the stratified electronegative pre-sheath for very low negative ion temperatures, and we have found that the difference between this case and the cold negative ions case is very small and beyond the precision of usual measurement methods. The geometric pre-sheath mechanism for both cylindrical and spherical geometries is not strong enough to eliminate the stratified electronegative pre-sheath completely.

We have shown that the main effect of the positive ion temperature is to serve as an additional source of energy for the ions to reach the probe. However, there is a range of small probe radii in spherical geometry for which the additional energy of the positive ions is translated directly in an increase in the potential profile, and, as a consequence, an increase in the floating potential. We have found that the floating potential is sensitive to the negative ion population density, and thus provides a convenient procedure for measuring the negative ions population.

ORCID iDs

Guillermo Fernando Regodón https://orcid.org/0000-0002-1782-9953
José Ignacio Fernández Palop https://orcid.org/0000-0002-2081-2095
Antonio Tejero-del-Caz https://orcid.org/0000-0002-9147-7909
Juan Manuel Díaz-Cabrera https://orcid.org/0000-0002-7388-7373

References

[1] Kostov K G, Machida M, Prysiazhnyi V and Honda R Y 2015 *Plasma Sources Sci. Technol.* **24** 025038
[2] Gyergyek T and Kovačič J 2017 *Phys. Plasmas* **24** 063505
[3] Popov T K, Dimitrova M, Ivanova P, Kovačič J, Gyergyek T, Dejarnac R, Stöckel J, Pedrosa M A, López-Bruna D and Hidalgo C 2016 *Plasma Sources Sci. Technol.* **25** 033001
[4] Merlino R L, Heinrich J R, Kim S H and Meyer J K 2012 *Plasma Phys. Control. Fusion* **54** 124014
[5] Jaiswal S, Bandyopadhyay P and Sen A 2016 *Plasma Sources Sci. Technol.* **25** 065021
[6] Lampe M 2001 *J. Plasma Phys.* **65** 171–80
[7] Allen J E, Boyd R L F and Reynolds P 1957 *Proc. Phys. Soc.* **70** 297–304
[8] Chen F F 1965 *J. Nucl. Energy* **7** 47–67
[9] Kuhn S, Riemann K U, Jelić N, Tskhakaya D D, Tskhakaya D and Stanojević M 2006 *Phys. Plasmas* **13** 013503
[10] Gyergyek T and Kovačič J 2017 *Phys. Plasmas* **24** 063506
[11] Tejero-del Caz A, Fernández Palop J, Díaz-Cabrera J, Regodón G, Carmona-Cabezas R and Ballesteros J 2017 *J. Comput. Phys.* **350** 747–58
[12] Tejero-del Caz A, Fernández Palop J I, Díaz-Cabrera J M and Ballesteros J 2016 *Plasma Sources Sci. Technol.* **25** 01LT03
[13] Fernández Palop J I, Ballesteros J, Colomer V and Hernández M A 1996 *J. Phys. D: Appl. Phys.* **29** 2832
[14] Fernández Palop J I, Ballesteros J, Hernández M A, Morales Crespo R and Borrego Del Pino S 2004 *J. Phys. D: Appl. Phys.* **37** 863
[15] Fernández Palop J I, Ballesteros J, Hernandez M A, Morales Crespo R and Borrego Del Pino S 2004 *J. Appl. Phys.* **95** 4585
[16] Fernández Palop J I, Ballesteros J, Hernández M A and Morales Crespo R 2007 *Plasma Sources Sci. Technol.* **16** S76–86
[17] Fernández Palop J I, Ballesteros J, Hernández M A and Morales Crespo R 2002 *J. Appl. Phys.* **91** 2587
[18] Kono A 2001 *J. Phys. D: Appl. Phys.* **34** 1083
[19] Kono A 1999 *J. Phys. D: Appl. Phys.* **32** 1357–63
[20] Kono A 2003 *J. Phys. D: Appl. Phys.* **36** 465–72
[21] Franklin R N and Snell J 2000 *J. Phys. D: Appl. Phys.* **33** 1990
[22] Franklin R and Snell J 1998 *J. Phys. D: Appl. Phys.* **31** 2532–42
[23] Franklin R 2000 *Plasma Sources Sci. Technol.* **9** 191–8
[24] Díaz-Cabrera J M, Fernández Palop J I, Morales Crespo R, Hernández M A, Tejero-del Caz A and Ballesteros J 2014 *Measurement* **55** 66–73
[25] Regodón G F, Fernández Palop J I, Tejero-del Caz A, Díaz-Cabrera J M, Carmona-Cabezas R and Ballesteros J 2017 *Phys. Plasmas* **24** 103516
[26] Fernández Palop J I, Ballesteros J, Colomer V and Hernández M A 1996 *J. Appl. Phys.* **80** 4282–91
[27] Swift J and Schwar M 1970 *Electrical Probes for Plasma Diagnosis* (London: Iliffe Books Ltd)
[28] Gudmundsson J, Kouznetsov I, Patel K and Lieberman M 2001 *J. Phys. D: Appl. Phys.* **34** 1100–9
[29] Mieno T, Kamo T, Hayashi D, Shoji T and Kadota K 1996 *Appl. Phys. Lett.* **69** 617–9
[30] Shintani H, Sakudo A, Burke P and McDonell G 2010 *Exp. Ther. Med.* **1** 731–8
[31] Franklin R 2002 *Plasma Sources Sci. Technol.* **11** A31–7
[32] Amemiya H 1990 *J. Phys. D: Appl. Phys.* **23** 999–1014

IOP Publishing Plasma Physics and Controlled Fusion
Plasma Phys. Control. Fusion **61** (2019) 095015 (9pp) https://doi.org/10.1088/1361-6587/ab3483

Floating potential calculation for a Langmuir probe in electronegative plasmas and experimental validation in a glow discharge

Guillermo Fernando Regodón[1], José Ignacio Fernández Palop[1], Juan Manuel Díaz-Cabrera[2] and Jerónimo Ballesteros[1]

[1] Departamento de Física, Universidad de Córdoba, E-14071 Córdoba, Spain
[2] Departamento de Ingeniería Eléctrica, Universidad de Córdoba, E-14071 Córdoba, Spain

E-mail: z62rehag@uco.es

Received 22 April 2019, revised 18 June 2019
Accepted for publication 23 July 2019
Published 13 August 2019

Abstract

A radial Langmuir probe sheath model is used to make a prediction of the floating potential of a Langmuir probe immersed in an electronegative plasma. The new electronegative plasma sheath model takes into account the positive ion and the negative ion thermal energies and is valid for any ion temperature value. The values predicted can be used for diagnosing and controlling an electronegative plasma, and we compare them with measurements of the floating potential in an Argon plasma and in a Neon plasma with with two distinct electron populations at different temperatures. We have found that the agreement is very good in a wide range of plasma pressure and discharge current values, and thus the model is applicable for electronegative plasmas. Moreover, the model can be used to measure the energy with which the ions will collide with the surface of the probe.

Keywords: Langmuir probe, floating potential, electronegative plasma, glow discharge, electron temperature, ion temperature

(Some figures may appear in colour only in the online journal)

1. Introduction

The Langmuir probe has been used in plasma laboratories since its invention more than eighty years ago, as it provides reliable local information in all kinds of plasmas. Nevertheless, the interpretation of the measurements made on a Langmuir probe immersed in a plasma requires a sound knowledge of the interaction between the probe and the plasma [1], the basic theories that model such interaction [2–4], and the limits of the validity of such theories. Despite the thorough research that has been performed in the scientific community in this field, there are still many aspects that are unclear [1, 5–7]. The importance of the understanding of the interaction between the Langmuir probe and the plasma can hardly be overstated: it is the simplest case of interaction between a plasma and a metallic surface. By means of the Langmuir probe measurement, we can characterize the plasma using the important plasma parameters: electron and ion densities and temperatures. Using these plasma parameters, the energy of the impact of the ions against a metallic surface can be related to the surface potential and the ion current.

The floating potential, that is, the potential reached by a metallic object immersed in a plasma, is of great significance in plasma physics. Dust grains can be considered as spherical Langmuir probes biased to their floating potential so that the collected net current is zero [8]. Metallic surfaces can be treated to obtain the desired modification by leaving the metallic object isolated in the plasma chamber, so that it attains its floating potential [9]. Moreover, the floating potential of the Langmuir probe is an important test of validity of Langmuir probe sheath models [10]. Electrons have higher mobility than ions. Therefore, a metallic probe in the bulk of plasma discharge at the same potential as the surrounding plasma collects more electrons than ions. In order to reach a steady situation and thus zero net current (positive

ion current minus electron and negative ion currents) the metallic surface becomes negatively charged, which is equivalent to being biased negatively to the floating potential (V_f). Thus, the measurement of the floating potential is very simple, although its theoretical prediction is usually a difficult task. A precise description of positive ions, negative ions and electrons is required in order to provide a theoretical floating potential value similar to the experimental one.

Regarding the movement of the positive ions towards a negatively biased Langmuir probe, there are two sets of theories, the orbital theory and the radial theory. The orbital theory, first proposed by Mott-Smith and Langmuir, which was developed by Laframboise based on the work by Bernstein and Rabinowitz, assumes that the positive ions will trace orbits from the quasineutral plasma around the probe, some of them reaching the probe and others orbiting back to the unperturbed plasma [2, 3, 11]. The radial theory, developed by Allen, Boyd and Reynolds for spherical probes and adapted by Chen to cylindrical probes (ABR-C), assumes that the positive ions fall radially towards the probe and can be described as a fluid [4, 12]. The limit of the validity of the two incompatible basic models for the movement of the positive ions in a plasma sheath in their fall towards the probe through the sheath is still not clear. A transition between both models has been found in experiments [13] and computer simulations [14]. The radial ABR-C model assumes cold ions and a Maxwellian Electron Energy Distribution Function (EEDF). Fernández Palop *et al* extended the ABR-C model to include the positive ion temperature but it still relied on Maxwellian electrons [15–17]. In the solution of this model, a mathematical singularity was found when the ions reach their local speed of sound. Recently, a complete numerical solution from the plasma to the probe has been obtained for any ion-to-electron temperature ratio for cylindrical and spherical probes, which allows us to obtain the potential profile of the sheath and the other physical magnitudes around the probe by bypassing the singularity [18, 19].

In magnetized plasmas, the direction of the magnetic field together with the Larmor radii of the particles can be used to determine the negative ion populations [20, 21]. We propose the measurement of the floating potential as a means of determining the negative ion population density in situ ations where other methods for magnetized plasmas are unavailable. In a recent paper, the authors calculated the floating potential for an electronegative plasma in which the radial model was used for the positive ions and the ions had non-negligible temperature in comparison with the electron temperature [19]. The electrons and the negative ions were assumed to follow a Maxwellian distribution with the negative ions having a lower temperature. However, electronegative plasmas almost always present a more complex chemical composition. Also, the assumption of Maxwellian negative ions cannot easily be confirmed, so that an experimental verification of the model is difficult. For these reasons, in order to experimentally confirm the model, we use the simplest case of a plasma with one positive ion species and two negative species, that is, an electropositive plasma with two distinct electron populations at different temperatures, or bi-Maxwellian EEDF [22–26], the cold electron population assuming the role of the negative ions. The model, when confirmed, will be applicable to electronegative plasmas in which the assumptions of the model are valid.

In this article, we study the floating potential in an electropositive glow discharge with bi-Maxwellian EEDF in order to check the validity of a Langmuir probe sheath model immersed in an electronegative plasma. We use the values obtained from the measurement of the EEDF [27, 28] in the radial model that considers non-zero ion temperature, to predict the value of the floating potential with respect to the plasma potential. We have found good agreement between the theory and the experiments using a wide range of pressure values and discharge currents. Thus, we also extend the validity of the radial model to the range of parameters in which the Maxwellian approximation is inappropriate.

2. Theoretical model

The radial model that we use in this article considers non-zero ion-to-electron temperature ratio. The effect of the positive ion temperature is to allow the positive ion pressure to be relevant in the model, allowing a finite ion sound velocity, with the characteristic change of fluid behavior from subsonic to super-sonic flow [18]. The model considers Poisson's equation in cylindrical coordinates with two negative populations, the negative ions and the electrons, with different characteristic parameters and one species of positive ions. The negative species experience a retarding field, so the use of the Boltzmann relation for both negative species is valid. Indeed, the negligible electron mass causes the dynamics of the electrons to be governed by the balance between the electric field and the electron pressure. The validity of the Boltzmann relation for negative ions was formally proved by Franklin and Snell [29] for collisionless and weakly collisional plasmas in the case of constant collision frequency. The Boltzmann relation for the negative ions is broken when one considers the mechanisms of attachment and detachment of electrons to negative ions and the mechanism of ionization of neutrals to form positive ions, which we suppose occurs in a much larger length scale than the Debye length, which is the scale of the collisionless sheath.We assume that the charge of the ions is $\pm e$. Let an infinite cylindrical Langmuir probe to be centered and aligned to the axis of symmetry. Poisson's equation for the electric potential $\phi(r)$, referred to the plasma potential, can then be written as follows for negative values of $\phi(r)$.

$$\begin{aligned}\frac{1}{r}\frac{\mathrm{d}}{\mathrm{d}r}\left(r\frac{\mathrm{d}\phi(r)}{\mathrm{d}r}\right) &= -\frac{e}{\varepsilon_0}(n_+(r) - n_e(r) - n_-(r)),\\ n_e(r) &= n_{e,0}\mathrm{e}^{\frac{e\phi(r)}{k_\mathrm{B}T_e}},\\ n_-(r) &= n_{-,0}\mathrm{e}^{\frac{e\phi(r)}{k_\mathrm{B}T_-}},\end{aligned} \tag{1}$$

r being the distance to the axis of symmetry, $n_+(r)$ the positive ions density at r, $n_{e,0}$ and $n_{-,0}$ the electron and

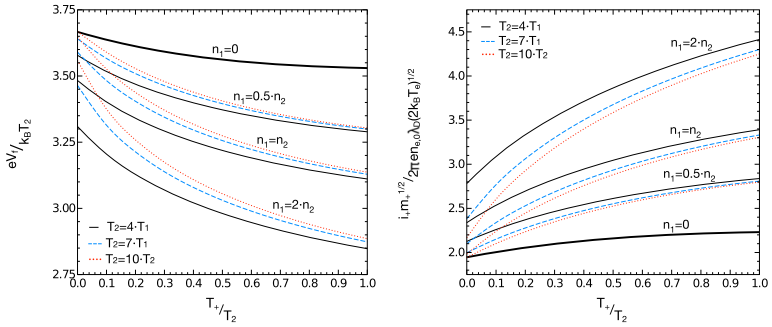

Figure 1. Theoretical floating potential, in $k_B T_e/e$ units, and positive ion current per unit length, in $m_+^{1/2}/2\pi e n_{e,0}\lambda_D(2k_B T_e)^{1/2}$ units, as a function of the positive ion to electron temperature ratio for an argon plasma with two distinct electron populations for $r_p = \lambda_D$.

negative ion densities in the plasma, respectively, and T_e and T_- the corresponding two negative species temperatures. In order to calculate the positive ion density, we consider its relation to the potential and the local ion gas partial pressure by means of the momentum balance equation

$$m_+ n_+(r) v_+(r) \frac{\mathrm{d}v_+(r)}{\mathrm{d}r} + e n_+(r) \frac{\mathrm{d}\phi(r)}{\mathrm{d}r} + \frac{\mathrm{d}p_+(r)}{\mathrm{d}r} = 0, \quad (2)$$

where m_+ is the mass of a positive ions, $v_+(r)$ stands for the ion velocity and $p_+(r)$ is the positive ion gas partial pressure. The partial pressure can be related to the positive ion temperature. We assume that the positive ion gas flow is adiabatic, so that the density and partial pressure can be related through a constant polytropic coefficient (or adiabatic constant) [16, 18, 19],

$$p_+(r) = k_B T_+ \frac{n_+(r)^\kappa}{n_{+,0}^{\kappa-1}}. \quad (3)$$

In this last equation, T_+ is the positive ion temperature in the plasma, and $n_{+,0}$ is the positive ion density in the plasma, that is related to the electron and negative ion densities in the plasma by means of the quasineutrality condition. We ignore ionization in the sheath, as well as collisions so that the positive ion current per unit length is constant and related to positive ion density and velocity by the continuity equation,

$$i_+ = e 2\pi r n_+(r) v_+(r). \quad (4)$$

This model can be solved numerically to obtain a potential profile, and all other physical magnitudes, continuously from the plasma to the probe, and to obtain the relation between the positive ion current and the probe potential for a given probe radius [18, 19]. The solution is found by matching the subsonic and the supersonic parts of the positive ion flow, which meet at the point where the positive ion flow reaches the local positive ion speed of sound. At this point, the equations have a singularity that is solved by forcing boundedness in the physical magnitudes. It is interesting to note that the solution makes no distinction between the sheath and the pre-sheath, but the model assumes that the solution reaches quasineutrality, and the quasineutral solution is found for a collisionless pre-sheath solution.

To obtain the floating potential, equality must be established between the positive ion current per unit length and the sum of the electron and negative ion currents per unit length. The latter are calculated for a probe of radius r_p as:

$$i_{e,-}(r_p) = e 2\pi r_p n_{e,-} \sqrt{\frac{k_B T_{e,-}}{2\pi m_{e,-}}}\, \mathrm{e}^{\frac{e\phi(r_p)}{k_B T_{e,-}}}. \quad (5)$$

For a given i_+ value, the potential profile $\phi(r)$ can be obtained, and hence both electron and negative ion currents, $i_{e,-}(r)$, for each distance to the axis r. The probe radius $r_p = r$ for which the equality between positive ion current and electron plus negative ion currents is found, is the radius of the probe for which zero net current is collected. From the potential profile, the floating potential ϕ_f can be obtained:

$$\phi_f = \phi(r_p). \quad (6)$$

Thus, the floating potential ϕ_f can be related to the probe radius r_p. The probe radius does not coincide, in general, with the radius of the probe in the experiments, so that it is necessary to test different i_+ values to get a probe radius close enough to the experimental one. The model is applicable to any negative ion species, and it can be used in the case that the second negative species is an electron. In figure 1, the theoretical floating potential and the corresponding theoretical ion current collected by the probeare shown for typical values of the plasma parameters, for $r_p = \lambda_D$, for an argon plasma with two electron populations, with densities n_1 and n_2 and temperatures T_1 and T_2, with $T_1 < T_2$. As the cold electron population increases, the floating potential decreases, while an increase in the electron temperatures implies an increase in the floating potential, in $k_B T_e/e$ units. The floating potential also increases, keeping all other parameters constant, as the quotient between the warm electron and the cold electron temperatures increases. The ion current has the opposite behavior to the floating potential: the ion current increases when the floating potential decreases. The cold electrons barely reach the probe when it is negatively biased, so the main effect of the cold electrons is to increase the ion population density in the plasma. On the other hand, when the warm electron population density is higher or when its

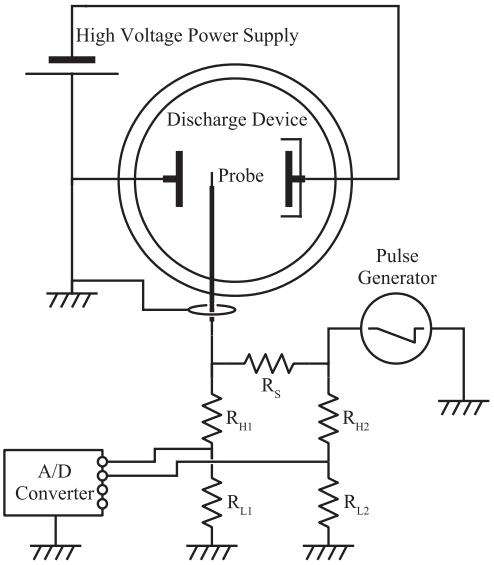

Figure 2. Schematics of the experimental device.

temperature is higher, the warm electrons penetrate more easily in the sheath and more electrons reach the probe, thus requiring a more negative probe potential to repel the electrons for a given ion current. From the other point of view, with the same probe potential an increased warm electron population density in the sheath requires more ions and an increased ion current to produce an electropositive sheath.

As a summary, the assumptions that we make in this model are: presence of two coexisting Maxwellian negative populations, small negative species currents, fluid model valid for positive ions without ionization or collisions, non-zero positive ion temperature and adiabatic flow for positive ions with constant polytropic coefficient. More details are given in previous articles [16, 18].

3. Experimental device

The DC discharge is performed in a large Pirex cylinder, 31 cm inner diameter and 40 cm height. A high voltage low noise power supply, configured as current supply, is connected to two circular 8 cm diameter stainless steel electrodes inside the cylinder. The distance between the electrodes is 15 cm, the anode being connected to ground. The gas entering the device is controlled by a mass gas flow controller, our experiment having a range of pressure between approximately 1 and 30 Pa. Figure 2 shows a simplified scheme of the experimental device with the elements that are relevant to the present work and more details of the discharge device can be found in the work by Díaz-Cabrera *et al* [13, 30, 31]. The power supply, model KEPCO BHK 2000-0.1MG, can be controlled as a constant potential source or as a constant current source. We choose to use it as a constant current source so that the plasma created in the plasma column does not change even if the temperature of the electrodes changes and consequently the volume of plasma close to them also changes. The discharge current is directly related to the charge carrier densities [32]. The discharge current thus becomes the governing variable in the experiments. After imposing the nominal value for the discharge current, both the discharge current and the discharge potential, which is limited to 2000 V, are measured. The DC discharge provides us with a reference potential, that is, the grounded anode. The glow discharge, with the wall far from the glow, allows the electron temperature to be very low, so that the positive ion temperature is not negligible. We assume that the positive ions are at room temperature, 300 K [10, 13, 30, 31, 33–35], and the electron temperatures that we measure are in the range [1500 K, 5000 K].

A cylindrical Langmuir probe is located between the electrodes, in the negative glow of the discharge, 8 cm away from the cathode where we have found the plasma to be more homogeneous. The dimensions are 6 mm long, 0.2 mm diameter, and the material of the probe is tungsten, to minimize secondary electron emission. The glass holder is carefully designed to perturb the plasma as little as possible around the base of the probe [30–32]. The probe is biased using a sawtooth signal that starts in the electron saturation zone of the *IV* characteristic. The Langmuir probe *IV* characteristic is measured using an analog-to-digital converter card PCI6122 from National Instruments. This card has four simultaneous, referenced-to-ground channels, with 16 bits of resolution, and takes $5 \cdot 10^5$ samples per second. An adaptation circuit, consisting of two voltage dividers and a series resistance, reduces the voltage to levels below 5V, the A/D card input ranges. Both shot noise and thermal noise have been calculated and proved to be negligible. A LabView Virtual Instrument controls all the process and makes the initial calculations: measurement of the plasma potential, the floating potential and the EEDF [31, 36]. The signal is smoothed in order to make the numerical derivation of the *IV* characteristic possible [1, 32]. For this fast A/D card, 2000 samples are taken in just 4 ms, which is fast enough to ensure that the temperature of the probe does not change during a measurement and, thus, the work-function of the probe surface is approximately constant and does not compromise the results [37]. The Langmuir probe is de-contaminated by electron bombardment, biasing the probe at a very high voltage for 10 min. Consecutive measurements were separated by one minute in order to ensure that the probe is at the same temperature for all the measurements.

4. Experimental results and discussion

In order to verify the validity of the model, we have performed three series of measurements of the floating potential of a Langmuir probe immersed in a plasma. The model is a radial Langmuir probe sheath model in an electronegative

plasma, and hence we have two distinct negative populations that, in the ion saturation part of the current to probe voltage characteristic, behave as fluids in equilibrium. That is, each negative population has its own density and temperature. However, it is known that electronegative plasmas almost always presents a more complex chemical composition. Besides, it is difficult to confirm that the negative ion population is Maxwellian, as the measurement of the negative ion energy distribution function is very difficult to perform. In order to verify and validate the model and the conclusions derived from it, we use electropositive argon and neon plasmas with two distinct, measurable Maxwellian electron populations, that is, with a bi-Maxwellian EEDF. As the model makes no assumption on the kind of negative species, it is applicable just by changing the mass of the negative ions for the mass of the electrons in (5).

The assumption of absence of collisions between positive ions and neutrals in the plasma sheath can be justified by calculating the mean free path λ_+ for the ion–neutral collision, for which we obtain values in around 1 mm for the low working pressure of the discharge [13, 30, 38, 39]; ten times the probe radius, $r_p = 0.1$ mm, or the Debye length, that is around of 0.1 mm in our measurements. We have also estimated the electron mean free path λ_e that is three orders of magnitude over the positive ion mean free path.

4.1. Separation of bi-Maxwellian distribution

The bi-Maxwellian electron population has been detected both in experiments [40] and in computer simulations [41]. According to the generally accepted results obtained by Hopkins and Graham for a DC plasma confined in a multipole magnetic plasma [1, 42], the directive high energy electrons that feed the plasma thermalize in the plasma creating the warm population. Collisions of the high energy electrons and the warm electrons, which ionize the neutrals in the bulk of the plasma, create the cold electrons. Methods for interpreting the two temperatures have been proposed [1, 7, 40]. However, for the present purpose, it is also necessary to find the values of the separated electron densities. The sensible approach to separate the two Maxwellian distributions is to obtain the values of the warm electrons, n_2 and T_2 from the tail of the EEDF, where the presence of the cold electrons is negligible, then subtract the warm Maxwellian distribution from the EEDF, and then obtain the values of the cold electrons, n_1 and T_1. In order to obtain the values of both the density and the temperature of an electron population, we use the well-known fact that the logarithm of the EEDF ($f(E)$) over the square root of the energy should be a straight line with respect to the energy, for a Maxwellian distribution

$$\log\left(\frac{f(E)}{\sqrt{E}}\right) = \log\left(\frac{2n}{\sqrt{\pi(k_B T)^3}}\right) - \frac{E}{k_B T}. \tag{7}$$

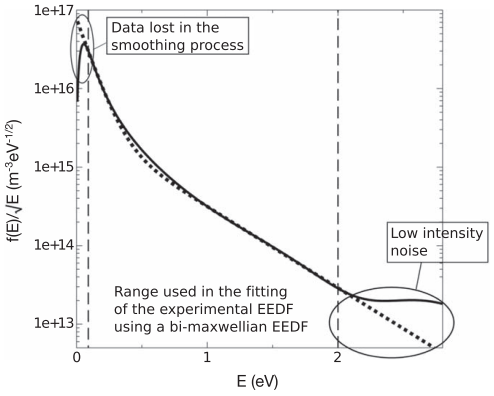

Figure 3. Experimental $f(E)$ over $\sqrt{E}$ (solid line) and bi-Maxwellian approximation (dotted line) for argon, pressure $P = 3.9$ Pa, discharge current $I_d = 2.0$ mA and discharge power $P_d = 2.58$ W. The energy range used in the calculations is $E \in [0.09\text{ eV}, 2.0\text{ eV}]$.

A linear regression should be performed over the appropriate part of the measured EEDF. The beginning of the EEDF should not be trusted [32]. The tail of the EEDF is affected by the noise that the smoothing process could not remove and by the increase in the ion current in the ion saturation zone, so that we truncate the EEDF when it deviates from an exponential shape [16, 32]. In the example in figure 3, measured in argon at 3.9 Pa and with a discharge power of 2.58 W, the EEDF is restricted to the range $E \in [0.09\text{ eV}, 2.0\text{ eV}]$ for calculations. The bi-Maxwellian fit is plotted with dots.

When this process is automatized, some criteria could be established to define the tail of the EEDF. However, as these calculations are done fast in a standard computer, and the EEDF that we measure has usually less than 200 points, we decided to calculate the optimal separation of the bi-Maxwellian EEDF using a brute force method. We iteratively calculate the separation of the bi-Maxwellian EEDF for shorter tails, starting with the assumption that the tail takes all the EEDF. We then compare the measured EEDF, $f(E)$, with the recomposed theoretical $f_{bi}(E)$, using a minimum squared error (MSE) method with the error parameter:

$$\mathrm{MSE} = \frac{\int_{E_{min}}^{E_{max}} [f(E) - f_{bi}(E)]^2 \cdot f(E)\,dE}{n_e^3 (E_{max} - E_{min})}. \tag{8}$$

Note that we weigh the MSE error with the experimental EEDF. There is a minimum of the MSE error which we take as the best fit of the experimental EEDF, $f(E)$, to a bi-Maxwellian EEDF, $f_{bi}(E)$. The whole calculation of the optimal separation of the bi-Maxwellian EEDF takes a fraction of a second in a standard computer. Two examples, with the separated cold (solid blue line) and warm (solid red line) electron populations and the added theoretical bi-Maxwellian electron population (dotted black line), are shown in figure 4.

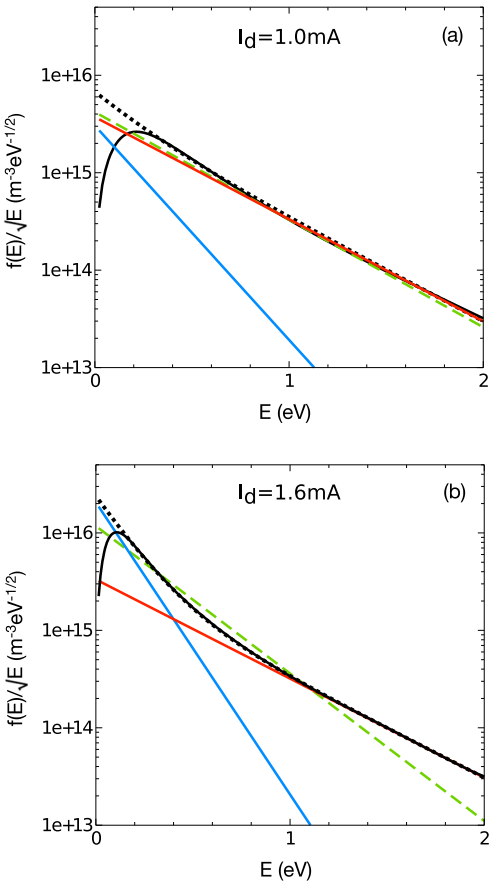

Figure 4. Comparison of experimental electron energy distribution function $f(E)$ (solid black line), bi-Maxwellian approximation (dotted black line), separated cold (solid blue line) and warm (solid red line) electron populations and Maxwellian approximation (dashed green line), for argon at $P = 10.2$ Pa pressure, for discharge currents 1 mA (a) and 1.6 mA (b).

We also show the Maxwellian population that would result from the density and temperature values obtained by direct integration of the experimental EEDF (dashed green line). It can be observed that, even in the cases in which the EEDF apparently is Maxwellian, the bi-Maxwellian approximation is a better fit to the EEDF. The low energy electron population (below 0.2 eV) is recovered with both Maxwellian and bi-Maxwellian fits. Therefore, the electron density obtained using these fits is higher than the one obtained from the direct integration of the EEDF.

4.2. Probe measurements and verification of the model

In order to compare the experimental floating potential with the theoretical one derived from the radial model that takes

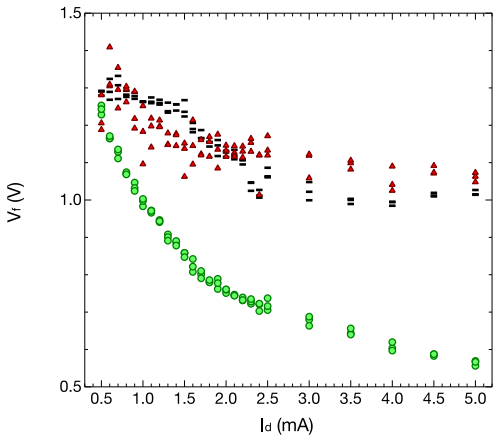

Figure 5. Comparison of measured floating potential V_f (horizontal lines), theoretical V_f using bi-Maxwellian EEDF (red triangles) and theoretical V_f using Maxwellian EEDF (green circles), versus discharge current I_d for argon at $P = 3.9$ Pa pressure.

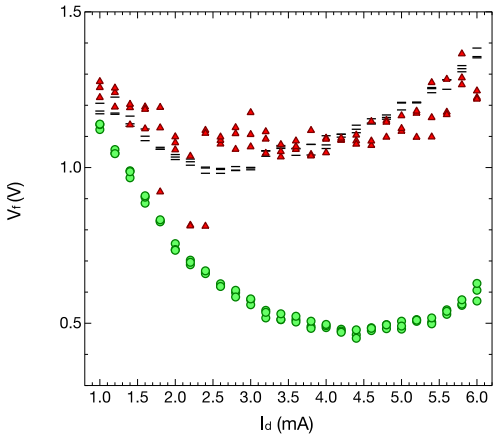

Figure 6. Comparison of measured floating potential V_f (horizontal lines), theoretical V_f using bi-Maxwellian EEDF (red triangles) and theoretical V_f using Maxwellian EEDF (green circles), versus discharge current I_d for argon at $P = 10.2$ Pa pressure.

into account positive ion temperature and two negatively charged particle populations, two series of measurements, for different background pressures, have been performed in an argon plasma and one in a neon plasma. For each measurement, the following calculations are made using the current to probe voltage characteristic:

- The plasma potential is obtained using the inflection point method [30, 32, 36, 43].
- The EEDF is obtained by means of the Druyvestein formula [27, 32].

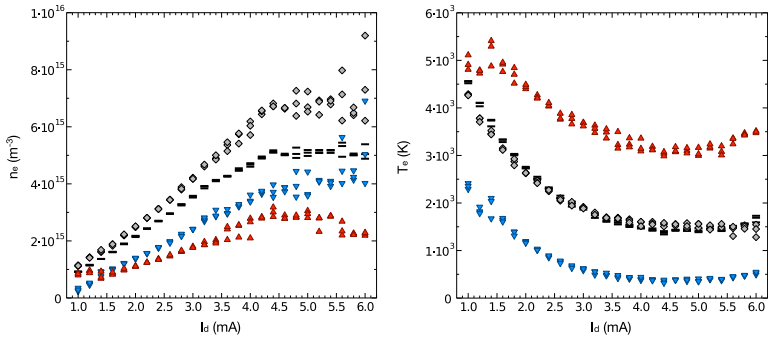

Figure 7. Comparison of electron density and temperature obtained from integration of the measured EEDF (horizontal lines), separated cold (blue inverted triangles) and warm (red triangles) electron populations and aggregated bi-Maxwellian electron population (rhombus), versus discharge current I_d for argon at $P = 10.2$ Pa pressure.

- The temperatures and the population densities of the separate cold and warm electron populations are obtained using the method described in the previous section, and the aggregated population density and the mean temperature are calculated by the integration of the EEDF.
- The Debye length is obtained using the warm electron population density and temperature, $\lambda_D = \sqrt{\frac{\varepsilon_0 k_B T_e}{e^2 n_{e,0}}}$, and the dimensionless probe radius is calculated, $x_p = r_p/\lambda_D$.
- The dimensionless numbers that characterize the plasma [18, 19] are obtained: the electronegativity parameter $\alpha_0 = n_{1,0}/n_{2,0}$, the ratio between the warm and the cold electron temperatures $\gamma = T_2/T_1$, and the ratio between the positive ion temperature and the warm electron temperature $\beta = T_+/T_2$.
- The floating potential in $k_B T_2/e$ units is obtained using the model [18, 19].

The ion temperature is not measured, and is estimated to be the room temperature, $T_+ = 300$ K. However, the calculations do not depend greatly on the positive ion temperature value used in the model related to the warm electron temperature, which is in the order of 5000 K. The calculation of the floating potential using an ion temperature 10% higher (330 K) produces a floating potential that is, in the worst case, 0.4% smaller.

For argon, with a constant pressure of $P = 3.9$ Pa, the discharge current was changed from $I_d = 0.5$ mA to $I_d = 2.5$ mA in 0.1 mA steps and from $I_d = 2.5$ mA to $I_d = 5.0$ mA in 0.5 mA steps. We measure the difference between the plasma potential and the potential for which the net current is null, both referenced to ground, and we give this result (positive) as the floating potential. Three measurements where performed for each discharge current. Figure 5 shows the comparison of the measured floating potential (horizontal lines), the theoretical floating potential using the bi-Maxwellian EEDF (red triangles) and the theoretical floating potential using a Maxwellian EEDF using the electron density and temperature from the experimental EEDF (green circles). We see that, even though the bi-Maxwellian floating potential is subjected to greater uncertainty, the trend clearly follows the experimental floating potential. Initially, the floating potential decreases, as the cold electron population increases, but this decrease is later compensated by the increase in the warm to cold electron temperature ratio. The Maxwellian floating potential gives the correct floating potential only for the lowest discharge currents, since in this case the cold electron population density is small, and the EEDF can be rendered Maxwellian, as in figure 4(a).

Another series of measurements was performed in argon, for a constant 10.2 Pa pressure. The discharge current varied from $I_d = 1.0$ mA to $I_d = 6.0$ mA in 0.2 mA steps. The results are plotted in figure 6. It can be seen that the bi-Maxwellian EEDF radial model again follows the correct value of the floating potential. As in the previous series of measurements in argon plasma, the floating potential that we calculate using the Maxwellian electron temperature and density from the EEDF is erroneous but for very low discharge currents. In figure 7 we plot the electron densities and temperatures. The cold electron density increases more than the warm electron density, and soon the cold electrons become predominant in the discharge, but the warm electrons have more energy and their influence in the floating potential is very important, as can be concluded from figure 6. The cold electron temperature reaches the lowest values 500–700 K and the warm electron temperature reaches 3000–3500 K, so that the positive ion to warm electron temperature ratio increases as we increase the discharge current. A similar analysis in the 3.9 Pa experiments shows that the trends in the electron population densities and temperatures are the same (figure 8), with the influence of an increase in the pressure being that it decreases the warm electron temperature, which is consistent with more frequent collisions in the plasma volume [1, 42]. Both electron population densities increase with pressure, albeit the cold electron population density increases more, so that the mean temperature, which takes into account both electron populations, decreases.

Another series of measurements was performed in neon, at a working $P = 23.6$ Pa pressure. Three measurements

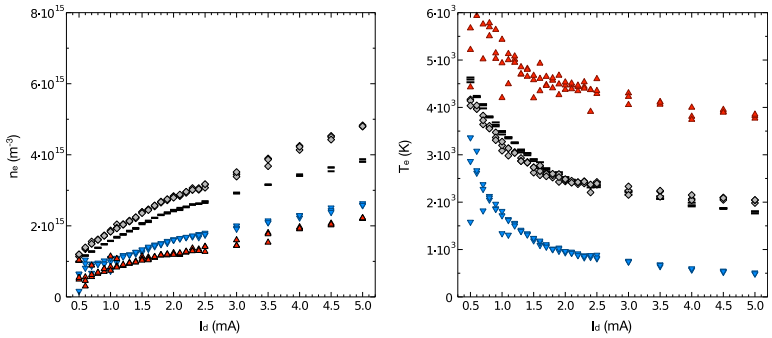

Figure 8. Comparison of electron density and temperature obtained from integration of the measured EEDF (horizontal lines), separated cold (blue inverted triangles) and warm (red triangles) electron populations and aggregated bi-Maxwellian electron population (rhombus), versus discharge current I_d for argon at $P = 3.9$ Pa pressure.

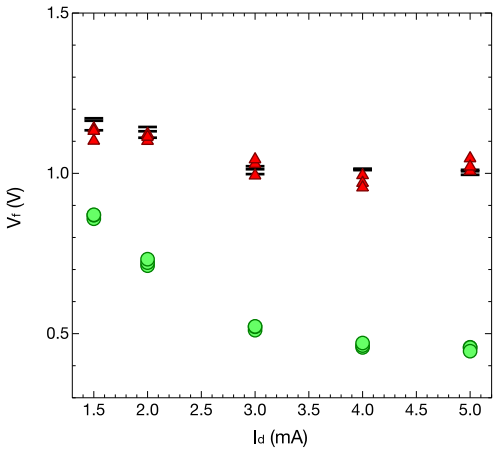

Figure 9. Comparison of measured floating potential V_f (horizontal lines), theoretical V_f using bi-Maxwellian EEDF (red triangles) and theoretical V_f using Maxwellian EEDF (green circles), versus discharge current I_d for neon at $P = 23.6$ Pa pressure.

where performed for $I_d = 1.5$, 2.0, 3.0, 4.0 and 5.0 mA. In figure 9, we can see that the floating potential is more precise using the bi-Maxwellian EEDF rather than the value obtained from the Maxwellian EEDF, compared to the experimental floating potential. In the conditions of the discharge, there is no qualitative difference between the two gases. The only quantitative difference is that the pressure needs to be increased for neon, as a lower pressure does not allow for a discharge with the same discharge current and plasma density.

5. Conclusions

The floating potential for a Langmuir probe immersed in an electronegative plasma in the regime without collision or ionization, has been predicted. The radial model of the ion sheath for an electronegative plasma with positive ion temperature $T_+ \neq 0$ developed by the authors is put to test using a series of measurements in argon and neon plasmas in conditions in which a bi-Maxwellian EEDF can be observed. The model included two negative populations, and has been applied for two electron populations. The theoretical floating potential assuming two electron populations, obtained from the measured EEDF, is accurate while the theoretical floating potential using a Maxwellian electron population, with parameters also obtained from the EEDF, deviates up to 50%. The model reduces the difference between the theoretical and the experimental floating potential to less than 0.15 V, in all cases lower than the electron mean energy. The bi-Maxwellian EEDF is used to make further measurements and to check the validity of the model, rather than simply being measured and characterized.

We use the floating potential as an easily measured parameter and a very important probe voltage in real applications, and we use it to easily verify the premises of the radial Langmuir probe sheath model in our test plasmas. Such premises regarding electron and ion mean free paths and the dimensions of the probe and the Debye length can be used to understand the interaction of the plasma with other materials.

Acknowledgments

The authors gratefully acknowledge the support of the Spanish Ministerio de Ciencia, Innovación y Universidades through the FPU program (ref. FPU17/01387).

ORCID iDs

Guillermo Fernando Regodón https://orcid.org/0000-0002-1782-9953
Juan Manuel Díaz-Cabrera https://orcid.org/0000-0002-7388-7373

References

[1] Stamate E 2014 *Surf. Coat. Technol.* **260** 401–10
[2] Bernstein I B and Rabinowitz I N 1959 *Phys. Fluids* **2** 112
[3] Laframboise J G 1966 Theory of spherical and cylindrical Langmuir probes in a collisionless, Maxwellian plasma at rest *Report No. 100* University of Toronto, Institute of Aeroespace Studies (http://dtic.mil/docs/citations/AD0634596)
[4] Allen J E, Boyd R L F and Reynolds P 1957 *Proc. Phys. Soc.* **70** 297–304
[5] Franklin R N 2004 *J. Phys. D: Appl. Phys.* **37** 1342–5
[6] Brinkmann R P 2011 *J. Phys. D: Appl. Phys.* **44** 042002
[7] Popov T K, Dimitrova M, Ivanova P, Kovačič J, Gyergyek T, Dejarnac R, Stöckel J, Pedrosa M A, López-Bruna D and Hidalgo C 2016 *Plasma Sources Sci. Technol.* **25** 033001
[8] Merlino R L, Heinrich J R, Kim S H and Meyer J K 2012 *Plasma Phys. Control. Fusion* **54** 124014
[9] Mohammadzadeh R, Akbari A and Drouet M 2014 *Surf. Coat. Technol.* **258** 566–73
[10] Ballesteros J, Fernández Palop J I, Hernández M A and Morales Crespo R 2006 *Appl. Phys. Lett.* **89** 101501
[11] Mott-Smith H M and Langmuir I 1926 *Phys. Rev.* **28** 727–63
[12] Chen F F 1965 *J. Nucl. Energy* **7** 47–67
[13] Díaz-Cabrera J M, Ballesteros J, Fernandez Palop J I and Tejero-del Caz A 2015 *Plasma Sources Sci. Technol.* **24** 025026
[14] Tejero-del Caz A, Fernández Palop J I, Díaz-Cabrera J M and Ballesteros J 2016 *Plasma Sources Sci. Technol.* **25** 01LT03
[15] Fernández Palop J I, Colomer V, Ballesteros J, Hernández M A and Dengra A 1996 *Surf. Coat. Technol.* **84** 341–7
[16] Fernández Palop J I, Ballesteros J, Colomer V and Hernández M A 1996 *J. Phys. D: Appl. Phys.* **29** 2832
[17] Morales Crespo R, Fernández Palop J I, Hernández M A and Ballesteros J 2004 *J. Appl. Phys.* **95** 2982
[18] Regodón G F, Fernández Palop J I, Tejero-del Caz A, Díaz-Cabrera J M, Carmona-Cabezas R and Ballesteros J 2017 *Phys. Plasmas* **24** 103516
[19] Regodón G F, Palop J I F, Tejero-del Caz A, Díaz-Cabrera J M, Carmona-Cabezas R and Ballesteros J 2018 *Plasma Sources Sci. Technol.* **27** 025014
[20] Demidov V I, Koepke M E and Raitses Y 2014 *Rev. Sci. Instrum.* **81** 10E129
[21] Popov T K, Mitov M, Bankova A, Ivanova P, Dimitrova M, Rupnik S, Kovačič J, Gyergyek T, Cerček M and Dias F M 2013 *Contrib. Plasma Phys.* **53** 51–6
[22] Godyak V A and Piejak R B 1990 *Phys. Rev. Lett.* **65** 996–9
[23] Li M, Dew S K and Brett M J 1999 *J. Phys. D: Appl. Phys.* **32** 2056–9
[24] Chung C 2005 *Phys. Plasmas* **12** 123505
[25] Gahan D, Dolinaj B and Hopkins M B 2008 *Plasma Sources Sci. Technol.* **17** 035026
[26] Godyak V and Alexandrovich B 2015 *Plasma Sources Sci. Technol.* **24** 052001
[27] Druyvesteyn M J 1930 *Z. Phys.* **64** 781–98
[28] Kagan Y M and Perel V I 1964 *Sov. Phys.—Usp.* **6** 767
[29] Franklin R N and Snell J 2000 *J. Plasma Phys.* **64** 131–53
[30] Díaz-Cabrera J M, Lucena-Polonio M V, Fernandez Palop J I, Morales Crespo R, Hernández M A, Tejero-del Caz A and Ballesteros J 2012 *J. Appl. Phys.* **111** 063303
[31] Díaz-Cabrera J M, Fernández Palop J I, Morales Crespo R, Hernández M A, Tejero-del Caz A and Ballesteros J 2014 *Measurement* **55** 66–73
[32] Fernández Palop J I, Ballesteros J, Colomer V and Hernández M A 1995 *Rev. Sci. Instrum.* **66** 4625–36
[33] Annaratone B M, Allen M W and Allen J E 1992 *J. Phys. D: Appl. Phys.* **25** 417–24
[34] Gudmundsson J T, Kimura T and Lieberman M A 1999 *Plasma Sources Sci. Technol.* **8** 22–30
[35] Lucena-Polonio M V, Díaz-Cabrera J M, Palop J I F, Crespo R M, Hernández M A and Ballesteros J 2011 *Plasma Phys. Control. Fusion* **53** 124024
[36] Ballesteros J, Fernandez Palop J I, Hernández M A and Morales Crespo R 2004 *Rev. Sci. Instrum.* **75** 90–3
[37] Godyak V A 1990 *Plasma-Surface Interactions and Processing of Materials* (*E: Applied Sciences* vol 176) (Dordrecht: Kluwer Scademic Publishers) pp 95–134
[38] Lieberman M A and Lichtenberg A J 2005 *Principles of Plasma Discharges and Material Processing* (New York: Wiley)
[39] Maiorov S A, Petrov O F and Fortov V E 2007 Calculation of resonant charge exchange cross-sections of ions Rubidium, Cesium, Mercury and noble gases *34th EPS Conf. on Plasma Physics (Warsaw, Poland)* vol 31FP–2.115
[40] Sahu B B, Han J G, Kim H R, Ishikawa K and Hori M 2015 *J. Appl. Phys.* **117** 033301
[41] Vender D and Boswell R 1990 *IEEE Trans. Plasma Sci.* **18** 725–32
[42] Hopkins M B and Graham W G 1987 *J. Phys. D: Appl. Phys.* **20** 838–43
[43] Chen X and Sánchez-Arriaga G 2018 *J. Phys.: Conf. Ser.* **958** 012001

IOP Publishing Plasma Sources Science and Technology
Plasma Sources Sci. Technol. **28** (2019) 115017 (10pp) https://doi.org/10.1088/1361-6595/ab515e

Influence of collisions in a fluid model for the warm-ion sheath around a cylindrical Langmuir probe

Guillermo Fernando Regodón[1], José Ignacio Fernández Palop[1], Juan Manuel Díaz-Cabrera[2] and Jerónimo Ballesteros[1]

[1] Departamento de Física, Universidad de Córdoba, E-14071 Córdoba, Spain
[2] Departamento de Ingeniería Eléctrica, Universidad de Córdoba, E-14071 Córdoba, Spain

E-mail: z62rehag@uco.es

Received 8 August 2019, revised 19 October 2019
Accepted for publication 25 October 2019
Published 25 November 2019

Abstract

A long cylindrical Langmuir probe immersed in a collisional plasma is modelled by using fluid equations in which the collision term is introduced assuming a constant ion mean free path. The physical magnitudes of the system are expanded in a perturbation series in the collision parameter, that is, the ratio between the Debye length and the ion mean free path, and the system is thus separated into zeroth-order and first-order perturbation systems. The ion temperature is arbitrary and a continuous solution from the plasma to the probe is obtained for the perturbation systems. Using this methodology, a continuous solution for the ion sheath around a cylindrical Langmuir probe is obtained for long ion mean free path, for any ion temperature with no need of two-scale study or asymptotic matching. It is found that the collisions and the ion temperature have opposite effects, and these effects are quantified. The solution for cold ions cannot be obtained directly using this method, but it can be recovered from the warm-ion solution. The methodology is usable for long cylindrical probes in which the scale of the probe is much higher than the scale of the sheath, so that the geometry is essentially cylindrical. The model is numerically solved to obtain the potential profile, the ion temperature profile, the ion density profile and the ion velocity profile, and the dependence of the sheath on the ion mean free path and the ion temperature is studied. The ion-current to probe-potential profiles for different probe radius are obtained. Finally, the Sonin plot is calculated, in order to use the solution in plasma diagnosis.

Keywords: Langmuir probe, fluid sheath model, collisional plasma, cylindrical probe, ion current, perturbation study

1. Introduction

The Langmuir probe is arguably the most important plasma diagnosis tool since its invention more than 80 years ago [1]. It is well known that it is routinely used in all kinds of plasmas like cold low pressure plasmas that may be used in metallic surface treatment or sterilisation, or warm magnetic moderate pressure plasmas that are used in tokamaks. The Langmuir probe is the only device that provides local, reliable information regarding the parameters that characterise the plasma. However, the interpretation of the data that is obtained from the Langmuir probe requires a good understanding of the Langmuir probe sheath theories. We may classify these into kinetic and fluid theories. Kinetic theories aim to obtain information from the carrier distribution functions, which is the most complete information available to describe the particles in the plasma in a continuum model [2–8]. The Boltzmann equation together with the Poisson equation comprise the set of equations that describe the plasma sheath around a Langmuir probe. However, even in the restricted geometry of the problem of the sheath around a planar, cylindrical or spherical Langmuir probe, the obtention of exact solutions is very difficult, and possible only in restricted situations [2–7]. Fluid equations

use only the first two moments of the Boltzmann's equation [9–11]. The validity of fluid equations is limited to the case in which it can be proved that the plasma behaves locally as thermalised gases. This fact limits the application of fluid models to the cases in which there is some collisionality between the particles that are present in the plasma, so it is natural and appropriate to consider collisions to some extent, and necessary if greater precision is required in the models.

The study of the sheath around a cylindrical Langmuir probe immersed in a collisional plasma has proved to pose a difficult mathematical problem [12]. In low pressure, low temperature plasmas in which collisions are not significant, the ions that reach the sheath around a negatively biased cylindrical Langmuir probe trace orbits with an eccentricity that depends on the azimuthal velocity and the radial velocity. The number of ions that are collected can be calculated, for a given ion velocity distribution function in the plasma, as the number of ions with an orbit that intersects the surface of the probe [13, 14]. If the pressure increases, the probability of a collision during an orbit becomes significant. The collision of an ion with a neutral atom during the orbit removes orbital energy, making the orbit more eccentric and facilitating the collection of ions. This effect of the collisions has been shown in theoretical models and in experimental measurements [15–18], and also in numerical PIC simulations [19–26].

However, as pressure further increases and collisions become frequent enough, the ion gas thermalises and can be modelled as a fluid. Charge-exchange collisions of ions with neutral atoms are introduced in the fluid equations as a term that removes random ions and creates ions with null mean velocity [27, 28]. Therefore, in the presence of collisions, the fluid locally presents two different ion populations, one with the fluid velocity and another with zero velocity which has to be accelerated by the electric field in order to reach the probe [3]. On the other hand, collisions are precisely the mechanism that locally thermalises the two ion populations into one to which fluid equations are applicable.

In fluid models, the collisionality term is usually introduced as a constant collision frequency (e.g. [29]), even though the introduction of the term as a constant ion mean free path has more physical meaning [27]. The infinitely long cylindrical Langmuir probe sheath model has strong divergences even in the case of no collision, and it is difficult to define a quasineutral solution or a pre-sheath solution. The matching of two or even three transition zones from the plasma to the probe surface have allowed more precise solutions which imply greater mathematical complexity [30–33]. Due to these difficulties, some alternatives have been proposed. The cylindrical geometry may be substituted by a prolate spheroid geometry, as proposed by Shih and Levi [34, 35], and the long cylindrical Langmuir probe is approximated by a prolate spheroid, limiting the validity of the model to cases in which the sheath extends into the plasma for a distance comparable to the length of the probe. When collisions are introduced in theoretical models that are valid in the range in which the ion fluid is thermalised, it is shown that the ion movement is impeded, due to the creation of slow ions, and the sheath is extended into the plasma [2, 3, 28]. This effect of collisions on the ion movement has been also found in experimental measurements [15, 16, 26, 29]. Plasma sheath PIC simulations that take into account charge-exchange collisions also demonstrate that the ion current is reduced in these circumstances [19–26].

This work studies the influence of collisions in fluid models in the range where collisions can be modelled as a drag force and the ion gas thermalises on a shorter time scale. The collision term is introduced as a constant ion mean free path and the ion temperature is allowed to have any value, varying from cold ions, $T_+ = 0$, to warm ions, $T_+ > 0.1$. In this article, we use the solution that was first presented in [36, 37] and that has been used successfully in experiments with an argon plasma to predict the floating potential [38], and we apply perturbation theory in the collisionality μ parameter, i.e. the ratio between the Debye length and the ion mean free path. The solution was based on establishing mathematical conditions at a point that was not included in the quasineutral solution, in this case the ion local speed of sound singularity that is reached in the sheath [39]. This condition was used to obtain a smooth continuous solution for all the physical magnitudes from the plasma to the sheath, in which no separation into sheath and pre-sheath is used. We show that this methodology can be used to study the case of weakly collisional plasmas, and that the case of cold ions and collisions can be recovered from this solution. We show that the introduction of collisions in the fluid model implies a decrease in the ion current collected by the probe and an expansion of the sheath. The results that are obtained using this model, without the need of asymptotic matching or an intermediate layer, are consistent with the results already reported in the bibliography in this range of collisionality [2, 3, 28].

2. Hypotheses and equations

Consider Poisson's equation in cylindrical geometry

$$\frac{1}{r}\frac{\mathrm{d}}{\mathrm{d}r}\left(r\frac{\mathrm{d}\phi}{\mathrm{d}r}\right) = -\frac{e}{\varepsilon_0}(n_+ - n_e), \tag{1}$$

where ϕ is the electric potential, ε_0 is the permittivity of free space, n_+ and n_e are the positive ion and electron densities and r is the distance to the cylindrical coordinates axis. We assume that the charge of the ions is e, the elementary charge. Let us consider an infinitely long cylindrical Langmuir probe placed so that the surface of the probe coincides with the coordinate surface $r = r_p$, the probe radius. Let the potential be negative, so that it attracts the positive ions and repels the electrons. We will consider that the electrons are in thermodynamic equilibrium with temperature T_e, so that they follow the Maxwell–Boltzmann distribution

$$n_e(\phi) = n_{e,0}\mathrm{e}^{\frac{e\phi}{k_\mathrm{B}T_e}}, \tag{2}$$

where $n_{e,0}$ is the electron density far from the axis and k_B is the Boltzmann constant. Quasineutrality ensures that the positive ion density $n_{+,0}$ in the plasma far from the probe,

for unity charge positive ions, equals the electron plasma density

$$n_{+,0} = n_{e,0}. \tag{3}$$

The ions are treated as a fluid in this model. Continuity equation for the positive ions reads, in absence of ionisation,

$$i_+ = 2\pi r e n_+ v_+ \tag{4}$$

being i_+ the constant ion current per unit length entering the Langmuir probe, and v_+ the velocity of the ion fluid. Using (4), the positive ion velocity can be removed from the system as a function of the distance to the axis r and the positive ion density n_+. We now write the momentum balance equation, in which we include the collision term, that translates into a loss of momentum term. It has been written both as a constant collision frequency or as a constant ion mean free path [27, 29] in the literature. It can be argued that the latter has more physical meaning [27, 40, 41], so that we choose to deal with the mathematical difficulties that it introduces in the system

$$m_+ v_+ \frac{\mathrm{d}v_+}{\mathrm{d}r} = \frac{m_+}{2}\frac{\mathrm{d}v_+^2}{\mathrm{d}r} = -\mathrm{e}\frac{\mathrm{d}\phi}{\mathrm{d}r} + m_+\frac{v_+^2}{\lambda_+} - \frac{1}{n_+}\frac{\mathrm{d}p_+}{\mathrm{d}r}, \tag{5}$$

where λ_+ is the ion mean free path for collisions with neutrals. We have also taken into account the positive ion gas pressure, p_+. We consider the positive ion gas as an adiabatic fluid with a polytropic coefficient κ, that is

$$p_+ = k_B T_+ \frac{n_+^\kappa}{n_{+,0}^{\kappa-1}}. \tag{6}$$

The value of κ depends on the number of degrees of freedom, 3, 2 and $\frac{5}{3}$ for one, two and three degrees of freedom, respectively. It has been discussed that the polytropic coefficient may not be well approximated by any of these values along the pre-sheath [42, 43]. However, Gyergyek and Kovacic prove that the polytropic coefficient is approximately constant along the sheath and pre-sheath and that the influence of the ion temperature is little sensitive to the value of the polytropic coefficient [36, 42, 43].

The pressure term was introduced in the work by Fernández Palop *et al* [11] who assumed that the positive ion temperature was small compared to the electron temperature. The problem has been recently solved for any ion temperature [36, 37], by means of considering the effect of the pressure in the ion local speed of sound and the change of behaviour from subsonic to supersonic flow. We summarise now the mathematical characteristics that allowed the exact solution of the problem, in order to explain the procedure that we have devised and present in this work. Let us first introduce the following dimensionless variables, where λ_D is the Debye length

$$\begin{aligned} I_i &= \frac{i_+ r_p e}{2\pi\varepsilon_0 k_B T_e}\left(\frac{m_+}{2k_B T_e}\right)^{\frac{1}{2}}, & \beta &= \frac{T_+}{T_e}, \\ x &= \frac{r}{\lambda_D}, & N_+(x) &= \frac{n_+}{n_{e,0}}, \\ x_p &= \frac{r_p}{\lambda_D}, & \lambda_D &= \sqrt{\frac{\varepsilon_0 k_B T_e}{e^2 n_{e,0}}}, \\ y &= -\frac{e\phi}{k_B T_e}, & V_+ &= v_+\sqrt{\frac{m_+}{2k_B T_e}}. \end{aligned} \tag{7}$$

Using these variables, Poisson's equation can be transformed into two first order differential equations in the following form

$$\begin{aligned} \frac{\mathrm{d}z}{\mathrm{d}x} &= -\frac{z}{x} + N_+ - \mathrm{e}^{-y}, \\ \frac{\mathrm{d}y}{\mathrm{d}x} &= z. \end{aligned} \tag{8}$$

The momentum balance equation, without collisions and using (6), reads

$$\frac{\mathrm{d}V_+^2}{\mathrm{d}x} = \frac{\mathrm{d}y}{\mathrm{d}x} - \beta\kappa N_+^{\kappa-2}\frac{\mathrm{d}N_+}{\mathrm{d}x}. \tag{9}$$

In this problem, the momentum balance equation (9), lacking the collision term, can be integrated to produce the energy balance equation, which is written in the form (10) after multiplying all terms by N_+^2. In this expression, the plasma conditions $y = 0$, $V_+ = 0$ and $N_+ = 1$ have been used. From the energy balance equation, one can obtain the dimensionless positive ion density N_+ from the electric potential y

$$\frac{I_i^2}{x^2 x_p^2} - \left(y(x) + \frac{\kappa}{\kappa-1}\beta\right)N_+^2(x) + \frac{\kappa}{\kappa-1}\beta N_+^{\kappa+1}(x) = 0. \tag{10}$$

The singularity that the ion local speed of sound introduced in the model, was treated imposing the condition that physical magnitudes cannot diverge in any point of the domain [39], in this case the radial distance to the axis. The system can be written in the form of a fraction of two expressions relating the physical magnitudes of the problem, so that the singularity becomes clear. Using the continuity equation (4) in dimensionless form and differentiating

$$I_i = x x_p N_+ V_+, \tag{11}$$

$$\frac{\mathrm{d}V_+}{V_+} + \frac{\mathrm{d}N_+}{N_+} + \frac{\mathrm{d}x}{x} = 0, \tag{12}$$

and using the definition of the ion local speed of sound in dimensionless units

$$C_+^2 = c_+^2\frac{m_+}{2k_B T_e} = \frac{1}{m_+}\frac{\partial p_+}{\partial n_+}\frac{m_+}{2k_B T_e} = \frac{\beta\kappa}{2}N_+^{\kappa-1}, \tag{13}$$

one can obtain the following expression for the derivative of the dimensionless positive ion density, by means of

introducing (12) and (13) into the momentum balance equation (9)

$$\frac{1}{N_+}\frac{\mathrm{d}N_+}{\mathrm{d}x} = \frac{\frac{V_+^2}{x} + \frac{z}{2}}{C_+^2 - V_+^2}. \tag{14}$$

The condition of boundedness for all physical magnitudes introduces an additional condition in the singularity, that is, when the denominator equals zero the numerator must equal zero as well. The denominator equating zero simply implies the equality of the ion velocity to the ion local speed of sound. The numerator equating zero implies a second condition in the singularity, relating the dimensionless electric field z to the ion velocity and hence to the positive ion density. This way, the system presents three dependent variables, the electric potential y, its first derivative, the electric field z, and the positive ion density N_+, and one independent variable, the distance to the axis x. The system has one condition of general validity, the energy balance equation, and two conditions in the singularity. The last condition that allows the obtention of the solution of the system is the quasineutrality condition in the plasma. A numerical search can be performed in the independent variable x, finding the electric potential y and its first derivative z using the singularity conditions, integrating the system to the plasma, and looking for the distance to the axis that fulfils the quasineutrality condition far from the probe [36, 37]. The solution that is obtained using this methodology is consistent with both computer simulations [44, 45] and with experiments [46–48] in cases in which the temperature of the ions is not negligible when compared to the electron temperature.

Unfortunately, the introduction of the collision term renders integration of the momentum balance equation impossible, so that one condition is lost. A similar numerical search could, in principle, be performed, however in a two-dimensional space. But in this case, our preliminary work shows that such numerical search is difficult. In phase space, several sets of initial conditions can fulfil quasineutrality in the plasma. We would need to know, not only the limiting value of N_+, but the functional form of the function $N_+(x)$ as $x \to \infty$. This is not known in the case of a collisional plasma so we introduce a perturbation method for the inverse of the ion mean free path. The solution is valid for any positive ion to electron temperature ratio, for long enough ion mean free path, compared to the Debye length.

3. The model with collisions as a perturbation term

When the collision term cannot be rendered insignificant, momentum balance equation (5) can be written in dimensionless form

$$\frac{\mathrm{d}V_+^2}{\mathrm{d}x} = \frac{\mathrm{d}y}{\mathrm{d}x} + \mu V_+^2 - \beta\kappa N_+^{\kappa-2}\frac{\mathrm{d}N_+}{\mathrm{d}x}, \tag{15}$$

where we introduce the dimensionless inverse of the ion mean free path, μ

$$\mu = \frac{2\lambda_\mathrm{D}}{\lambda_+}. \tag{16}$$

Using this new parameter μ, and considering it small enough, we expand the physical magnitudes of the system in terms of powers of μ

$$\begin{aligned} y &= y_0 + y_1\mu + y_2\mu^2 + \cdots, \\ z &= z_0 + z_1\mu + z_2\mu^2 + \cdots, \\ V_+^2 &= V_0^2 + V_1^2\mu + V_2^2\mu^2 + \cdots, \\ N_+ &= N_0 + N_1\mu + N_2\mu^2 + \cdots. \end{aligned} \tag{17}$$

The relationship between the expansion for V_+^2 and N_+ is obtained by means of the continuity equation in dimensionless form (11). Using the Taylor expansion for $f(x) = x^{-2}$ around $x = x_0$, that is, $\frac{1}{x^2} \simeq \frac{1}{x_0^2} - 2\frac{1}{x_0^3}(x - x_0) + 6\frac{1}{x_0^4}\frac{1}{2!}(x - x_0)^2$, and substituting $f(x) = V_+^2$, $x = N_+$ and $x_0 = N_0$, we obtain the relation between the first two terms of V_+^2 and N_+

$$V_+^2 = \frac{I_i^2}{x^2 x_p^2}\frac{1}{N_+^2}, \tag{18}$$

and introducing (17)

$$\begin{aligned} V_0^2 + V_1^2\mu + V_2^2\mu^2 = \frac{I_i^2}{x^2 x_p^2} \\ \left(\frac{1}{N_0^2} - 2\frac{1}{N_0^3}(N_1\mu + N_2\mu^2 + \cdots)\right. \\ \left. +3\frac{1}{N_0^4}(N_1\mu + N_2\mu^2 + \cdots)^2 + \cdots\right). \end{aligned} \tag{19}$$

The difference $x - x_0 = N_+ - N_0 = N_1\mu + N_2\mu^2 + \cdots$ contains the perturbation terms with the infinite powers of μ, which we regroup to produce the following relations

$$\begin{aligned} V_0^2 &= \frac{I_i^2}{x^2 x_p^2}\left(\frac{1}{N_0^2}\right), \\ V_1^2 &= \frac{I_i^2}{x^2 x_p^2}\left(\frac{-2N_1}{N_0^3}\right), \\ V_2^2 &= \frac{I_i^2}{x^2 x_p^2}\left(\frac{3N_1^2}{N_0^4} - \frac{2N_2}{N_0^3}\right). \end{aligned} \tag{20}$$

In the following treatment, we will assume that the polytropic coefficient value in (15) is $\kappa = 2$, which is the appropriate value for a system of two degrees of freedom [11, 42, 43, 49]. This choice will also simplify the expansion of the last term in (15). Using these expressions, the zeroth order terms of the

momentum balance equation and the Poisson's equation are

$$\frac{\mathrm{d}V_0^2}{\mathrm{d}x} = \frac{\mathrm{d}y_0}{\mathrm{d}x} - 2\beta\frac{\mathrm{d}N_0}{\mathrm{d}x},$$
$$\frac{1}{x}\frac{\mathrm{d}}{\mathrm{d}x}\left(x\frac{\mathrm{d}y_0}{\mathrm{d}x}\right) = N_0 - \mathrm{e}^{-y_0}. \tag{21}$$

These equations coincide, as they should, with the problem first stated in [50] and solved in [36, 37] by studying the subsonic to supersonic ion flow transition. The momentum balance equation is exactly integrable. The whole zeroth order system is solvable, and the singularity [36] is located at the point where the ion fluid velocity equals the ion local speed of sound. In order to obtain a useful condition that is fulfilled in the singularity, we use the singularity condition in which the ion velocity equals the ion local speed of sound, $C_0^2 = V_0^2$ in terms of the zeroth order system. Together with (11) and (13) we obtain this condition that is written in terms of the variable N_0 of the zeroth order system (21)

$$N_0^3 = \frac{I_i^2}{x^2 x_p^2 \beta}. \tag{22}$$

The first order terms of the momentum balance equation and the Poisson's equation are

$$\frac{\mathrm{d}V_1^2}{\mathrm{d}x} = \frac{\mathrm{d}y_1}{\mathrm{d}x} + V_0^2 - 2\beta\frac{\mathrm{d}N_1}{\mathrm{d}x}, \tag{23}$$
$$\frac{1}{x}\frac{\mathrm{d}}{\mathrm{d}x}\left(x\frac{\mathrm{d}y_1}{\mathrm{d}x}\right) = N_1 + y_1\mathrm{e}^{-y_0}. \tag{24}$$

Equation (23) is also integrable, given that V_0 has already been obtained in the zeroth order solution

$$V_1^2 = y_1 + \int_\infty^x V_0^2\,\mathrm{d}x - 2\beta N_1, \tag{25}$$

where we have used the fact that in the plasma, $x \to \infty$, the perturbation produced by the finiteness of the ion mean free path must vanish. Using (20), we can solve for N_1, finding the following expression

$$N_1 = \frac{y_1 + \int_\infty^x V_0^2\,\mathrm{d}x}{2\beta - 2\frac{I_i^2}{x^2 x_p^2 N_0^3}}. \tag{26}$$

The denominator of (26) is null at the point where the same singularity condition (22) is met. For the perturbation to be finite, we impose the condition that the numerator must also be null, obtaining

$$y_1 = \int_x^\infty V_0^2\,\mathrm{d}x. \tag{27}$$

As the distance to the axis x_s where the ion fluid reaches the ion local speed of sound has already been obtained in the zeroth order terms solution, and y_1 in the singularity is obtained from (27), we can test z_1 values in Poisson's equation and integrate the system from x_s to the plasma in order to find the value that fulfils the condition of a null first order perturbation term in the plasma. In order to do this, we move a small distance δx to the plasma, assuming that z_1 does not change. We obtain y_1 using:

$$y_1(x_s + \delta x) = y_1(x_s) + z_1(x_s)\delta x, \tag{28}$$

and N_1 using (26), so that the first order system is exactly solvable.

We may state the second order system as well

$$V_2^2 = y_2 + \int_\infty^x V_1^2\,\mathrm{d}x - 2\beta N_2, \tag{29}$$

$$\frac{1}{x}\frac{\mathrm{d}}{\mathrm{d}x}\left(x\frac{\mathrm{d}y_2}{\mathrm{d}x}\right) = N_2 + \left(y_2 - \frac{y_1^2}{2}\right)\mathrm{e}^{-y_0}, \tag{30}$$

$$N_2 = \frac{y_2 + \int_\infty^x V_1^2\,\mathrm{d}x - \frac{5I_i^2N_1^2}{x^2x_p^2N_0^4}}{2\beta - 2\frac{I_i^2}{x_2x_p^2N_0^3}}. \tag{31}$$

The same strategy can be used for the second order system, and indeed we could continue. In subsequent results, the calculations are limited to a long ion mean free path or small μ parameter, so that we do not need more terms. Our preliminary study of the second order solution shows that the solution is of the same order of magnitude as the first order solution, and that the second order solution is more important when the ion current I_i is higher. In this case we only use the first order solution and we restrict the perturbation parameter μ to small values.

4. Results

The methodology that we describe in this paper has been used to obtain the physical magnitudes of the plasma sheath around a cylindrical probe that is negatively biased with respect to the plasma. The model can be solved for any value of the ion temperature, and we restrict the problem to small Debye length to ion mean free path ratio μ parameter values, so that we can use the first order perturbation term and ignore higher order terms In figure 1 we show the potential profile for two different ion currents, $I_i/x_p = 2.5$ and $I_i/x_p = 5$, for the same collisionality parameter values $\mu = 0$, 0.025 and 0.05. We also show the effect of the ion temperature for temperature ratios $\beta = 0.01$, 0.4 and 1: as the ions have more energy in the plasma, the potential needed to attract them to the probe is smaller, hence the reduction of the potential profile and the size of plasma sheath, for the same current. For these ion currents and temperature ratios, we have six potential profiles to which we apply the perturbation model in order to study the effect of collisions using a constant ion mean free path. We see in figure 1 that the main effect of the collisions is to hinder the ion movement, requiring a higher potential for the same ion current and ion temperature. As we restrict the collisionality parameter to small values, the effect of collisions is secondary compared to the effect of the ion temperature. We note that the effect of collisions is opposed to the effect of the ion temperature, that is, an increase in the ion temperature enables the ions to reach the probe more easily due to the increased thermal energy of the ions in the plasma, contrary to collisions, which make it more difficult for the ions to reach the probe. It is interesting to note that the

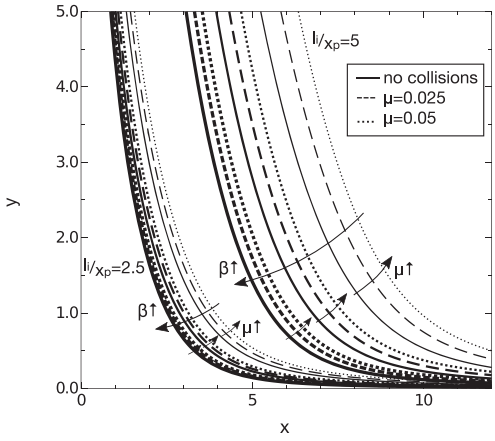

Figure 1. Potential profile for ion currents $I_i/x_p = 2.5$ and $I_i/x_p = 5$, for temperature ratios $\beta = 0.01$ (thin lines), $\beta = 0.4$ (medium thick lines) and $\beta = 1$ (bold lines), for collisionality parameter values $\mu = 0$ (solid lines), $\mu = 0.025$ (dashed lines) and $\mu = 0.05$ (dotted lines). Note that the potential is displaced to the left for increasing ion to electron temperature ratio β and to the right for increasing collisionality parameter μ.

perturbative model cannot be solved for cold ions, because the singularity would be infinitely distant from the axis of symmetry. Therefore, we prefer to study ion to electron temperature ratio $\beta = 0.01$ instead of $\beta = 0$, knowing that the difference in the solutions will be very small. When needed, we may extrapolate the solution for $\beta = 0$ from the next solved cases, $\beta = 0.01$ and $\beta = 0.1$.

We can also see in figure 1 that the effect of collisions is more important when the size of the sheath is increased. This is understandable, as the ions traverse a longer distance at higher velocities, so that collisions, which essentially stop the ions that collide with a neutral atom, are more important in the momentum balance equation (15). For this reason, we consider that it is more interesting to compare the ion mean free path with the sheath size. The solution for the ion sheath based in the study of the singularity [11, 36, 37] provides us with a continuous solution from the probe surface to the plasma and does not define a point that could easily be designated as the sheath edge. In order to define a sheath edge, we use the quasineutral collisionless solution and find the classical solution for the sheath edge. From equality of the positive ion density and the electron density $n_+ = n_e$, that is valid in the pre-sheath, we obtain

$$N_+ = \mathrm{e}^{-y}, \tag{32}$$

while from continuity equation, which is of general validity, we can write

$$x = \frac{I_i}{x_p V_+ N_+}. \tag{33}$$

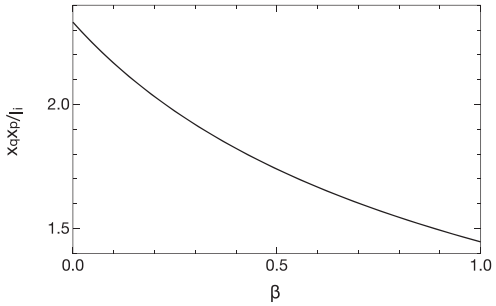

Figure 2. Classical sheath edge over ion current dependence on the ion to electron temperature ratio.

Finally, we solve the ion velocity V_+ from energy balance equation (10), also of general validity, to obtain

$$V_+ = \sqrt{y - 2\beta(N_+ - 1)}. \tag{34}$$

We therefore find an expression relating x and y

$$x = \frac{I_i}{x_p \mathrm{e}^{-y}\sqrt{y - 2\beta(\mathrm{e}^{-y} - 1)}}. \tag{35}$$

In order to find the classical sheath edge, we look for the point where the quasineutral solution is vertical, that is, $\dfrac{\mathrm{d}x}{\mathrm{d}y} = 0$. Obtaining the expression for the derivative and solving the condition, we numerically obtain the classical sheath edge x_q. We note that the point depends on the temperature ratio β, and is proportional to the quotient between ion current I_i and the probe radius x_p. In figure 2 we show the dependence of the classical sheath edge on the ion to electron temperature ratio β.

We define the classical sheath edge to ion mean free path ratio μ' as

$$\mu' = \mu x_q. \tag{36}$$

In figure 3 we show a complete example of the potential, ion density, velocity and ion temperature profiles. The effect of collisions in the potential profile has already been discussed in figure 1. We see in figure 3(b) that the higher ion temperature reduces the dip in the ion density in the sheath when the ions are accelerated. Increasing collisions of the ions with the neutral atoms reduces the ion density, similarly to the effect of reducing the ion temperature. The ion temperature of the ion flow, as shown in 3(d), is reduced with respect to the ion temperature in the plasma as the ion density is reduced.

We also see in figure 3(c) that the ion velocity is higher when collisions increase. We note that the effect of collisions is more important when the ions move with higher velocity. However, this is an effect of the enlargement of the ion sheath, rather than an effect of the collisions, which hinder the movement of the ions. In order to study this double effect, in figure 4 we show the potential profile and the velocity profile for the ion currents that polarise the probe at $y_p = 5$ when the probe radius is $x_p = 1$ for the cases of sheath edge to ion mean free path ratios $\mu' = 0$, 0.1, 0.2, 0.3, 0.4 and 0.5. We

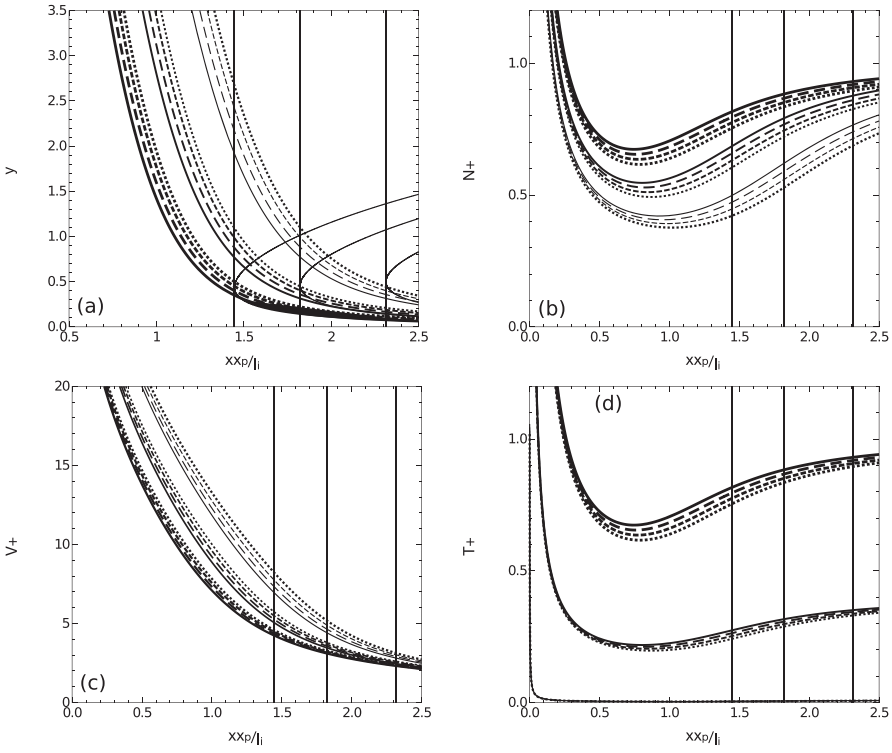

Figure 3. Potential profile (a), ion density profile (b), velocity profile (c) and ion temperature profile (d) for ion current $I_i/x_p = 5$ for ion to electron temperature ratios $\beta = 0.01$ (thin lines), $\beta = 0.4$ (medium thick lines) and $\beta = 1$ (bold lines), for sheath edge to ion mean free path ratio $\mu' = 0$ (solid line), $\mu' = 0.1$ (long dashed line), $\mu' = 0.2$ (short dashed line) and $\mu' = 0.3$ (dotted line). Indicated with vertical lines, the classical sheath edge for the three β values and, in the potential profile, the quasineutral solutions for the three β values.

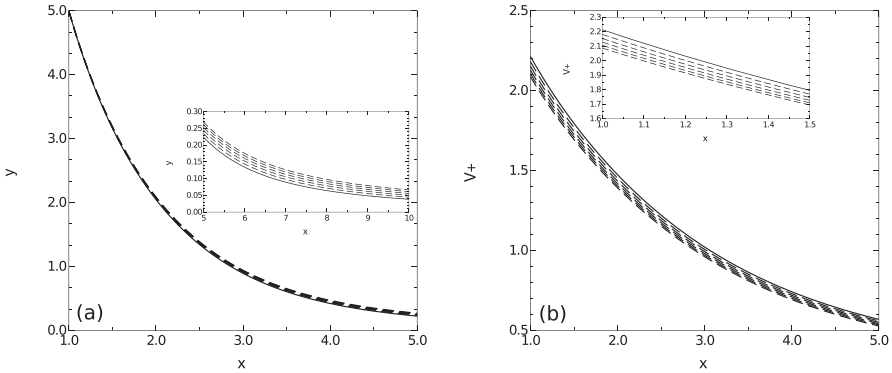

Figure 4. Potential profiles (a) and velocity profiles (b) for probe radius $x_p = 1$, probe potential $y_p = 5$ and for sheath edge to ion mean free path ratio $\mu' = 0$ (solid line), $\mu' = 0.1$–0.5 in 0.1 steps (long dashed lines).

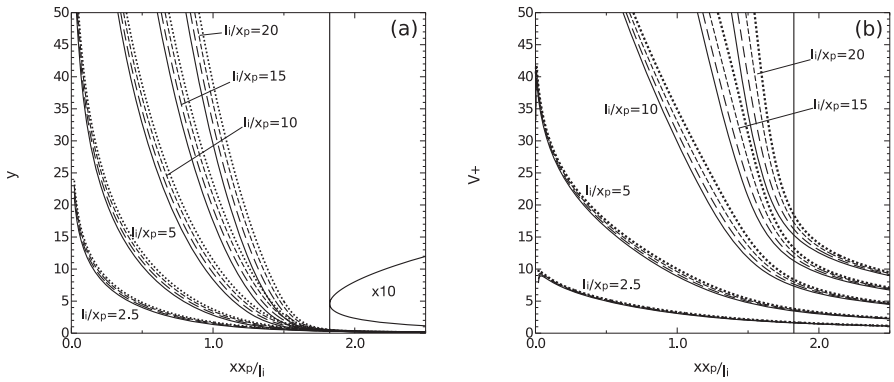

Figure 5. Potential profiles (a) and velocity profiles (b) ion to electron temperature ratio $\beta = 0.4$, for ion currents $I_i/x_p = 2.5$, 5, 10, 15, and 20 and for sheath edge to ion mean free path ratio $\mu' = 0$ (solid line), $\mu' = 0.1$ (long dashed line), $\mu' = 0.2$ (short dashed line) and $\mu' = 0.3$ (dotted line). The classical sheath edge is indicated with a vertical line and, in the potential profile, the quasineutral solution is plotted, scaled $\times 10$ for better visibility.

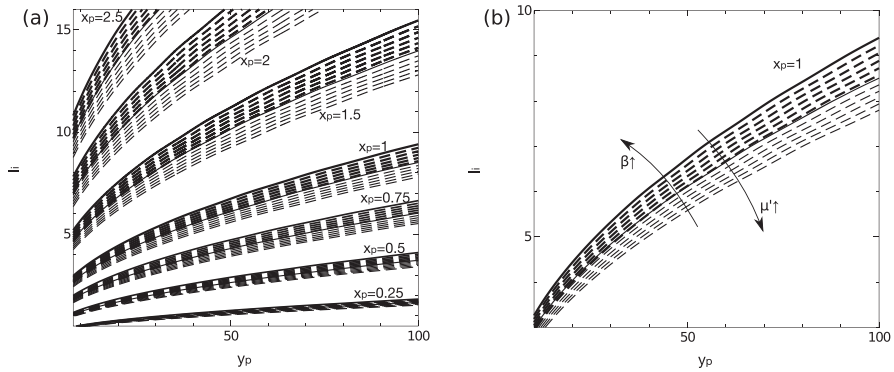

Figure 6. Ion current to probe potential characteristics for probe radius $x_p = 0.25$, 0.5, 0.75, 1 and 2 for ion to electron temperature ratios $\beta = 0$ (thin lines) and 0.25 (bold lines) and for sheath edge to ion mean free path ratio $\mu' = 0$ (solid lines), and 0.1–0.5 in 0.1 steps (dashed lines).

see that the effect of collisions is a decrease in the ion velocity and a slight increase in the size of the sheath.

In figure 5 we compare several potential profiles and the velocity profiles for different ion currents $I_i/x_p = 2.5$, 5, 10, 15 and 20 for the same ion to electron temperature ratio. We see that an increase in the ion current implies an increase in the potential profile and the ion velocity, and that the higher the ion velocity, the more important the effect of collisions is.

In figure 6(a) we show the plot of the ion current to probe potential characteristics that we calculate based in this model. We see that the main effect of the collisions is that it reduces the current collected for a fixed probe potential. In figure 6(b) it is again clearly evident that the effect of collisions is opposed to the effect of the ion temperature. A sheath edge to ion mean free path ratio of $\mu' = 0.5$ for the ion to electron temperature ratio $\beta = 0.25$ produces an ion current to probe potential characteristic that is very close to the $\mu' = \beta = 0$ case for probe radius in the range $x_p \in [0.25, 2]$.

In order to make the results of this study readily usable in plasma diagnosis, we have produced a Sonin plot that we show in figure 7, in which we show the influence of collisions. The Sonin plot is a convenient plot in which the following dimensionless current is represented [35, 51–55]

$$I_i'(15) = I_i 2\sqrt{\pi}\left(\frac{\lambda_D}{r_p}\right)^2 = \frac{i_+}{e r_p n_{e0}}\sqrt{\frac{m_+}{2\pi k_B T_e}}, \qquad (37)$$

versus

$$I_i'(15)x_p^2 = \frac{I_i e r_p}{\varepsilon_0}\left(\frac{m_+}{2\pi k_B^3 T_e^3}\right)^{\frac{1}{2}}. \qquad (38)$$

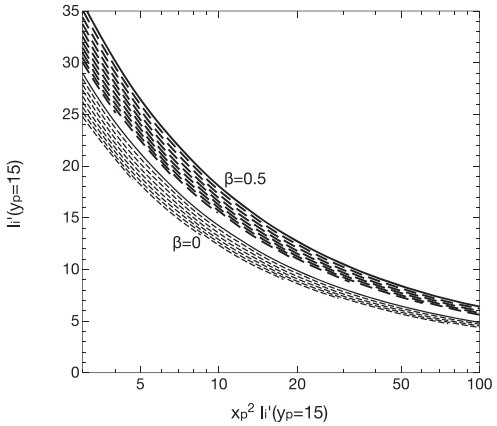

Figure 7. Sonin plot for probe potential $y_p = 15$ for ion to electron temperature ratios $\beta = 0$ (thin lines) and 0.5 (bold lines) and for Debye length to ion mean free path ratio $\mu = 0$ (solid lines), and increasing in 0.1 steps (dashed lines).

$I_i'(15)$ is used to denote this dimensionless ion current for $y_p = 15$. The abscissa in the Sonin plot does not depend on the plasma density n_e.

In plasma laboratories, the parameter of reference is the Debye length. For that reason, the Sonin plot has been produced using the Debye length to ion mean free path μ as the collisionality parameter. Once more, in figure 7 we note that the effect of collisions and of ion temperature is opposed, the former displacing the Sonin plot downwards and the latter displacing the Sonin plot upwards. The plots for each Debye length to ion mean free path μ parameter value is cut when the sheath edge to ion mean free path ratio μ' raises above 0.5, that is, as can be deduced from (16) and (36), the ion mean free path is four times the size of the sheath edge. The maximum μ value that results from this limitation is $\mu_{\max} = 0.11879$ for $x_p = 0.2$ and $\beta = 0.5$. In terms of laboratory units, for an argon discharge with $T_e = 2.5\,\mathrm{eV}$, $n_{e,0} = 10^{11}\ \mathrm{cm}^{-3}$, the Debye length is $\lambda_D = 37.2\ \mu\mathrm{m}$. The ion mean free path follows the following formula, after Lieberman [40] with the argon charge-exchange cross-section by Maiorov [41] for ion temperatures $T_+ = 0.025\,\mathrm{eV}$ and $T_+ = 0.25\,\mathrm{eV}$

$$\lambda_+(T_+ = 0.025\ \mathrm{eV}) = \frac{1}{264P(\mathrm{Torr})}\ \mathrm{cm}, \tag{39}$$

$$\lambda_+(T_+ = 0.25\ \mathrm{eV}) = \frac{1}{21.3P(\mathrm{Torr})}\ \mathrm{cm}. \tag{40}$$

The size of the classical sheath, defined as the turning point of (35), depends on the ion current and the probe radius. For a typical probe radius $r_p \approx 2.5\lambda_D \approx 0.1$ mm, the non-dimensional ion current for the value $y_p = 15$ that is used in the Sonin plot in figure 7, is $I_i \approx 12 \pm 2$ (see figure 6). The classical sheath size is $x_q \approx 2.25 I_i/x_p \approx 11$, or $r_q \approx 0.4$ mm. The limit of applicability, as stated before, is the ion mean free path being four times the size of the sheath edge, that is, $\lambda_i > 1.6$ mm. In this example, the pressure must be:

$$P(T_+ = 0.025\ \mathrm{eV}) < 24\ \mathrm{mTorr}, \tag{41}$$

$$P(T_+ = 0.25\ \mathrm{eV}) < 290\ \mathrm{mTorr}. \tag{42}$$

On the other hand, the pressure should be high enough for the radial fluid model to be valid, so that the orbital motion of the ions can be ignored. When using the Sonin plot in plasma diagnosis, if the experimental point lies in the range of the plots for a given ion to electron temperature ratio, which are presented in figure 7, then the limit of the validity of the model is fulfilled, under the assumption of the validity of fluid theories to describe the movement of the ions.

5. Conclusions

In this article we have presented a procedure to obtain the potential sheath profile, and all the relevant physical magnitudes, for the plasma sheath around a cylindrical Langmuir probe immersed in a collisional electropositive plasma with one predominant positive ion species. The methodology is a perturbative approximation in the collisionality parameter, which is proportional to the inverse of the ion mean free path. The solution is continuous from the plasma to the surface of the probe, with no asymptotic solution matching involved, and is valid for any positive ion temperature for weakly collisional plasmas. The applicability of the model is limited to long enough probes, as collisional plasmas tend to form a sheath that is between the cylindrical and the spherical solution. The quasineutral solution is reached at a shorter distance from the probe when the current is lower, so that the Langmuir probe length limitation can be understood as a collected ion current limitation. The obtention of the solution was possible by studying the singularity that is present in the system when the ions reach their local speed of sound: the singularity is also present in the higher order perturbative systems. Our test cases show that the validity of the model can be stated in terms of the relation between the Debye length and the ion mean free path μ, that should be lower than $\mu \lesssim 0.1$, and in terms of the relation between classical sheath edge and ion mean free path μ', that should be lower than $\mu' \lesssim 0.5$, that is, the ion mean free path should be higher or similar than 10 times the Debye length and 4 times the classical sheath edge.

We have proved that the effect of collisionality is opposed to the effect of the positive ion temperature, and they essentially cancel out in the range of parameters studied when the relation between the ion to electron temperature ratio β and the sheath edge to ion mean free path ratio μ' is $2\beta = \mu'$. The results show that the effect of collisions is more important when the sheath edge is farther from the probe and when the ions traverse the pre-sheath with higher velocity. Finally, in order to make the application of the model readily usable in plasma laboratories, we have produced the Sonin plot, which is restricted to the range in which the two conditions of validity of the model $\mu \lesssim 0.1$ and $\mu' \lesssim 0.5$ are fulfilled.

Acknowledgments

The authors gratefully acknowledge the support of the Spanish Ministerio de Ciencia, Innovación y Universidades through the FPU program (ref. FPU17/01387).

ORCID iDs

Guillermo Fernando Regodón https://orcid.org/0000-0002-1782-9953
Juan Manuel Díaz-Cabrera https://orcid.org/0000-0002-7388-7373

References

[1] Mott-Smith H M and Langmuir I 1926 *Phys. Rev.* **28** 727–63
[2] Chou Y S 1966 *Phys. Fluids* **9** 2150
[3] Riemann K U 1981 *Phys. Fluids* **24** 2163
[4] Riemann K U 1991 *J. Phys. D: Appl. Phys.* **24** 493–518
[5] Benilov M S 1997 *Phys. Plasmas* **4** 521–8
[6] Sheridan T E and Baalrud S D 2017 *Phys. Rev.* E **96** 053201
[7] Tsankov T V and Czarnetzki U 2017 *Plasma Sources Sci. Technol.* **26** 055003
[8] Kos L, Jelić N, Gyergyek T, Kuhn S and Tskhakaya D D 2018 *AIP Adv.* **8** 105311
[9] Allen J E, Boyd R L F and Reynolds P 1957 *Proc. Phys. Soc.* **70** 297–304
[10] Chen F F 1965 *J. Nucl. Energy* **7** 47–67
[11] Fernández Palop J I, Ballesteros J, Colomer V and Hernández M A 1996 *J. Phys. D: Appl. Phys.* **29** 2832
[12] Chen F F 1965 *Plasma Diagnostic Techniques* (New York: Academic)
[13] Bernstein I B and Rabinowitz I N 1959 *Phys. Fluids* **2** 112
[14] Laframboise J G 1966 Theory of spherical and cylindrical Langmuir probes in a collisionless, Maxwellian plasma at rest Technical Report 100 *Toronto Univ. Downsview Inst. for Aerospace Studies* (http://dtic.mil/docs/citations/AD0634596)
[15] Tichý M, Šícha M, David P and David T 1994 *Contrib. Plasma Phys.* **34** 59–68
[16] Zakrzewski Z and Kopiczynski T 1974 *Plasma Phys.* **16** 1195–8
[17] Sternovsky Z, Robertson S and Lampe M 2003 *Phys. Plasmas* **10** 300–9
[18] Sternovsky Z, Robertson S and Lampe M 2003 *J. Appl. Phys.* **94** 1374–81
[19] Trunec D, Španěl P and Smith D 1995 *Contrib. Plasma Phys.* **35** 203–12
[20] Trunec D, Španěl P and Smith D 2002 *Contrib. Plasma Phys.* **42** 91–8
[21] Taccogna F, Longo S and Capitelli M 2003 *Eur. Phys. J. Appl. Phys.* **22** 29–39
[22] Taccogna F, Longo S and Capitelli M 2004 *Contrib. Plasma Phys.* **44** 594–600
[23] Cenian A, Chernukho A, Bogaerts A, Gijbels R and Leys C 2005 *J. Appl. Phys.* **97** 123310
[24] Iza F and Lee J K 2006 *J. Vac. Sci. Technol.* A **24** 1366–72
[25] Taccogna F, Longo S and Capitelli M 2008 *Contrib. Plasma Phys.* **48** 509–14
[26] Voloshin D, Kovalev A, Mankelevich Y, Proshina O, Rakhimova T and Vasilieva A 2015 *Eur. Phys. J.* D **69** 23
[27] Franklin R N and Snell J 2001 *Phys. Plasmas* **8** 643–7
[28] Robertson S 2013 *Plasma Phys. Control. Fusion* **55** 093001
[29] Bryant P M 2009 *Plasma Sources Sci. Technol.* **18** 014013
[30] Franklin R N and Ockendon J R 1970 *J. Plasma Phys.* **4** 371–85
[31] Riemann K U 2006 *Phys. Plasmas* **13** 063508
[32] Brinkmann R P 2011 *J. Phys. D: Appl. Phys.* **44** 042002
[33] Almeida N A and Benilov M S 2012 *Phys. Plasmas* **19** 073514
[34] Shih C and Levi E 1971 *AIAA J.* **9** 1673–80
[35] Bryant P, Dyson A and Allen J E 2001 *J. Phys. D: Appl. Phys.* **34** 1491
[36] Regodón G F, Fernández Palop J I, Tejero-del Caz A, Díaz-Cabrera J M, Carmona-Cabezas R and Ballesteros J 2017 *Phys. Plasmas* **24** 103516
[37] Regodón G F, Palop J I F, Tejero-del Caz A, Díaz-Cabrera J M, Carmona-Cabezas R and Ballesteros J 2018 *Plasma Sources Sci. Technol.* **27** 025014
[38] Regodón G F, Palop J I F, Cabrera J M M D and Ballesteros J 2019 *Plasma Phys. Control. Fusion* **61** 095015
[39] Valentini H B 1988 *J. Phys. D: Appl. Phys.* **21** 311–21
[40] Lieberman M A and Lichtenberg A J 2005 *Principles of Plasma Discharges and Material Processing* (New York: Wiley)
[41] Maiorov S A, Petrov O F and Fortov V E 2007 Calculation of resonant charge exchange cross-sections of ions rubidium, cesium, mercury and noble gases *34th EPS Conf. on Plasma Physics* vol 31F *(Warsaw, Poland)* p P–2.115
[42] Gyergyek T and Kovačič J 2017 *Phys. Plasmas* **24** 063505
[43] Gyergyek T and Kovačič J 2017 *Phys. Plasmas* **24** 063506
[44] Tejero-del Caz A, Fernández Palop J I, Díaz-Cabrera J M, Regodón G F, Carmona-Cabezas R and Ballesteros J 2017 *J. Comput. Phys.* **350** 747–58
[45] Tejero-del Caz A, Fernández Palop J I, Díaz-Cabrera J M and Ballesteros J 2016 *Plasma Sources Sci. Technol.* **25** 01LT03
[46] Díaz-Cabrera J M, Lucena-Polonio M V, Fernandez Palop J I, Morales Crespo R, Hernández M A, Tejero-del Caz A and Ballesteros J 2012 *J. Appl. Phys.* **111** 063303
[47] Díaz-Cabrera J M, Ballesteros J, Fernandez Palop J I and Tejero-del Caz A 2015 *Plasma Sources Sci. Technol.* **24** 025026
[48] Díaz-Cabrera J M, Fernández Palop J I, Morales Crespo R, Hernández M A, Tejero-del Caz A and Ballesteros J 2014 *Measurement* **55** 66–73
[49] Kuhn S, Riemann K U, Jelić N, Tskhakaya D D, Tskhakaya D and Stanojević M 2006 *Phys. Plasmas* **13** 013503
[50] Fernández Palop J I, Ballesteros J, Colomer V and Hernández M A 1996 *J. Appl. Phys.* **80** 4282–91
[51] Sonin A A 1966 *AIAA J.* **4** 1588–96
[52] Klindworth M, Arp O and Piel A 2006 *J. Phys. D: Appl. Phys.* **39** 1095–104
[53] Ballesteros J, Fernández Palop J I, Hernández M A and Morales Crespo R 2006 *Appl. Phys. Lett.* **89** 101501
[54] Pilling L S and Carnegie D A 2007 *Plasma Sources Sci. Technol.* **16** 570–80
[55] Barth S, Bartzsch H, Glöß D, Frach P, Gittner M and Labitzke R 2016 *Surf. Coat. Technol.* **290** 73–6

applied sciences

MDPI

Article

Influence of the Ion Mass in the Radial to Orbital Transition in Weakly Collisional Low-Pressure Plasmas Using Cylindrical Langmuir Probes

Guillermo Fernando Regodón [1], Juan Manuel Díaz-Cabrera [2,*], José Ignacio Fernández Palop [1] and Jerónimo Ballesteros [1]

[1] Departamento de Física, Campus Universitario de Rabanales, Universidad de Córdoba, 14071 Córdoba, Spain; z62rehag@uco.es (G.F.R.); fa1fepai@uco.es (J.I.F.P.); fa1bapaj@uco.es (J.B.)
[2] Departamento de Ingeniería Eléctrica y Automática, Campus Universitario de Rabanales, Universidad de Córdoba, 14071 Córdoba, Spain
* Correspondence: el1dicaj@uco.es

Received: 15 July 2020; Accepted: 17 August 2020; Published: 19 August 2020

Abstract: This paper presents an experimentally observed transition from the validity of the radial theories to the validity of the orbital theories that model the ion current collected by a cylindrical Langmuir probe immersed in low-pressure, low-temperature helium plasma when it is negatively biased with respect to the plasma potential, as a function of the positive ion-neutral collision mean free path to the Debye length ratio $\Lambda = \lambda_+/\lambda_D$. The study has been also conducted on argon and neon plasmas, which allows a comparison based on the mass of the ions, although no transition has been observed for these gases. As the radial or orbital behavior of the ions is essential to establish the validity of the different sheath theories, a theoretical analysis of such a transition not only as a function of the parameters Λ and $\beta = T_+/T_e$, T_+ and T_e being the positive ion and electron temperature, respectively, but also as a function of the ion mass is provided. This study allows us to recognize the importance of the mass of the ion as the parameter that explains the transition in helium plasmas. Motivated by these theoretical arguments, a novel set of measurements has been performed to study the relationship between the Λ and β parameters in the transition that demonstrate that the effect of the ion mean free path cannot be completely ignored and also that its influence on the ion current collected by the probe is less important than the effect of the ion temperature.

Keywords: plasma surface technology; cold plasma; ion temperature; ion-neutral charge-exchange collisions; ion mean free path; plasma diagnosis; Langmuir probe; sheath theories

1. Introduction

In low-pressure, low-temperature plasmas, the study of the positive ion current collected by the Langmuir probe is very important, as the smallness of the positive ion current collected by the Langmuir probe when it is polarized negatively with respect to the plasma potential allows local diagnosis of the plasma parameters with very low disturbance to the plasma. In other words, the positive ion sheath that is formed around the probe shields out the influence of the probe, which in plasmas with low plasma density is crucial [1–7]. On the other hand, many surface technological processes that use plasmas depend on the ion current that reaches the surface, and thus the control of the ion current is essential in this kind of technology. Among these processes, we have plasma-assisted chemical vapor deposition (PACVD), ion implantation, etching, surface coating, thin films, nanotechnology, etc. [8–13]. In the semiconductor industry, which is a major application of PACVD, the properties of the plasma must be closely examined in order to control the energy and the frequency of the ion

impacts against the surface, so that the optimal conditions for ion implantation are obtained [8,10]. Therefore, both theoretical analysis and experimental studies of the ion sheath surrounding the surface to be treated are important.

The ion current collected by a Langmuir probe has been extensively studied from a theoretical point of view. There are two main groups of theories to explain the fall of the ions towards the probe. The orbital theories, of which orbital motion limited (OML) is the most frequently used, study the movement of the ions in orbits around the probe that are calculated using the applicable laws of conservation. Some ions have a trajectory that does not intersect with the probe surface and orbit back to the plasma, so that not all of the ions are collected by the probe [14–16]. The radial theories, the first being the Allen–Boyd–Reynolds (ABR) theory for a spherical Langmuir probe, study the plasma as a fluid, so that all the ions fall radially towards the probe and therefore all the ions that enter the sheath are collected by the probe [17]. The Allen–Boyd–Reynolds theory, which was soon adapted to cylindrical Langmuir probes by Chen [18], is valid for ions that have an ion temperature that is negligible when compared to the electron temperature, so that the parameter $\beta = T_+/T_e$, with T_+ and T_e as the positive ion and electron temperature, respectively, can be given a value of $\beta = 0$. The cylindrical radial model has been extended by the authors to $\beta \neq 0$ [1,2,19–24].

Both orbital and radial theories are used to diagnose plasmas to obtain plasma parameters such as plasma density. However, the values obtained using the two theories can be very different, the one predicted by the radial theory being up to an order of magnitude higher than the one predicted by the orbital theory. When the values of the plasma parameters deduced from these theories are compared to the values of the plasma parameters obtained using the much higher electron current in the electron saturation zone, depending on the plasma conditions, it is found that either the radial or the orbital theories are consistent with the well-established electron saturation zone theory. This implies a paradox when the ion current is used in plasma diagnosis, given that the appropriate theory that should be used is not known a priori before it is used in plasma diagnosis [1,4,25]. Actually, in many situations which depend on the plasma discharge power and the pressure, values for the ion current collected by the probe between the two theories are measured in experiments [5,26–28]. In two previous papers [26,28], the authors showed an experimentally observed transition in the positive ion current values that are derived from the radial theories and the orbital ones, as a function of the β parameter. The transition takes place only for helium plasmas. Similar experiments on argon and neon plasmas [1,2,19–24] show that the radial theory developed by the authors that takes into account the temperature of the ions, but does not take into account the mass of the ions or the ion mean free path, is successful in predicting the positive ion current.

Neither radial nor orbital models consider collisions in the calculation of the positive ion current of a negatively biased cylindrical Langmuir probe relative to the plasma. The most frequent collision of the ions in their fall towards the probe in low-pressure, low-temperature plasmas is the ion-neutral charge-exchange collision (INCEC) with the neutral atoms of the background gas [29,30]. In INCEC, an electron transitions from the neutral atom to the ion, effectively interchanging the moment between them. In radial models, this loss of moment is similar to a friction force in the fluid, so that the positive ion current is reduced. In the orbital models, the ions may lose their orbital velocity, so that, after the last collision, the ions will lose their angular momentum and fall radially towards the probe [1,2,5,7,17,18,26,28], increasing the positive ion current collected by the probe. The effect of collisions is opposed in both models and will affect not only surface technology but plasma diagnosis methods, both depending on the positive ion current.

Electropositive plasmas can be studied by means of three parameters—that is, the ion to electron temperature ratio, the ion mean free path to Debye length ratio and the ion mass [22,31]. The effect of the ion to electron temperature ratio was studied in previous works [4,22,24,26,28]. The INCEC mean free path is recognized as an important parameter to discriminate between the ABR and the OML behavior in recent theoretical works [29–32]. This article shows an experimentally observed transition from the ABR to the OML behavior as a function of the INCEC mean free path, λ_+, to the Debye length,

λ_D, ratio $\Lambda = \lambda_+/\lambda_D$ [26,28]. This study allowed us to recognize the mass of the ion, m_+, as the critical parameter in the presence of the observed transition in helium plasmas. A theoretical justification of the transition as a function of the β, Λ and ion mass parameters is proposed.

In the Section 2, after this introduction, the experimental setup and measurement method are briefly cited. The Section 3 states the experimental measurement conditions and the methodology. The Section 4 presents the results. In the Section 5, supported by a set of novel measurements, a theoretical discussion about why the transition takes place only for the helium plasmas is proposed. Finally, the Section 6 is an exposition of the conclusions.

2. Experimental Setup and Measurement Method

A high-voltage DC discharge has been chosen for these experiments. The gas is introduced in a large Pyrex cylinder, 40 cm high and with an inner diameter of 31 cm, where two stainless steel electrodes are held 15 cm from each other, each electrode having a diameter of 8 cm. The anode is connected to the ground. The electrodes are supplied a high DC voltage by means of the low ripple/low noise-to-signal ratio KEPCO BHK 2000-0.1MG high-voltage DC power supply. The DC power supply is configured as a current supply, given that the discharge current is related to the electron density and it better serves to characterize the discharge compared to the DC voltage or the discharge power. The entering gas flow is controlled by a mass gas flow controller, MKS 247. A tungsten cylindrical, 6 mm long, 0.1 mm diameter Langmuir probe is placed in the diffuse afterglow of the plasma discharge. In this zone, the plasma is spatially homogeneous and the electron temperature is found to be the lowest, so that the effect of the ion temperature cannot be neglected and the ion to electron temperature ratio, β, is not negligible [1,2,4,7,26,28]. The neutral and positive ions are supposed to be thermalized. As the electrodes are very hot during the measurements, the ion and neutral atom common temperature is estimated to be 350 K [1,2,5,7,24,26,28,33,34].

The current-voltage characteristic of the cylindrical Langmuir probe can be used to obtain an indirect measurement of the parameters that characterize the plasma in the zone of the discharge where it is placed. The plasma potential, V_{plasma}, the floating potential, V_{float}, and the electron energy distribution function, EEDF, can be measured [1,2,4,6,26,34–41]. Regarding the measured EEDF, it is checked that, in every measurement, the EEDF can be considered as following the distribution of Maxwell–Boltzmann [1,4,6,26,28], which is essential since the assumption of a Maxwellian EEDF is made in both radial and orbital theories. The EEDF is used to perform the calculation of the electron temperature, T_e, and the electron density, n_e, which is equal to the ion density, n_+, by means of the quasi-neutrality condition, $n_e \approx n_+$. These values for n_e and T_e have been used as in all further calculations since they do not depend on the radial or orbital theory used to obtain the results. The discharge and the measurements are controlled, and the initial calculations are performed, using a LabView Virtual Instrument [1,4,6,7].

The experimental device has been designed with the objective of obtaining a low electron temperature plasma, so that the ion temperature, in the range of the ambient temperature, becomes non-negligible when compared to the electron one [1]. This property of the DC discharge allowed us to check the validity of the radial theory developed by the authors, which takes into account the temperature of the ions in argon and neon plasmas in the conditions of the discharge [1,2,19–24]. On the other hand, the size of the probe was chosen to be small enough so that the small-radius OML theory would be of applicability in the cases in which the orbital theories are applicable, as was found in the helium plasma in some conditions of the discharge. The LabView-controlled measuring system makes fast measurements, each taking only 4 ms, so that the temperature of the probe does not change during the measurement of the current-voltage characteristic. In order to make sure that the measurements are quick enough, the current-voltage characteristics were measured, starting both in the electron saturation zone and in the ion saturation zone, making no difference to the results of the measurements.

3. Experimental Measurement Conditions and Methodology

The high-voltage DC power supply has an upper limit of 2000 V and 100 mA. The discharge currents are typically much lower, so that the voltage limitation is the relevant one. For argon, neon and helium plasmas, the discharge DC current is always lower than 12.5 mA. The pressure range for the argon plasma is $p(\text{Pa}) \in [2, 10]$; for the neon plasma, it is $p(\text{Pa}) \in [10, 35]$, and for the helium plasma, it is $p(\text{Pa}) \in [13, 37]$. Given that the transition in the validity of the orbital and radial theories is found in the helium plasma, a total of 448 current-voltage characteristics were measured, while in argon and neon plasmas, for which no transition was found, a total of 171 and 111 current-voltage characteristics, respectively, were measured. This set of measurements includes the measurements already published [26,28] together with additional measurements in which we explored the higher electron temperature range in the three kinds of plasmas, although no new insight was gained, as the measurements followed the same trend as the rest of the measurements, albeit extending the range in which the trend was observed. The measured electron density, n_e, gives values in the range from 9×10^{14} to 7×10^{15} m^{-3}, while the electron temperature, T_e, ranges from 1000 to 4400 K, corresponding to β values which vary from 0.08 to 0.35. The $\Lambda = \lambda_+/\lambda_D$ parameter is obtained from the following expression.

$$\lambda_+ = \frac{1}{n_+ \sigma_{+-n}}, \tag{1}$$

with $\sigma_{+-\text{n}}$ being the cross-section for positive ion-neutral collision [10,42], and $\lambda_D = \sqrt{\frac{\epsilon_0 k_B T_e}{e^2 n_e}}$ [10]. For each of the plasmas, the following apply.

- For argon plasmas, the cross-section for positive ion-neutral collision, under our experimental conditions, is $\sigma_{+-\text{n}} = 7.84 \times 10^{-15}$ cm^2 [10,42]. Therefore, the ion mean free path for argon is the following:

$$\lambda_+ = \frac{133}{218 \cdot p(\text{Pa})} (\text{cm}). \tag{2}$$

  Therefore, the Λ values vary from 3.98 to 29.71 for the argon discharges studied in this article.
- For neon plasmas, the cross-section for the ion-neutral collision is $\sigma_{+-\text{n}} = 4.25 \times 10^{-15}$ cm^2 [10,42]. Therefore, the ion mean free path for neon is the following:

$$\lambda_+ = \frac{133}{118 \cdot p(\text{Pa})} (\text{cm}). \tag{3}$$

  Therefore, the Λ values vary from 1.52 to 24.27 for the neon discharges studied in this article.
- For helium plasmas, the cross-section for the ion-neutral collision is $\sigma_{+-\text{n}} = 3.99 \times 10^{-15}$ cm^2 [10,42]. Therefore, the ion mean free path for helium is the following:

$$\lambda_+ = \frac{133}{111 \cdot p(\text{Pa})} (\text{cm}). \tag{4}$$

  Therefore, the Λ values vary from 2.27 to 14.29 for the helium discharges studied in this article.

Note that the upper limit for the ion mean free path to Debye length ratio Λ for the three gases decreases with decreasing ion mass, such that for argon, the upper limit is $\Lambda_{max,Ar} = 29.31$, close to the double the helium Λ upper limit, $\Lambda_{max,He} = 14.29$. It is also interesting to compare these Λ ranges with the sheath edge, which has values always lower than $k \cdot \lambda_D$. The k value depends on the sheath edge criteria used, usually considered to be $4 < k < 8$ [20,34,36], but regardless of the criteria used, there is a range in which the ion mean free path is comparable to the size of the sheath.

Two novel series of measurements were performed in the helium plasma, one for constant background pressure $P = 20.2$ Pa and one for constant discharge current $I_d = 5.0$ mA.

The methodology that is followed in this work is based on the use of the Sonin plot [1,2,4,26,28], which uses the positive ion current per unit length collected by the probe, $I_{+,}$ when it is biased at a fixed electric potential, V_p in $k_B T_e/e$ units, e being the elementary charge and k_B the Boltzmann constant, referring to the plasma potential, V_{plasma} [43]. In the Sonin plot, the ordinate of the plot is the non-dimensional ion current,

$$y_{Sonin} = I'(y_{SP}) = \frac{I_+(y_{SP})}{e r_p n_+} \sqrt{\frac{m_+}{2\pi k_B T_e}}, \tag{5}$$

where r_p is the probe radius and y_{SP} is defined as the non-dimensional probe potential $y_{SP} = -eV_p/k_B T_e$. The abscissa of the plot has the following expression:

$$x_{Sonin} = {x_p}^2 I'(y_{SP}) = \frac{I_+(y_{SP}) e r_p}{\varepsilon_0} \sqrt{\frac{m_+}{2\pi {k_B}^3 {T_e}^3}}, \tag{6}$$

which does not depend on the ion density, with x_p being the non-dimensional probe radius $x_p = r_p/\lambda_D$. The V_p value must be chosen carefully, so that it is negative enough to ensure that the current collected by the probe is almost exclusively positive ion current, and the electron current can be neglected. Regarding the other extreme, if the difference between the plasma potential and the probe potential is too high, the emission of secondary electrons from the probe would be accounted for as an increase in the positive ion current collected by the Langmuir probe [1,2,4,5,26,28]. As in other articles, we have chosen $y_{SP} = -eV_p/k_B T_e = 25$ [1,2,4,26,28], which accounts for V_p values in the range $V_p(\mathrm{V}) \in [2.15, 9.48]$ for the given range of electron temperatures $T_e(\mathrm{K}) \in [1000, 4400]$. A single point in the Sonin plot is obtained for each set of plasma conditions—that is, for each set of experimental values for $I_+\left(V_p\right)$, n_e and T_e [1,4,5,26,28]. The experimental Sonin plot point is placed in the Sonin plot and its position relative to the theoretical orbital and radial curves is analyzed. The plasma conditions are studied in relation to the position of the experimental Sonin plot points.

4. Results

The experimental points are plotted for the different plasmas in Figures 1–3. The experimental Sonin plot points are grouped in terms of the INCEC mean free path to Debye length ratio Λ, which allows a comparison between the three plasmas in which the scale of the sheath varies with the Debye length. We show the Sonin plot that includes the theoretical curves that correspond to the orbital and the radial theories in Figures 1–3. The complete solution by Laframboise [16] for the orbital theory is used, calculated from the fitting curves obtained by Peterson and Talbot [44]. The radial model developed by the authors for several β values, which converge to the Allen–Boyd–Reynolds model adaptation to cylindrical Langmuir probes by Chen for negligible ion temperature with respect to the electron temperature [19,21,22]. In Figure 1, we also show the experimental Sonin plot points corresponding to different ranges in the Λ parameter for argon plasmas. The results of the measurements show that the radial theory describes appropriately the positive ion current collected by a cylindrical Langmuir probe immersed in an argon plasma, in the conditions of the DC discharge used in the measurements.

Figure 2 shows the experimental Sonin plot points obtained from the different neon plasma discharge conditions measured. Figure 2 also includes the experimental points colored and symbolized as a function for the Λ parameter. As can be seen in Figures 1 and 2, the Λ parameter shows an evolution in the Sonin plot points—that is, the points for which the ion mean free path is longer are grouped to the right, while the points for which the ion mean free path is short are grouped to the left. These points are located over the radial model theoretical curves for $\beta \neq 0$ and fit well with the experimental β values for each point. Therefore, the influence of Λ is not very important in terms of the ions' behavior in this range for argon and neon plasmas.

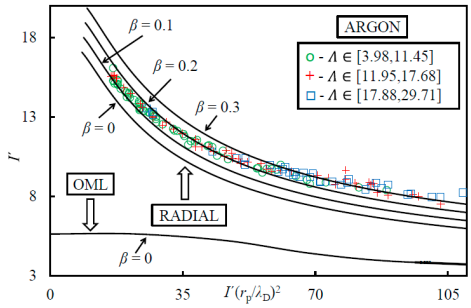

Figure 1. Argon plasma Sonin plot for the normalized probe potential $y_{SP} = 25$. Experimental data for the argon plasma: green circles for $3.98 \leq \Lambda \leq 11.45$, red crosses for $11.95 \leq \Lambda \leq 17.68$ and blue squares for $17.88 \leq \Lambda \leq 29.71$. In solid lines, the orbital and radial theoretical curves are shown.

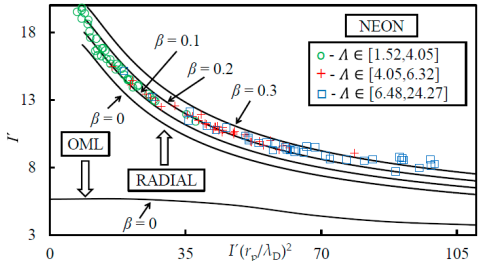

Figure 2. Neon plasma Sonin plot for the normalized probe potential $y_{SP} = 25$. Experimental data for the neon plasma: green circles for $1.52 \leq \Lambda \leq 4.05$, red crosses for $4.05 \leq \Lambda \leq 6.32$ and blue squares for $6.48 \leq \Lambda \leq 24.27$. In solid lines, the orbital and radial theoretical curves are shown.

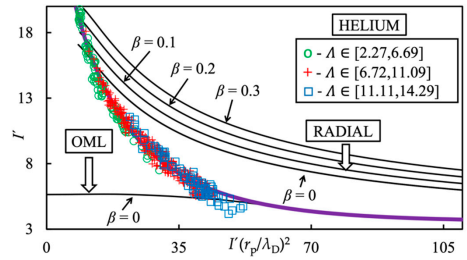

Figure 3. Helium plasma Sonin plot for the normalized probe potential $y_{SP} = 25$. Experimental data for the helium plasma: green circles for $2.27 \leq \Lambda \leq 6.69$, red crosses for $6.72 \leq \Lambda \leq 11.09$ and blue squares for $11.11 \leq \Lambda \leq 14.29$. In solid lines, the orbital and radial theoretical curves are shown. In purple bold line, the fitting curve for the experimental helium plasma Sonin plot points is shown.

As in Figures 1 and 2, Figure 3 shows the Sonin plot for the experimental points colored and symbolized as a function of the Λ parameter. On one hand, those points corresponding to the lower Λ values (green circles for $2.27 \leq \Lambda \leq 6.69$) are mainly placed in the radial zone or close to it, and none of them are placed in the orbital zone. On the other hand, those points corresponding to the higher Λ values (blue squares for $11.11 \leq \Lambda \leq 14.29$) are mainly placed in the orbital zone or close to it, and none of them are placed in the radial zone. Finally, those points corresponding to intermediate Λ values (red crosses for $6.72 \leq \Lambda \leq 11.09$) are mainly placed in the intermediate zone, where none of the theories

are verified, and only a few of them are placed in the other zones. Nevertheless, Figures 1–3 show that the dependence on Λ does not seem to be so critical than that on β [26,28], since the Λ parameter depends not only on T_+ and T_e but also on $n_e \approx n_+$ and p through λ_+ and λ_D. Finally, Figure 3 also shows a fitting curve that may be used to diagnose this helium plasma in these conditions of pressure and discharge current, and that converges with OML in the range of abscissa of the Sonin plot, x_{Sonin}, of $[70, 100]$. However, although it is of great theoretical interest, the transition range of plasma conditions for the helium plasma should be avoided in plasma diagnosis by means of the Sonin plot, and the plasma conditions should be used in which one of the two theories, ABR or OML, is valid. The fitting curve, in purple bold line in Figure 3, follows the following formula:

$$y_{Sonin\ He,exp} = ae^{-b(x_{Sonin\ He,exp})^c} + d, \tag{7}$$

with $a = 32.11693$, $b = 0.13901$, $c = 0.77237$ and $d = 3.56418$.

5. Discussion

The finiteness of the ion mean free path and the experimental observation of its influence in the transition from radial to orbital behavior can be justified theoretically. After the last collision, the ions lose their orbital motion, so, for small β and Λ values, the OML theory cannot appropriately describe the ion current collected by the probe. For higher ion temperatures, after the last collision, the ions have a non-negligible velocity in a random direction. For the ions that have a direction that is predominantly in the azimuthal direction of cylindrical coordinates, the mean thermal velocity is important enough so that the trajectory of the ion will not intersect the probe and the ion will orbit around the probe back to the plasma. The mass of the ion thus becomes an essential parameter, since the mass of the ion is inversely proportional to the square of the thermal velocity.

$$\overline{v_{+,th}} = \sqrt{\frac{2k_B T_+}{m_+}}, \tag{8}$$

where m_+ is the mass of the ion. This fact explains why the transition is only found in the helium plasma but not in neon or argon plasmas.

The most frequent ion collision in this kind of plasma is INCEC, which removes an accelerated ion and results in a new ion with the temperature of the background gas [45,46]. It is interesting to note that the effect of INCEC in both radial and orbital models is the opposite: on one hand, in orbital models, usually the new ion created after an INCEC has a lower orbital kinetic energy, so the ion is more likely to be collected by the probe. If the orbital motion limited model is used, the exact potential profile of the sheath can be ignored, and the probability of the ion being collected can be calculated using the conservation laws. Therefore, the positive ion current collected by the probe is increased when INCEC is taken into account [47–49]. On the other hand, the effect of collisions in radial models is to reduce the mean velocity of the fluid particle, which is composed by many ions, in its fall towards the probe. That is, the positive ion current collected by the probe is reduced, having an effect similar to that of the transition from radial to orbital behavior. This effect can be estimated using the radial model that takes into account the ion temperature and the collisions of ions with neutral atoms developed by the authors [31] and proved to be opposite to the effect of the positive ion temperature in radial models, which increases the positive ion current [1,2,4,5,19,21,22,26,28]. It is interesting to note that, in neon and argon plasmas, the points in the Sonin plot shift up into regions of higher theoretical β values with increasing Λ, as can be seen in Figures 1 and 2, which is consistent with this development for radial theories—that is, less collisions in the ion sheath and a higher ion to electron temperature ratio have a similar effect in radial theories of increasing the current both in neon and argon plasmas, in the range of discharge parameters studied.

In the helium plasmas, the same increase in the ion mean free path to Debye length ratio Λ and in the ion to electron temperature ratio β has a very different influence on the movement of the ions in their fall towards the probe. The effect of collisions in the helium plasma can be studied with the available experimental data of the discharge. If the discharge current is decreased while maintaining the background pressure, the plasma and the electron density decrease [40,41]. Therefore, the Debye length increases, and the ion mean free path to Debye length ratio—that is, the Λ parameter—is decreased. We note in Equation (1) that the λ_+ parameter is constant if the background pressure is kept constant. Moreover, the measurements show that the electron temperature is higher when the discharge current is lower [40,41], so that the effect of a decrease in the discharge current is to cause a decrease in the β parameter value and a decrease in the Λ parameter (Figure 4). We have performed a series of novel measurements at constant background pressure, changing the discharge current, which show that the predicted trend is correct. This does not allow us to distinguish between the effect of the ion to electron temperature ratio β and the effect of the ion mean free path to Debye length ratio Λ in the experiments. However, if the discharge current is kept constant, the plasma density remains constant and so does the electron density [40]. Moreover, if the background pressure is decreased, the measurements show that the electron temperature, T_e, increases [40,41], causing a decrease in β. Accordingly, regarding the Λ parameter, we predict two opposite influences: (a) the Debye length increases with T_e, and thus the Λ parameter decreases; (b) the collisions are less frequent, increasing λ_+, and so the Λ parameter increases. Therefore, the trend that the Λ parameter will follow with changing background pressure alone cannot be predicted for a constant discharge current. We have also performed a series of novel measurements at constant discharge current to verify the influence of the background pressure on both the β and Λ parameters. Figure 5 shows that a decrease in the β parameter and an increase in the Λ parameter are experimentally found when the gas pressure decreases, according to argument (b) above. As the transition is found for decreasing background pressure, this proves that the most relevant parameter in the transition between radial and orbital behavior of the ions in the helium plasma is the positive ion to electron temperature ratio, β.

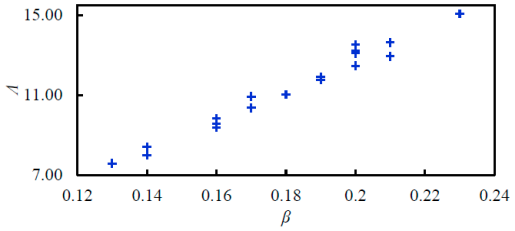

Figure 4. Increasing figure between β and Λ for constant background helium pressure $p = 20.2$ Pa.

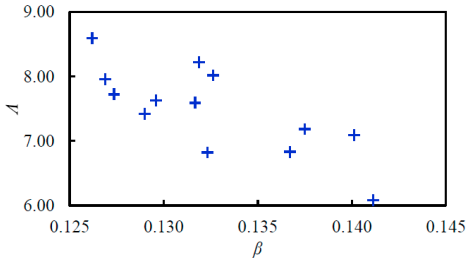

Figure 5. Decreasing figure between β and Λ for constant discharge current $I_d = 5.0$ mA in a helium discharge.

6. Conclusions

In plasma diagnosis experiments, when measuring the ion current collected by a cylindrical Langmuir probe, it is found that sometimes the orbital theories correctly predict the ion current and, at other times, the radial theories are found to be valid. Therefore, a transition from the validity of the orbital theories towards the validity of the radial theories is expected, depending on the experimental conditions of the plasma—that is, the ion temperature to electron temperature ratio, β, and the ion mean free path to Debye length ratio, Λ.

The transition has been theoretically justified in the context of INCEC, so that positive ions lose their translation kinetic energy in collisions with the neutral atoms of the background gas. Therefore, for small β and Λ values, after the last collision, the ions lose their orbital motion and the OML model is no longer valid to describe the ion current collected by the probe. This way, when collisions are included, the OML model provides higher positive ion current collected by the probe, i.e., approaching the values predicted by the ABR model. Alternatively, for higher Λ values, after the last collision, the ions are far away from the probe, and the orbital component of the ion thermal motion is high enough for those ions to fall towards the probe, following an orbital trajectory, diminishing the ion current collected by probe, i.e., approaching the OML model.

The aforementioned transition has been experimentally observed only for helium plasmas and not for argon and neon plasmas, and it has been justified due to the lower mass of the helium ions, which makes the helium thermal velocity higher for the same ion temperature. Therefore, only for higher Λ and β values in helium plasmas, the transition has been observed. Moreover, as an extreme case comparison, for electrons of even lower mass, the OML theory always predicts well the electron current collected when the probe is positively biased with respect to the plasma potential. Although it has been proven that the positive ion to electron temperature ratio, β, is a more relevant parameter than the INCEC mean free path to Debye length ratio Λ in the transition between radial and orbital behavior of the ions, the ion mass is crucial, since it determines the existence of the transition.

In view of these experimental results and theoretical arguments, the positive ion thermal motion and the collisions must be included in the sheath models, since they influence the radial or orbital behavior of the positive ion current to the substrate/probe, even though the collisions included in this article mainly take place outside of the sheath. This fact also explains that the β parameter has a more definite influence on the transition than the Λ one, as shown in Figures 4 and 5, but the influence of the ion mean free path to Debye length ratio Λ cannot be altogether ignored.

Author Contributions: Conceptualization, J.M.D.-C. and J.B.; methodology, J.M.D.-C. and J.B.; software, G.F.R. and J.M.D.-C.; validation, J.I.F.P. and J.B.; formal analysis, J.B.; investigation, G.F.R. and J.M.D.-C.; resources, J.I.F.P. and J.B.; data curation, G.F.R. and J.M.D.-C.; writing—original draft preparation, J.B.; writing—review and editing, G.F.R., J.M.D.-C., J.I.F.P. and J.B.; visualization, J.I.F.P. and J.B.; supervision, J.I.F.P. and J.B.; project administration, J.M.D.-C.; funding acquisition, G.F.R. and J.I.F.P. All authors have read and agreed to the published version of the manuscript.

Funding: This research has been partially funded by the Spanish Ministry of Science and Innovation, ref. no FIS2010-19951, which is partially financed with FEDER funds, and the FPU Program of the Spanish Ministry of Education (ref. FPU17/01387).

Conflicts of Interest: The authors declare no conflict of interest.

References

1. Díaz-Cabrera, J.M.; Fernández Palop, J.I.; Morales Crespo, R.; Hernández, M.A.; Tejero-Del-Caz, A.; Ballesteros, J. Virtual Instrument for automatic low temperature plasmas diagnostic considering finite positive ion temperature. *Measurement* **2014**, *55*, 66–73. [CrossRef]
2. Ballesteros, J.; Fernández Palop, J.I.; Hernández, M.A.; Morales Crespo, R. Influence of the positive ion temperature in cold plasma diagnosis. *Appl. Phys. Lett.* **2006**, *89*, 101501. [CrossRef]
3. Dengra, A.; Ballesteros, J.; Colomer, V.; Hernández, M.A. Investigation of the creation process in dc pulsed discharges. *J. Appl. Phys.* **1990**, *68*, 5507–5510. [CrossRef]

4. Díaz-Cabrera, J.M.; Lucena-Polonio, M.V.; Fernández Palop, J.I.; Morales Crespo, R.; Hernández, M.A.; Tejero-Del-Caz, A.; Ballesteros, J. Experimental study of the ion current to a cylindrical Langmuir probe taking into account a finite ion temperature. *J. Appl. Phys.* **2012**, *111*, 063303. [CrossRef]
5. Annaratone, B.M.; Allen, M.W.; E Allen, J. Ion currents to cylindrical Langmuir probes in RF plasmas. *J. Phys. D Appl. Phys.* **1992**, *25*, 417–424. [CrossRef]
6. Ballesteros, J.; Fernández Palop, J.I.; Hernaández, M.A.; Morales Crespo, R.; Del Pino, S.B. LabView virtual instrument for automatic plasma diagnostic. *Rev. Sci. Instruments* **2004**, *75*, 90–93. [CrossRef]
7. Lucena-Polonio, M.V.; Díaz-Cabrera, J.M.; Fernández Palop, J.I.; Morales Crespo, R.; Hernández, M.A.; Ballesteros, J. Mass spectrometry diagnosis of ion species in low-pressure plasmas. *Plasma Phys. Control. Fusion* **2011**, *53*, 124024. [CrossRef]
8. Chen, F.F. Industrial applications of low-temperature plasma physics. *Phys. Plasmas* **1995**, *2*, 2164–2175. [CrossRef]
9. Annemie, B.; Neyts, E.; Gijbels, R.; van der Mullen, J. Gas Discharge Plasmas and Their Applications. *Spectrochim. Acta Part B At. Spectrosc.* **2002**, *57*, 609–658.
10. Lieberman, M.A.; Lichtenberg, A.J. *Principles of Plasma Discharges and Materials Processing*; John Wiley & Sons: Hoboken, NJ, USA, 2005.
11. Shashurin, A.; Li, J.; Zhuang, T.; Keidar, M.; Beilis, I.I. Application of electrostatic Langmuir probe to atmospheric arc plasmas producing nanostructures. *Phys. Plasmas* **2011**, *18*, 073505. [CrossRef]
12. Weltmann, K.-D. Future trends in plasma science. *Plasma Process. Polym.* **2018**, *16*, e1890001. [CrossRef]
13. Laroussi, M. Cold Plasma in Medicine and Healthcare: The New Frontier in Low Temperature Plasma Applications. *Front. Phys.* **2020**, *8*. [CrossRef]
14. Mott-Smith, H.M.; Langmuir, I. The Theory of Collectors in Gaseous Discharges. *Phys. Rev.* **1926**, *28*, 727–763. [CrossRef]
15. Bernstein, I.B.; Rabinowitz, I.N. Theory of Electrostatic Probes in a Low-Density Plasma. *Phys. Fluids* **1959**, *2*, 112–121. [CrossRef]
16. LaFramboise, J.G. Theory of Spherical and Cylindrical Langmuir Probes in a Collisionless, Maxwellian Plasma at Rest. Ph.D. Thesis, University of Toronto, Toronto, ON, Canada, 1 June 1966.
17. E Allen, J.; Boyd, R.L.F.; Reynolds, P. The Collection of Positive Ions by a Probe Immersed in a Plasma. *Proc. Phys. Soc. Sect. B* **1957**, *70*, 297–304. [CrossRef]
18. Chen, F.F. Numerical computations for ion probe characteristics in a collisionless plasma. *J. Nucl. Energy. Part C Plasma Physics, Accel. Thermonucl. Res.* **1965**, *7*, 47–67. [CrossRef]
19. Fernández Palop, J.I.; Ballesteros, J.; Colomer, V.; Hernández, M.A. Theoretical ion current to cylindrical Langmuir probes for finite ion temperature values. *J. Phys. D Appl. Phys.* **1996**, *29*, 2832–2840. [CrossRef]
20. Morales Crespo, R.; Fernández Palop, J.I.; Hernaández, M.A.; Ballesteros, J. Analytical fit of the I–V characteristic for cylindrical and spherical Langmuir probes. *J. Appl. Phys.* **2003**, *94*, 4788. [CrossRef]
21. Morales Crespo, R. Analytical fit of the I–V probe characteristic for finite ion temperature values: Justification of the radial model applicability. *J. Appl. Phys.* **2004**, *95*, 2982. [CrossRef]
22. Regodón, G.F.; Fernández Palop, J.I.; Tejero-Del-Caz, A.; Díaz-Cabrera, J.M.; Carmona-Cabezas, R.; Ballesteros, J. Removal of singularity in radial Langmuir probe models for non-zero ion temperature. *Phys. Plasmas* **2017**, *24*, 103516. [CrossRef]
23. Regodón, G.F.; Fernández Palop, J.I.; Tejero-Del-Caz, A.; Díaz-Cabrera, J.M.; Carmona-Cabezas, R.; Ballesteros, J. Floating potential in electronegative plasmas for non-zero ion temperatures. *Plasma Sources Sci. Technol.* **2018**, *27*, 025014. [CrossRef]
24. Tejero-Del-Caz, A.; Fernández Palop, J.I.; Díaz-Cabrera, J.M.; Ballesteros, J. Radial-to-orbital motion transition in cylindrical Langmuir probes studied with particle-in-cell simulations. *Plasma Sources Sci. Technol.* **2015**, *25*, 01LT03. [CrossRef]
25. Pilling, L.S.; A Carnegie, D. Validating experimental and theoretical Langmuir probe analyses. *Plasma Sources Sci. Technol.* **2007**, *16*, 570–580. [CrossRef]
26. Díaz-Cabrera, J.M.; Ballesteros, J.; Fernández Palop, J.I.; Tejero-Del-Caz, A. Experimental radial motion to orbital motion transition in cylindrical Langmuir probes in low pressure plasmas. *Plasma Sources Sci. Technol.* **2015**, *24*, 25026. [CrossRef]
27. Tejero-Del-Caz, A.; Fernández Palop, J.I.; Díaz-Cabrera, J.M.; Regodón, G.F.; Carmona-Cabezas, R.; Ballesteros, J. Ion injection in electrostatic particle-in-cell simulations of the ion sheath. *J. Comput. Phys.* **2017**, *350*, 747–758. [CrossRef]

28. Díaz-Cabrera, J.M.; Fernández Palop, J.I.; Regodón, G.F.; Ballesteros, J. Accurate measurement of the ion saturation current collected by a cylindrical Langmuir probe in cold plasmas. *Plasma Process. Polym.* **2020**, 1–12. [CrossRef]
29. Franklin, R.N.; Snell, J. The plasma-sheath transition with a constant mean free path model and the applicability of the Bohm criterion. *Phys. Plasmas* **2001**, *8*, 643–647. [CrossRef]
30. Robertson, S. Sheaths in laboratory and space plasmas. *Plasma Phys. Control. Fusion* **2013**, *55*, 093001. [CrossRef]
31. Regodón, G.F.; Fernández Palop, J.I.; Díaz-Cabrera, J.M.; Ballesteros, J. Influence of collisions in a fluid model for the warm-ion sheath around a cylindrical Langmuir probe. *Plasma Sources Sci. Technol.* **2019**, *28*, 115017. [CrossRef]
32. Tsankov, T.V.; Czarnetzki, U. Information hidden in the velocity distribution of ions and the exact kinetic Bohm criterion. *Plasma Sources Sci. Technol.* **2017**, *26*, 055003. [CrossRef]
33. Gudmundsson, J.T.; Kimura, T.; A Lieberman, M. Experimental studies of O2/Ar plasma in a planar inductive discharge. *Plasma Sources Sci. Technol.* **1999**, *8*, 22–30. [CrossRef]
34. Godyak, V.A.; Piejak, R.B.; Alexandrovich, B.M. Probe diagnostics of non-Maxwellian plasmas. *J. Appl. Phys.* **1993**, *73*, 3657–3663. [CrossRef]
35. Regodón, G.F.; Fernández Palop, J.I.; Díaz-Cabrera, J.M.; Ballesteros, J. Floating potential calculation for a Langmuir probe in electronegative plasmas and experimental validation in a glow discharge. *Plasma Phys. Control. Fusion* **2019**, *61*, 095015. [CrossRef]
36. Swift, J.D.; Schwar, M.J.R. *Electrical Probes for Plasma Diagnosis*; Iliffe Books Ltd.: London, UK, 1970.
37. Demidov, V.I.; Ratynskaia, S.V.; Rypdal, K. Electric probes for plasmas: The link between theory and instrument. *Rev. Sci. Instruments* **2002**, *73*, 3409–3439. [CrossRef]
38. Curreli, D.; Chen, F.F. Equilibrium theory of cylindrical discharges with special application to helicons. *Phys. Plasmas* **2011**, *18*, 113501. [CrossRef]
39. Stamate, E. Status and challenges in electrical diagnostics of processing plasmas. *Surf. Coat. Technol.* **2014**, *260*, 401–410. [CrossRef]
40. Fernández Palop, J.I.; Ballesteros, J.; Colomer, V.; Hernaández, M.A. A new smoothing method for obtaining the electron energy distribution function in plasmas by the numerical differentiation of the I-V probe characteristic. *Rev. Sci. Instruments* **1995**, *66*, 4625–4636. [CrossRef]
41. Fernández Palop, J.I.; Ballesteros, J.; Colomer, V.; Hernaández, M.A. Transient processes in an Ar+I2 dc discharge. *J. Appl. Phys.* **1996**, *80*, 4282–4291. [CrossRef]
42. Maiorov, S.A.; Petrov, O.F.; Fortov, V.E. Calculation of resonant charge exchange cross-sections of ions Rubidium, Cesium, Mercury and noble gases. In Proceedings of the 34th EPS Conference on Plasma Physics, Warsaw, Poland, 2–6 July 2007.
43. Sonin, A.A. Free-molecule Langmuir probe and its use in flow-field studies. *AIAA J.* **1966**, *4*, 1588–1596. [CrossRef]
44. Peterson, E.W.; Talbot, L. Langmuir probe response in a turbulent plasma. *AIAA J.* **1970**, *8*, 1391–1398. [CrossRef]
45. Phelps, A.V. The application of scattering cross sections to ion flux models in discharge sheaths. *J. Appl. Phys.* **1994**, *76*, 747–753. [CrossRef]
46. Riemann, K.-U. Kinetic theory of the plasma sheath transition in a weakly ionized plasma. *Phys. Fluids* **1981**, *24*, 2163. [CrossRef]
47. Zakrzewski, Z.; Kopiczynski, T. Effect of collisions on positive ion collection by a cylindrical Langmuir probe. *Plasma Phys.* **1974**, *16*, 1195–1198. [CrossRef]
48. Sternovsky, Z.; Robertson, S.; Lampe, M. Ion collection by cylindrical probes in weakly collisional plasmas: Theory and experiment. *J. Appl. Phys.* **2003**, *94*, 1374. [CrossRef]
49. Sternovsky, Z.; Robertson, S.; Lampe, M. The contribution of charge exchange ions to cylindrical Langmuir probe current. *Phys. Plasmas* **2003**, *10*, 300–309. [CrossRef]

4.2 Como coautor

Journal of Computational Physics 350 (2017) 747–758

Contents lists available at ScienceDirect

Journal of Computational Physics

www.elsevier.com/locate/jcp

Ion injection in electrostatic particle-in-cell simulations of the ion sheath

A. Tejero-del-Caz [a,*], J.I. Fernández Palop [b], J.M. Díaz-Cabrera [c], G.F. Regodón [b], R. Carmona-Cabezas [b], J. Ballesteros [b]

[a] Instituto de Plasmas e Fusão Nuclear, Instituto Superior Técnico, Universidade de Lisboa, Av Rovisco Pais, 1049-001 Lisboa, Portugal
[b] Departamento de Física, Universidad de Córdoba, E-14071 Córdoba, Spain
[c] Departamento de Ingeniería Eléctrica, Universidad de Córdoba, E-14071 Córdoba, Spain

ARTICLE INFO

Article history:
Received 17 June 2017
Received in revised form 31 August 2017
Accepted 9 September 2017
Available online 12 September 2017

Keywords:
Plasma diagnostic
Langmuir probes
Sheath theories
PIC
Simulations

ABSTRACT

A particle injection algorithm has been developed for its use in electrostatic particle-in-cell (PIC) simulations of the ion sheath which takes place in the surroundings of a planar electrode immersed in a plasma when negatively biased. The algorithm takes into account the acceleration of ions along the presheath and evaluates their flux and velocity distribution when entering the simulation at the sheath edge. It has been verified by comparing the results obtained from the PIC simulation with those provided by fluid models of the ion sheath. The algorithm can be easily extended to cylindrical or spherical geometries and, in fact, it has already been successfully used to study the transition from radial to orbital behaviour of ions in the surroundings of cylindrical Langmuir probes.

1. Introduction

Nowadays, many surface treatment techniques rely on plasma technology [1] which, ultimately, depend on the sheath that takes place between a neutral plasma and the surface that is going to be treated. In many cases, in order to perform the functionalisation of the surface, it is polarised in such a way that it attracts positive ions. Also, plasma diagnosis by using electrostatic Langmuir probes, which constitutes one of the few methods that provides local measurements on plasma parameters [2–7], depends on the plasma-sheath properties. Likewise, one of the most attractive conditions to perform the diagnose with Langmuir probes, is to negatively bias them with respect to the plasma as, by doing so, the current collected by the probe and drained from the plasma is diminished and so the disturbance produced by the presence of the probe [8–10]. Because of the aforementioned reasons, the theoretical knowledge of the structure of the ion sheath that is developed between a neutral plasma and a negatively biased metallic surface, results of great importance.

There are two main approaches when it comes to obtain theoretical knowledge about the ion sheath: fluid or kinetic modelling and particle simulations [11]. On the one hand, fluid or kinetic modelling is fast and sometime allow us to obtain analytical expressions that are useful when it comes to diagnose a plasma. However, because of their lack of selfconsistency and macroscopic nature, in the case of fluid models, they are not always the most suitable approach. On the other hand, particle simulations [11–13] constitute a selfconsistent first principles approach that provides the most detailed information about the system. Nevertheless, there are some drawbacks when it comes to use particle simulations. The computational

* Corresponding author.
E-mail address: antonio.tejero@tecnico.ulisboa.pt (A. Tejero-del-Caz).

http://dx.doi.org/10.1016/j.jcp.2017.09.018
0021-9991/

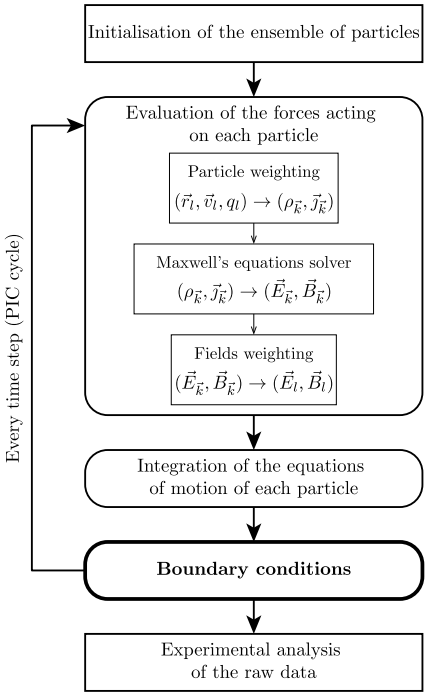

Fig. 1. General scheme of a PIC simulation. The l subindex refers to particles while the $\vec{k}$ subindex refers to grid nodes.

resources needed are huge, and one has to be careful with the different physical mechanisms and algorithms implemented in the simulation, since they can greatly affect its behaviour and the results provided by it, as we will see in this paper.

When we talk about particle simulations in plasma science, we mostly refer to the well known particle-in-cell (PIC) codes [13]. The main difference between PIC and any other particle simulation lies in the force evaluation algorithm. In PIC simulations, the simulation domain is gridded and, the forces acting on each particle are evaluated by considering a macroscopic field which is evaluated at the nodes of the grid. In Fig. 1 the general scheme of a PIC simulation can be seen. However, in this paper we will be focused on the case of electrostatic simulations, *i.e.* non magnetised plasmas.

PIC simulations are well known algorithms [11–13] and, the effects of the different numerical schemes that can be used in the various steps, that can be seen in Fig. 1, have been extensively studied [14–16]. However, there exists a common problem that appears when simulating an ion sheath, *i.e.* the contact of a plasma with a negatively biased metallic surface. When the loading of particles, or more precisely of the ions, is not performed properly a "source sheath" may appear [17–19].

Some solutions to this problem have been proposed [20], however, they depend on macroscopic coefficients such as diffusion or mobility coefficients, which are not usually easy to obtain. In this paper, we present an iterative selfconsistent algorithm that allows to avoid the appearance of this source sheath, without the need of macroscopic coefficients.

The rest of the paper is organised as follows: in 2 the statement of the problem is presented, defining what a source sheath is and explaining the reasons of its appearance. In 3 the proposed algorithm for the ion injection is introduced. Then, in 4, the results obtained when using the proposed injection algorithm are shown. Finally, in 5, the conclusions of the present research are outlined.

2. Statement of the problem

Let us start by defining what a source sheath is. A source sheath is a sheath-like potential drop that occurs at the boundary where particles are injected into the simulation, *i.e.* the source of particles. Source sheaths appear in PIC simulations of the contact of an electrode with an unperturbed plasma. They are more pronounced when the electrode that is being simulated has planar geometry, however, it has also impact when other geometries are considered. The appearance of source sheaths has been observed since long time ago [17], however they are still a common problem [18,19].

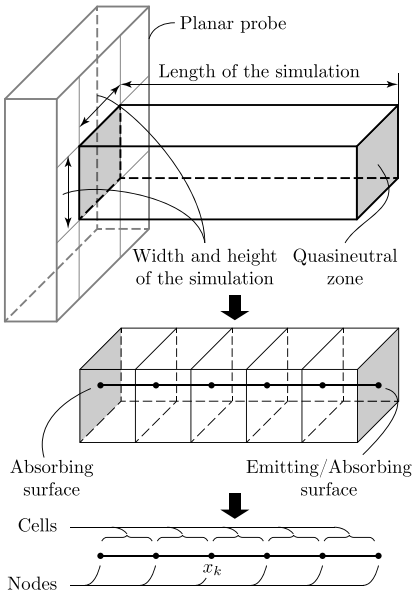

Fig. 2. Computational abstraction for the simulation (1d1v) of the ion sheath developed in front of a planar electrode.

When developing a PIC simulation of a plasma, there are four main boundary conditions that can be implemented: reflecting, cyclic, absorbing and emitting boundary conditions. On the one hand, when implementing the three former conditions, one has to be careful in order to avoid numerical errors [21], nevertheless, there is not much physics involved in those. But, on the other hand, when developing emitting boundary conditions, the physical properties of the boundary have to be carefully taken into account. That is, the properties of the particles injected into the simulation, in particular their velocity distribution function (VDF), must exactly match those of the real particles at the physical boundary. Otherwise, problems such as source sheaths may appear.

For the sake of simplicity, let us consider the case of a planar electrode immersed in a plasma consisting of singly ionised ions and electrons. In the planar case, the problem of the ion sheath is monodimensional. So, let us think of a 1d1v PIC simulation of the contact of a negatively biased electrode with a plasma. The computational abstraction of such simulation can be seen in Fig. 2. It has to be noticed that the right boundary (RB) of Fig. 2 has been labeled as *Quasineutral zone*, however, that boundary is usually considered to be located at the unperturbed plasma and particles are injected there with a maxwellian VDF. This seems to be a reasonable assumption, as long as the length of the simulation is large enough. In this case, we can assume that particles at the plasma are thermalised and therefore follow a maxwellian distribution function. Nonetheless, we are going to see how these assumptions are wrong and, consequently, they lead to wrong results.

First, we are going to perform a PIC simulation just as has been described in the previous paragraph, *i.e.* the RB of the simulation is assumed to be located at the unperturbed plasma, and particles are injected into the simulation with maxwellian distributed velocities corresponding to a certain prescribed temperature, as given by:

$$f(v)\,\mathrm{d}v = v\sqrt{\frac{m}{2\pi k_\mathrm{B} T}}\exp\left(-\frac{mv^2}{2k_\mathrm{B}T}\right)\mathrm{d}v, \tag{1}$$

m being the particle mass, T its temperature and k_B the Boltzmann constant.

We have to notice that (1) is normalised to the unity, so it gives us the probability of particles entering the simulation to have velocities $v \in [v, v + \mathrm{d}v]$. In order to obtain the number of particles entering the simulation per time and surface units, *i.e.* the incoming flux of particles that the simulation is fed with, we have to multiply (1) by the number density of particles at the boundary and integrate the resulting expression for all the velocities. In this case, since we are considering the right boundary of the simulation to be located at the unperturbed plasma, the number density of particles there is given by the electron plasma density, $n_{\mathrm{e}0}$. So, the thermal flux of particles entering the simulation is given by:

$$\Phi_\mathrm{th} = n_{\mathrm{e}0}\sqrt{\frac{k_\mathrm{B}T}{2\pi m}}. \tag{2}$$

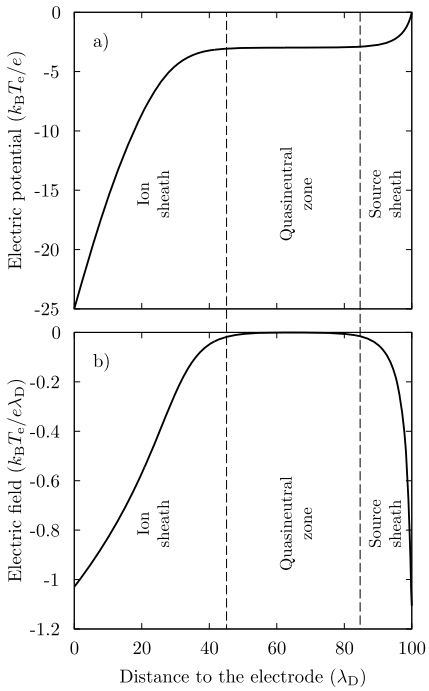

Fig. 3. Source sheath developed in a PIC simulation.

In the simulation, all the magnitudes are measured in dimensionless units and the plasma is the reference for the electric potential. The electrode is biased at $-25\ k_B T_e/e$, the length of the simulation is 100 λ_D and the ion temperature is set to $0.1T_e$. Also, regarding the numerical parameters of the simulation: the space step is set to 0.2 λ_D and the time step is set to 0.01 ω_{pe}^{-1}. Where e represents the elementary charge, λ_D the Debye length and ω_{pe} the electron plasma frequency.

With the previous configuration, the electric potential distribution in the simulation domain, obtained once the simulation reaches the steady state, is shown in Fig. 3a). The electric field distribution, whose derivative is proportional to the net charge density, is also shown in Fig. 3b). There we can see the appearance of a source sheath at the RB of the simulation, then we have a quasineutral zone, *i.e.* flat electric potential and null field, and finally the ion sheath is developed near the electrode. Sometimes it is argued that the quasineutral zone in Fig. 3 must be considered as the unperturbed plasma, since quasineutrality holds in that zone. However that zone does no meet the conditions of an unperturbed plasma. This is somehow said because the source sheath is considered to be a numerical artefact produced by the simulation. However, there are physical reasons for its appearance, that should not be misled. Actually, even the most simple fluid model of the ion sheath in front of a planar electrode [22] can predict the appearance of a source sheath.

The main difference between the physics of our PIC simulation and the basic model developed in [22], resides in the boundary conditions. While in our simulation we have set the energy with which ions cross the boundary opposite to the electrode, by prescribing their VDF, in the fluid model the boundary condition is imposed in the value of the electric field. It has to be said that, the later approach makes much more sense. The reason being that, while it is usually difficult, or even impossible, to know what is the velocity or energy with which particles, in particular ions, enter the sheath, it is a true fact that quasineutrality must be fulfilled at the sheath edge. This means that the electric field at the sheath edge must go to zero. When this boundary condition is imposed in the fluid model, it is found that the ions entering the sheath must have a minimum energy in order for the sheath to be able to develop. This is usually known as the Bohm criterion:

$$v_{0i}^2 \geq v_B^2 = \frac{k_B T_e}{m_i}, \tag{3}$$

where v_{0i} is the velocity with which ions enter the sheath.

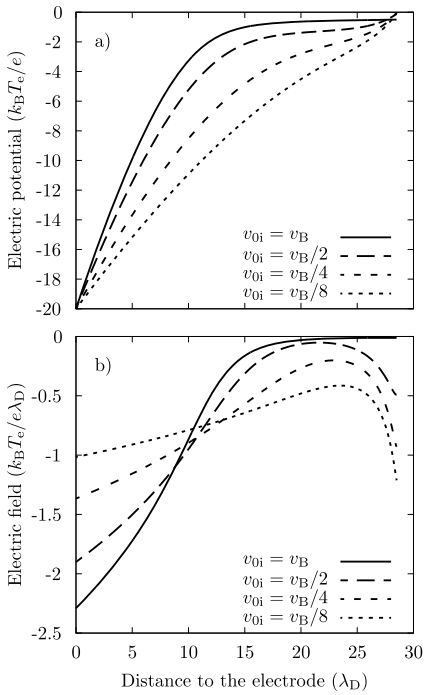

Fig. 4. Appearance of a source sheath in a fluid model as the ion velocity at the sheath edge is decreased.

So, regarding the boundary conditions at the sheath edge, there are two different approaches:

(BC 1). to fix the drift velocity with which ions enter the sheath and let the electric field evolve towards a value in accordance with the drift velocity
(BC 2). to fix the electric field at the sheath edge and let the ion drift velocity evolve towards a value in accordance the electric field

On the one hand we have the first approach, (i), which is the one we choose in the PIC simulation. The problem of this approach is that, if the flux of incoming ions is not set properly, the electric field at the sheath edge evolve towards a value that is not in accordance with the quasineutrality condition, as can be seen in Fig. 3b). On the other hand we have the second approach, (ii), which is the one chosen in the fluid model. There, the electric field at the sheath edge is set to have a negligible value and the Bohm criterion is obtained, as well as a physically reasonable solution.

It has to be noticed that the first approach can be also implemented in the fluid model. However, if this is done and the energy of ions entering the sheath is not in accordance with the Bohm criterion, a "source sheath" also appears. This is shown in Fig. 4, where the electric potential and field distributions are shown for different values of the velocity of ions at the sheath edge. Obviously, the solutions corresponding to ion velocities $v_{0i} < v_B$ are not physically acceptable. Actually, the physical reason behind this behaviour was already explained by Riemann [22], which is the fact that ions should move fast enough so that their density decreases slower than the electron density as the electric potential decreases, otherwise a negative space charge, *i.e.* a source sheath, appears.

As we have seen, the main difference between the boundary conditions in the PIC simulation and the fluid model resides in which parameter is fixed at the boundary: the electric field or the ion drift velocity. However, from a physical point of view, the difference is much more noticeable, being: to take into account the existence of a presheath or to neglect it. The presheath is the zone that connects the unperturbed plasma with the sheath. This is done through a "presheath mechanism" that allows the net ion current to increase while maintaining quasineutrality. Once that the ion current has reached a certain value, *i.e.* ions move fast enough, the sheath can be developed and quasineutrality can be broken in order to shield the electrode. So, when we are using the unperturbed plasma conditions on the RB of Fig. 2 without implementing a presheath mechanism, *e.g.* ionisation, we are trying to connect the unperturbed plasma with the sheath directly. This is not physically possible, and for this reason, a source sheath appears.

The previous explanation is also the reason why, at the beginning of this section, we said that source sheaths are more pronounced when simulating planar electrodes. When the planar geometry is considered, the presheath mechanism has to be explicitly implemented. But, when simulating cylindrical or spherical electrodes, the own geometry of the problem acts as a presheath mechanism [22]. However, even though a presheath mechanism is taken into account in those cases, we still don't know if the RB of the simulation is located at the unperturbed plasma. The reason being that the unperturbed plasma is only reached asymptotically as we move away from the electrode. So, even though very close to the unperturbed plasma, the RB of the simulation is going to be located, in general, at some point along the presheath.

Finally, if source sheaths appear in fluid models when using boundary conditions (BC 1), it seems reasonable to think that they can be avoided in PIC simulations by using boundary conditions (BC 2) adequately. This means that, we have to fix a value of the electric field at the sheath edge which must be in accordance with the quasineutrality condition, and then adjust the velocity with which ions enter into the simulation.

3. Particle injection algorithm

In this section we are going to describe a selfconsistent algorithm for the injection of particles, in particular ions, at the boundary of the simulation. In order to set up this algorithm we are going to need the value of three magnitudes at the RB of the simulation: the electric potential, ψ_s, the electric field, E_s, and the VDF of the particles entering the simulation.

For the sake of simplicity, we still are going consider the 1d1v PIC simulations described in the previous section. However, this algorithm can be extended to other geometries, as we will see later on.

Let us start with the value of the electric field. As we have previously mentioned, the electric field must be negligible at the boundary of the simulation in order to recover quasineutrality. The easiest approach is to set up a value which is negligible when compared with the electric field developed along the sheath. If the dimensionless units of Fig. 3 and Fig. 4 are used, a negligible electric field means something like $|E_s| \lesssim 10^{-2}$. Even though this might seem a very coarse approximation, we have found that, in the case of planar geometry, results do not depend too much on the exact value that we set for E_s, as long as it is small enough. A second approach, which has more physical content, is to use the value obtained from the quasineutral solution of a certain fluid model. This solution is usually easy to find by equating the densities of electrons and ions, and provides a functional dependency between the electric field and potential along the presheath, *i.e.* $E_s = f(\psi_s)$. Once we have this dependency and the value of the electric potential at the boundary is set up, we can obtain the corresponding value of the electric field.

Once the quasineutral value of the electric field is defined, we have to adjust the drift velocity of the incoming ions accordingly. This is done by the modification of their VDF, which is no longer going to be maxwellian. At the unperturbed plasma, particles can be assumed to be thermalised at a certain temperature, thus can be described by a maxwellian VDF. However, as we have previously said, ions are accelerated along the presheath until they reach the necessary velocity for the sheath to develop. For this reason, ions arrive at the sheath edge with a certain drift velocity. So, ions at the boundary of the simulation can be assumed to have the following VDF:

$$f_{\mathrm{i}}(v)\,\mathrm{d}v = v\sqrt{\frac{m_{\mathrm{i}}}{2\pi k_{\mathrm{B}} T_{\mathrm{i}}}}\exp-\frac{m_{\mathrm{i}}(v-v_{\mathrm{d}})^2}{2k_{\mathrm{B}}T_{\mathrm{i}}}\,\mathrm{d}v, \tag{4}$$

which is a maxwellian distribution with a drift velocity, v_{d}. Actually, this velocity is the parameter that we are going to adjust in order to fulfil the quasineutrality condition at the RB of the simulation. Then, as we did with (1), we can integrate (4) in order to obtain the flux of ions that we have to feed the simulation with. By doing so, the following expression is obtained:

$$\Phi = \underbrace{\frac{n_{\mathrm{s}} v_{\mathrm{th}}}{2\sqrt{\pi}}\exp\left(-\frac{v_{\mathrm{d}}^2}{v_{\mathrm{th}}^2}\right)}_{\Phi_{\mathrm{th}}} + \underbrace{\frac{n_{\mathrm{s}} v_{\mathrm{d}}}{2}\left[1+\mathrm{erf}\left(\frac{v_{\mathrm{d}}}{v_{\mathrm{th}}}\right)\right]}_{\Phi_{\mathrm{d}}}, \tag{5}$$

where v_{th} is the thermal velocity, which can be defined as $v_{\mathrm{th}} = \sqrt{2k_{\mathrm{B}}T_{\mathrm{i}}/m_{\mathrm{i}}}$, and n_{s} is the ion density at the boundary of the simulation. The two terms in (5) represent the thermal and drift contributions to the ion flux. It can be seen that, when $v_{\mathrm{d}} \to 0$, $\Phi_{\mathrm{d}} \to 0$ and Φ_{th} recovers the value we obtained in (2). Also, if we make $T_{\mathrm{i}} \to 0$, we have that $\Phi_{th} \to 0$ and $\Phi_{\mathrm{d}} \to n_{\mathrm{s}} v_{\mathrm{d}}$, which is the flux of a monoenergetic beam of ions that moves with velocity v_{d}.

It has to be noticed that there is a significant difference in using (5) instead of (2) when it comes to evaluate the flux of ions entering the simulation. The reason being that, when the ratio of the drift to thermal velocity is not negligible, the ion current injected in the simulation that predicts each expression is quite different. This can be seen in Fig. 5, where it is shown how the total ion flux goes from purely thermal to purely drift as the ratio v_{d}/v_{th} is increased for a given ion temperature. As we can see, when the value of the drift velocity is only half of the value of the thermal one, the ion current injected in the simulation is more than doubled with respect to the thermal contribution. Obviously, the closer the RB of the simulation is to the unperturbed plasma, the smaller the drift velocity is going to be. However, Fig. 5 highlights the importance of taking into account the drift velocity of ions at the boundary, even if it is small, since any change in the ion

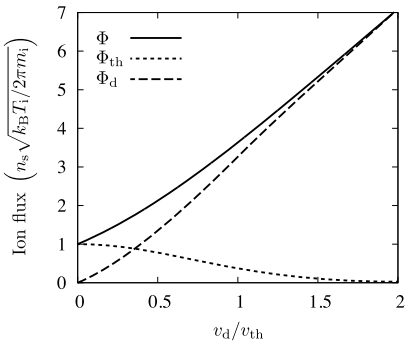

Fig. 5. Dependence of the ion flux entering the simulation with the ratio of drift to thermal velocity.

current injected into the simulation greatly affects the results obtained with it. This is particularly important when the ion current collected by the electrode is going to be measured as we will see in 4.

Finally, in order to complete the description of the boundary condition, we need to know the value of the electric potential, ψ_s, and the particle density, n_s, that we are going to impose at the RB of the simulation.

Let us start by taking into account that, in the approach described in 2, we considered the RB of the simulation to be located at the unperturbed plasma. That allowed us to take it as a reference point, which is very convenient in order to compare results with experiments, since quantities such as particle densities and temperatures can be measured at the unperturbed plasma. For this reason, we would like to keep the unperturbed plasma as a reference for our simulations, so that the input parameters are referred to it. For this reason, the electric potential at the RB of the simulation, ψ_s, is the potential drop between the unperturbed plasma and the boundary of our simulation. Now, by assuming energy conservation for ions between the plasma and the RB of the simulation, we have that:

$$e\psi_s = \frac{1}{2}m_i v_d^2 \Rightarrow \psi_s = \frac{m_i v_d^2}{2e}. \tag{6}$$

Thus, once we set the drift velocity of ions at the boundary, the electric potential can be evaluated from (6).

Also, it has to be noticed that, since we are dealing with negatively biased electrodes, electrons are repelled by them. Consequently, their VDF is still given by 1 and, it is known that their number density distribution is given by the following Boltzmann factor:

$$n_e(\psi) = n_{e0}\exp -\frac{e\psi}{k_{BT_e}}. \tag{7}$$

Now, because of the quasineutrality condition at the boundary, we can obtain $n_s = n_e(\psi_s)$. The only requirement is to know the value of ψ_s, which is obtained from (6) as we have already mentioned.

Once we have all this information, the selfconsistent particle injection algorithm is schematised in Fig. 6, and can be summarised as follows:

(i). An initial guess for the drift velocity of ions, v_d, is considered.
(ii). The electric potential at the boundary, ψ_s, is evaluated from (6) with the considered v_d value.
(iii). The particle number density at the boundary, n_s, is evaluated from (7) and the ψ_s value.
(iv). In case we are considering a quasineutral solution for the electric field at the boundary, E_s is evaluated from the ψ_s value, instead of having a fixed value.
(v). The right fluxes for the particles are obtained from (5) and (2).
(vi). A complete PIC iteration is performed, as shown in Fig. 1.
(vii). The value obtained for the electric field at the boundary of the simulation, E_b, is compared with E_s:
  (a) If $E_b < E_s$, the v_d value is not enough for the sheath to be developed, so it is increased.
  (b) If $E_b > E_s$, the v_d value is larger than necessary for the sheath to be developed, so it is decreased.
(viii). We go back to step (ii).

4. Results

In this section some results obtained with the previously defined particle injection algorithm are shown. The results that are going to be showcased pursuit two different objectives:

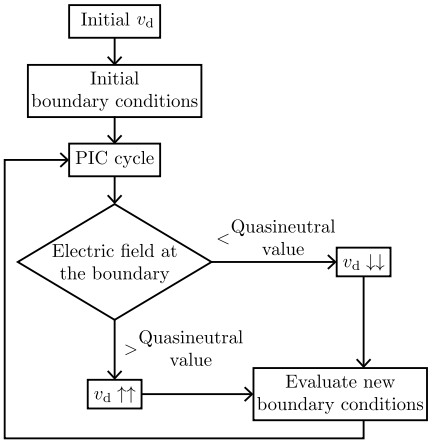

Fig. 6. Flow diagram of the drift velocity calibration algorithm.

- In 4.1, we have validated the algorithm by checking its ability to avoid the appearance of source sheaths. Also, we have verified it by comparing the results of the simulation with those provided by the simple fluid model in [22].
- In 4.2 we explain the extension of the algorithm to other geometries and show off its importance in the proper evaluation of the input fluxes of ions.

4.1. Validation and verification of the injection algorithm

On the one hand, to validate the algorithm is pretty simple, we just have to check if the source sheaths appear or not. On the other hand, if our PIC simulation is to provide physically meaningful results in cases that can not be solved by fluid or kinetic models, under simple circumstances, it should retrieve the same results than those theories. So, in order to validate the particle injection algorithm, we have compared the distribution of the electric field and potential obtained with the PIC simulation with those provided by a fluid model. The fluid model chosen for the comparison is the simple model developed by Riemann [22] of a planar electrode in contact with a plasma. This simple model considers: continuity equation and conservation of energy for ions (assumed to be monoenergetic), Boltzmann relation for electrons and Poisson's equation for the electric potential. The reason for choosing this model is that, despite its simplicity, it provides some important physical results that are widely accepted, in particular, the already mentioned Bohm criterion.

It has to be noticed that, in order to perform a fair comparison between the PIC and fluid results, the ion temperature in the PIC simulation was set to zero. The reason being that, the fluid model considers monoenergetic ions. Other than this, the parameters used for the PIC simulation were the same than those used for the obtention of the results shown in Fig. 3. Also, regarding the particle injection algorithm, the value used for the quasineutral electric field was $E_s = -10^{-2}\ k_B T_e / e\lambda_D$.

With the previous setup, we obtained the electric potential and field distributions shown in Fig. 7. There it can also be seen the results provided by the fluid model. By looking at the graphs in Fig. 7, the first thing we notice is that the appearance of a source sheath in the PIC simulation has been avoided, so the main objective of the algorithm has been clearly achieved. In Fig. 7b) it can be seen that the electric field approach a negligible value and its derivative tend to zero at the RB of the simulation, so, quasineutrality is achieved. Also, the agreement obtained between the PIC simulation and the fluid model is so good that both solutions are nearly indistinguishable.

For the previous reason, in order to quantify the discrepancy between both models, we evaluated the relative difference between them as:

$$\text{Relative error} \equiv 100 \times \frac{\text{Value(PIC)} - \text{Value(fluid)}}{\text{Value(fluid)}}. \tag{8}$$

In Fig. 8 it is shown that the relative difference between both results is negligible along the sheath, and it only start to arise at the RB as we approach the presheath. Nevertheless it should be noticed that it is reasonable to obtain larger relative errors at this boundary, specially in the case of the electric field, since its value there goes to zero. However, the maximum difference between the prediction of the PIC simulation and the fluid model is less than 1% for the electric potential and less than 10% for the electric field.

The last result that validates the particle injection algorithm, and the whole PIC simulation, is the steady state value reached for the drift velocity of the ions at the boundary, v_d. In Fig. 10 we can see the evolution of this parameter along with the electric field at the boundary, E_b, as the simulation advances. In the inset of this graph it can be seen how E_b

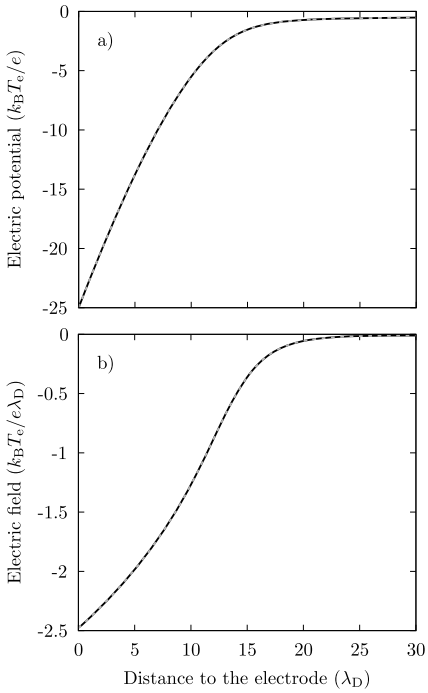

Fig. 7. Comparison of the electric potential and field distributions obtained with the PIC simulation (solid black) and with the simple fluid model in [22] (dashed grey).

tends to the quasineutral value, E_s, quickly as the drift velocity of ions is adjusted. The speed of the particle injection algorithm is remarkable, as it only needs around 25k iterations in order to achieve the quasineutrality, or negligible electric field conditions, at the RB of the simulation. However, it is even more interesting to observe the evolution of v_d with a larger timescale, in order to examine its steady state value. In the graph, we can see that the drift velocity approaches the Bohm velocity, given by (3), as limiting value. This result can be seen as a "quasiempirical" obtention of the Bohm criterion.

The graphs in Fig. 7, 8 and 9 validate the proposed algorithm. Particularly the last one, since it describes the same behaviour than the widely accepted Bohm criterion, which is a theoretical result obtained via a completely different approach, *i.e.* a fluid model. Also, it has to be noticed that this result has been obtained by simply imposing the electric field at the RB to be negligible.

4.2. Extension to other geometries

The injection algorithm that is being described here, is not only applicable to the case of planar electrodes. Actually, it is applicable for any electrode geometry as long as the problem is symmetric along the dimensions parallel to the surface of the electrode, *e.g.* spherical or cylindrical electrodes.

For example, in Fig. 10 we can see the case of a cylindrical electrode (the same reasoning applies to the case of spherical electrodes). Here we must consider two components of the velocity, *i.e.* radial and orbital velocities. In this case, the radial velocity of ions, v_r, is going to be affected by a drift velocity, due to the potential drop in the radial dimension as we approach the surface of the electrode. For this reason, this component of the velocity should be described by a drifted maxwellian distribution, as given by (4). On the other hand, the orbital velocity, v_θ, should follow a regular maxwellian distribution as given by (1), since there is no acceleration of the ions in the orbital dimension. This is the approach that was followed in order to study the transition from radial to orbital behaviour of ions in the surroundings of a negatively biased cylindrical electrode [23].

It may be argued that, in the case of cylindrical or spherical electrodes, there is no need to implement such an injection algorithm, since source sheaths are not observed. As it was explained in 2, this is due to the fact that a presheath mechanism is implicitly implemented, *i.e.* the own geometry of the problem. Nevertheless, it was also mentioned that even in these cases, in general, the RB of the simulation is going to lie at some point along the presheath. For this reason, even though

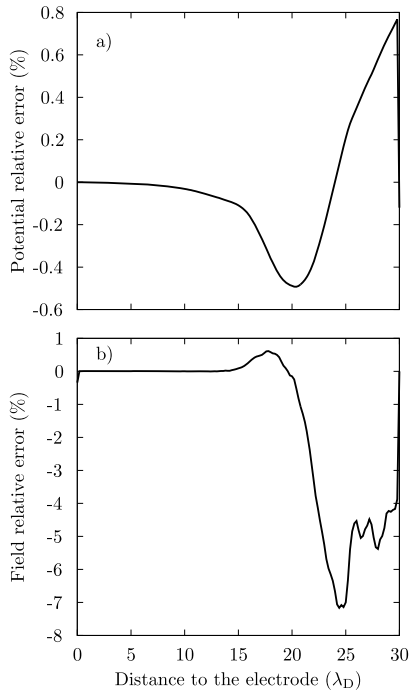

Fig. 8. Relative difference between PIC and fluid solutions as given by (8).

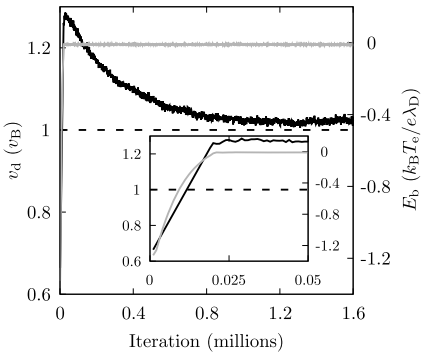

Fig. 9. Evolution of the ion drift velocity (black) and electric field (grey) at the boundary according to the selfconsistent particle injection algorithm (planar electrode).

a source sheath is not observed, the use of the proposed injection algorithm is essential in order to evaluate the right ion flux that the simulation is fed with. This is a critical feature when we want to evaluate the ion current collected by the electrode, as it was done in [23]. Actually, without this proper evaluation of the influx of ions, it had not been possible to obtain the results shown there.

In order to illustrate the importance of this effect we are going to consider one of the simulations performed to obtain the results shown in [23]. The parameters of the simulation are the following ones: ions mass (He^+) 7296 m_e, ion temperature 0.1 T_e, electron temperature 2000 K, electron plasma density 10^{15} m^{-3}, radius of the electrode 1 λ_D and biasing potential of the electrode -25 $k_B T_e/e$. Also, in this case the quasineutral value of the electric field at the RB was obtained from the quasineutral solution of a fluid model [8].

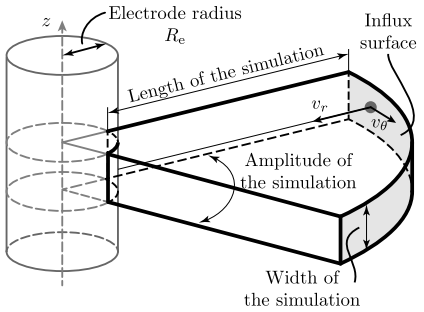

Fig. 10. Simulation domain of the ion sheath developed in front of a cylindrical electrode (1d2v simulation).

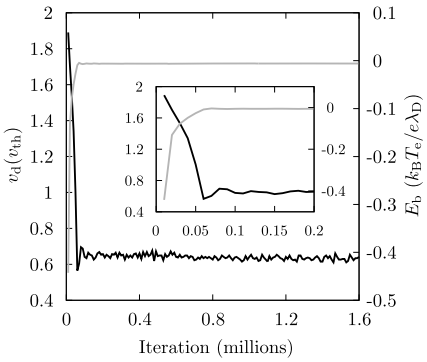

Fig. 11. Evolution of the ion drift velocity (black) and electric field (grey) at the boundary according to the selfconsistent particle injection algorithm (cylindrical electrode).

In Fig. 11 it is shown the evolution of the radial drift velocity of ions, measured in thermal velocity units, along with the evolution of the value of the electric field at the RB. It can be seen that, the electric field at the RB goes quickly to a quasineutral value as the drift velocity is adjusted, which is the expected behaviour that we saw in Fig. 9.

However, the important fact that we would like to highlight from Fig. 11 is that, the steady state value reached by the drift velocity is $v_d \sim 0.6\ v_{th}$. With this ratio of drift to thermal velocity we can see in Fig. 5 that the ion flux that feeds the simulation is $\Phi \sim 2.5\ n_s\sqrt{k_B T_i/2\pi m_i}$. That is, the influx of ions into the simulation is more than double when compared to the case of fully maxwellian ions. Obviously, this fact has a huge impact into the ion current collected by the electrode, and the results described in [23].

5. Conclusions

The problem of the appearance of source sheaths in PIC simulations has been studied. The physical reasons behind this effect have been explained. It has been shown that those reasons are related to the injection of slow ions into the simulation, which is incompatible with the Bohm criterion. In order to solve the problem, a selfconsistent particle injection algorithm has been developed. The algorithm relies on the injection of ions with a drifted maxwellian velocity distribution function. The drift velocity of the distribution is the parameter that is selfconsistently adjusted in order to obtain the quasineutrality condition at the presheath/plasma boundary.

On the one hand, the algorithm has been validated by comparing the results provided by the PIC simulation of a planar electrode with a fluid model under simple physical conditions. Not only the agreement between both models has been outstanding, but also the Bohm criterion, which is a theoretical result from the fluid theory, has been obtained.

On the other hand, the extension of the algorithm to other geometries, cylindrical in particular, has been explained. Even though in this case source sheaths do not appear, because of the existence of a presheath mechanism in the simulation, it has been shown that the use of the proposed injection algorithm has a huge impact of the ion current injected into the simulation. Obviously this leads to the prediction, by the simulation, of different values of the ion current collected by the electrode.

The proposed algorithm has been shown to solve the problem of the appearance of source sheaths and, at the same time, to improve the quality of the results provided by PIC simulations of the contact of an electrode with an unperturbed plasma.

Acknowledgements

The authors greatly acknowledge the support of the FPU Program of the Spanish Ministry of Education (ref. AP2010/0639) and the Spanish Ministry of Science and Innovation (ref. No FIS2010-19951) which is partially financed with FEDER funds.

References

[1] Shi Qian, Huiliang Cao, Xuanyong Liu, Chuanxian Ding, Nanotube array controlled carbon plasma deposition, Appl. Phys. Lett. 102 (2013) 243109.
[2] T.E. Sheridan, Ion focusing by an expanding, two-dimensional plasma sheath, Appl. Phys. Lett. 68 (1996) 1918–1920.
[3] G.D. Severn, Xu Wang, Eunsuk Ko, N. Hershkowitz, Experimental studies of the Bohm criterion in a two-ion-species plasma using laser-induced fluorescence, Phys. Rev. Lett. 90 (2003) 145001.
[4] V. Demidov, C. DeJoseph, A. Kudryavtsev, Anomalously high near-wall sheath potential drop in a plasma with nonlocal fast electrons, Phys. Rev. Lett. 95 (2005) 215002.
[5] Dongsoo Lee, Lutfi Oksuz, Noah Hershkowitz, Exact solution for the generalized Bohm criterion in a two-ion-species plasma, Phys. Rev. Lett. 99 (2007) 155004.
[6] M.D. Campanell, A.V. Khrabrov, I.D. Kaganovich, Absence of Debye sheaths due to secondary electron emission, Phys. Rev. Lett. 108 (2012) 255001.
[7] J.I. Fernández Palop, V. Colomer, J. Ballesteros, M.A. Hernández, A. Dengra, Theoretical aspects of the metal—electronegative plasma interface, Surf. Coat. Technol. 84 (1996) 341–347.
[8] J.I. Fernández Palop, J. Ballesteros, V. Colomer, M.A. Hernández, Theoretical ion current to cylindrical Langmuir probes for finite ion temperature values, J. Phys. D, Appl. Phys. 29 (1996) 2832–2840.
[9] J.M. Díaz-Cabrera, M.V. Lucena-Polonio, J.I. Fernández Palop, R. Morales Crespo, M.A. Hernández, A. Tejero-del Caz, J. Ballesteros, Experimental study of the ion current to a cylindrical Langmuir probe taking into account a finite ion temperature, J. Appl. Phys. 111 (2012) 063303.
[10] J.M. Díaz-Cabrera, J.I. Fernández Palop, R. Morales Crespo, M.A. Hernández, A. Tejero-del Caz, J. Ballesteros, Virtual instrument for automatic low temperature plasmas diagnostic considering finite positive ion temperature, Measurement 55 (2014) 66–73.
[11] C.K. Birdsall, A.B. Langdon, Plasma Physics via Computer Simulations, 1st ed., Adam Hilger, 1991.
[12] R.W. Hockney, J.W. Eastwood, Computer Simulation Using Particles, Adam Hilger, 1988.
[13] D. Tskhakaya, K. Matyash, R. Schneider, F. Taccogna, The particle-in-cell method, Contrib. Plasma Phys. 47 (2007) 563–594.
[14] J.P. Verboncoeur, Symmetric spline weighting for charge and current density in particle simulation, J. Comput. Phys. 174 (2001) 421–427.
[15] Ming-chih Lai, Wei-Cheng Wang, Fast direct solvers for Poisson equation on 2D polar and spherical geometries, Numer. Methods Partial Differ. Equ. 18 (2002) 56–68.
[16] M.M. Turner, Kinetic properties of particle-in-cell simulations compromised by Monte Carlo collisions, Phys. Plasmas 13 (2006) 033506.
[17] M. Surendra, D. Vender, Collisionless electron heating by radio-frequency plasma sheaths, Appl. Phys. Lett. 65 (1994) 153.
[18] T. Gyergyek, J. Kovačič, Floating potential of an electron emitting collector that terminates a bounded plasma system, Contrib. Plasma Phys. 52 (2012) 699–721.
[19] T. Gyergyek, J. Kovačič, Potential formation in a bounded plasma system which is terminated by an electron emitting floating collector studied by a particle-in-cell computer simulation, Contrib. Plasma Phys. 53 (2013) 189–201.
[20] G. Gozadinos, D. Vender, M.M. Turner, Boundary conditions and particle loading for the modeling of a semi-infinite plasma, J. Comput. Phys. 172 (2001) 348–355.
[21] H.C. Kim, Y. Feng, J.P. Verboncoeur, Algorithms for accurate collection, ejection, and loading in particle simulations, J. Comput. Phys. 223 (2007) 629–642.
[22] K.U. Riemann, The Bohm criterion and sheath formation, J. Phys. D, Appl. Phys. 24 (1991) 493–518.
[23] A. Tejero-del Caz, J.I. Fernández Palop, J.M. Díaz-Cabrera, J. Ballesteros, Radial-to-orbital motion transition in cylindrical Langmuir probes studied with particle-in-cell simulations, Plasma Sources Sci. Technol. 25 (2016) 01LT03.

Received: 3 April 2020 | Revised: 21 May 2020 | Accepted: 29 May 2020

DOI: 10.1002/ppap.202000073

FULL PAPER

PLASMA PROCESSES AND POLYMERS

Accurate measurement of the ion saturation current collected by a cylindrical Langmuir probe in cold plasmas

Juan Manuel Díaz-Cabrera[1] | **José I. Fernández Palop**[2] | **Guillermo F. Regodón**[2] | **Jerónimo Ballesteros**[2]

[1]Departamento de Ingeniería Eléctrica, Campus Universitario de Rabanales, Universidad de Córdoba, Córdoba, Spain

[2]Departamento de Física, Campus Universitario de Rabanales, Universidad de Córdoba, Córdoba, Spain

Correspondence
Juan Manuel Díaz-Cabrera, Departamento de Ingeniería Eléctrica, Campus Universitario de Rabanales, Universidad de Córdoba, 14071 Córdoba, Spain.
Email: jmdiaz@uco.es

Funding information
FPU Program of the Spanish Ministry of Education, Grant/Award Number: FPU17/01387; Ministerio de Ciencia e Innovación, Grant/Award Number: No FIS2010-19951

Abstract

This paper analyzes the results of accurate measurements of the ion current collected by a cylindrical Langmuir probe immersed in cold argon, neon, and helium plasmas. These measurements make it possible to study the influence of the positive ion-to-electron temperature ratio $\beta = T_+/T_e$ on the collected ion current, providing valuable information about the trajectory described by the positive ions when falling toward the probe. Several criteria have been applied to discriminate whether the ion current is described by using the orbital motion limited theory or the radial motion theory. In all the studied argon and neon plasma discharge conditions, the criteria indicate that the positive ion current collected by the probe is appropriately described by the radial motion theory; however, as β increases, some criteria indicate a trend toward the orbital theory. In contrast, for the studied helium plasmas discharge conditions, a transition from radial to orbital motion has been measured.

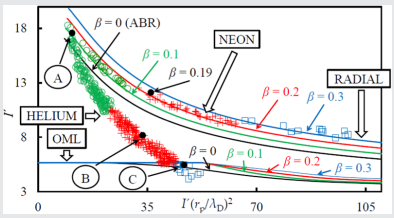

KEYWORDS

cold plasma, DC discharges, Langmuir electrostatic probe, noble gases, surfaces

1 | INTRODUCTION

The analysis of the ion current collected by a surface immersed in a cold plasma is essential in both Langmuir probe plasma diagnosis and surface treatment enhanced by plasmas. However, the measurement of the positive ion current by means of a Langmuir probe allows the diagnosis of plasma local parameters with a very low disturbance to the plasma due to the ion sheath, which shields from the effect of the probe.[1–7] In contrast, when an electrically isolated surface is introduced inside a plasma, due to the greater mobility of electrons, the surface acquires a negative charge and attracts the positive ions from the plasma, so that many technological processes depend on the positive ion current reaching it. Among these processes, we have plasma-assisted chemical vapor deposition, ion implantation, etching, surface coating, thin films, nanotechnology, and so forth.[8–13]

In all these processes, the positive ion thermal motion influences the trajectory of the positive ions when falling toward the probe/surface and thus the positive ion current collected by it.

From the theoretical point of view, we can address the description of a cylindrical Langmuir probe, negatively biased with respect to the plasma potential, by considering two essentially different descriptions. The orbital theories consider that the positive ions orbit around the probe and, according to the conservation laws, not all the ions reach the probe. In this study, we use the orbital motion limited (OML) model, which is a particular case of the orbital theories in which $r_p/\lambda_D \ll 1$, where r_p is the probe radius and λ_D is the Debye length, which is related to the thickness of the sheath. For this case, there is no absorption radius. It is the opposite case to thin sheath limit where $r_p/\lambda_D \gg 1$.[14–16] The Allen–Boyd–Reynolds (ABR) theory considers the positive ions to fall toward the probe by following a radial trajectory so that all the ions reach the probe.[17] The original ABR theory, adapted by Chen[18] for cylindrical geometry, is valid only for positive ions having a null temperature ($\beta = T_+/T_e = 0$, with T_+ and T_e being the positive ion and electron temperature, respectively), and it has been extended by the authors for $\beta \neq 0$.[2,19–24] It is important to be able to discriminate which theory is applicable in each plasma condition, as each one provides different results for the ion density in the plasma diagnosis. Moreover, this fact implies a paradox in the analysis of positive ion saturation zone in the Langmuir probe current–voltage characteristic when used in plasma diagnosis, as we do not know a priori which theory is valid before it is applied in the diagnosis.[1,4,25] Furthermore, in many situations, values for the ion current between the two limiting theories are observed in experiments.[5,26,27] However, both models do not consider the influence of the collisions on the positive ion current collected by the probe. Therefore, if the ion current is to be used in plasma diagnosis, we must know the effect produced by phenomena such as positive ion thermal motion or positive ion–neutral collisions on the positive ion current. Several authors have published several works dealing with the problem of positive ions collection when the collisions of positive ions and neutral particles are considered.[28–32] In this way, the authors have just developed a radial model that not only considers the positive ions' thermal motion, but also the influence of those collisions.[33]

This paper presents the experimental results obtained in the application of several criteria to distinguish if the positive ion current measured by a cylindrical Langmuir probe is explained by the OML or ABR models in low-pressure, low-temperature argon, neon, and helium plasmas. The results are obtained as a function of the β parameter in all the criteria and also as a function of the ion–neutral collision mean free path (λ_+) in one criterion. All the criteria are based on the study of the positive ion current measured for high negative biasing potentials (ion saturation in the current–voltage characteristic curve). These measurements are very delicate, as the ion saturation current is very small, for example, in the plasma conditions studied in this article, which is always lower than 10^{-5} A. The authors have developed a diagnosis method in low-temperature plasmas by using Langmuir probes, which permits this study. The accuracy is high enough to discriminate variations in the ion saturation current, with variations being lower than 10^{-6} A, which are caused by the positive ion thermal motion.[1]

The structure of the article is as follows: in Section 2, the experimental setup and measurement method are briefly cited. Section 3 describes the experimental measurement conditions of the argon, neon, and helium plasmas studied. Section 4 is devoted to the presentation and discussion of the applied criteria and the experimental results obtained. Finally, Section 5 is an exposition of the conclusions.

2 | EXPERIMENTAL SETUP AND MEASUREMENT METHOD

Figure 1 shows the discharge device and measurement setup. It produces a stable plasma from a high-voltage DC discharge and has been previously used by the authors.[1,2,4,6,7,26,34,35]

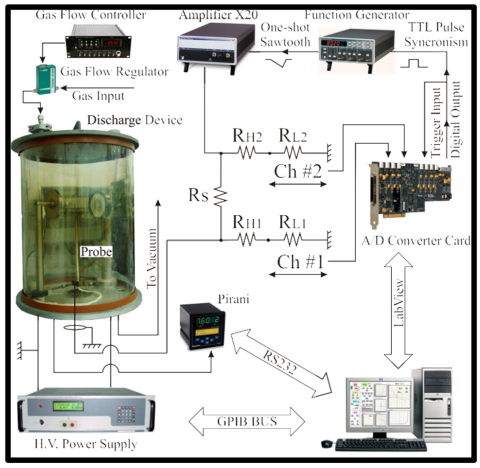

FIGURE 1 The experimental device and measurement setup. Reproduced with permission from Díaz-Cabrera et al.[1] 2014, Elsevier

As it can be seen, it consists of a large Pyrex cylinder, with 31-cm inner diameter and 40-cm height, including two stainless steel electrodes, with 8-cm diameter, which are 15 cm apart. These electrodes are connected to the low ripple/noise to signal ratio KEPCO BHK 2000-0.1 MG high-voltage DC power supply, configured as a current supply, since the discharge current is related to the electron density,[1,2,4,6,7,26,34,35] so it characterizes the discharge better than other parameters like the discharge voltage or the gas discharge pressure. The gas pressure is controlled by using a mass gas flow controller, MKS 247. A tungsten cylindrical Langmuir probe, 6 mm in length and 0.1 mm in radius, is placed in the afterglow with its axis parallel to the electrode surfaces. In this position, the effect produced by a finite ion-to-electron temperature ratio, β, may be significant in the measurements,[1,2,4,6,7,26,34,35] as the mean free path for positive ion–neutral collisions (λ_+) is small, compared with the plasma dimensions, so that positive ions and neutrals are thermalized and their temperature (T_+) is estimated to be about 350 K.[1,2,5,7,26,36–38] Actually, the mean free path of the ion–neutral collision for Ar is about 0.74 mm, for Ne is about 0.8 mm, and for He is about 1 mm for the gas pressures studied in this paper,[10,38,39] so that positive ions are thermalized with neutrals.

The measurement of the current–voltage (*I-V*) probe characteristic curve of the Langmuir probe provides the indirect measurement of parameters such as the plasma potential V_{plasma}, the floating potential V_{float}, and the electron energy distribution function (EEDF).[1,2,4,6,26,34,38,40–43] As the measurement range of this study is very broad, the EEDF can deviate from the Maxwellian form, for example, in pressure dependence.[44–48] This is an important issue, as both radial and OML models assume the EEDFs to be Maxwellian.[1,4,6,16,18,19,21,42] To simplify the study, the measurement method has been designed to check that all the obtained EEDFs included in this study can be considered as Maxwellians, discarding those cases for which this condition is not accomplished. To do so, we use a parameter that is quite sensitive to ensure the measured EEDF to be Maxwellian, that is, the linear correlation coefficient, r, of the curve $ln(d^2I/dV^2)$ versus V in the electron-retarding zone, which will approach a straight line if the EEDF is Maxwellian; thus, all the cases for which $r < 0.9$ are discarded.[1,4,49]

The electron density n_e and electron temperature T_e are measured by direct integration of the EEDF. These n_e and T_e values have been used as the reference ones in further calculations. The measured values of electron density, n_e, vary from 9×10^{14} to $7 \times 10^{15}\ m^{-3}$, and the values of electron temperature, T_e, vary from 1,000 to 4,400 K, approximately, corresponding to β values that vary from 0.08 to 0.35, because, as has been commented before, $T_+ \approx 350$ K. All the control and acquisition of the discharge conditions, the current-to-voltage probe characteristic curve data acquisition, and the following calculation to obtain these parameters are conducted by a Virtual Instrument developed in the LabView environment.[1,6,7]

3 | EXPERIMENTAL MEASUREMENT CONDITIONS

The measurements are performed in plasma discharges using three different gases:

(a) Argon: its pressure is in the interval $p\,(\text{Pa}) \in [2, 10]$, whereas the discharge conditions are as follows: discharge current $I_d\,(\text{mA}) \in [1, 12.5]$ and discharge voltage $V_d\,(\text{V}) \in [0, 2000]$. In total, 153 different current–voltage probe characteristic curves corresponding to the different argon plasma conditions have been measured. We have selected one current–voltage probe characteristic, corresponding to intermediate plasma conditions and β values as an example, to illustrate how the ion current is analyzed. The experimental conditions for the argon example case are as follows: $p = 2.14$ Pa, $I_d = 1.8$ mA, and $\beta = 0.16$. Nevertheless, for the rest of plasma conditions, the results are quite similar to the ones obtained for this argon example case.[1,2,4,34]

(b) Neon: $p\,(\text{Pa}) \in [10, 35]$, $I_d\,(\text{mA}) \in [1, 12]$, and $V_d\,(\text{V}) \in [0, 2000]$. In total, 86 different current–voltage probe characteristic curves corresponding to the different neon plasma conditions have been measured, with the following being the discharge conditions for the neon example case: $p = 14.9$ Pa, $I_d = 2$ mA, and $\beta = 0.19$. Similar to argon plasmas, for the rest of neon plasma conditions, the results are similar to the ones obtained for this neon example case.

(c) Finally, helium: $p\,(\text{Pa}) \in [13, 37]$, $I_d\,(\text{mA}) \in [0.6, 12.5]$, and discharge voltage $V_d\,(\text{V}) \in [0, 2000]$. In total, 433 different current–voltage probe characteristic curves corresponding to different helium plasma conditions have been measured. The higher number of measurements in helium than for argon and neon is due to the transition in the ion current from radial to orbital with the increase in β values. Also, three different current–voltage characteristic curves have been selected as helium plasma example cases, each one corresponding to a different behavior: the A case corresponds to one of the lowest β values, when the radial motion theory is verified, with the following being the discharge conditions: $p = 20.3$ Pa, $I_d = 0.8$ mA, and $\beta = 0.09$; the C case corresponds to one of the highest β values, when the orbital motion theory is verified, with the following being the discharge conditions: $p = 26.4$ Pa, $I_d = 8$ mA, and

$\beta = 0.26$; and the intermediate case, the B case, represents a β value for which neither the OML nor the ABR provides a good description for the ion current collected by the probe, with the following being the discharge conditions: $p = 28.4$ Pa, $I_d = 4$ mA, and $\beta = 0.2$.

4 | DESCRIPTION OF THE CRITERIA AND OBTAINED RESULTS

Several criteria to discriminate the behavior of ions reaching the probe have been used. The study of different criteria is interesting, as there are differences among the criteria in critical aspects: (a) the possibility of using the criterion for plasma diagnosis, (b) the possibility of plotting the result versus the β parameter, (c) the number of points used from the experimental current–voltage characteristic curve and, (d) the influence of the experimental noise on the result of the criterion. Finally, as it will be shown, the OML or radial character of the positive ions obtained does not depend on the employed criterion.

Let us present the description of the criteria and the corresponding obtained results:

(a) The first criterion is related to the Sonin plot.[50] This is a useful representation of the positive ion current collected by the probe. For cylindrical probes, the Sonin plot is the representation of the dimensionless ion current for a fixed probe biasing potential:

$$I'(x_p, y_{SP}, \beta) = \frac{I_+(x_p, y_{SP}, \beta)}{e r_p n_+} \sqrt{\frac{m_+}{2\pi k_B T_e}} \quad (1)$$

versus

$$I'(x_p, y_{SP}, \beta) \times x_p^2 = \frac{I_+(x_p, y_{SP}, \beta) e r_p}{\varepsilon_0} \sqrt{\frac{m_+}{2\pi k_B^3 T_e^3}}, \quad (2)$$

where m_+ is the positive ion mass, e is the elementary charge, k_B is the Boltzmann constant, ε_0 is the vacuum dielectric permittivity, r_p is the probe radius, x_p is the dimensionless probe radius ($x_p = r_p/\lambda_D$), λ_D is the (experimental) Debye length, $\lambda_D = \sqrt{\varepsilon_0 k_B T_e / e^2 n_e}$ (n_e and T_e obtained from direct integration of the EEDF),[42] y_{SP} is the dimensionless probe biasing potential ($y_{SP} = -eV_{SP}/k_B T_e$), I_+ is the positive ion current collected by the probe per unit length when the probe is biased to a chosen V_{SP} potential, referred to the plasma potential, in the positive ion saturation zone and the positive ion density, $n_+ \approx n_e$ (due to the quasi-neutrality condition in the plasma). Similar to several other articles, we have chosen $y_{SP} = 25$ in this study.[1,4,23] A discussion about this choice is made later. As it can be seen, the corresponding V_{SP} value is illustrated in all the figures where the probe potential is plotted.

In this study, the criterion consists of how well the experimental points in the Sonin plot for each plasma condition fit the theoretical curves obtained from the OML and radial theories. These experimental points are obtained from the experimental values for the I_+, x_p, y_{SP}, β, n_e, and T_e values, measured from the experimental current–voltage characteristic curve and by direct integration of the EEDF.[1,5,26,42]

Figures 2 and 3 illustrate the Sonin plots including the points corresponding to each set of experimental conditions: the theoretical curves corresponding to the orbital model developed by Laframboise,[16] which were calculated from the fitting curves given by Peterson and Talbot,[51] and the theoretical curves corresponding to the radial model developed by the authors for $\beta = 0$, 0.1, 0.2, and 0.3.[1,19,21,22]

Figure 2 shows the experimental points in the Sonin plot for argon plasmas. The example case has been highlighted. According to the results plotted, we can conclude that the ion current in argon plasmas is well described by the radial theory, even in the cases of finite β values, as the experimental points match the corresponding theoretical ABR curves calculated by the authors for the $\beta \neq 0$ illustrated values.[1,19,21,22]

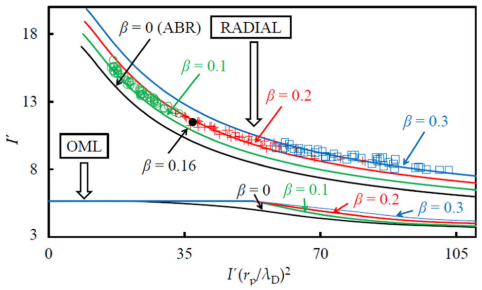

FIGURE 2 Argon plasma Sonin plots for the normalized probe potential $y_{SP} = 25$, including the points corresponding to experimental data (symbols) and several theoretical curves (solid lines). The example case and its corresponding β value have been highlighted in the graph (black dot). Circles denote $0.08 \leq \beta \leq 0.15$, crosses denote $0.16 \leq \beta \leq 0.25$, and squares denote $0.26 \leq \beta \leq 0.34$. Reproduced with permission from Díaz-Cabrera et al.[26] 2015, IoP

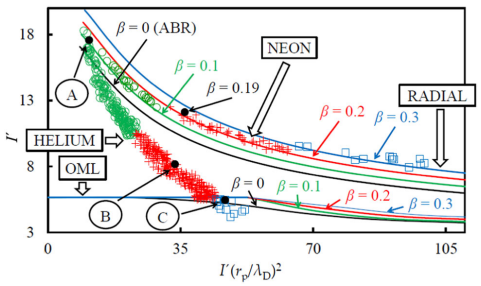

FIGURE 3 Neon plasma and helium plasma Sonin plots for the normalized probe potential $y_{SP} = 25$, including the points corresponding to experimental data (symbols) and several theoretical curves (solid lines). The example cases have been highlighted in the graph (black dots). Neon plasmas: circles denote $0.08 \leq \beta \leq 0.15$, crosses denote $0.16 \leq \beta \leq 0.25$, and squares denote $0.26 \leq \beta \leq 0.34$. Helium plasmas: circles denote $0.09 \leq \beta \leq 0.15$, crosses denote $0.16 \leq \beta \leq 0.25$, and squares denote $0.26 \leq \beta \leq 0.34$. Reproduced with permission Díaz-Cabrera et al.[26] 2015, IoP

A similar radial behavior is obtained in neon plasmas, as illustrated in Figure 3. In this case, the points obtained from each measured neon discharge are plotted. The example case has also been highlighted. In addition, Figure 3 shows the experimental Sonin plot points obtained from the different helium plasma discharge conditions measured. Moreover, the three example cases, A, B, and C, have been highlighted. As it can be seen, a transition is found, as the points corresponding to He plasmas are close to the radial curves for low β values and approach the orbital ones as β increases, crossing an intermediate zone where none of the theories is verified. It can be supposed that some ions fall toward the probe by following a radial trajectory, whereas the rest orbit before they fall or escape from the probe.

This transition can be justified if we consider that positive ions lose their translation kinetic energy when they collide, mainly with neutrals.[1–5,7,26,36–38] So, after the last collision, for the smallest mean free paths, λ_+, and for β values close to zero, the ions fall toward the probe by following radial trajectories. Nevertheless, for the highest λ_+ and/or β values, the ions are far enough from the probe and/or the azimuthal component of the ion thermal velocity is high enough for the ions to fall toward the probe following an orbital trajectory. The behavior observed in our argon, neon, and helium plasmas verifies this hypothesis, as, on the one hand, the mean free path of the neutral–ion collisions, λ_+, is higher for the helium plasma than for argon or neon, at it will be shown later. On the other hand, the azimuthal component of the ion thermal velocity is higher for the He^+ ions, as their mass is lower than that of Ar^+ or Ne^+. So, only for the highest β values in helium plasmas, the transition has been observed.

The favorable aspect of this criterion is that it provides a plasma diagnostic technique for the positive ion density, $n_+ \approx n_e$, considering the influence of the positive ion temperature.[1,2,4] This diagnostic technique has several advantages: (a) it uses the positive ion saturation zone of the *I-V* characteristic curve, where the disturbance produced in the plasma by the probe is shielded by the sheath; (b) the perturbation due to the drainage of plasma charge by the probe is negligible due to the small value of I.[2,4,49] The technique consists on evaluating the abscissa value in the Sonin Plot, which does not depends on n_+ (Equation 1), by using the corresponding parameters obtained from the experimental current–voltage characteristic curve, and thus obtaining the corresponding ordinate (Equation 2) by cross-plotting from the theoretical Sonin plot curve for the corresponding β value, that ordinate value provides n_+.[1,2,4] As it can be seen, this implies a paradox: Before using this diagnostic method, the radial or orbital behavior of the ions must be known, as different curves must be used for the cross-plotting, giving different values for the ion density. So, this study about the several radial and orbital criteria is very useful. In addition, the study of the evolution of this criterion as a function of the β parameter can be obtained. An inconvenience of this criterion is that it uses a single experimental point of the whole current-to-voltage characteristic curve. Moreover, this criterion is quite sensible, as, on the one hand, a small variation in the measured ion current may produce a large displacement in the Sonin plot; on the other hand, a small variation in β may also correspond to a large displacement in the Sonin plot. Therefore, this criterion is influenced by a low signal-to-noise ratio in the ion saturation zone, as the corresponding current values are very small in this zone of the characteristic curve. In this way, although our measurements are very accurate, smoothed current–voltage characteristic curves are used in the diagnosis process.

As commented above, there should be a discussion about the value chosen for y_{SP}, as its value must be high enough to ensure that the current collected by the probe is exclusively due to the positive ions; nevertheless, it must be low enough to avoid secondary electron emission phenomenon from the probe, which can be confused with an increase of the positive ion current to the probe. This is important to be analyzed, as the value of I_+ is very small and this phenomenon could influence the obtained results.[5] In this way, we have observed that the values obtained for n_+ from the Sonin plot method, considering the influence of T_+, for y_{SP} in the interval $15 < y_{SP} < 30$ are quite similar. So, in several articles, we have chosen

$y_{SP} = 25$,[1,4,23] as it corresponds to higher values for I_+, therefore increasing the signal-to-noise ratio of the measured current-to-voltage characteristic curve in the positive ion saturation zone. Moreover, we have obtained a very good agreement in the comparison between the results obtained for the n_+, from the I_+ value ($y_{SP} = 25$) in the positive ion saturation zone of the *I-V* characteristic curve, by using the Sonin plot method considering the influence of T_+, and the reference cases for the n_e values, from the electron-retarding zone, by direct integration of the EEDF. This is confirmed in the Sonin plots illustrated in Figures 2 and 3 for Ar and neon gases, where the experimental points, obtained from n_e, match the evolution of the theoretical curves due to β values ranging from 0.1 to 0.3 from which n_+ is obtained. Hence, we can conclude that the measurements of n_+ conducted in this article for argon and neon discharges are not influenced by the secondary electron emission from the probe. Similar results have been observed for other authors.[5] However, in the helium plasma, the presence of metastable high-energy helium atoms[52] may still produce a secondary electron emission, even though the metastable helium proportion is very small. However, in helium plasma, the additional current due to the secondary emission of electrons would shift the points of the Sonin plot to higher values. Therefore, if this phenomenon influences the results, the OML behavior points will be displaced toward the ABR curves, whereas in the measured transition, these points go to lower ordinates that reach the OML curves. Furthermore, the probe is made of tungsten to diminish secondary electron emission, as its work function is close to 4.5 eV, high enough for the secondary electron emission from the probe to be almost negligible due to the small value of T_e and T_+ obtained in this discharge.[52] Hence, we can conclude that the transition observed in this study for the helium discharges is not related to the secondary electron emission from the probe.

(b) The second criterion consists of the comparison between the experimental current-to-voltage characteristic curve, for $V < V_{plasma}$ values (V being the biasing probe potential), and the theoretical ones obtained from our radial model and the OML theory, that is, by subtracting, either to our radial theoretical I_+ versus V curve[1,2,19,21,22] or to the OML one (Equation 3),[42] the theoretical contribution due to the electrons following a Maxwellian distribution function in the electron-retarding zone of the *I-V* characteristic curve, $I_e = I_{es} e^{\frac{e(V-V_{plasma})}{k_B T_e}}$, with I_{es} being the electron current at the plasma potential, $I_{es} = eAn_e(k_B T_e/2\pi m_e)^{\frac{1}{2}}$, and A being the cylindrical probe surface.

Figure 4a illustrates such a comparison for an argon example case, using the radial theory to evaluate the positive ions contribution. As it can be seen, there is a very good agreement between the curves along the full V measured interval, even for the very critical floating potential. So, the OML theoretical curves have not been included. Moreover, as for the rest of the cases, the results are similar, we can conclude again that, under the studied argon plasma conditions, the ion current is well described by the radial theories. Figure 4b illustrates such a comparison for the neon example case. The results are also similar for the rest of the neon cases, so we can also conclude that, under the neon studied plasma conditions, the radial theories provide again a good description for the ion current.

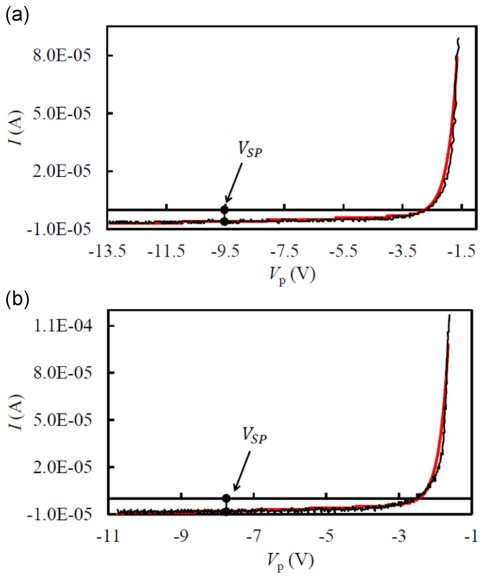

FIGURE 4 (a,b) Theoretical (red solid line) and experimental (black solid line) nonsmoothed current–voltage, *I-V*, characteristic curves for the argon and neon example cases, respectively. The point indicates the V_{SP} datum selected for the Sonin plots

Figure 5a–c illustrates such a comparison for the three helium example cases, A, B, and C, respectively. As it can be seen, the radial curves are illustrated for $V < V_{plasma}$, whereas the OML curves are illustrated for V values lower than the floating potential, V_{float}, as the used equation is an approximation that is only valid for values far from the plasma potential, V_{plasma} ($V < V_{plasma} - 2k_B T_+/e$).[42] As it can be seen for the Case A, there is a good agreement between both the radial theoretical curve and the experimental one along a wide zone of the ion saturation, corresponding to β values close to zero, whereas the OML

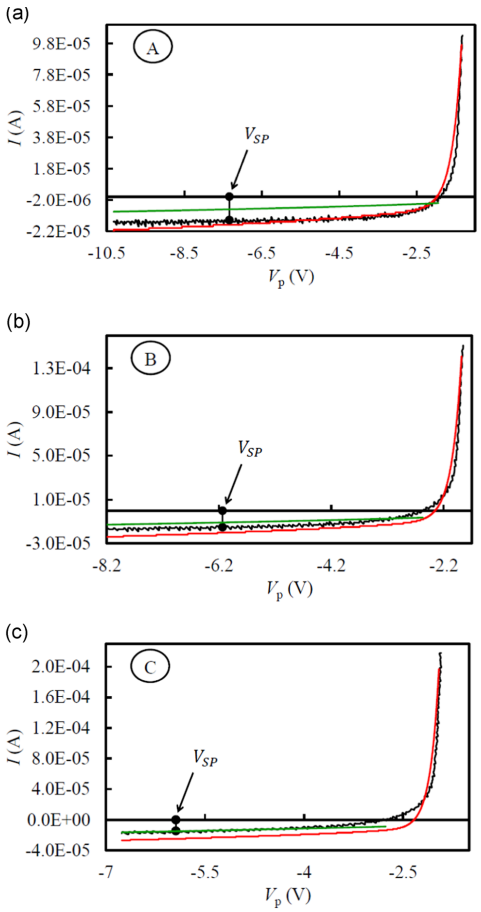

FIGURE 5 (a–c) Theoretical radial (red solid line), theoretical orbital motion limited (green solid line), and experimental (black solid line) nonsmoothed current–voltage, *I-V*, characteristic curves for the helium A, B, and C example cases, respectively. The point indicates the V_{SP} datum selected for the Sonin plot

theoretical curve does not match the experimental curve, so the radial theory is fulfilled. For the B case (intermediate β value), the experimental curve is in an intermediate zone between the OML and the radial theoretical curves. Finally, for the C case, corresponding to the highest β values, the experimental curve fits quite well with the one corresponding with the OML theoretical one. So, this criterion enables to observe the transition between OML and radial theories.

The favorable aspect of this criterion is that it ensures that the agreement with the radial or OML behavior extends to a wide range of values of the measured probe potential, so it is not exclusively confined to probe potential values close to the one used in the Sonin plot criterion, $y_{SP} = 25$. In this sense, it can be seen from Figure 5a that for values of the probe potential, V, below the one selected for the Sonin plot, the experimental curve diverges from the radial one, hence resulting in a nonradial behavior. This evidences the problem mentioned about the Sonin plot criterion, as it depends on a single point of the current–voltage characteristic curve, and so the conclusion would be different, depending on the y_{SP} selected value. Moreover, as the n_+ obtained value depends on the theoretical radial or OML curves used for the cross-plotting, we conclude that both (a) and (b) criteria are complementary. Furthermore, the signal-to-noise ratio of the experimental data does not influence this criterion. The inconvenience of this criterion is that it does not let us study the evolution as a function of the β parameter; furthermore, it is a qualitative criterion.

(c) The third criterion is the study of the linear behavior of the experimental plot I_+^2 versus V, in the positive ion saturation zone, which must be followed if the OML motion theory is fulfilled.

It should be noted that in the cases in which the OML well describes the ion current collected by the probe, this current depends on the probe potential as follows[14]:

$$I_+ = -An_+e\sqrt{\frac{k_b T_+}{2\pi m_+}}\frac{2}{\sqrt{\pi}}\left(1-\frac{e|V-V_{plasma}|}{k_B T_+}\right)^{\frac{1}{2}}, \quad (3)$$

for $V < V_{plasma} - 2k_B T_+/e$.

Therefore, similar to the Sonin plot, this criterion can be used to diagnose the positive ion density, as the slope of a linear fitting, of the I_+^2 versus V curve, provides an experimental value for n_+.[1,6,14,34,42,43,49,53]

Figure 6 shows the I_+^2 versus V points and the corresponding linear fit, obtained from the experimental current-to-voltage characteristic, for the argon example case in an interval centered at y_{SP}, which is few $k_B T_+/e$ wide, to ensure that the current is only due to positive ions. Linear correlation coefficients lower than 0.5, for intervals always containing more than 50 points, have been obtained for all the argon plasma measured cases. Moreover, there is always a difference >60% between the n_e reference values obtained from the EEDF and the one obtained for n_+ from the slope of the I_+^2 versus V linear fit for all those cases. So, we can conclude that, under our discharge conditions in argon plasmas, the current collected by the probe is not described by the OML theory. Similar results have been obtained in the case of neon plasmas.

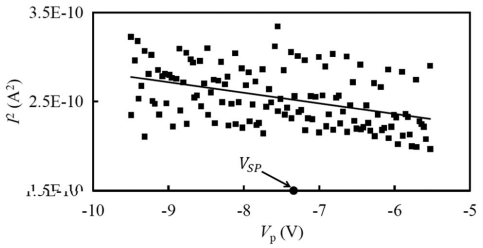

FIGURE 6 I_+^2 versus V experimental linear fit for nonsmoothed experimental data in the ion saturation zone for the argon example case

Figure 7a–c illustrate such a comparison for the three helium example cases, A, B, and C, respectively. The evolution found in previous criteria is shown again. The correlation coefficient for the A case, where β is close to zero, is $r = 0.41$, obtained from an interval containing 131 points, whereas for the B case, for intermediate β values, $r = 0.78$, obtained from an interval containing 130 points, and for the C case, for the highest β values, $r = 0.96$, obtained from an interval containing 113 points. Similar to argon and neon plasmas, there is a big difference between the n_+ values obtained from the EEDF and those obtained from the slope of the I_+^2 versus V linear fit for the A and B cases. Nevertheless, for the C case, the value obtained for the ion density by means of this representation, $n_+ = 7.6 \times 10^{15}\,\mathrm{m}^{-3}$, is quite similar to the one obtained from the EEDF, $n_e = 7.4 \times 10^{15}\,\mathrm{m}^{-3}$. So, it can be concluded that in the C case, the OML theory provides a good description of the ion current collected by the probe, whereas for the other A and B cases, the OML theory is not appropriate. This result is similar to those obtained for the rest of the measured cases for helium, that is, only for the highest β value cases, n_e approaches n_+.

Finally, as in the (b) criterion, the favorable aspect of this one is that it uses a wide interval of the current–voltage characteristic curve and it can be used to diagnose n_+ if the OML theory is accomplished[53]; however, the inconvenience is that the low experimental signal-to-noise ratio in the ion saturation zone of the current-to-voltage characteristic curve will contribute to diminish the linear correlation coefficient, so the results may not be conclusive. In contrast, this criterion only ensures the orbital or nonorbital behavior of the ions trajectory, that is, it is only an OML criterion and no information about the radial behavior, if the criterion is not fulfilled, can be concluded.

(d) The Pilling–Carnegie criterion[25] is a consequence of the previous one. These authors proposed the study

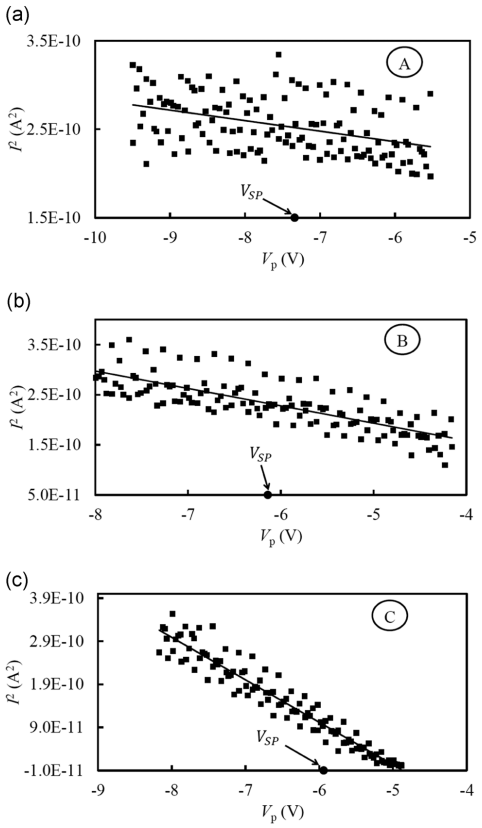

FIGURE 7 (a–c) I_+^2 versus V experimental linear fit for nonsmoothed experimental data in the ion saturation zone for the helium example cases A, B, and C, respectively

of the plot $d(\log_{10}V)/d(\log_{10}I_+)$ versus V. Obviously, for V values very distant from the plasma potential, V_{plasma}, the curve will tend to the limiting value 2 if the charged particles fall toward the probe, fulfilling the OML theory.

Figure 8a shows the $d(\log_{10}V)/d(\log_{10}I_+)$ versus V plots for the ion saturation zone, $V \ll V_{plasma}$, for several argon plasma conditions in the interval $y_{SP} \pm 3k_BT_e/e$. As it can be seen, the curves do not tend to the limiting value 2, corresponding to the OML theory. So, we can conclude that under the studied discharge conditions, the ions do not fall toward the probe by following an orbital trajectory. For the case of neon plasmas, the behavior is quite similar. Nevertheless, Figure 8b illustrates the plot for several helium plasma conditions. As it can be seen, for

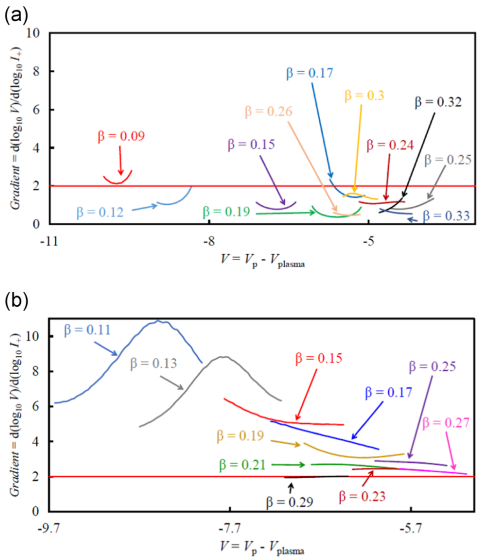

FIGURE 8 (a,b) Pilling–Carnegie criterion in the ion saturation zone: Evolution of experimental measurements with the β parameter for argon and helium plasmas, respectively. In these graphs, the limiting value 2 is represented

the highest β values, the curves tend to the limiting value 2, as expected for the orbital motion theory. So, a transition to the OML theory is again observed by using this criterion, as the β value increases in helium plasmas.

Finally, as in the (b) and (c) criteria, the favorable aspect of this criterion is that it does not just use a single point but an interval of the current–voltage characteristic curve. Moreover, it lets us study its evolution as a function of the β parameter. The disadvantages of this criterion include the experimental noise, since the logarithmic scale can mask the trend to the limiting value 2, as can be seen even in the original article from Pilling and Carnegie.[25] Also, similar to the (c) criterion, it only ensures the orbital or nonorbital behavior of the ions' trajectory, and no information about the radial behavior, if the criterion is not fulfilled, can be concluded.

(e) The Allen–Annaratone criterion[5] considers that the OML theory will not be valid if

$$\lambda_+ < r_p\left(-eV/k_B T_+\right)^{1/2}. \quad (4)$$

The right term of the inequality is the effective radius of the probe for ion capture, r_{eff}, when the energy of the ions at large distances from the probe is a small quantity compared with $|eV|$. This condition is quite restrictive, as $\lambda_+/r_p < 28.79[T_e(eV)]^{1/2}$ for $T_+ = 350$ K and $-eV/k_B T_+ = 25$. As shown in Figure 9a, when β increases, the behavior of Ar^+ ions falling toward the probe does not become orbital, as the experimental measurements do not cross the λ_+ limiting value of 0.74 mm (straight line). Obviously, all the results of the illustrated discharges have been made at the same argon pressure, corresponding to the indicated lambda value, $\lambda_+ = 0.74$ mm. Figure 9b shows similar results for Ne^+ ($\lambda_+ = 0.8$ mm). Nevertheless, as it can be seen in both gases, if our discharge device would allow us to achieve higher β values, a transition from radial to orbital motion could be observed. Finally, Figure 9c shows the results obtained for the helium plasmas ($\lambda_+ = 1$ mm). As it can be seen, similar to the previous criteria, a transition from nonorbital motion to orbital motion behavior is clearly illustrated for the highest β values.

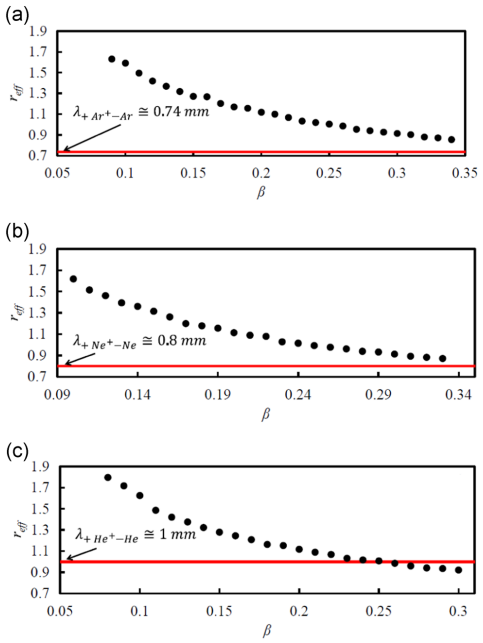

FIGURE 9 (a–c) Allen–Annaratone criterion as a function of the β parameter for argon, neon, and helium plasmas, respectively, under several discharge conditions. The red straight lines for 0.74, 0.8, and 1 mm are the mean free path values for neutral–ion collisions for the case of argon, neon, and helium case, respectively

TABLE 1 Comparison of criteria

Criteria	Advantages	Inconveniences
Sonin plot	**1.** It provides a plasma diagnostic technique for the positive ion density, $n_+ \approx n_e$ **2.** The evolution of this criterion as a function of the β parameter can be obtained	**1.** It uses a single experimental point of the whole current-to-voltage characteristic curve **2.** This criterion is quite sensible. A small variation in β may also correspond to a large displacement in the Sonin plot **3.** This criterion is influenced by the low signal-to-noise ratio in the ion saturation zone
Comparison between the experimental current–voltage characteristic curve, for $V < V_{plasma}$ values, and the theoretical ones obtained from the radial and the OML theories	**1.** It ensures that the agreement with the radial or OML behavior extends to a wide range of values of the measured probe potential **2.** The signal-to-noise ratio of the experimental data is not critical in this criterion	**1.** It does not let us to study the evolution as a function of the β parameter; furthermore, it is a qualitative criterion
Linear behavior of the experimental plot I_+^2 versus V	**1.** It uses a wide interval of the current–voltage characteristic curve	**1.** The low experimental signal-to-noise ratio in the ion saturation zone of the current-to-voltage characteristic curve will contribute to diminish the linear correlation coefficient, so the results may not be conclusive **2.** It only ensures the orbital or nonorbital behavior of the ions' trajectory
Pilling–Carnegie	**1.** It does not just use a single point but an interval of the current–voltage characteristic curve **2.** It lets us study its evolution as a function of the β parameter	**1.** The experimental noise, as the logarithmic scale can mask the trend to the limiting value 2 **2.** It only ensures the orbital or nonorbital behavior of the ions trajectory, and no information about the radial behavior can be concluded
Allen–Annaratone	**1.** It is the only one that considers both λ_+ and β parameters **2.** It is the only one that does not use the measured ion current **3.** It uses a wide interval of the current–voltage characteristic curve to obtain T_e **4.** It is a quantitative criterion, so it lets us study its evolution as a function of both the λ_+ and β parameters	**1.** It is an OML criterion

Abbreviation: OML, orbital motion limited.

Finally, this criterion has two very favorable aspects: On the one hand, it is the only criterion that considers both λ_+ and β parameters; on the other hand, it is the only one that does not use the measured ion current. Moreover, similar to the (b), (c), and (d) criteria, another favorable aspect of this criterion is that it uses a wide interval of the current–voltage characteristic curve to obtain T_e. Furthermore, it is a quantitative criterion; hence, it lets us study its evolution as a function of both the λ_+ and β parameters. The disadvantage of this criterion is similar to other presented criteria: It is an OML criterion, as it only ensures the orbital or nonorbital behavior of the ion trajectory, and no information about radial behavior, if the criterion is not fulfilled, can be concluded.

As a summary, Table 1 shows the main aspects of these criteria to be considered.

5 | CONCLUSIONS

There are two different theories describing the positive ion current collected by a cylindrical Langmuir probe immersed in a plasma: the radial and orbital theories. They assume radial or orbital trajectories, respectively, for positive ions when falling toward the probe. This is an important subject of study, as the trajectory of the ions when falling toward the probe/surface is extremely important in plasma diagnosis and plasma surface technology.

Moreover, in many situations, values for the ion current between the two limiting theories are observed in experiments, such that a transition from the radial to the orbital positive ion behavior should be expected when the influence of different parameters, such as β and λ_+, is considered. This transition can be theoretically justified by supposing that positive ions lose their translation kinetic energy by collisions with other particles composing the plasma, mainly neutrals. So, for small β and λ_+ values, after the last collision, the ions can be expected to follow a quasi-radial trajectory when falling toward the probe. Nevertheless, for the highest λ_+ and/or β values, for ions far away from the probe, the azimuthal component of the ion thermal velocity is high enough to fall toward the probe by following an orbital trajectory.

In this article, we have reported the experimental results obtained in the application of five criteria to discriminate whether the positive ion current collected by a cylindrical Langmuir probe is described by the orbital or radial theories in low-pressure, low-temperature argon, neon, and helium plasmas as a function of the β parameter and of the λ_+ parameter. Moreover, a discussion of the favorable and unfavorable aspects of each criterion has been included, describing whether the criterion is qualitative or quantitative, if it can be used to diagnose the plasma, the amount of data used, the influence of the signal-to-noise ratio, or the possibility of illustrating the criterion as a function of β.

The study begins with argon plasmas, finding that, under our discharge conditions, the Ar^+ ion current collected by the probe is well described by the radial theory for all the β values. In neon plasmas, as λ_+ is higher for Ne^+ than for Ar^+, and as its atomic mass is lower and consequently the azimuthal component of the ion thermal velocity is higher than in argon, we could expect a transition from radial to orbital behavior for the ion current collected by the probe with the increase in β. Nevertheless, an identical radial Ne^+ behavior was obtained. Finally, a transition was found in helium plasma discharges, as its atomic mass is much lower and λ_+ is much higher, compared with the neon ones. As theoretically expected, we have found that for the lower β values, the He^+ ions fall toward the probe by following a radial trajectory. Nevertheless, as β increases, the transition takes place, and for the highest β values, the He^+ ions follow an orbital trajectory, and the He^+ current is well described by the OML theory. This is the first time that such a transition has been experimentally observed. Moreover, these results confirm the proposed theoretical justification for the measured ion current between the two limiting theories.

ACKNOWLEDGMENTS

This study has been partially supported by the Spanish Ministry of Science and Innovation, Ref. No. FIS2010-19951, which is partially financed with FEDER funds, and the FPU Program of the Spanish Ministry of Education (Ref. FPU17/01387).

ORCID

Juan Manuel Díaz-Cabrera http://orcid.org/0000-0002-7388-7373

José I. Fernández Palop http://orcid.org/0000-0002-2081-2095

Guillermo F. Regodón http://orcid.org/0000-0002-1782-9953

Jerónimo Ballesteros http://orcid.org/0000-0002-6481-0462

REFERENCES

[1] J. M. Díaz-Cabrera, J. I. Fernández Palop, R. Morales Crespo, M. A. Hernández, A. Tejero-del Caz, J. Ballesteros, *Measurement* **2014**, *55*, 66.

[2] J. Ballesteros, J. I. Fernández Palop, M. A. Hernández, R. Morales Crespo, *Appl. Phys. Lett.* **2006**, *89*, 101501.

[3] A. Dengra, J. Ballesteros, M. A. Hernández, V. Colomer, *J. Appl. Phys.* **1990**, *68*, 5507.

[4] J. M. Díaz-Cabrera, M. V. Lucena-Polonio, J. I. Fernández Palop, R. Morales Crespo, M. A. Hernández, A. Tejero-del Caz, J. Ballesteros, *J. Appl. Phys.* **2012**, *111*, 063303.

[5] B. M. Annaratone, M. W. Allen, J. E. Allen, *J. Phys. D: Appl. Phys.* **1992**, *25*, 417.

[6] J. Ballesteros, J. I. Fernández Palop, M. A. Hernández, R. Morales Crespo, *Rev. Sci. Instrum.* **2004**, *75*, 90.

[7] M. V. Lucena-Polonio, J. M. Díaz-Cabrera, J. I. Fernández Palop, R. Morales Crespo, M. A. Hernández, J. Ballesteros, *Plasma Phys. Controlled Fusion* **2011**, *53*, 124024.

[8] F. F. Chen, *Phys. Plasmas* **1995**, *2*, 2164.

[9] A. Bogaerts, E. Neyts, R. Gijbels, J. van der Mullen, *Spectrochim. Acta, Part B* **2002**, *57*, 609.

[10] M. A. Lieberman, A. J. Lichtemberg, *Principles of Plasma Discharges and Materials Processing*, John Wiley & Sons Inc., Hoboken, NJ **2005**, pp. 8–11.

[11] A. Shashurin, J. Li, T. Zhuang, M. Keidar, I. I. Beilis, *Phys. Plasmas* **2011**, *18*, 073505.
[12] K.-D. Weltmann, J. F. Kolb, M. Holub, D. Uhrlandt, M. Šimek, K. Ostrikov, S. Hamaguchi, U. Cvelbar, M. Černák, B. Locke, A. Fridman, P. Favia, K. Becker, *Plasma Processes Polym.* **2019**, *16*, e1800118.
[13] M. Laroussi, *Front. Phys.* **2020**, *8*, 1.
[14] H. M. Mott-Smith, I. Langmuir, *Phys. Rev.* **1926**, *28*, 727.
[15] I. B. Bernstein, I. N. Rabinowitz, *Phys. Fluids* **1959**, *2*, 112.
[16] J. G. Laframboise, *Theory of Spherical and Cylindrical Langmuir Probes Collisionless, Maxwellian Plasma at Rest*, Tech. rep. Toronto University Downsview (Ontario) Institute for Aerospace Studies **1966**.
[17] J. E. Allen, R. L. F. Boyd, P. Reynolds, *Proc. Phys. Soc.* **1957**, *70*, 297.
[18] F. F. Chen, *J. Nucl. Energy* **1965**, *7*, 47.
[19] J. I. Fernández Palop, J. Ballesteros, V. Colomer, M. A. Hernández, *J. Phys. D: Appl. Phys.* **1996**, *29*, 2832.
[20] R. Morales Crespo, J. I. Fernández Palop, M. A. Hernández, J. Ballesteros, *J. Appl. Phys.* **2003**, *94*, 4788.
[21] R. Morales Crespo, J. I. Fernández Palop, M. A. Hernández, J. Ballesteros, *J. Appl. Phys.* **2004**, *95*, 2982.
[22] G. F. Regodón, J. I. Fernández Palop, A. Tejero-del Caz, J. M. Díaz-Cabrera, R. Carmona-Cabezas, J. Ballesteros, *Phys. Plasmas* **2017**, *24*, 103516.
[23] G. F. Regodón, J. I. Fernández Palop, A. Tejero-del Caz, J. M. Díaz-Cabrera, R. Carmona-Cabezas, J. Ballesteros, *Plasma Sources Sci. Technol.* **2018**, *27*, 025014.
[24] G. F. Regodón, J. I. Fernández Palop, J. M. Díaz-Cabrera, J. Ballesteros, *Plasma Phys. Controlled Fusion* **2019**, *61*, 095015.
[25] L. S. Pilling, D. A. Carnegie, *Plasma Sources Sci. Technol.* **2007**, *16*, 570.
[26] J. M. Díaz-Cabrera, J. Ballesteros, J. I. Fernández Palop, A. Tejero-del Caz, *Plasma Sources Sci. Technol.* **2015**, *24*, 025026.
[27] A. Tejero-del-Caz, J. I. Fernández Palop, J. M. Díaz-Cabrera, G. F. Regodón, R. Carmona-Cabezas, J. Ballesteros, *J. Comput. Phys.* **2017**, *350*, 747.
[28] Y. S. Chou, *Phys. Fluids* **1966**, *9*, 2150.
[29] Z. Zakrzewski, T. Kopiczynski, *Plasma Phys.* **1974**, *16*, 1195.
[30] K. U. Riemann, *Phys. Fluids* **1981**, *24*, 2163.
[31] M. Tichý, M. Šícha, P. David, T. David, *Contrib. Plasma Phys.* **1994**, *34*, 59.
[32] S. Robertson, *Plasma Phys. Controlled Fusion* **2013**, *55*, 093001.
[33] G. F. Regodón, J. I. Fernández Palop, J. M. Díaz-Cabrera, J. Ballesteros, *Plasma Sources Sci. Technol.* **2019**, *28*, 115017.
[34] J. I. Fernández Palop, J. Ballesteros, V. Colomer, M. A. Hernández, *Rev. Sci. Instrum.* **1995**, *66*, 4625.
[35] J. I. Fernández Palop, J. Ballesteros, V. Colomer, M. A. Hernández, *J. Appl. Phys.* **1996**, *80*, 4282.
[36] J. T. Gudmundsson, *Plasma Sources Sci. Technol.* **1999**, *8*, 58.
[37] A. Tejero-del Caz, J. I. Fernández Palop, J. M. Díaz-Cabrera, J. Ballesteros, *Plasma Sources Sci. Technol.* **2016**, *25*, 01LT03.
[38] V. A. Godyak, R. B. Piejak, B. M. Alexandrovich, *J. Appl. Phys.* **1993**, *73*, 3657.
[39] S. A. Maiorov, O. F. Petrov, V. E. Fortov *Calculation of Resonant Charge Exchange Cross-Sections of Ions Rubidium, Cesium, Mercury and Noble Gases*, 34th EPS Conf. on Plasma Phys. (Warsaw), **2007**, *31F*, P-2.115.
[40] D. Curreli, F. F. Chen, *Phys. Plasmas* **2011**, *18*, 113501.
[41] E. Stamate, *Surf. Coat. Technol.* **2014**, *260*, 401.
[42] J. D. Swift, M. J. R. Schwar, *Electrical Probes for Plasma Diagnostics*, Ilife Books Ltd., London **1970**.
[43] V. I. Demidov, S. V. Ratynskaia, K. Rypdal, *Rev. Sci. Instrum.* **2002**, *73*, 3409.
[44] V. Godyak, R. B. Piejak, *Phys. Rev. Lett.* **1990**, *65*, 996.
[45] M. Li, S. K. Dew, M. J. Brett, *J. Phys. D: Appl. Phys.* **1999**, *32*, 2056.
[46] C. Chung, *Phys. Plasmas* **2005**, *12*, 123505.
[47] D. Gahan, B. Dolinaj, M. B. Hopkins, *Plasma Sources Sci. Technol.* **2008**, *17*, 035026.
[48] V. Godyak, B. Alexandrovich, *Plasma Sources Sci. Technol.* **2015**, *24*, 052001.
[49] F. F. Chen, *Langmuir Probe Diagnostics Mini-course on Plasma Diagnostics*, IEEE-ICOPS meeting, Jeju, Korea, **2003**.
[50] A. A. Sonin, *AIAA J.* **1966**, *4*, 1588.
[51] E. W. Peterson, L. Talbot, *AIAA J.* **1970**, *8*, 1391.
[52] M. L. E. Oliphant, E. Rutherford, *Proc. R. Soc. London, Ser. A* **1997**, *124*, 228.
[53] F. F. Chen, *Plasma Sources Sci. Technol.* **2009**, *18*, 035012.

How to cite this article: Díaz-Cabrera JM, Fernández Palop JI, Regodón GF, Ballesteros J. Accurate measurement of the ion saturation current collected by a cylindrical Langmuir probe in cold plasmas. *Plasma Process Polym.* 2020;e2000073.
https://doi.org/10.1002/ppap.202000073

5 Otras contribuciones

Removal of supersonic ion singularity in radial Langmuir probe models

G.F. Regodón[1], J.I. Fernandez Palop[1], A. Tejero-del-Caz[2], J.M. Diaz-Cabrera[3], R. Carmona-Cabezas[1], J. Ballesteros[1]

[1] *Departamento de Física, Universidad de Córdoba, E-14071 Córdoba, Spain*
[2] *Instituto de Plasmas e Fusão Nuclear, Instituto Superior Técnico, Universidade de Lisboa, Lisboa, Portugal*
[3] *Departamento de Ingeniería Eléctrica, Universidad de Córdoba, E-14071 Córdoba, Spain*

It is well known that a singularity appears when the ions reach the speed of sound in an electropositive plasma. For cold ions, the singularity is at infinity, and so it poses no problem the numerical integration of radial Langmuir probe models. However, for warm ions the singularity typically occurs between the quasi-neutral plasma and the sheath. We have found that we can continuously join the solution at the plasma with the probe thanks to a careful analysis of the mathematical structure of the problem. The technique can be applied to different geometries and to electronegative plasmas as well. For the case of cylindrical Langmuir probes, we have derived potential profiles, ion population profiles and ion current to probe voltage characteristics. These results are used to refine diagnosis techniques by means of Langmuir probes in laboratory plasmas.

In the interest of obtaining the potential profile $\phi(r)$ around a Langmuir probe in electropositive plasmas one should solve **Poisson's equation**. In the case of cylindrical geometry, we have

$$\frac{1}{r}\frac{\mathrm{d}}{\mathrm{d}r}\left(r\frac{\mathrm{d}\phi}{\mathrm{d}r}\right) = -\frac{e}{\varepsilon_0}[n_+(r) - n_e(r)]. \quad (1)$$

The electron density $n_e(r)$ will be described by the Maxwellian distribution function, whereas the ion density $n_+(r)$ depends on the ion motion theory used. When using a radial motion theory**, the thermal motion of the ions introduces an additional term in the energy balance equation** [1], giving

$$\frac{1}{2}m_+v_+^2(r) + e\phi(r) + \frac{\kappa}{\kappa-1}k_BT_+\left(\frac{n_{+(r)}}{n_{e0}}\right)^{\kappa-1} = \frac{\kappa}{\kappa-1}k_BT_+, \quad (2)$$

where κ is the adiabatic coefficient of the thermal flow. As $v_+(r)$ is inversely related to the ion density through continuity equation, i being the ion current per unit length collected by the probe,

$$i = e2\pi n_+(r)v_+(r), \quad (3)$$

we get a polynomic equation in $n_+(r)$, with defining parameters r and $\phi(r)$, which should be solved in order to introduce its value into Poisson's equation. We have found that **this polynomial has two positive roots** that coalesce into one for certain values of the problem variables r and ϕ. We further found that one of the roots is valid in the plasma in the limit $x \to \infty$, where the ions are at rest, while the other root is valid in the sheath in the cold ions limit $T_+ \to 0$.

We have proved that the transition between these roots must occur, in the variable space (r, ϕ), in the curve where the two positive roots of the energy balance polynomial coalesce in a sort of bifurcation line, and that the only possible smooth and continuous crossing through the **regular singularity [2] where the ions reach the speed of sound** is tangent to that bifurcation curve. In figure 1 we show an example of solution of the potential profile.

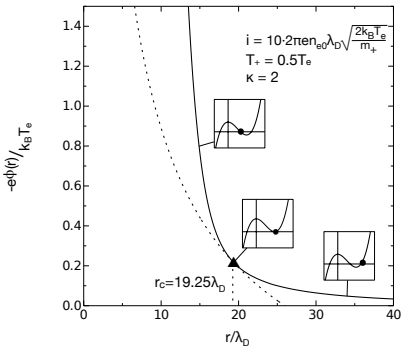

Figure 1: Potential profile and bifurcation curve solution. The small inserts are qualitative plots of the polynomic equation for $n_+(r)$.

This method is **valid for any ion temperature**. We indicate with a triangle the point where the speed of sound is reached. To the plasma or to the sheath we use the right energy balance polynomial root, as we mark with a dot in the inserts in the figure.

2. References

[1] J.I. Fernández Palop *et al* 1996 *J. Phys. D: Appl. Phys* **29** 2831.

[2] H.B. Valentini 1988 *J. Phys. D: Appl. Phys* **21** 311-321

Removal of supersonic ion singularity in radial Langmuir probe models

Regodon GF, Fernández Palop JI, Tejero-del-Caz A, Díaz-Cabrera JM, Carmona Cabezas R, Ballesteros J

Cylindrical radial model considering ion temperature

The potential profile is given by **Poisson's equation**:

$$\frac{1}{r}\frac{\mathrm{d}}{\mathrm{d}r}\left(r\frac{\mathrm{d}\phi}{\mathrm{d}r}\right) = -\frac{e}{\varepsilon_0}[n_{+(r)} - n_e(r)]$$

The **energy balance equation** [1] of the ion fluid:

$$\frac{1}{2}m_+ v_+^2(r) + e\phi(r) + \frac{\kappa}{\kappa-1}k_B T_+\left(\frac{n_+(r)}{n_{+0}}\right)^{\kappa-1} = \frac{\kappa}{\kappa-1}k_B T_+$$

In absence of ionisation, the **ion current is constant**.

$$i = e2\pi n_+(r)v_+(r)$$

We are considering a cylindrical Langmuir probe in the ion saturation zone of the IV characteristic. As ions fall to the probe:
- Increase of the pressure due to compression.
- Increase in density of the field lines.

When the ions reach the local speed of sound the relation between density and volume is inverted, as in jet engine exhausts. **This inversion of fluid behaviour creates a singularity**.

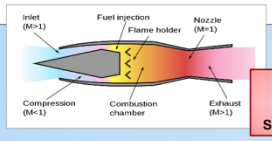

Jet engines are designed using this supersonic singularity

Integrating the equations starting in the quasineutral solution

The **quasineutral solution** (green line in the figures) includes a point in which the supersonic singularity is reached. When integrating from the plasma towards the probe **(to the left)**:

- If **the integration starts before the singularity**, all solutions diverge to $\Phi \to -\infty$ (blue solutions, short lines down in the figures).
- If **the integration starts after the singularity**, many solutions are possible (red solutions). But...
  - **Where** is the most correct position for the **initial conditions**?
  - Does the singularity **necessarily** belong **to the quasineutral solution**?

Furthermore, for increasing ion temperature (all other variables constant) solutions **separate from each other**.

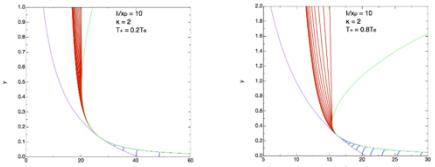

There were no arguments to choose one solution over the others.

All plots in adimensional units:
- Potential: $\Phi \to y$
- Radial coordinate: $r \to x$

Removal of supersonic ion singularity

Following the proposal by Valentini [2], we take the limit of physical variables and force them to stay bounded. We have found that the following statement must be true.

In the supersonic ion singularity, the potential must be tangent to a **regular supersonic singularity curve** (that depends on the current and on the ion temperature).

Regular supersonic singularity curve

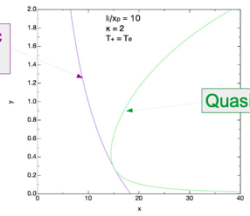

Quasineutral solution

Numerical search of the fluid solution

We check all the solutions that start in the **regular supersonic singularity curve**, and find that **only one of them fulfils quasineutrality** in the plasma. When integrating from the singularity to the plasma **(to the right)**:

- If **the starting potential is too high**, if will diverge to $\Phi \to +\infty$ (blue solutions).
- If **the starting potential is too low**, if will diverge to $\Phi \to -\infty$ (orange solutions).

Once the singularity is located, we can integrate towards the probe and obtain the whole **potential profile** (red solution) and any other physical variable or plot of interest.

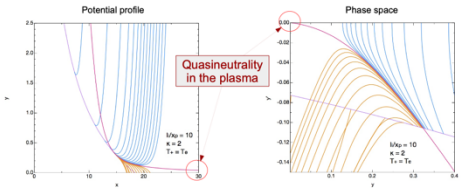

This methodology is valid for any ion to electron temperature ratio

We are now able to firmly stablish the limits of validity of radial models comparing to experiments

References:
[1] J.I. Fernández Palop *et al* 1996 *J. Phys. D: Appl. Phys* **29** 2831.
[2] H.B. Valentini 1988 *J. Phys. D: Appl. Phys* **21** 311-321

Radial Langmuir probe models for electronegative plasmas: Dependance of the floating potential on the geometry

Guillermo Fernando Regodón(*)[1], José Ignacio Fernandez Palop[1], Antonio Tejero-del-Caz[2], Juan Manuel Díaz-Cabrera[3], Rafael Carmona-Cabezas[1], Jerónimo Ballesteros[1]

[1] *Departamento de Física, Universidad de Córdoba, E-14071 Córdoba, Spain*
[2] *Instituto de Plasmas e Fusão Nuclear, Instituto Superior Técnico, Universidade de Lisboa, Lisboa, Portugal*
[3] *Departamento de Ingeniería Eléctrica, Universidad de Córdoba, E-14071 Córdoba, Spain*
(*) z62rehag@uco.es

We have extended the radial Langmuir probe sheath model by Fernández Palop J I *et al.* [*J Appl Phys* **80** 4282-91 (1996)] for non-zero positive ion temperature to the case of electronegative plasmas with one negative ion species. The negative ions are considered to be well characterised as a second maxwellian population, the first being the electrons. The model is valid for cylindrical and spherical geometry and we have found that there is and essential difference in the behaviour of the floating potential in both cases for probes with a small radius. We prove that the floating potential correctly estimates the electronegativity of the plasma almost independently of the temperature of the ions.

Since electronegative plasmas are commonly used in microelectronic industry, there is interest in enhancing diagnosing techniques in such plasmas. In our work we study a fluid model of a Langmuir probe in either cylindrical or spherical geometry immersed in an electronegative plasma with one positive ion species and one negative ion species. The positive ion species is modelled by means of the fluid equations, that is, the momentum balance equation, in which an ion gas pressure term is added. The pressure term is described by an adiabatic process in an ideal gas, the pressure force depending on the gradient of the ion density:

$$\frac{\mathrm{d}p_+(r)}{\mathrm{d}r} = k_B T_+ \kappa \left(\frac{n_+}{n_{+,0}}\right)^{\kappa-1} \frac{\mathrm{d}n_+(r)}{\mathrm{d}r}, \tag{1}$$

where n_+, $n_{+,0}$ stand for the positive ion densities at distance r from the axis or the center of symmetry and the positive ion density in the plasma. The constant κ is the adiabatic coefficient of the process. The negative ion species and the electrons are modelled with enough accuracy using maxwellian distribution functions of their respective temperatures. These equations can be used in Poisson's equation to establish a differential equation for the potential profile in both geometries ($D = 1$ corresponds to cylindrical geometry and $D = 2$ to spherical geometry). Poisson equation, written simultaneously for both cylindrical and spherical geometry, is therefore read:

$$\frac{1}{r^D}\frac{\mathrm{d}}{\mathrm{dr}}\left(r^D \frac{\mathrm{d}\phi(\mathrm{r})}{\mathrm{dr}}\right) = -\frac{e}{\varepsilon_0}\left[n_+(r) - n_-(r) - n_e(r)\right]. \tag{2}$$

The equations have a singularity when the positive ions reach their local speed of sound. At this point, the relative behaviour between the ion density and the pressure is inverted, that is, in a subsonic flow an increase in the pressure implies an increase in the density, while the opposite occurs in a supersonic flow. This singularity has been recently solved [1, 2] for cylindrical geometry and a solution valid from the plasma limit to the probe has been found. This procedure can be extended to two negative species and to spherical geometry, which is the aim of our present work.

The floating potential is the potential with respect to the plasma potential for which the net current collected by the probe is zero. The negative ions are much heavier than the electrons, so that the negative ion current is generally very small in comparison. It could only be comparable to the electron current if the negative ions density is much higher than the electron density in the plasma, and if the negative ion temperature is comparable to the electron temperature. In any other case, the only influence of the negative ions is the increase of the positive ion density through quasineutrality condition in the plasma.

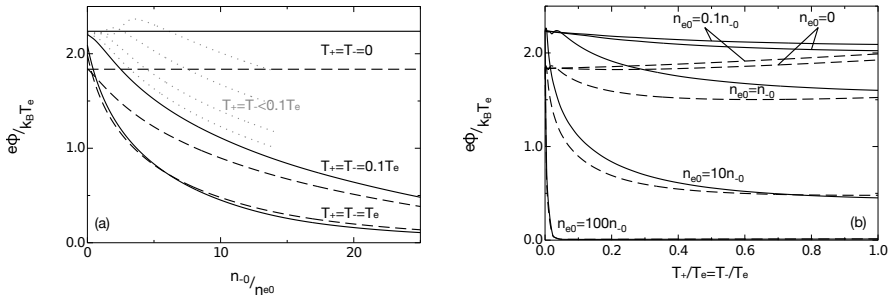

Fig. 1: Floating potential, with respect to the ions temperature (a) and with respecto to the electronegativity (b) for probe radius equating $1.5\lambda_D$, in cylindrical geometry (bold lines) and in spherical geometry (broken lines).

When the floating potential is calculated for several electronegativity parameters α_0, defined as the ratio between the negative ion and the electron density in the plasma, we find that the floating potential is largely insensitive to the negative ion temperature (we have assumed equality of both ion temperatures although this assumption is not important, as long as they are in the same order of magnitude). This renders the floating potential to be a good parameter to estimate the electronegativity of the plasma. As a case of study we plot the floating potential for an electronegative plasma in which both ions species are oxygen, with charges $\pm e$.

In the model studied, the effect of the pressure depends on the geometry. In both geometries studied in the model, cylindrical and spherical, the pre-sheath mechanism is the reduction of available volume closer to the symmetry axis. We have found that for small probes in spherical geometry, the pre-sheath mechanism is so strong as to surpass the effect of the acceleration due to the electric field of the electronegative sheath. In such case, the positive ion density is ever increasing as the positive ion fluid approaches the probe, and thus the ion pressure exerts a force on the ions away from the probe. As the pressure is proportional to the temperature, through the ideal gases law, an increase in the ion temperature makes more difficult for the ions to reach the probe, and the floating potential increases, which is the opposite to the behaviour in most circumstances.

We can appreciate in Fig. 1 that for very low ion temperature there appear oscillations in the floating potential (the dotted lines in (a)). These oscillations occur due to the same phenomena that generate the stratified pre-sheath that has been predicted but not experimentally observed [3]. In Fig.1, it can be observed that the range of values for which the stratified pre-sheath can be measured is very small and beyond experimental measuring procedures.

Acknowlegments

This work has been co-financed by the Plan Propio de Investigación de la Universidad de Córdoba and by the Programa Operativo FEDER Andalucía

References

[1] Fernández Palop J I, Ballesteros J, Colomer V and Hernández M A 1996 *J. Phys. D: Appl. Phys* **29** 2832
[2] Regodón G F, Fernández Palop J I, Tejero-del Caz A, Díaz-Cabrera J M, Carmona-Cabezas R and Ballesteros J 2017 *Phys. Plasmas* **24** 103516
[3] Kono A 1999 *J. Phys. D: Appl. Phys* **32** 1357–1363

Radial Langmuir probes for electronegative plasmas: dependance of the floating potential on the geometry

Regodón GF, Fernández Palop JI, Tejero-del-Caz A, Díaz-Cabrera JM, Carmona-Cabezas R, Ballesteros J

Radial model considering ion temperature: hypotheses

The model for the **ion saturation** part of the ion current-to-probe voltage characteristic (IV characteristic) considers the following assumptions:

- Plasma with **one positive** ion species and **two negative** species.
- **Fluid model** valid for the positive ions. → $\frac{1}{r^D}\frac{\mathrm{d}}{\mathrm{d}r}\left(r^D\frac{\mathrm{d}\phi}{\mathrm{d}r}\right) = -\frac{e}{\varepsilon_0}[n_{+(r)} - n_1(r) - n_2(r)]$
- **Small negative species** currents to avoid depletion of negative species.
- **Non-zero positive ion temperature** which introduces effect of pressure and sub-sonic/super-sonic flow.
- **Adiabatic flow** for the positive ions. → $p_+ = k_B T_+ \frac{n_+(r)^\kappa}{n_{+,0}^{\kappa-1}}$

Case of electronegative plasma

The main effect of the presence of a negative ion population, is the decrease of the floating potential, other plasma parameters having secondary influence.

Floating potential VS electronegativity

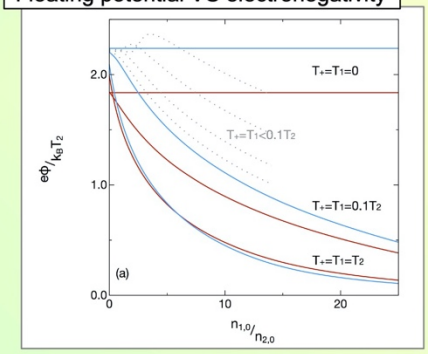

The effect of the ion temperature depends on the probe radius (in λ_D units) and on the geometry

Cylindrical geometry

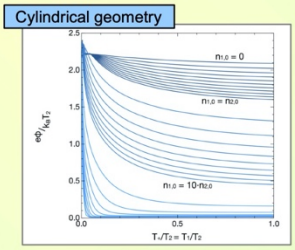

Spherical geometry

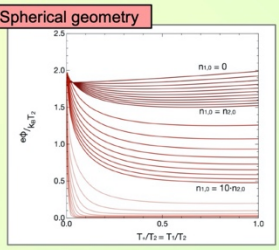

The stronger geometric compression in spherical coordinates inverts the pressure gradient

Case of electropositive plasma with bi-maxwellian EEDF

We can prove experimentally that the model works in a wide range of discharge conditions. We have performed a series of measurements in argon, with maxwellian to bi-maxwellian EEDF transition.

Experimental measurement of the floating potential

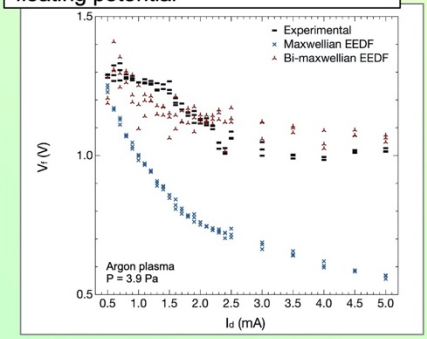

We have found that, when the EEDF can be considered maxwellian, the floating potential is correctly given by the model with one negative population.

But when the EEDF is bi-maxwellian, the radial model for electronegative plasmas with non-zero ion temperatures gives the correct value for the floating potential.

This work has been co-financed by the Plan Propio de Investigación de la Universidad de Córdoba and by the Programa Operativo FEDER Andalucía

References:
[1] J.I. Fernández Palop *et al* 1996 *J. Phys. D: Appl. Phys* **29** 2831.
[2] G.F. Regodón *et al.* 2018 *Plasma Sources Sci. Technol.* **27** 025014.

PIC simulation of a collisional planar pre-sheath

Guillermo Fernando Regodón(*)[1], José Ignacio Fernandez Palop[1], Antonio Tejero-del-Caz[2], Juan Manuel Díaz-Cabrera[3], Rafael Carmona-Cabezas[1], Jerónimo Ballesteros[1]

[1] *Departamento de Física, Universidad de Córdoba, E-14071 Córdoba, Spain*
[2] *Instituto de Plasmas e Fusão Nuclear, Instituto Superior Técnico, Universidade de Lisboa, Lisboa, Portugal*
[3] *Departamento de Ingeniería Eléctrica, Universidad de Córdoba, E-14071 Córdoba, Spain*
(*) z62rehag@uco.es

A Particle-in-Cell (PIC) simulation has been performed for the pre-sheath that is formed in front of a planar Langmuir probe negatively biased with respect to the plasma in which collisions have been included. The plasma is composed of positive ions and electrons, as well as a background of neutrals: both kinds of charged particles are simulated. NVIDIA CUDA parallel technology has been used to implement the simulations in a General Purpose Graphics Processing Unit (GPGPU). We have tested the validity of the programmed collisions procedure by comparison with a theoretical, exactly solvable model. In the testing simulation, the mean free path for the collision of ions with neutrals is 50 Debye lengths, while the length of the simulation is 200 Debye lengths, which proved to be enough distance for the collisional pre-sheath to form.

Models that are exactly solvable in plasma physics are scarce. Therefore, simulations that allow researchers to introduce different pre-sheath mechanisms are an essential tool in order to check new theories. For that task, Particle-in-Cell (PIC) algorithms are commonly used to perform simulations of plasmas. They have been studied for several decades and the numerical effects of the different parameters that characterise the simulation are well known. The simplification introduced in the calculation of the force over the particles using a grid and Poisson's equation does not reduce accuracy in an appreciable way, and greatly reduces the amount of required calculations.

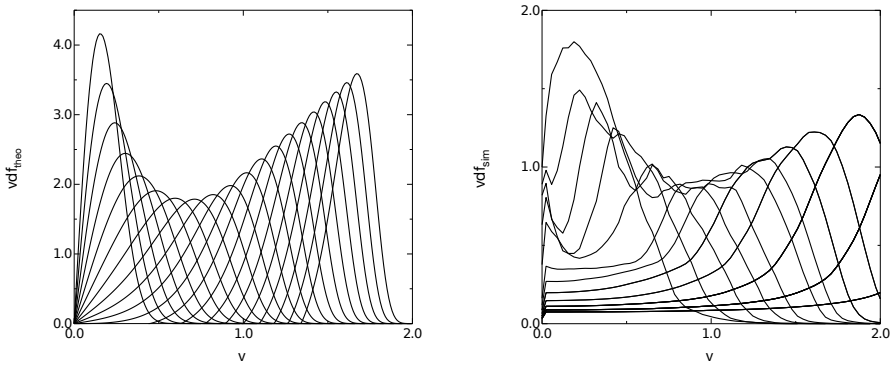

Fig. 1: Ion velocity distribution function (IVDF) of a collisional pre-sheath for several potential values. On the left, the exact IVDF calculated using Riemann's solution [1]. On the right, the IVDF obtained using CUDA PIC simulations in which collisions are included, with a mean free path of 50 Debye lengths. The difference in the potential between each two consecutive IVDFs is $0.2k_BT_e/e$. The velocity axis is normalised to $v_{th} = \sqrt{\frac{k_BT_e}{m_+}}$.

Collisions are an important pre-sheath mechanism, especially in planar metallic surfaces in contact with the plasma. The parameter that characterises the collisional plasma is the ratio between the collision

mean free path and the sheath scale, that is, the Debye length. The only case for which there exists an exact solution is the asymptotic case of infinite collision mean free path to Debye length ratio [1]. In other cases, we must rely on asymptotic matching techniques.

In this work, we continue the development of PIC 1d1v sheath simulations by Tejero-del-Caz *et al.* and introduce several updates. They are programmed using NVIDIA CUDA parallel computing framework over a General Purpose Graphics Processing Unit (GPGPU) [2, 3]. Using this technology we can use the thousands of small Processing Units that GPGPUs have in a coordinated way to solve a problem. Tejero-del-Caz original work was centred in the development and the validation of the PIC algorithm for a non-collisional sheath. We have now been able to extent the simulations to include collisions and ionisation, as well as to include some enhancement on the code.

The PIC simulation was used to obtain the ion velocity distribution function (IVDF) of a collisional pre-sheath, and we compare it to the theoretical ion velocity distribution function that we obtained using the method developed in [1]. The simulation was performed in a one dimensional grid that simulated the space next to a metallic planar surface in contact with a plasma. The length of the simulation was 200 Debye lengths with 4000 cells. The simulation included approximately $4 \cdot 10^5$ ions and $3.95 \cdot 10^5$ electrons. On the metallic surface end we forced the potential to a fixed value, $-25 k_B T_e / e$. The IVDFs were averaged from times $1.1 \cdot 10^5 \omega_p^{-1}$ to $1.2 \cdot 10^5 \omega_p^{-1}$ in $0.01 \omega_p^{-1}$ steps. The ions were introduced as a mono-energetic beam so that the electric field at the plasma end of the simulation is as close to zero as possible [2]. A comparison is shown in Fig. 1, where it can be appreciated that the IVDFs that we obtain follows the correct trend, although the IVDFs are smoothed out. This is a consequence of the averaging on a cell with a limited number of particles. The leftmost IVDFs correspond to the plasma, and, as the ions get closer to the metallic surface, they are accelerated. In the case of the simulation IVDFs we can observe a peak close to 0 velocity, corresponding to the collisions of the mono energetic ion beam, and also that the peak disappears as the collisional pre-sheath forms. The peak is absent in the theoretical solution. We estimate that the peak would disappear in the simulation if the ions were injected following Riemann's distribution.

The main computational improvement is that we solve Poisson's equation using Crank-Nicholson method, which is faster and more exact than Jacobi iterative method, although the programming of this method is far more complex in CUDA framework. Although other improvements were performed, this substitution turned out to be the most important: the computation time was reduced greatly, to one third or even one tenth of the original computation time.

Acknowlegments

This work has been co-financed by the Plan Propio de Investigación de la Universidad de Córdoba and by the Programa Operativo FEDER Andalucía

References

[1] Riemann K U 1981 *Phys. Fluids* **24** 2163
[2] Tejero-del Caz A, Fernández Palop J I, Díaz-Cabrera J M, Regodón G F, Carmona-Cabezas R and Ballesteros J 2017 *J. Comput. Phys.* **350** 747–758
[3] Tejero-del Caz A, Fernández Palop J I, Díaz-Cabrera J M and Ballesteros J 2016 *Plasma Sources Science and Technology* **25** 01LT03

PIC simulation of a collisional planar pre-sheath

Regodón GF, Fernández Palop JI, Tejero-del-Caz A, Díaz-Cabrera JM, Carmona-Cabezas R, Ballesteros J

PIC simulations of sheaths and pre-sheaths

We use a **1d-1v Particle-in-Cell (PIC)** simulation [1] for the interaction between a **plasma** and a **plane metallic surface**. It is a standard PIC simulations with:

- a particle collecting boundary (the metallic surface) and
- a boundary that injects particles according to a defined algorithm (the plasma).

The simulation considers collisions using a Montecarlo method.

CUDA technology for parallel processing

We use Nvidia CUDA technology for the programming of the simulation. It allows to use the parallel computing power of Graphics Processing Units (GPU) for scientific computations.

This technology can be used effectively as a library for high level languages like C++, Fortran or Matlab. However, to unleash all the computing power of GPUs, we use it as a low level C-style language.

Implementation of the simulation

- The plasma boundary should have as small electric field as possible.
- The ion being injected should have the velocity that avoids the apparition of a source sheath [2].
- The potential is solved with a direct method (Crank-Nicholson, FEM...).
- The size of the simulation is limited by GPU memory constraints.

Results of the simulation

Example of 200 Debye length (λ_D) simulation in 0.01 ω_p^{-1} timesteps with 5 λ_D mean free path (mfp).

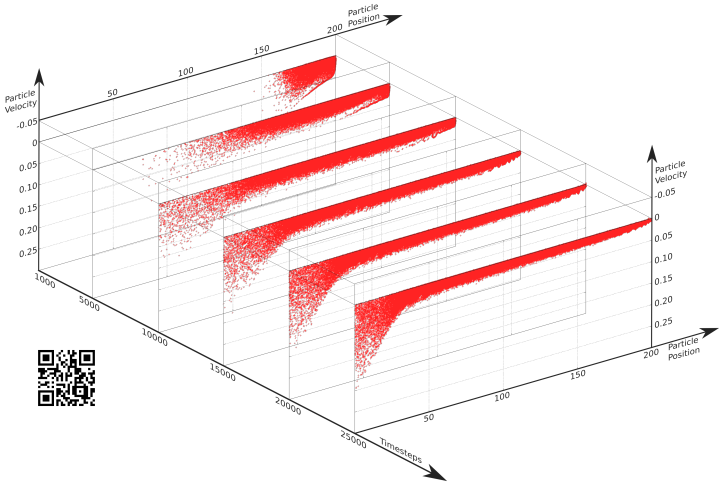

Velocity distribution function for a 50 λ_D mean free path (mfp) simulation and the asymptotic theoretical limit [3].

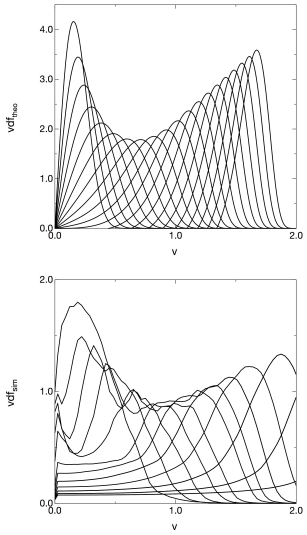

This work has been co-financed by the Plan Propio de Investigación de la Universidad de Córdoba and by the Programa Operativo FEDER Andalucía

References:
[1] Tejero-del-Caz A *et al.* 2016 *Plasma Sources Sci. Technol.* **25** 01LT03
[2] Tejero-del-Caz A *et al.* 2017 *J. Comput. Phys.* **350** 747–758
[3] Riemann K U 1981 *Phys. Fluids* **24** 2163

Sistema de control de la medida de la característica I-V en un plasma luminiscente.

***Abstract*—El plasma, conocido como el cuarto estado de la materia, es un gas de iones, electrones y átomos neutros que presenta un comportamiento inherentemente complejo cuando interacciona con superficies metálicas o no metálicas, con líquidos, con flujos de partículas, con radiación electromagnética... Para describir su comportamiento es necesario utilizar las leyes físicas del electromagnetismo, de la termodinámica y de la física cuántica. En este trabajo se presenta el dispositivo, basado en la utilización de una sonda de Langmuir (un conductor con geometría cilíndrica o esférica), con el que puede obtener la característica IV de la sonda de Langmuir inmersa en el plasma. El sistema está automatizado y controlado por ordenador mediante LabView para realizar diagnosis de un plasma luminiscente (glow plasma), es decir, un plasma frío generado en una cavidad amplia. Con este sistema se permite la caracterización del mismo en base a magnitudes medibles con significado físico, en condiciones óptimas de forma que la medida sea confiable y útil para contrastar las teorías que se desarrollan sobre la interacción del plasma con superficies metálicas y utilizar las medidas en aplicaciones industriales.**

I. Introduccion

El plasma es un gas de iones y electrones que presenta comportamiento colectivo [1]. Los iones poseen carga que genera campos eléctricos y magnéticos, los cuales a su vez condicionan el movimiento de las demás cargas del plasma mediante la fuerza de Lorentz.

$$m \cdot \frac{\mathrm{d}\vec{v}}{\mathrm{d}t} = q \cdot (\vec{E} + \vec{v} \times \vec{B})$$

Por lo tanto, un plasma es un sistema físico en que el propio movimiento de las partículas se realimenta en el sistema condicionando el movimiento posterior de las mismas. Este es un ejemplo paradigmático de sistema no lineal. Los plasmas aparecen de forma natural en gases a alta presión y temperatura, como ocurre en el sol y las estrellas (el plasma constituye más del 99% de la materia del Universo). En la Tierra, donde temperaturas y presiones suficientemente altas no ocurren naturalmente, generamos el plasma mediante grandes descargas eléctricas que, en condiciones apropiadas de presión y composición química, permiten la formación de un plasma estable. Los plasmas generados en la Tierra se utilizan en gran cantidad de aplicaciones industriales: La más importante es la implantación de iones en el tratamiento de superficies mediante deposición química de vapor asistida por plasma (PACVD), que se utiliza en la industria de semiconductores y para modificar las propiedades físico-químicas de superficies de componentes usados en la industria [2]. Otras aplicaciones son iluminación, esterilización, biocompatibilidad o generación de especies químicas.

En las aplicaciones industriales del plasma es esencial controlar las propiedades del plasma. Muchas de las aplicaciones industriales del plasma se basan en colisionar iones, positivos o negativos, con una superficie. Si la velocidad de la partícula que colisiona es demasiado baja, el ion no se implantará o no tendrá energía para esterilizar la superficie. Si la velocidad es demasiado alta, dañará la estructura de la superficie. Por otra parte, el plasma generado es susceptible a cambios de presión temperatura ambiental. por lo que puede ser necesario realizar correcciones en la potencia de la descarga o la presión para encontrar las condiciones ideales para cada aplicación. Por lo tanto, controlar el plasma y conocer la manera en que los iones caen a la superficie es esencial para garantizar que el plasma puede ser utilizado con éxito en aplicaciones industriales.

Para poder diagnosticar el plasma, es decir, para poder describirlo en base a un conjunto de magnitudes físicas medibles, se utilizan principalmente dos métodos importantes. En primer lugar tenemos la sonda de Langmuir, que es un conductor con simetría radial (cilíndrica o esférica) que se introduce en el plasma. En base a teorías sobre dicha interacción, podemos relacionar la característica I-V (extremadamente no lineal) que presenta la sonda de Langmuir inmersa en el plasma y medir las magnitudes de interés, que son principalmente la temperatura de los iones y electrones y la densidad de iones y electrones. El otro método de diagnosis de plasma es la espectroscopia de la radiación luminosa emitida por el plasma luminiscente cuando iones y electrones se recombinan para generar un nuevos átomos o iones.

La sonda de Langmuir presenta algunas ventajas que hacen que aún sea uno de los métodos más utilizados para diagnosticar el plasma más de 80 años después de su invención [3]. Las ventajas principales frente a la espectroscopia de plasmas luminiscentes es que es relativamente sencilla de construir y proporciona información local de la región del plasma donde se coloca, permitiendo el estudio de la descarga completa en relación a la posición de ánodo y cátodo. Como desventaja, la sonda interactúa de forma eléctrica con el plasma, por lo que sólo puede obtener el flujo neto de carga y no es capaz de discriminar especies químicas con distintas cargas o masas. Para poder obtener toda la información sobre cada una de las corrientes eléctricas generadas por cada especie química es necesario desarrollar teorías sobre el movimiento de cada especie, agregar todas las corrientes presentes y compararlo con la corriente total, además de con otros métodos de medida, lo que permite dar validez a dichas teorías. Una vez se conoce el comportamiento de cada especie química, se puede utilizar el plasma en aplicaciones industriales y relacionar

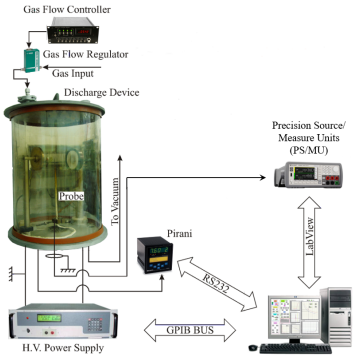

Fig. 1. Esquema del dispositivo experimental

las características del plasma con los efectos producidos en dichas aplicaciones (cantidad y ritmo de implantación iónica, potencia y cualidad lumínica, tiempo de esterilización, etc). Es interesante observar que las diferentes especies químicas componentes del plasma pueden ser modeladas correctamente con distintas teorías: En algunos casos una especie química se podrá considerar como un gas en equilibrio, mientras que en otros caso es necesario modelarlo como un fluido, o mediante una función de densidad que se rige por la ecuación de Boltzmann.

II. Dispositivo experimental

El dispositivo se muestra esquematizado en la figura 1. El plasma es generado en una campana de vacío de Pirex cilíndrica de 40 cm de altura y 31 cm de diámetro interior. En la parte superior tiene la entrada del circuito de gas por donde se inyecta el gas estudiado. En nuestro caso usamos Argon, Neón y Helio, que son gases nobles con actividad química casi nula, lo que crea plasmas con una composición sencilla de especies químicas. Además, el Argon es especialmente importante por que se usa a menudo como medio auxiliar en descargas con compuestos con mayor actividad química, para controlar y estabilizar la descarga. El flujo de gas es controlado mediante cuatro reguladores de flujo másico de gas MKS, modelo 179A. Los reguladores tienen un caudal de 10, 20, 50 y 100 sccm (Standard Cubic Centimeter per Minute). Para alcanzar las presiones de trabajo con Argon, Neón y Helio es necesario usar los dos primeros, el tercero y el cuarto respectivamente, dado que la diferente masa atómica de los gases hace que sea necesario un flujo mayor de masa para alcanzar la misma presión. Los reguladores de flujo másico están controlados mediante un controlador MKS modelo 247. Con este controlador se pueden controlar los cuatro reguladores simultáneamente, de forma que es posible conseguir la mezcla de gases que se desee.

En la parte inferior de la campana se encuentra la salida de gas, que es extraído mediante una bomba de vacío rotatoria de dos etapas de Varian, modelo DS 402, que es capaz de aspirar $17.4\ \mathrm{m}^3/\mathrm{min}$ y de mantener un vacío con una presión inferior a $10^{-7}\mathrm{atm}$ o 0.01 Pa, más de cuatro ordenes de magnitud de lo necesario para poder tener un plasma estable. El motor consume una potencia de 0.75 kW y tiene una frecuencia de rotación de 1500 rpm. Se ha incorporado una trampa de zeolita en la linea de escape para minimizar el aceite que puede retornar desde la bomba a la campana y que se incorporaría a la descarga de plasma. La presión es controlada mediante un manómetro Pirani MKS, modelo PDR900.

Dentro de la campana tenemos dos electrodos circulares de acero inoxidable de 8 cm de diámetro, a una altura de 25 cm entre base de la campana y centro de los discos, separados 15 cm entre si y estableciendo un volumen cilíndrico entre ellos, que es donde se va a concentrar la descarga generadora del plasma luminiscente. Los electrodos se conectan a una fuente de alimentación de bajo ruido KEPCO BHK 2000-0.1MG, que puede ser controlado por tensión o por corriente y que puede mantener el valor estable con un rizado garantizado menor a 0.1 V y 0.1 mA. Puede generar hasta 2000 V y 100 mA.

En la zona en la que el plasma es generado se coloca la sonda de Langmuir, que es un cilindro de Tungsteno de 0.1 mm de radio y 6.0 mm de longitud. El Tungsteno se elige por que tiene muy baja emisión de electrones cuando los iones colisionan con la sonda para capturar un electrón del metal (emisión secundaria). El soporte de la sonda debe ser diseñado cuidadosamente para no perturbar excesivamente el plasma que rodea la sonda [4], [5]. La tensión de la sonda es impuesta por una unidad de medida/generación de precisión (PS/MU) de Agilent, modelo B2901A, que es capaz de imponer la tensión deseada y de medir la corriente que drena, de manera que podemos medir la característica I-V de la sonda inmersa en el plasma. La unidad Agilent puede medir muestras cada $20\ \mu$s, por lo que la característica completa de 4000 puntos se mide en 80 ms, tiempo suficientemente rápido como para que la sonda no varíe su temperatura en dicho intervalo de tiempo, de forma que las propiedades físicas de extracción de electrones (su función trabajo), que es muy sensible a la temperatura, sea constante a lo largo de la medida.

Todo el sistema está controlado de forma automatizada mediante un instrumento virtual programado en LabView instalado en un ordenador PC provisto de entradas USB, RS-232 y IEEE 488.2. Permite automatizar las características de la descarga generada por la fuente de alta tensión KEPCO y la medida de la característica I-V mediante la unidad PS/MU de Agilent de forma sencilla mediante el puerto IEEE 488.2, y la medida de presión del Pirani mediante el puerto RS-232. El resto de los datos, temperatura ambiente, composición química del gas, etc. se deben introducir manualmente. Los resultados teóricos de los modelos más importantes de sondas de Langmuir están programados en el instrumento virtual, de forma que se puede comprobar el grado de coincidencia de los modelos con las medidas y por lo tanto se puede definir el rango de validez de las hipótesis de cada uno de los modelos.

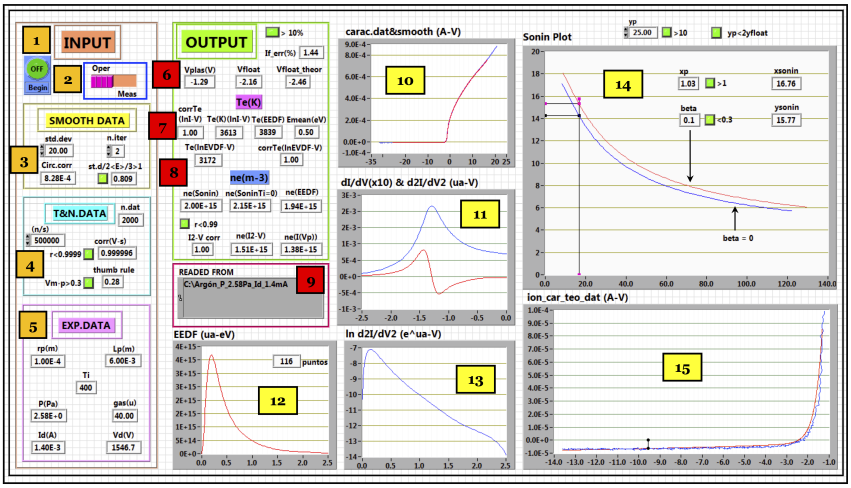

Fig. 2. Visualización de controles del instrumento virtual en LabView

III. Medidas experimentales

Con el dispositivo experimental descrito en la sección II se han realizado descargas de plasma y se han medido las magnitudes físicas características del plasma. La presión de trabajo se encuentra entre 2 Pa y 36 Pa. La presión inferior está limitada por la potencial de la fuente de alimentación. A menor presión, y por lo tanto, a menor cantidad de gas, mayor tensión interelectródica es necesaria para superar el umbral necesario para generar el plasma: antes de generar la descarga, el espacio interelectródico es un dieléctrico en el que hay que provocar la ruptura del aislamiento eléctrico, de forma similar a la descarga de un relámpago en la tierra. De hecho, el límite superior de presión está limitado por la estabilidad de la descarga. A mayor cantidad de gas en la campana, empiezan a formarse caminos preferentes para la corriente creando un plasma inestable e inhomogéneo, y si la presión fuera suficientemente elevada, se formaría un arco eléctrico entre los electrodos.

Las corrientes de descarga varian desde 1.0 mA hasta los 3.5 mA aproximadamente para las descargas a menor presión y desde 1.5 mA hasta los 10.0 mA para las descargas a mayor presión. El límite inferior esta dado por la presencia de plasma y por el rizado de corriente de la fuente de alta tensión. A menor corriente, la densidad de las especies del plasma es menor y el plasma puede llegar a ser demasiado tenue como para poder ser de utilidad. Y si el rizado es importante, las magnitudes físicas del plasma son cambiantes, invalidando la aplicación de ningún modelo. El límite inferior de corriente corresponde con 400-600 V. El límite superior está dado por la tensión máxima de la fuente, de 2000 V. El rizado en tensión, de 0.1 V, es menos importante que el rizado de corriente.

La unidad PS/MU de Agilent puede registrar medidas simultáneas de tensión y corriente con unas incertidumbres de 0.1 μV y de 1 pA, con un rango en tensión de [-20V, 10V]. La característica I-V de la sonda de Langmuir inmersa en el plasma varia desde casi 1 mA de corriente saliente a la sonda cuando los portadores principales de carga son los electrones (zona electrónica), hasta 10 μA de corriente entrante cuando los portadores principales son los iones positivos (zona iónica), que es el regimen en que los modelos funcionan peor y existe más interés científico en la actualidad [6]. La corriente más problemática es por tanto la segunda, en la que la relación señal ruido debida a la unidad PS/MU de Agilent es muy buena, mucho mayor que la relación señal/ruido inherente del plasma que puede ser de hasta 20 dB, es decir, un ruido en torno a 1 μA sobre una señal de 10 μA.

En la figura 2 se muestra la visualización de controles de LabView, en la que se pueden introducir los datos necesarios y se opera el dispositivo experimental automatizado. En el gráfico, las diferentes subsecciones están indicadas:

1) Botón de inicio de operación automatizada.
2) Interruptor de selección entre operación del dispositivo experimental o carga de fichero con una medida previa.
3) Características del filtrado para eliminación de ruido [2].
4) Características del muestreo.
5) Datos de la campana de vacío: Algunos datos son leídos desde la fuente de alta tensión KEPCO o del manómetro Pirani, y otros datos son para establecer el gas o la temperatura ambiente.
6) Potenciales eléctricos relevantes de la característica I-V.
7) Valores de temperatura de los electrones del plasma interpretadas de la característica I-V.
8) Valores de densidad de los electrones del plasma inter-

pretadas de la característica I-V.
9) Nombre y ruta del fichero de lectura/escritura.
10) Característica I-V medida y filtrada.
11) Derivadas 1ª y 2ª de la característica I-V, para obtener la Función de Densidad de Energía Electrónica [7], [8],
12) Función de Densidad de Energía Electrónica.
13) Logaritmo de la Función de Densidad de Energía Electrónica.
14) Sonin Plot, de utilidad para medir la densidad de electrones del plasma, considerando temperatura de iones despreciable y no despreciable.
15) Zona ampliada y filtrada para eliminación de ruido de la característica I-V en que los portadores principales son los iones positivos.

La medida se realiza, tal y como se ha calculado previamente, en 80 ms, y los cálculos del instrumento virtual en LabView se realizan en menos de un segundo, por lo que se puede tener información del plasma prácticamente en tiempo real, y ver de forma dinámica cómo varian las magnitudes del plasma cuando varían las condiciones.

A. Teorías importantes

Es interesante destacar que las teorías válidas en la zona electrónica se pueden resolver de forma que los resultados quedan expresados como una ecuación cerrada. Los electrones, cuando la sonda presenta un potencial positivo con respecto al potencial al que se encuentra el plasma envolvente, son atraídos hacia la sonda, pero dado que en el plasma se encuentran desplazándose aleatoriamente en todas direcciones, algunos electrones alcanzan la sonda, mientras que otros orbitan alrededor de ella de la misma forma que un cometa alrededor del sol. Así, la corriente saliente de la sonda debida a los electrones se puede integrar y resulta ser para una sonda cilíndrica de radio r_p y longitud L_p [3]:

$$I_e = e2r_pL_pn_e\sqrt{\frac{k_BT_e}{2m_e}}\left(1+\frac{e\phi_p}{k_BT_e}\right)^{\frac{1}{2}}$$

Donde n_e, T_e, k_B, m_e, e y ϕ_p son la densidad y la temperatura de los electrones, la constante de Boltzmann, la masa y la carga del electrón y el potencial de la sonda respectivamente. Los iones por otra parte, dependiendo de su masa y de la densidad de iones en el plasma, pueden orbitar la sonda de la misma manera que los electrones (aunque a menor velocidad) [10], [11], o pueden caer en la misma dirección hacia la sonda, como el agua de lluvia [9]. Sin embargo, las teorías de la zona iónica ofrecen resultados que requieren la solución numérica de un sistema de ecuaciones diferenciales ordinarias acopladas, que requieren más tiempo en general para obtener resultados numéricamente precisos. Por esto, se ha realizado un ajuste numérico de los resultados en base a los parámetros de interés en el rango de valores que suele aparecer en nuestros plasmas, con lo que la corriente debida a los iones en la zona iónica se puede obtener en un tiempo igualmente muy corto.

IV. Resultados

El resultado principal de la medida es la característica I-V del plasma, medida de la que mostramos un ejemplo en la figura 3. En ella se indican los valores de potencial de la sondas importantes que tiene la característica. El potencial del plasma es el potencial al que se encuentra el plasma envolvente, es decir, que entre la sonda y el plasma no hay diferencia de potencial. Observamos que la corriente saliente de la sonda no es 0, debido a que los electrones tienen mayor movilidad y alcanzan la sonda con más facilidad que los iones. El potencial flotante es el potencial al que la corriente neta es nula, que es muy fácil de medir pero muy difícil de predecir teóricamente. El esfuerzo en física teórica en física de plasmas se dedica en gran parte a entender el comportamiento de los iones y en predecir esta corriente, ya que es la que tiene más importantes aplicaciones tecnológicas.

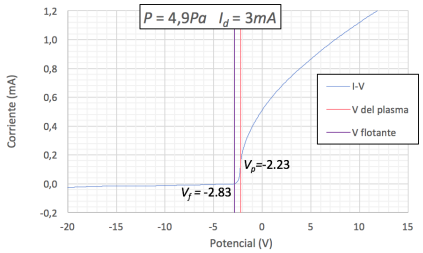

Fig. 3. Ejemplo de característica IV para corriente de descarga 3 mA y presión 4.9 Pa.

Gracias al instrumento virtual de LabView que controla el dispositivo experimental se pueden realizar medidas automatizadas de forma rápida sobre los parámetros más importantes de un plasma luminiscente. Con este sistema automatizado, un científico puede obtener varias series de datos en el intervalo de unas pocas horas sin necesidad de procesar los datos posteriormente, con lo que sólo queda interpretar los resultados y presentarlos en gráficas, etc. Por ejemplo, la figura 4 muestra 4 series de datos a distintas presiones con los resultados de densidad electrónica, según tres métodos teóricos distintos, a medida que se varía la corriente de la descarga generadora del plasma luminiscente. Si aumenta la corriente de descarga, aumenta la cantidad de iones y electrones generados en el plasma, lo que se comprueba en todas las series. Vemos que las tres teorías, la que utiliza la función de distribución de energía electrónica (EEDF), la que utiliza la zona electrónica (I2-V) y la que utiliza la corriente medida cuando la sonda se polariza al mismo potencial al que se encuentra el plasma envolvente (I(Vp)), ofrecen los mismos valores en un rango, pero valores distintos en otro. En este caso, la causa de las diferencias es que la medida de la función de distribución de energía electrónica se mide con pocos puntos (sólo en torno a 100 puntos de la característica I-V sirven para obtenerla), lo que es poco para esta medida [5], mientras que la corriente cuando

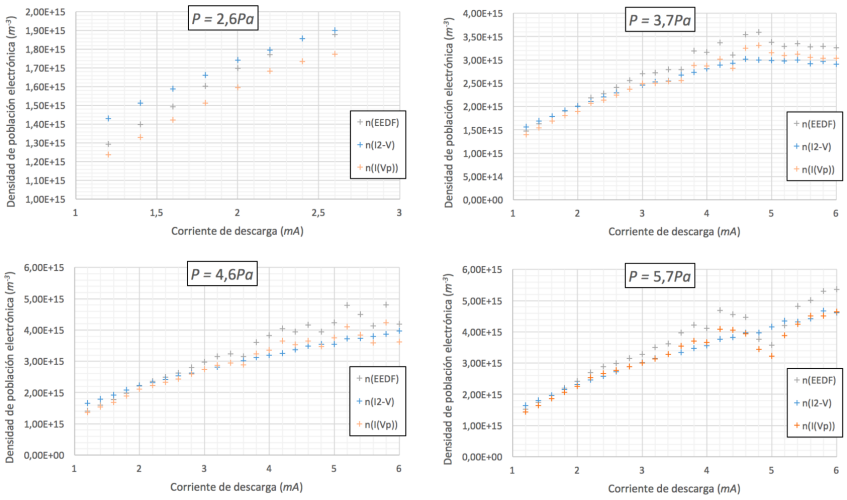

Fig. 4. Medida de la densidad de electrones con respecto a la corriente de descarga para presión 2.6 Pa, 3.7 Pa, 4.6 Pa y 5.7 Pa.

la sonda está polarizada al mismo potencial del plasma supone que todos los electrones tienen la misma temperatura, aunque en muchos plasmas se encuentran dos tipos de electrones con distintas temperaturas (EEDF bi-maxwelliana) [12], [13], [14], [15], [16]. La medida más fiable se considera la de la zona electrónica, aunque tiene la desventaja de que drena mucha corriente del plasma y por lo tanto puede causar una disminución de la población de electrones del plasma. Es decir, que esta medida perturba el plasma en mayor medida.

V. Conclusión

En esta contribución se presenta un dispositivo de medida automatizada mediante un instrumento virtual de LabView con el que podemos realizar medidas de las magnitudes físicas importantes de un plasma de forma sencilla y rápida. LabView ha resultado ser un entorno de programación perfecto para instrumentación automatizada de dispositivos de medida de las magnitudes físicas de un plasma luminiscente. El esfuerzo dedicado a desarrollar el sistema se ve compensado con la rapidez con la que se pueden tomar series de datos, de forma que el trabajo del científico se puede invertir en la interpretación de los resultados más que en el tratamiento de los datos. Permite enfocar la atención en la física de lo que está ocurriendo en el plasma, en particular a las magnitudes de interés, la densidad de iones y electrones, y la temperatura de iones y electrones. Con el conocimiento de estas magnitudes, sabiendo qué resultados dan las distintas teorías, con el conocimiento de las teorías, se puede entender con precisión la forma en que caen los iones y los electrones hacia una superficie metálica polarizada. Desde el punto de vista de la aplicación industrial, la obtención rápida de estos resultados permite realizar los ajustes necesarios para obtener un plasma de las características deseadas para la aplicación tecnológica en la que se quiera utilizar el plasma.

References

[1] J. Swift and M. Schwar, *Electrical Probes for Plasma Diagnosis*. London, United Kingdom: Iliffe Books Ltd., 1970.

[2] E. Stamate, "Status and challenges in electrical diagnostics of processing plasmas," *Surf. Coat. Technol.*, vol. 260, pp. 401–410, Dec. 2014. [Online]. Available: http://linkinghub.elsevier.com/retrieve/pii/S0257897214009086

[3] H. M. Mott-Smith and I. Langmuir, "The Theory of Collectors in Gaseous Discharges," *Phys. Rev.*, vol. 28, no. 4, pp. 727–763, 1926. [Online]. Available: https://journals.aps.org/pr/abstract/10.1103/PhysRev.28.727

[4] V. A. Godyak, R. B. Piejak, and B. M. Alexandrovich, "Electron energy distribution function measurements and plasma parameters in inductively coupled argon plasma," *Plasma Sources Sci. Technol.*, vol. 11, no. 4, pp. 525–543, Nov. 2002. [Online]. Available: http://stacks.iop.org/0963-0252/11/i=4/a=320?key=crossref.a8168d151a959a3b9a590332d47c7ede

[5] V. A. Godyak, "Measuring EEDF in gas plasma discharges," in *Plasma-Surface Interactions and Processing of Materials*, ser. E: Applied Sciences. Dordrecht, The Netherlands: Kluwer Scademic Publishers, 1990, vol. 176, pp. 95–134.

[6] T. K. Popov, M. Dimitrova, P. Ivanova, J. Kovačič, T. Gyergyek, R. Dejarnac, J. Stöckel, M. A. Pedrosa, D. López-Bruna, and C. Hidalgo, "Advances in Langmuir probe diagnostics of the plasma potential and electron-energy distribution function in magnetized plasma," *Plasma Sources Sci. Technol.*, vol. 25, no. 3, p. 033001, Jun. 2016. [Online]. Available: http://stacks.iop.org/0963-0252/25/i=3/a=033001?key=crossref.88afe59ce51c1567040b3a8c1d462e05

[7] M. J. Druyvesteyn, "Der Niedervoltbogen," *Z. Phys*, vol. 64, no. 11-12, pp. 781–798, Sep. 1930. [Online]. Available: http://link.springer.com/10.1007/BF01773007

[8] Y. M. Kagan and V. I. Perel, "Probe methods in plasma research," *Sov. Phys.—Usp*, vol. 6, no. 6, p. 767, 1964. [Online]. Available: http://dx.doi.org/10.1070/PU1964v006n06ABEH003611

[9] J. E. Allen, R. L. F. Boyd, and P. Reynolds, "The Collection of Positive Ions by a Probe Immersed in a Plasma," *Proc. Phys. Soc.*, vol. 70, pp. 297–304, 1957. [Online]. Available: http://iopscience.iop.org/article/10.1088/0370-1301/70/3/303/meta

[10] I. B. Bernstein and I. N. Rabinowitz, "Theory of Electrostatic Probes in Low-Density Plasma," *Phys. Fluids*, vol. 2, no. 2, p. 112, 1959. [Online]. Available: http://dx.doi.org/10.1063/1.1705900

[11] J. G. Laframboise, "Theory of spherical and cylindrical Langmuir probes in a collisionless, Maxwellian plasma at rest," TORONTO UNIV DOWNSVIEW (ONTARIO) INST FOR AEROSPACE STUDIES, Tech. Rep., 1966. [Online]. Available: http://www.dtic.mil/docs/citations/AD0634596

[12] M. S. Barnes, J. C. Forster, and J. H. Keller, "Electron energy distribution function measurements in a planar inductive oxygen radio frequency glow discharge," *Appl. Phys. Lett.*, vol. 62, no. 21, pp. 2622–2624, May 1993. [Online]. Available: http://aip.scitation.org/doi/10.1063/1.109265

[13] C. Chung, "Experimental investigation on the floating potential of cylindrical Langmuir probes in non-Maxwellian electron distributions," *Phys. Plasmas*, vol. 12, no. 12, p. 123505, Dec. 2005. [Online]. Available: http://aip.scitation.org/doi/10.1063/1.2135280

[14] D. Gahan, B. Dolinaj, and M. B. Hopkins, "Comparison of plasma parameters determined with a Langmuir probe and with a retarding field energy analyzer," *Plasma Sources Sci. Technol.*, vol. 17, no. 3, p. 035026, Aug. 2008. [Online]. Available: http://stacks.iop.org/0963-0252/17/i=3/a=035026?key=crossref.4fab76e1556318c6643cb41fde261488

[15] V. A. Godyak and R. B. Piejak, "Abnormally low electron energy and heating-mode transition in a low-pressure argon rf discharge at 13.56 MHz," *Phys. Rev. Lett.*, vol. 65, no. 8, pp. 996–999, Aug. 1990. [Online]. Available: https://link.aps.org/doi/10.1103/PhysRevLett.65.996

[16] B. B. Sahu, J. G. Han, H. R. Kim, K. Ishikawa, and M. Hori, "Experimental evidence of warm electron populations in magnetron sputtering plasmas," *J. Appl. Phys.*, vol. 117, no. 3, p. 033301, Jan. 2015. [Online]. Available: http://aip.scitation.org/doi/10.1063/1.4905901

Sistema de control de la medida de la característica I-V en un plasma luminiscente

Guillermo Fernando Regodón Harkness
José Ignacio Fernández Palop
Juan Manuel Díaz Cabrera
Jerónimo Ballesteros Pastor

Departamento de Física

Física de plasmas

- Plasma
  - Gas (comportamiento colectivo) -> Termodinámica
  - Partículas con carga eléctrica -> Electromagnetismo
  - Quasineutro -> Carga neta casi nula

Ejemplo de Plasma: El Sol

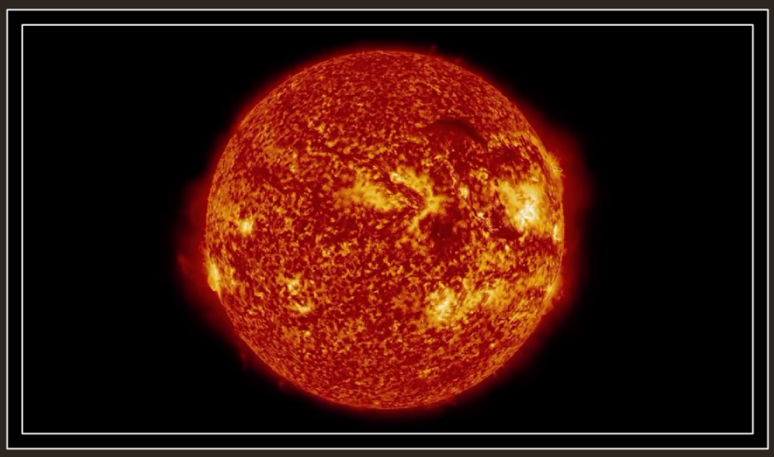

Aplicaciones tecnológicas

- En laboratorios donde se crean plasmas por descargas eléctricas o radiofrecuencia
- Implantación de iones

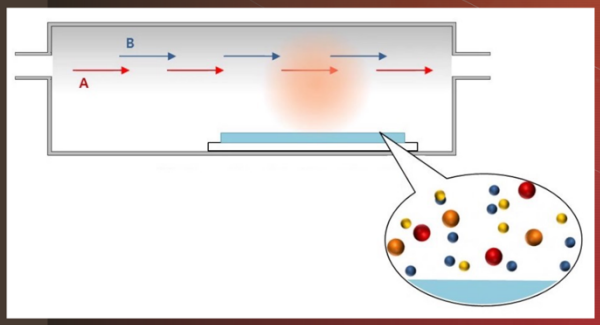

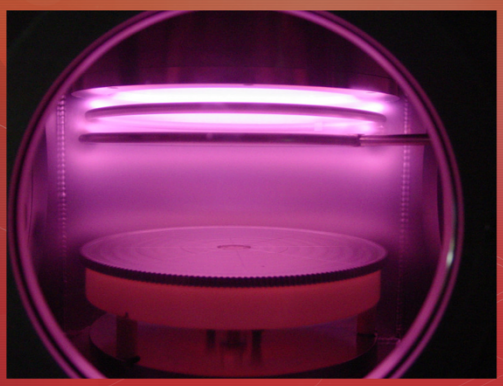

Aplicaciones tecnológicas

- Modificar las propiedades físico-químicas de la superficie
- Dificultad -> Controlar la energía con la que los iones chocan contra la superficie

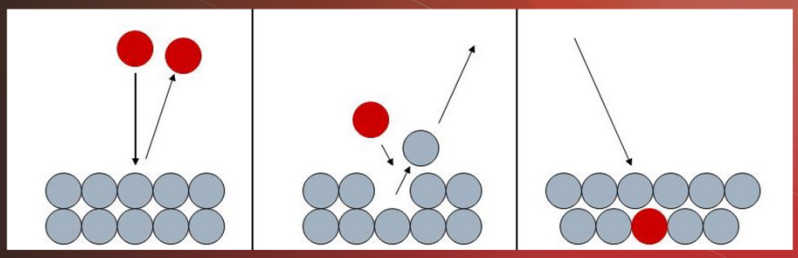

La sonda de Langmuir

- Es una estructura metálica de referencia
  - Geometría sencilla -> Un cilindro, una esfera o un plano
- Muy estudiado

Controlar y diagnosticar el plasma

Explicar la forma en que los iones llegan al metal

El dispositivo experimental

- Circuito de gas
  - Bomba de vacio: P<0.01Pa
  - Regulador de flujo
- Circuito de descarga
  - Fuente de alimentación de alta tensión y bajo rizado
  - Dos electrodos circulares
- Circuito de señal
  - Sonda de Langmuir
  - Precision Source/Measuring Unit
- PC con Labview

El dispositivo experimental

- Dos electrodos circulares de 8 cm de diámetro, separados 15 cm
  - Tensión interelectródica de ~1000 V
- La sonda se coloca en la zona donde el plasma es más homogéneo
  - Es la posición donde se colocaría la muestra a tratar
- La unidad PS/MU impone tensión y mide la corriente recogida por la sonda
  - Frecuencia de muestreo de 50 Khz
  - 4000 puntos (I,V) en 80 ms
- La referencia de tierra es de muy buena calidad

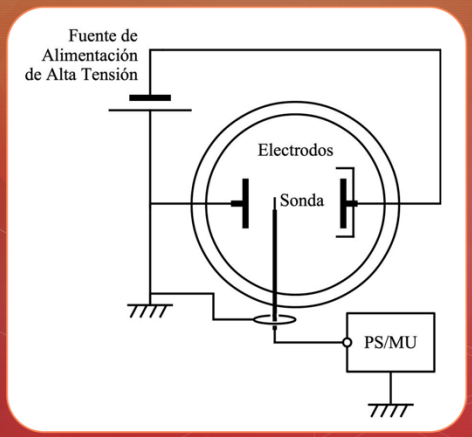

La característica corriente-tensión de la sonda de Langmuir

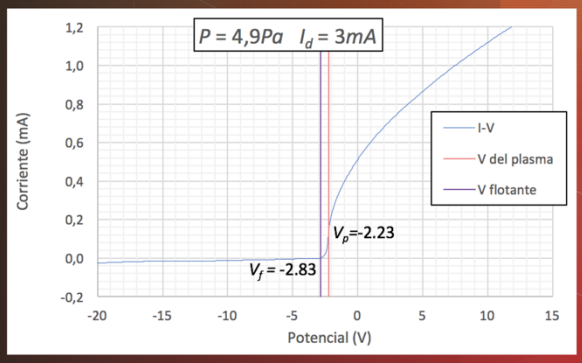

- Potencial del plasma V_p<0 V
- Polarización positiva
  - La sonda recoge exclusivamente electrones
- Polarización negativa
  - Principalmente iones, y unos pocos electrones
- Potencial flotante
  - Corriente neta nula
  - Difícil de calcular teóricamente

Labview

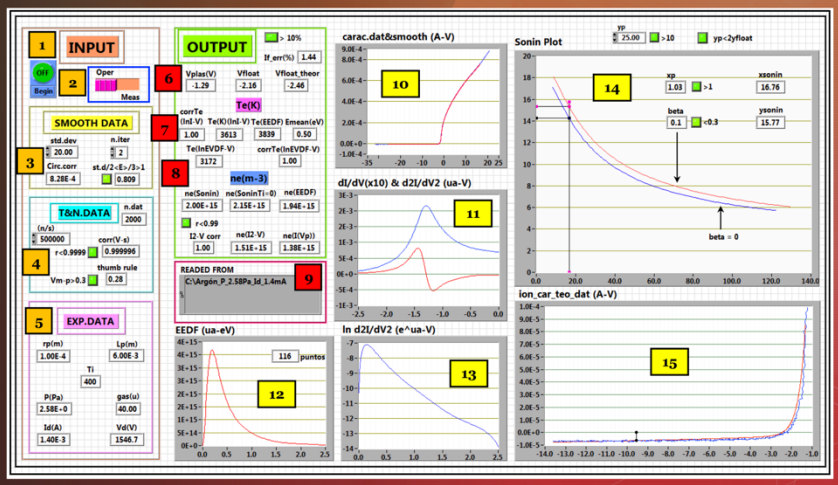

La física condiciona el diseño

- La sonda es de tungsteno, por que tiene muy baja emisión de electrones
  - La función trabajo depende de la temperatura -> Medidas muy rápidas
- El plasma es un sistema inherentemente ruidoso
  - Filtrado o suavizado de los datos
- Origen de los electrones: dos poblaciones de electrones con distinta temperatura
  - Medidas en los rangos en los que una población de electrones es despreciable
- El plasma es un entorno químicamente muy activo
  - Composición del plasma depende de presión, corriente interelectródica, composición y temperatura del gas neutro...
  - Se suelen usar gases nobles, principalmente Argon, para controlar la descarga
- Para la corriente iónica, la física plantea sistemas EDO de solución numérica lenta
  - Ajuste numérico para obtener expresiones aproximadas

Resultados rápidos

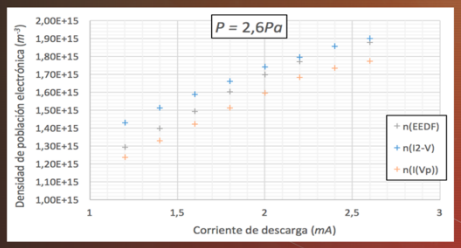

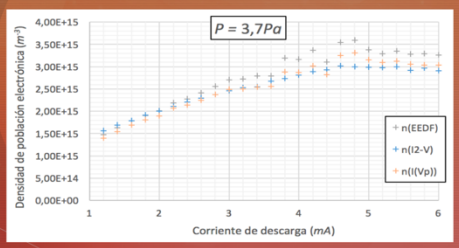

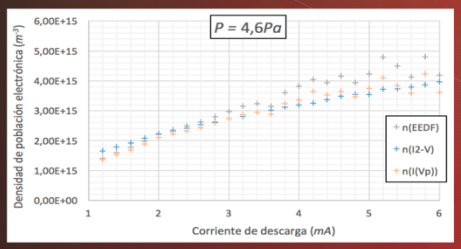

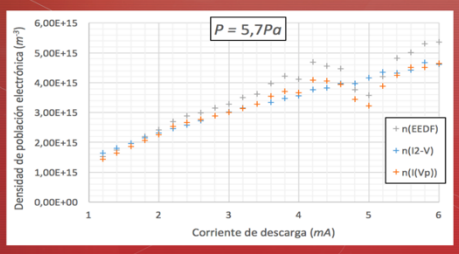

6 Conclusiones

Durante el desarrollo de esta tesis se han conseguido varios hitos relacionados con la diagnosis de plasmas fríos mediante la utilización de modelos radiales de fluidos.

- Se ha desarrollado una metodología para resolver, por primera vez y de forma numérica, las ecuaciones planteadas por Fernández Palop en el año 96 [11] para modelar la corriente iónica recogida por una sonda electrostática de Langmuir cilíndrica inmersa en un plasma electropositivo que tiene en cuenta el valor finito de la temperatura de los iones positivos. La solución se ha basado en el tratamiento de la singularidad [103] que aparece en las ecuaciones cuando el fluido de iones alcanza la velocidad del sonido [18]. Un trabajo preliminar se llevó como contribución en forma de póster al congreso ICPIG2017 celebrado en Lisboa.
- Se ha generalizado la metodología desarrollada para modelar plasmas electronegativos en los que hay una población de iones positivos, una población de electrones y una población de iones negativos de cualquier masa, y se han obtenido gráficas útiles en los laboratorios de plasma en los que es necesario tener en cuenta la presencia de una segunda población de partículas de carga negativa. En particular, se ha calculado el potencial flotante, de gran importancia práctica, en función del grado de electronegatividad y de la temperatura de los iones negativos en comparación con la temperatura de los electrones [19].
- Se han realizado medidas en el laboratorio de plasma en una descarga DC de plasma de neón y de argón para comprobar la validez del modelo desarrollado para la corriente iónica en presencia de dos poblaciones de electrones de distinta temperatura, y se ha comprobado que el modelo es capaz de predecir el potencial flotante mejor que el modelo que incluye solo una población de electrones [21].
- Se ha generalizado la metodología desarrollada para introducir el efecto de las colisiones de intercambio de carga o C-E entre los iones positivos y los átomos neutros del plasma. De esta forma, se ha conseguido una solución general que permite tener en cuenta tanto las colisiones de intercambio de carga como la temperatura de los iones en el caso de recorrido libre medio constante. Se ha demostrado que el efecto de ambos en los modelos radiales es opuesto, lo que explica la dificultad para estudiar experimentalmente el efecto aislado de los dos [20].

- Se han realizado una serie de medidas enmarcadas en el objetivo del grupo de investigación TEP-230 Contacto plasma-superficie de estudiar la transición entre validez de los modelos radiales a validez de los modelos orbitales encontrada en un plasma de helio. Se ha analizado la transición en función del cociente entre la temperatura de los iones y la temperatura de los electrones, y en función del cociente entre el recorrido libre medio de colisión de tipo intercambio de carga o C-E y la longitud de Debye [16,17]. Se ha demostrado que ninguno de los dos puede ser el parámetro que permite que la transición se observe tan solo en el plasma de helio, y que la masa del ion debe ser el parámetro que diferencia el plasma de helio de los plasmas de neón y argón estudiados y que permite la aparición de la transición.
- Se ha propuesto una metodología para estimar la población de iones negativos en un plasma electronegativo mediante la medición del potencial flotante, y que se ha llevado como una contribución en forma de póster al congreso ESCAMPIG2018 celebrado en Glasgow.
- Se ha mejorado el rendimiento de las simulaciones PIC desarrolladas en el grupo de investigación TEP-230 Contacto plasma-superficie para simular la interacción entre un plasma y una superficie metálica. Asimismo, se han introducido las colisiones de tipo intercambio de carga o C-E y la ionización. La pre-vaina de colisiones calculada por Riemann [37] ha podido ser obtenida en las simulaciones, dando validez a la simulación, y los resultados de esta comparativa entre teoría y simulaciones se ha llevado como contribución en forma de póster al congreso ESCAMPIG2018 celebrado en Glasgow.
- Se han realizado algunas mejoras sobre el instrumento virtual en LabView que controla todo el proceso de medida en la descarga DC del grupo de investigación TEP-230 Contacto plasma-superficie. Una exposición del dispositivo de medida completo, incluyendo la automatización en LabView y sus aplicaciones, se llevó como contribución oral al congreso SAAEI2019 celebrado en Córdoba.

7 Resúmenes

El modelo de fluidos propuesto por Fernández Palop *et al.* (Fernández Palop J I *et al.* 1996 *J. Phys. D: Appl. Phys.* **29** 2832–40) para modelar la vaina electronegativa de una sonda electrostática de Langmuir cilíndrica inmersa en un plasma electropositivo que incluye el efecto de la temperatura de los iones no nula ha sido resuelto de forma exacta estudiando la singularidad que aparece en las ecuaciones de fluidos cuando los iones alcanzan la velocidad local del sonido en el movimiento del fluido de iones en su caída hacia la sonda polarizada negativamente con respecto al plasma. Este avance permite establecer el límite de validez de las teorías radiales cuando se enfrentan los resultados de dicho modelo a las medidas experimentales realizadas en el laboratorio de plasma. Además, la solución propuesta se ha utilizado y se ha generalizado a dos casos importantes desde el punto de vista teórico y práctico: la sonda electrostática de Langmuir inmersa en un plasma electronegativo y la sonda electrostática de Langmuir inmersa en un plasma electropositivo con colisiones de tipo intercambio de carga o C-E en el que el recorrido libre medio de los iones positivos es comparable con las dimensiones de la vaina. Para la generalización realizada para el caso de un plasma electronegativo sin colisiones, se ha calculado el potencial flotante, de gran importancia práctica ya que es el potencial al que se polariza una superficie metálica eléctricamente aislada con respecto al potencial del plasma. Los cálculos realizados se han aplicado en la predicción del potencial flotante en medidas experimentales en el caso del plasma más sencillo en el que se puede encontrar una sola especie positiva y dos especies negativas, que es un plasma electropositivo en el que la población de electrones se puede descomponer en dos poblaciones de electrones de distintas temperaturas, o lo que es lo mismo, puede ser caracterizada mediante una función de distribución de energía de los electrones o EEDF bi-maxwelliana. Los resultados demuestran que dicho modelo predice correctamente el potencial flotante mientras que el modelo con una única población de electrones no coincide en el caso de que las dos poblaciones de electrones son comparables. Esto quiere decir que la población de electrones bi-maxwelliana en general no puede ser sustituida por una población equivalente con una temperatura y una densidad efectivas. En el caso del plasma en el que el recorrido libre medio es comparable con la escala de la vaina, debido a las dificultades de estabilidad numérica la

solución se ha planteado teóricamente y se ha resuelto para el caso de plasmas en los que las colisiones están presentes pero no son predominantes. En este caso, los resultados teóricos obtenidos y una serie de medidas experimentales en el laboratorio de plasma han permitido establecer que la transición entre validez de las teorías radiales y validez de las teorías orbitales viene determinada por la masa del ion y que el efecto de la temperatura del ion es predominante frente al efecto de las colisiones en la transición encontrada en un plasma de helio. Para facilitar la aplicación de los resultados en medidas experimentales en laboratorios de plasma, se ha obtenido el Sonin Plot en todos los casos y los límites de aplicabilidad de los resultados se han establecido claramente. Se ha encontrado que en los modelos radiales el efecto de las colisiones de intercambio de carga es opuesto al efecto de la temperatura de los iones y se ha cuantificado la medida en que ambos efectos se cancelan. Este hecho puede explicar y justificar por qué es muy difícil realizar medidas experimentales en los que se aíslen los efectos tanto de las colisiones de intercambio de carga con los átomos neutros como de la temperatura de los iones.

The fluid model proposed by Fernández Palop *et al.* (Fernández Palop J I *et al.* 1996 *J. Phys. D: Appl. Phys.* **29** 2832–40) to model the electronegative sheath around a cylindrical Langmuir probe immersed in an electropositive plasma that includes the effect of the non-null ion temperature has been solved exactly studying the singularity that fluid equations have when the ions reach the local speed of sound in the movement of the ion fluid in their fall towards the probe negatively polarised with respect to the plasma. This advance allows to establish the limit of validity of the radial theories when the results from these models are compared to the experimental measurements that are performed in the plasma laboratory. Moreover, the proposed methodology has been used and it has been generalised to two important cases from both theoretical and applied points of view: The Langmuir probe immersed in an electronegative plasma and the Langmuir probe immersed in an electropositive plasma with Charge-Exchange collisions, or C-E collisions, in which the ion mean free path is of the same scale as the sheath thickness. For the generalisation to the case of a collisionless electronegative plasma, the floating potential, of great practical importance, has been calculated, that is, the potential that a metallic surface reaches with respect to the plasma when it is electrically isolated when immersed in the plasma. The produced calculations have been applied to predict the floating potential in experimental measurements to the simplest case of a plasma with one positive species and two negative species, that is, an electropositive plasma in which an electron population that can be decomposed into two different electron populations of different temperatures, or equivalently, that can be characterised by a bi-maxwellian Electron Energy Distribution Function or EEDF. The results show that such a model correctly predicts the floating potential while the model with only one electron population does not correctly predicts the floating potential in the case when both electron population densities are comparable. This means that the bi-maxwellian electron population cannot be, in general, substituted by a single equivalent electron population with one effective electron temperature and electron population density. In the case when the ion mean free path is comparable to the sheath thickness, due to the numerical difficulties, the solution has been investigated theoretically and it has been solved in the case when the collisions are not predominant. In this case, the theoretical results and a series of experimental measurements in the plasma laboratory allowed to prove that the transition between the validity of radial theories to the validity of orbital theories in determined by the ion mass and that the effect of the ion temperature is predominant when compared to the effect of collisions in the transition that was

observed in a Helium plasma. In order to facilitate the application of the results in the plasma laboratory, the Sonin plot was obtained in all cases and the limits of applicability of the results have been clearly established. It was found that in the radial models, the effect of Charge-Exchange collisions is the contrary of the effect of the ion temperature and the cancellation between both effects have been quantified. This fact can explain why it is very difficult to produce experimental measurements in which both the effect of Charge-Exchange collisions with the neutral atoms and the effect of the ion temperature are isolated.

8 Informes de cuartil

8.1 Physics of Plasmas 2017

Clarivate Analytics

2017 Journal Performance Data for: PHYSICS OF PLASMAS

ISSN: 1070-664X
eISSN: 1089-7674
AMER INST PHYSICS
1305 WALT WHITMAN RD, STE 300, MELVILLE, NY 11747-4501
USA

TITLES
ISO: Phys. Plasmas
JCR Abbrev: PHYS PLASMAS

LANGUAGES
English

CATEGORIES
PHYSICS, FLUIDS & PLASMAS -- SCIE

PUBLICATION FREQUENCY
12 issues/year

The data in the two graphs below and in the Journal Impact Factor calculation panels represent citation activity in 2017 to items published in the journal in the prior two years. They detail the components of the Journal Impact Factor. Use the "All Years" tab to access key metrics and additional data for the current year and all prior years for this journal.

2017 Journal Impact Factor & percentile rank in category for: PHYSICS OF PLASMAS

1.941
2017 Journal Impact Factor

2017 JIF Citation Distribution for: PHYSICS OF PLASMAS

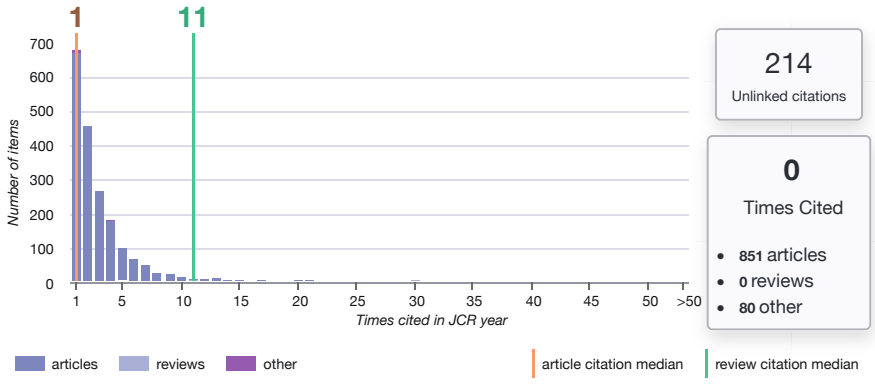

Journal Impact Factor Calculation

$$\text{2017 Journal Impact Factor} = \frac{5,230}{2,694} = 1.941$$

How is Journal Impact Factor Calculated?

$$\text{JIF} = \frac{\text{Citations in 2017 to items published in } \textbf{2015 (2,810) + 2016 (2,420)}}{\text{Number of citable items in } \textbf{2015 (1,333) + 2016 (1,361)}} = \frac{5,230}{2,694}$$

Box plot

Category Box Plot 2017

Category Box Plot

The category box plot depicts the distribution of Impact Factors for all journals in the category. The horizontal line that forms the top of the box is the 75th percentile (Q1). The horizontal line that forms the bottom is the 25th percentile (Q3). The horizontal line that intersects the box is the median Impact Factor for the category.
Horizontal lines above and below the box, called whiskers, represent maximum and minimum values.
The top whisker is the smaller of the following two values:
the maximum Impact Factor (IF)
Q1 IF + 3.5(Q1 IF - Q3 IF)
The bottom whisker is the larger of the following two values:
the minimum Impact Factor (IF)
Q1 IF - 3.5(Q1 IF - Q3 IF)
Box Plots are provided for the current JCR year for each of the categories in which the journal is indexed.

PHYS PLASMAS, IF: 1.941

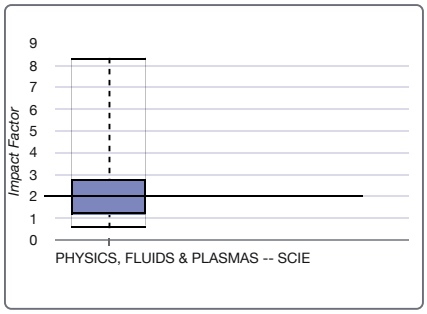

Rank

Rank

JCR Impact Factor

JCR Year	PHYSICS, FLUIDS & PLASMAS -- SCIE		
	Rank	Quartile	JIF Percentile
2018	18/32	Q3	45.313
2017	16/31	Q3	50.000
2016	14/31	Q2	56.452
2015	11/30	Q2	65.000
2014	11/31	Q2	66.129
2013	11/31	Q2	66.129
2012	8/31	Q2	75.806
2011	11/31	Q2	66.129
2010	9/31	Q2	72.581
2009	6/28	Q1	80.357
2008	7/26	Q2	75.000
2007	5/25	Q1	82.000
2006	8/24	Q2	68.750
2005	6/24	Q1	77.083
2004	6/21	Q2	73.810
2003	5/21	Q1	78.571
2002	4/20	Q1	82.500
2001	4/20	Q1	82.500
2000	4/19	Q1	81.579
1999	4/19	Q1	81.579
1998	4/19	Q1	81.579
1997	5/19	Q2	76.316

8.2 Plasma Sources Science and Technology 2018

2018 Journal Performance Data for: PLASMA SOURCES SCIENCE & TECHNOLOGY

ISSN: 0963-0252
eISSN: 1361-6595
IOP PUBLISHING LTD
TEMPLE CIRCUS, TEMPLE WAY, BRISTOL BS1 6BE, ENGLAND
ENGLAND

TITLES
ISO: Plasma Sources Sci. Technol.
JCR Abbrev: PLASMA SOURCES SCI T

LANGUAGES
English

CATEGORIES
PHYSICS, FLUIDS & PLASMAS -- SCIE

PUBLICATION FREQUENCY
6 issues/year

The data in the two graphs below and in the Journal Impact Factor calculation panels represent citation activity in 2018 to items published in the journal in the prior two years. They detail the components of the Journal Impact Factor. Use the "All Years" tab to access key metrics and additional data for the current year and all prior years for this journal.

2018 Journal Impact Factor & percentile rank in category for: PLASMA SOURCES SCIENCE & TECHNOLOGY

4.128
2018 Journal Impact Factor

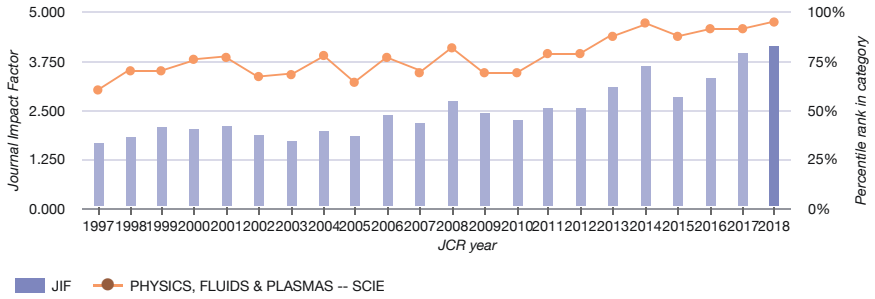

2018 JIF Citation Distribution for: PLASMA SOURCES SCIENCE & TECHNOLOGY

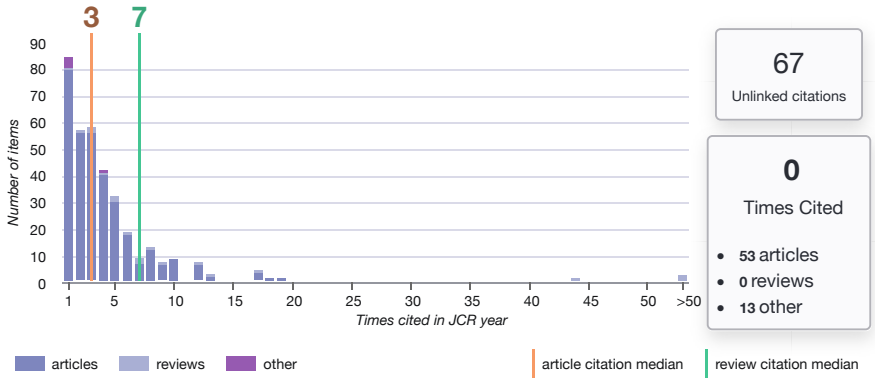

67
Unlinked citations

0
Times Cited

- **53** articles
- **0** reviews
- **13** other

Journal Impact Factor Calculation

$$\text{2018 Journal Impact Factor} = \frac{1{,}639}{397} = 4.128$$

How is Journal Impact Factor Calculated?

$$\text{JIF} = \frac{\text{Citations in 2018 to items published in } \textbf{2016 (932) + 2017 (707)}}{\text{Number of citable items in } \textbf{2016 (204) + 2017 (193)}} = \frac{1{,}639}{397}$$

Box plot

Category Box Plot 2018

Category Box Plot

The category box plot depicts the distribution of Impact Factors for all journals in the category. The horizontal line that forms the top of the box is the 75th percentile (Q1). The horizontal line that forms the bottom is the 25th percentile (Q3). The horizontal line that intersects the box is the median Impact Factor for the category.
Horizontal lines above and below the box, called whiskers, represent maximum and minimum values.
The top whisker is the smaller of the following two values:
the maximum Impact Factor (IF)
Q1 IF + 3.5(Q1 IF - Q3 IF)
The bottom whisker is the larger of the following two values:
the minimum Impact Factor (IF)
Q1 IF - 3.5(Q1 IF - Q3 IF)
Box Plots are provided for the current JCR year for each of the categories in which the journal is indexed.

PLASMA SOURCES SCI T, IF: 4.128

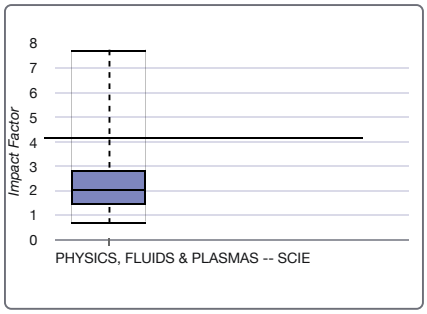

Rank

Rank

JCR Impact Factor

JCR Year	PHYSICS, FLUIDS & PLASMAS -- SCIE		
	Rank	Quartile	JIF Percentile
2018	2/32	Q1	95.313
2017	3/31	Q1	91.935
2016	3/31	Q1	91.935
2015	4/30	Q1	88.333
2014	2/31	Q1	95.161
2013	4/31	Q1	88.710
2012	7/31	Q1	79.032
2011	7/31	Q1	79.032
2010	10/31	Q2	69.355
2009	9/28	Q2	69.643
2008	5/26	Q1	82.692
2007	8/25	Q2	70.000
2006	6/24	Q1	77.083
2005	9/24	Q2	64.583
2004	5/21	Q1	78.571
2003	7/21	Q2	69.048
2002	7/20	Q2	67.500
2001	5/20	Q1	77.500
2000	5/19	Q2	76.316
1999	6/19	Q2	71.053
1998	6/19	Q2	71.053
1997	8/19	Q2	60.526

8.3 Plasma Physics and Controlled Fusion 2019

2019 Journal Performance Data for: PLASMA PHYSICS AND CONTROLLED FUSION

ISSN: 0741-3335
eISSN: 1361-6587
IOP PUBLISHING LTD
TEMPLE CIRCUS, TEMPLE WAY, BRISTOL BS1 6BE, ENGLAND
ENGLAND

TITLES
ISO: Plasma Phys. Control. Fusion
JCR Abbrev: PLASMA PHYS CONTR F

LANGUAGES
Multi-Language

CATEGORIES
PHYSICS, FLUIDS & PLASMAS -- SCIE

PUBLICATION FREQUENCY
12 issues/year

The data in the two graphs below and in the Journal Impact Factor calculation panels represent citation activity in 2019 to items published in the journal in the prior two years. They detail the components of the Journal Impact Factor. Use the "All Years" tab to access key metrics and additional data for the current year and all prior years for this journal.

2019 Journal Impact Factor & percentile rank in category for: PLASMA PHYSICS AND CONTROLLED FUSION

2.829
2019 Journal Impact Factor

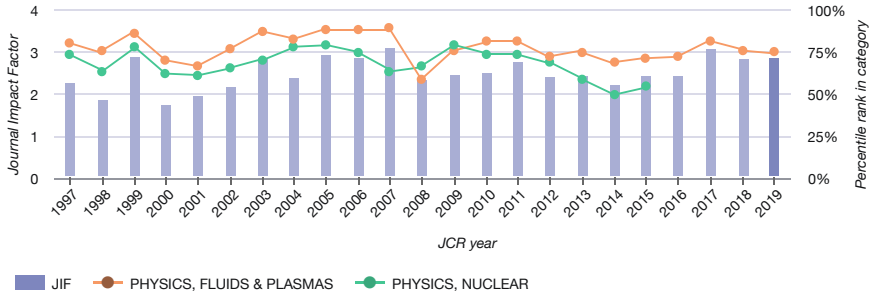

2019 JIF Citation Distribution for: PLASMA PHYSICS AND CONTROLLED FUSION

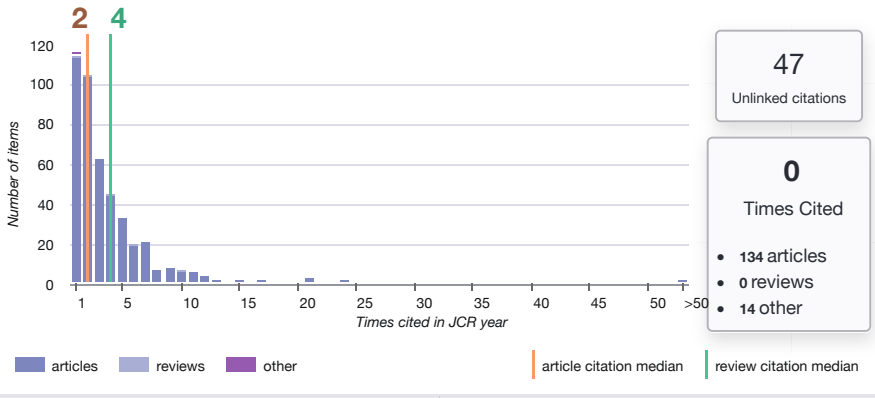

Journal Impact Factor Calculation

$$\text{2019 Journal Impact Factor} = \frac{1{,}604}{567} = 2.829$$

How is Journal Impact Factor Calculated?

$$\text{JIF} = \frac{\text{Citations in 2019 to items published in } \mathbf{2017\ (808) + 2018\ (796)}}{\text{Number of citable items in } \mathbf{2017\ (272) + 2018\ (295)}} = \frac{1{,}604}{567}$$

Box plot

Category Box Plot 2019

Category Box Plot

The category box plot depicts the distribution of Impact Factors for all journals in the category. The horizontal line that forms the top of the box is the 75th percentile (Q1). The horizontal line that forms the bottom is the 25th percentile (Q3). The horizontal line that intersects the box is the median Impact Factor for the category.
Horizontal lines above and below the box, called whiskers, represent maximum and minimum values.
The top whisker is the smaller of the following two values:
the maximum Impact Factor (IF)
Q1 IF + 3.5(Q1 IF - Q3 IF)
The bottom whisker is the larger of the following two values:
the minimum Impact Factor (IF)
Q1 IF - 3.5(Q1 IF - Q3 IF)
Box Plots are provided for the current JCR year for each of the categories in which the journal is indexed.

PLASMA PHYS CONTR F, IF: 2.829

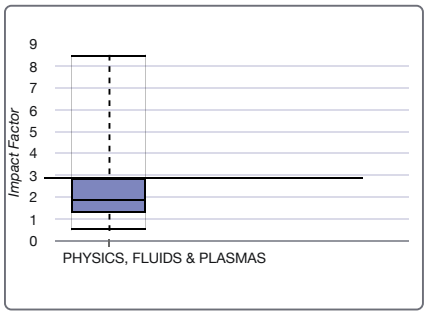

Rank

Rank

JCR Impact Factor

JCR Year	PHYSICS, FLUIDS & PLASMAS			PHYSICS, NUCLEAR		
	Rank	Quartile	JIF Percentile	Rank	Quartile	JIF Percentile
2019	9/34	Q2	75.000	n/a	n/a	n/a
2018	8/32	Q1	76.563	n/a	n/a	n/a
2017	6/31	Q1	82.258	n/a	n/a	n/a
2016	9/31	Q2	72.581	n/a	n/a	n/a
2015	9/30	Q2	71.667	10/21	Q2	54.762
2014	10/31	Q2	69.355	11/21	Q3	50.000
2013	8/31	Q2	75.806	9/21	Q2	59.524
2012	9/31	Q2	72.581	7/21	Q2	69.048
2011	6/31	Q1	82.258	6/21	Q2	73.810
2010	6/31	Q1	82.258	6/21	Q2	73.810
2009	7/28	Q1	76.786	5/22	Q1	79.545
2008	11/26	Q2	59.615	7/20	Q2	67.500
2007	3/25	Q1	90.000	8/21	Q2	64.286
2006	3/24	Q1	89.583	6/22	Q2	75.000
2005	3/24	Q1	89.583	5/22	Q1	79.545
2004	4/21	Q1	83.333	5/21	Q1	78.571
2003	3/21	Q1	88.095	7/22	Q2	70.455
2002	5/20	Q1	77.500	8/22	Q2	65.909
2001	7/20	Q2	67.500	9/22	Q2	61.364
2000	6/19	Q2	71.053	8/20	Q2	62.500
1999	3/19	Q1	86.842	5/21	Q1	78.571
1998	5/19	Q2	76.316	8/21	Q2	64.286
1997	4/19	Q1	81.579	6/21	Q2	73.810

8.4 Plasma Sources Science and Technology 2019

2019 Journal Performance Data for: PLASMA SOURCES SCIENCE & TECHNOLOGY

ISSN: 0963-0252
eISSN: 1361-6595
IOP PUBLISHING LTD
TEMPLE CIRCUS, TEMPLE WAY, BRISTOL BS1 6BE, ENGLAND
ENGLAND

TITLES
ISO: Plasma Sources Sci. Technol.
JCR Abbrev: PLASMA SOURCES SCI T

LANGUAGES
English

CATEGORIES
PHYSICS, FLUIDS & PLASMAS -- SCIE

PUBLICATION FREQUENCY
6 issues/year

The data in the two graphs below and in the Journal Impact Factor calculation panels represent citation activity in 2019 to items published in the journal in the prior two years. They detail the components of the Journal Impact Factor. Use the "All Years" tab to access key metrics and additional data for the current year and all prior years for this journal.

2019 Journal Impact Factor & percentile rank in category for: PLASMA SOURCES SCIENCE & TECHNOLOGY

3.193
2019 Journal Impact Factor

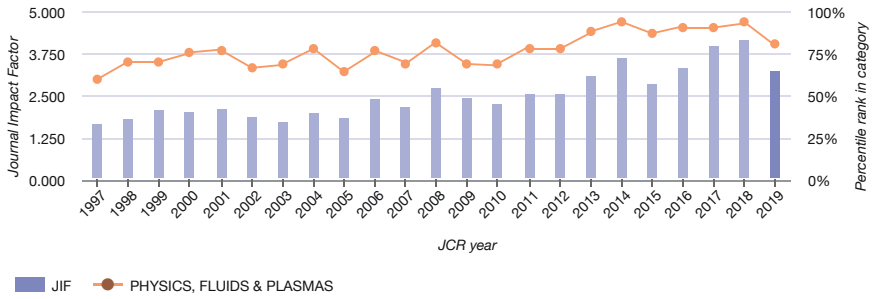

2019 JIF Citation Distribution for: PLASMA SOURCES SCIENCE & TECHNOLOGY

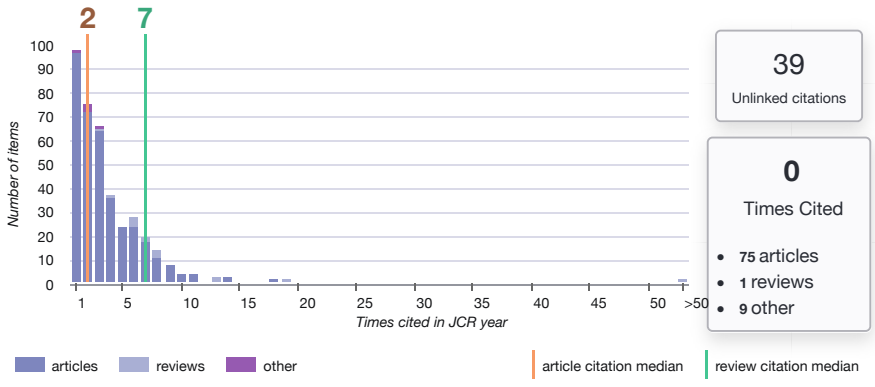

Journal Impact Factor Calculation

$$\text{2019 Journal Impact Factor} = \frac{1{,}440}{451} = 3.193$$

How is Journal Impact Factor Calculated?

$$\text{JIF} = \frac{\text{Citations in 2019 to items published in } \textbf{2017 (709) + 2018 (731)}}{\text{Number of citable items in } \textbf{2017 (193) + 2018 (258)}} = \frac{1{,}440}{451}$$

Box plot

Category Box Plot 2019

Category Box Plot

The category box plot depicts the distribution of Impact Factors for all journals in the category. The horizontal line that forms the top of the box is the 75th percentile (Q1). The horizontal line that forms the bottom is the 25th percentile (Q3). The horizontal line that intersects the box is the median Impact Factor for the category.
Horizontal lines above and below the box, called whiskers, represent maximum and minimum values.
The top whisker is the smaller of the following two values:
the maximum Impact Factor (IF)
Q1 IF + 3.5(Q1 IF - Q3 IF)
The bottom whisker is the larger of the following two values:
the minimum Impact Factor (IF)
Q1 IF - 3.5(Q1 IF - Q3 IF)
Box Plots are provided for the current JCR year for each of the categories in which the journal is indexed.

PLASMA SOURCES SCI T, IF: 3.193

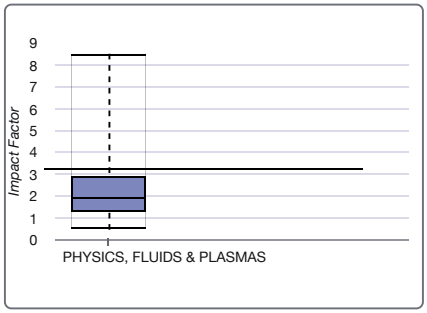

Rank

Rank

JCR Impact Factor

JCR Year	PHYSICS, FLUIDS & PLASMAS		
	Rank	Quartile	JIF Percentile
2019	7/34	Q1	80.882
2018	2/32	Q1	95.313
2017	3/31	Q1	91.935
2016	3/31	Q1	91.935
2015	4/30	Q1	88.333
2014	2/31	Q1	95.161
2013	4/31	Q1	88.710
2012	7/31	Q1	79.032
2011	7/31	Q1	79.032
2010	10/31	Q2	69.355
2009	9/28	Q2	69.643
2008	5/26	Q1	82.692
2007	8/25	Q2	70.000
2006	6/24	Q1	77.083
2005	9/24	Q2	64.583
2004	5/21	Q1	78.571
2003	7/21	Q2	69.048
2002	7/20	Q2	67.500
2001	5/20	Q1	77.500
2000	5/19	Q2	76.316
1999	6/19	Q2	71.053
1998	6/19	Q2	71.053
1997	8/19	Q2	60.526

8.5 Applied Sciences 2019

2019 Journal Performance Data for: Applied Sciences-Basel

ISSN: ****-****
eISSN: 2076-3417
MDPI
ST ALBAN-ANLAGE 66, CH-4052 BASEL, SWITZERLAND
SWITZERLAND

TITLES
ISO: Appl. Sci.-Basel
JCR Abbrev: APPL SCI-BASEL

LANGUAGES
English

CATEGORIES
CHEMISTRY, MULTIDISCIPLINARY -- SCIE

PHYSICS, APPLIED -- SCIE

ENGINEERING, MULTIDISCIPLINARY -- SCIE

MATERIALS SCIENCE, MULTIDISCIPLINARY -- SCIE

PUBLICATION FREQUENCY
24 issues/year

Open Access from 2011

The data in the two graphs below and in the Journal Impact Factor calculation panels represent citation activity in 2019 to items published in the journal in the prior two years. They detail the components of the Journal Impact Factor. Use the "All Years" tab to access key metrics and additional data for the current year and all prior years for this journal.

2019 Journal Impact Factor & percentile rank in category for: Applied Sciences-Basel

2.474
2019 Journal Impact Factor

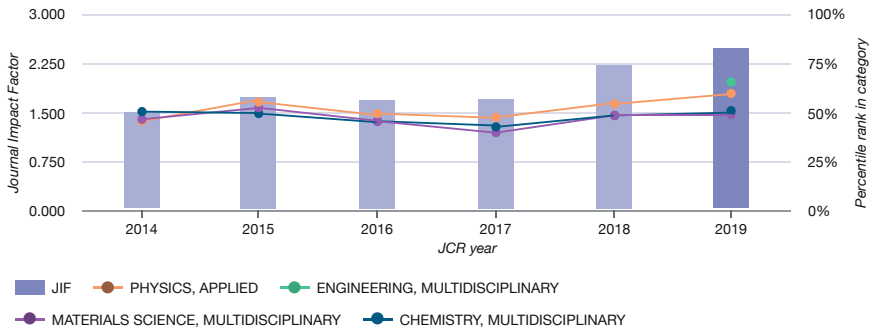

2019 JIF Citation Distribution for: Applied Sciences-Basel

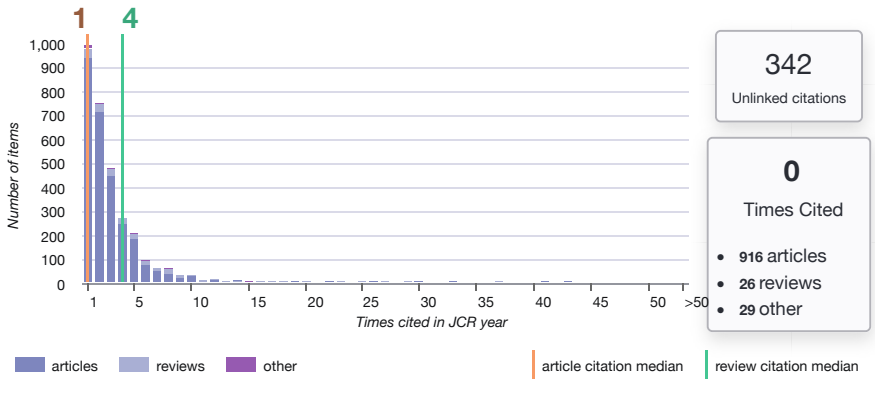

Journal Impact Factor Calculation

$$\text{2019 Journal Impact Factor} = \frac{9,860}{3,985} = 2.474$$

How is Journal Impact Factor Calculated?

$$\text{JIF} = \frac{\text{Citations in 2019 to items published in } \textbf{2017 (3,779) + 2018 (6,081)}}{\text{Number of citable items in } \textbf{2017 (1,313) + 2018 (2,672)}} = \frac{9,860}{3,985}$$

Box plot

Category Box Plot 2019

Category Box Plot

The category box plot depicts the distribution of Impact Factors for all journals in the category. The horizontal line that forms the top of the box is the 75th percentile (Q1). The horizontal line that forms the bottom is the 25th percentile (Q3). The horizontal line that intersects the box is the median Impact Factor for the category.
Horizontal lines above and below the box, called whiskers, represent maximum and minimum values.
The top whisker is the smaller of the following two values:
the maximum Impact Factor (IF)
Q1 IF + 3.5(Q1 IF - Q3 IF)
The bottom whisker is the larger of the following two values:
the minimum Impact Factor (IF)
Q1 IF - 3.5(Q1 IF - Q3 IF)
Box Plots are provided for the current JCR year for each of the categories in which the journal is indexed.

APPL SCI-BASEL, IF: 2.474

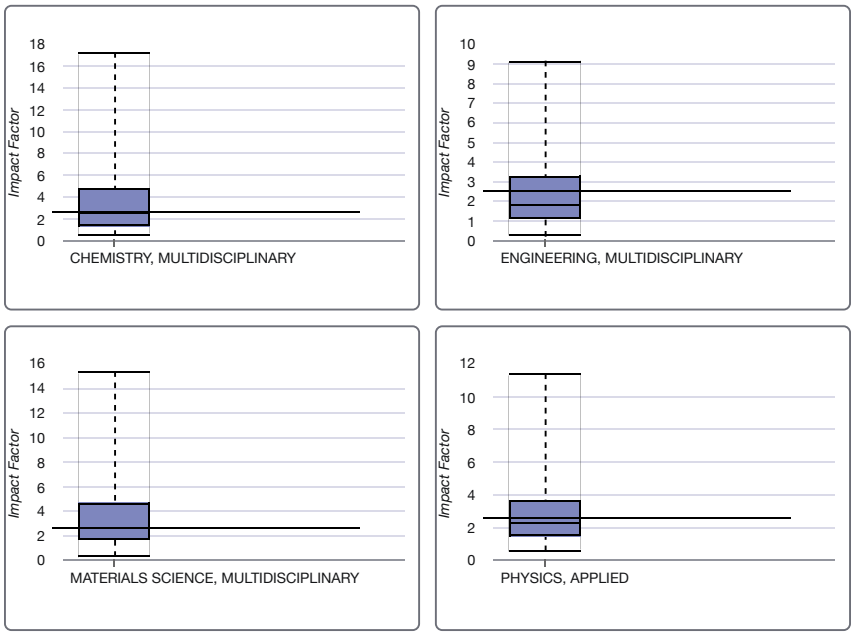

Rank

Rank

JCR Impact Factor

JCR Year	CHEMISTRY, MULTIDISCIPLINARY			ENGINEERING, MULTIDISCIPLINARY			MATERIALS SCIENCE, MULTIDISCIPLINARY			PHYSICS, APPLIED		
	Rank	Quartile	JIF Percentile	Rank	Quartile	JIF Percentile	Rank	Quartile	JIF Percentile	Rank	Quartile	JIF Percentile
2019	88/177	Q2	50.565	32/91	Q2	65.385	161/314	Q3	48.885	62/154	Q2	60.065
2018	89/172	Q3	48.547	n/a	n/a	n/a	151/293	Q3	48.635	67/148	Q2	55.068
2017	98/171	Q3	42.982	n/a	n/a	n/a	171/285	Q3	40.175	77/146	Q3	47.603
2016	91/166	Q3	45.482	n/a	n/a	n/a	150/275	Q3	45.636	75/148	Q3	49.662
2015	83/163	Q3	49.387	n/a	n/a	n/a	129/271	Q2	52.583	64/145	Q2	56.207
2014	78/157	Q2	50.637	n/a	n/a	n/a	139/260	Q3	46.731	79/144	Q3	45.486

9 Bibliografía

1. Mieno T, Kamo T, Hayashi D, Shoji T, Kadota K. Efficient production of O + and O – ions in a helicon wave oxygen discharge. Appl Phys Lett [Internet]. 1996 Jul 29;69(5):617–9. Available from: http://aip.scitation.org/doi/10.1063/1.117925

2. Gudmundsson JT, Kouznetsov IG, Patel KK, Lieberman MA. Electronegativity of low-pressure high-density oxygen discharges. J Phys D Appl Phys [Internet]. 2001 Apr 7;34(7):1100–9. Available from: http://stacks.iop.org/0022-3727/34/i=7/a=312?key=crossref.7550c26d8974b2dd859fbf96b5abcf72

3. Mott-Smith HM, Langmuir I. The Theory of Collectors in Gaseous Discharges. Phys Rev [Internet]. 1926 Oct 1;28(4):727–63. Available from: https://link.aps.org/doi/10.1103/PhysRev.28.727

4. Godyak V, Alexandrovich BM. Comparative analyses of plasma probe diagnostics techniques. J Appl Phys [Internet]. 2015 Dec 21;118(23):233302. Available from: http://aip.scitation.org/doi/10.1063/1.4937446

5. Popov TK, Dimitrova M, Ivanova P, Kovačič J, Gyergyek T, Dejarnac R, et al. Advances in Langmuir probe diagnostics of the plasma potential and electron-energy distribution function in magnetized plasma. Plasma Sources Sci Technol [Internet]. 2016 Jun 1;25(3):033001. Available from: http://stacks.iop.org/0963-0252/25/i=3/a=033001?key=crossref.88afe59ce51c1567040b3a8c1d462e05

6. Han J, Pribyl P, Gekelman W, Paterson A, Lanham SJ, Qu C, et al. Three-dimensional measurements of plasma parameters in an inductively coupled plasma processing chamber. Phys Plasmas. 2019;26(10).

7. Stamate E. Status and challenges in electrical diagnostics of processing plasmas. Surf Coatings Technol [Internet]. 2014 Dec 4;260:401–10. Available from: https://linkinghub.elsevier.com/retrieve/pii/S0257897214009086

8. Ionita C, Schneider BS, Costea S, Vasilovici O, Kovačič J, Gyergyek T, et al. Plasma potential probes for hot plasmas: A review and some news. Eur Phys J D. 2019;73(4).

9. Allen JE, Boyd RLF, Reynolds P. The Collection of Positive Ions by a Probe Immersed in a Plasma. Proc Phys Soc Sect B [Internet]. 1957 Mar 1;70(3):297–304. Available from: http://iopscience.iop.org/article/10.1088/0370-1301/70/3/303/meta

10. Chen FF. Numerical computations for ion probe characteristics in a collisionless plasma. J Nucl Energy Part C, Plasma Physics, Accel Thermonucl Res [Internet]. 1965 Jan 1;7(1):47–67. Available from: http://iopscience.iop.org/article/10.1088/0368-3281/7/1/306/meta

11. Fernández Palop JI, Ballesteros J, Colomer V, Hernández MÁ. Theoretical ion current to cylindrical Langmuir probes for finite ion temperature values. J Phys D Appl Phys [Internet]. 1996 Nov 14 [cited 2016 Dec 2];29(11):2832–40. Available from: http://iopscience.iop.org/article/10.1088/0022-3727/29/11/017/meta

12. Bernstein IB, Rabinowitz IN. Theory of Electrostatic Probes in a Low-Density Plasma. Phys Fluids [Internet]. 1959 Oct 4;2(2):112. Available from: https://aip.scitation.org/doi/10.1063/1.1705900

13. Laframboise JG. Theory of spherical and cylindrical Langmuir probes in a collisionless, Maxwellian plasma at rest [Internet]. TORONTO UNIV DOWNSVIEW (ONTARIO) INST FOR AEROSPACE STUDIES; 1966 [cited 2017 Sep 5]. Available from: http://www.dtic.mil/docs/citations/AD0634596

14. Díaz-Cabrera JM, Lucena-Polonio M V, Fernández Palop JI, Morales Crespo R, Hernández MÁ, Tejero-del-Caz A, et al. Experimental study of the ion current to a cylindrical Langmuir probe taking into account a finite ion temperature. J Appl Phys [Internet]. 2012 Mar 15 [cited 2019 Oct 4];111(6):063303. Available from: http://aip.scitation.org/doi/10.1063/1.3698313

15. Díaz-Cabrera JM, Fernández Palop JI, Morales Crespo R, Hernández MÁ, Tejero-del-Caz A, Ballesteros J. Virtual Instrument for automatic low temperature plasmas diagnostic considering finite positive ion temperature. Measurement [Internet]. 2014 Sep 4 [cited 2019 Oct 4];55:66–73. Available from: https://linkinghub.elsevier.com/retrieve/pii/S0263224114001870

16. Díaz-Cabrera JM, Ballesteros J, Fernández Palop JI, Tejero-del-Caz A. Experimental radial motion to orbital motion transition in cylindrical Langmuir probes in low pressure plasmas. Plasma Sources Sci Technol [Internet]. 2015 Mar 16;24(2):025026. Available from: http://stacks.iop.org/0963-0252/24/i=2/a=025026?key=crossref.08974592357ce5d559b8bbd790e86aec

17. Díaz-Cabrera JM, Fernández Palop JI, Regodón GF, Ballesteros J. Accurate measurement of the ion saturation current collected by a cylindrical Langmuir probe in cold plasmas. Plasma Process Polym [Internet]. 2020 Jun 16;(April):1–12. Available from: https://onlinelibrary.wiley.com/doi/abs/10.1002/ppap.202000073

18. Regodón GF, Fernández Palop JI, Tejero-del-Caz A, Díaz-Cabrera JM, Carmona-Cabezas R, Ballesteros J. Removal of singularity in radial Langmuir probe models for non-zero ion temperature. Phys Plasmas [Internet]. 2017 Oct 4;24(10):103516. Available from: http://aip.scitation.org/doi/10.1063/1.4997844

19. Regodón GF, Fernández Palop JI, Tejero-del-Caz A, Díaz-Cabrera JM, Carmona-Cabezas R, Ballesteros J. Floating potential in electronegative plasmas for non-zero ion temperatures. Plasma Sources Sci Technol [Internet]. 2018 Feb 21;27(2):025014. Available from: http://stacks.iop.org/0963-0252/27/i=2/a=025014?key=crossref.5ffd9261858eacbf1779e892618f4f79

20. Regodón GF, Fernández Palop JI, Díaz-Cabrera JM, Ballesteros J. Influence of collisions in a fluid model for the warm-ion sheath around a cylindrical Langmuir probe. Plasma Sources Sci Technol [Internet]. 2019 Nov 28;28(11):115017. Available from: https://iopscience.iop.org/article/10.1088/1361-6595/ab515e

21. Regodón GF, Fernández Palop JI, Díaz-Cabrera JM, Ballesteros J. Floating potential calculation for a Langmuir probe in electronegative plasmas and experimental validation in a glow discharge. Plasma Phys Control Fusion [Internet]. 2019 Sep 1;61(9):095015. Available from: https://iopscience.iop.org/article/10.1088/1361-6587/ab3483

22. Regodón GF, Díaz-Cabrera JM, Fernández Palop JI, Ballesteros J. Influence of the Ion Mass in the Radial to Orbital Transition in Weakly Collisional Low-Pressure Plasmas Using Cylindrical Langmuir Probes. Appl Sci [Internet]. 2020 Aug 19;10(17):5727. Available from: https://www.mdpi.com/2076-3417/10/17/5727

23. Morales Crespo R, Fernández Palop JI, Hernández MÁ, Ballesteros J. Analytical fit of the I–V probe characteristic for finite ion temperature values: Justification of the radial model applicability. J Appl Phys [Internet]. 2004 Mar 15;95(6):2982–90. Available from: http://aip.scitation.org/doi/10.1063/1.1650540

24. Morales Crespo R, Fernández Palop JI, Ballesteros J, Hernández MÁ, Lucena-Polonio M V. Effect of Positive-Ion Temperature in the Sheaths Surrounding Cylindrical and Spherical Probes in Electronegative Plasmas. IEEE Trans Plasma Sci [Internet]. 2009 Sep 4;37(9):1715–22. Available from: http://ieeexplore.ieee.org/document/5200503/

25. Morales Crespo R, Fernández Palop JI, Hernández MÁ, Borrego del Pino S, Ballesteros J. Analytical fit of the I-V characteristic for cylindrical and spherical probes in electronegative plasmas. J Appl Phys [Internet]. 2004 Nov 4;96(9):4777–83. Available from: http://aip.scitation.org/doi/10.1063/1.1796517

26. Morales Crespo R, Fernández Palop JI, Hernández MÁ, Ballesteros J. Analytical fit of the I-V characteristic for cylindrical and spherical Langmuir probes. J Appl Phys. 2003;94(8):4788–95.

27. Ballesteros J, Fernández Palop JI, Hernández MÁ, Morales Crespo R, Borrego del Pino S. LabView virtual instrument for automatic plasma diagnostic. Rev Sci Instrum [Internet]. 2004 Jan;75(1):90–3. Available from: https://aip.scitation.org/doi/10.1063/1.1634356

28. Lucena-Polonio M V, Díaz-Cabrera JM, Fernández Palop JI, Morales Crespo R, Hernández MÁ, Ballesteros J. Mass spectrometry diagnosis of ion species in low-pressure plasmas. Plasma Phys Control Fusion [Internet]. 2011 Dec 1;53(12):124024. Available from: http://stacks.iop.org/0741-3335/53/i=12/a=124024?key=crossref.c97438b77993398044b59d02a5c807a6

29. Tejero-del-Caz A, Fernández Palop JI, Díaz-Cabrera JM, Ballesteros J. Radial-to-orbital motion transition in cylindrical Langmuir probes studied with particle-in-cell simulations. Plasma Sources Sci Technol [Internet]. 2016 Feb 1;25(1):01LT03. Available from: http://stacks.iop.org/0963-0252/25/i=1/a=01LT03?key=crossref.bdfa4e1a1769664e9fa8a9eafcfffd76

30. Tejero-del-Caz A, Fernández Palop JI, Díaz-Cabrera JM, Regodón GF, Carmona-Cabezas R, Ballesteros J. Ion injection in electrostatic particle-in-cell simulations of the ion sheath. J Comput Phys [Internet]. 2017 Dec 4;350:747–58. Available from: https://linkinghub.elsevier.com/retrieve/pii/S0021999117306770

31. Chen FF. Plasma Diagnostic Techniques. New York: Academic; 1965.

32. Wiesemann K. A short introduction to plasma physics. CAS-CERN Accel Sch Ion Sources - Proc. 2013;(1):85–122.

33. Goldston RJ, Rutherford PH. Introduction to Plasma Physics. Introduction to Plasma Physics. IOP Publishing Ltd; 1995.

34. Godyak V, Piejak RB, Alexandrovich BM. Electron energy distribution function measurements and plasma parameters in inductively coupled argon plasma. Plasma Sources Sci Technol [Internet]. 2002 Oct 4;11(4):525–43. Available from: http://stacks.iop.org/0963-0252/11/i=4/a=320?key=crossref.a8168d151a959a3b9a590332d47c7ede

35. Franklin RN, Snell J. The Boltzmann relation in electronegative plasmas: When is it permissible to use it? J Plasma Phys [Internet]. 2000 Jun 14;64(2):131–53. Available from: https://www.cambridge.org/core/product/identifier/S0022377800008576/type/journal_article

36. Annaratone BM, Allen MW, Allen JE. Ion currents to cylindrical Langmuir probes in RF plasmas. J Phys D Appl Phys [Internet]. 1992 Mar 14;25(3):417–24. Available from: http://stacks.iop.org/0022-3727/25/i=3/a=012?key=crossref.509bbda5f87a36599674095462d65dad

37. Riemann K-U. Kinetic theory of the plasma sheath transition in a weakly ionized plasma. Phys Fluids [Internet]. 1981 Oct 4;24(12):2163. Available from: https://aip.scitation.org/doi/10.1063/1.863332

38. Tonks L, Langmuir I. A General Theory of the Plasma of an Arc. Phys Rev [Internet]. 1929 Sep 15;34(6):876–922. Available from: https://link.aps.org/doi/10.1103/PhysRev.34.876

39. Franklin RN. Where is the sheath edge? J Phys D Appl Phys [Internet]. 2004 May 7;37(9):1342–5. Available from: http://stacks.iop.org/0022-3727/37/i=9/a=007?key=crossref.9265841284dd0ad3793c56638189e3f3

40. Nanbu K. Probability theory of electron-molecule, ion-molecule, molecule-molecule, and Coulomb collisions for particle modeling of materials processing plasmas and gases. IEEE Trans Plasma Sci. 2000;28(3):971–90.

41. Franklin RN, Snell J. The plasma-sheath transition with a constant mean free path model and the applicability of the Bohm criterion. Phys Plasmas [Internet]. 2001 Feb;8(2):643–7. Available from: http://aip.scitation.org/doi/10.1063/1.1334609

42. Riemann K-U. The Bohm criterion and sheath formation. J Phys D Appl Phys [Internet]. 1991 Apr 14;24(4):493–518. Available from: http://stacks.iop.org/0022-3727/24/i=4/a=001?key=crossref.8ef018f33cb54573928abc7217c3932b

43. Brinkmann RP. The plasma–sheath transition in low temperature plasmas: on the existence of a collisionally modified Bohm criterion. J Phys D Appl Phys [Internet]. 2011 Feb 2;44(4):042002. Available from: http://stacks.iop.org/0022-3727/44/i=4/a=042002?key=crossref.735290290bde3797f268d06c54b1e9cd

44. Franklin RN. You cannot patch active plasma and collisionless sheath. IEEE Trans Plasma Sci. 2002 Feb 4;30(1):352–6.

45. Druyvesteyn MJ. Der Niedervoltbogen. Zeitschrift für Phys [Internet]. 1930 Sep 4 [cited 2019 Oct 4];64(11–12):781–98. Available from: http://link.springer.com/10.1007/BF01773007

46. Kagan YM, Perel' VI. Probe methods in plasma research. Sov Phys Uspekhi [Internet].

1964 Jun 30;6(6):767–93. Available from: http://dx.doi.org/10.1070/PU1964v006n06ABEH003611

47. Fernández Palop JI, Ballesteros J, Colomer V, Hernández MÁ. A new smoothing method for obtaining the electron energy distribution function in plasmas by the numerical differentiation of the I - V probe characteristic. Rev Sci Instrum [Internet]. 1995 Sep;66(9):4625–36. Available from: https://aip.scitation.org/doi/10.1063/1.1145300

48. Ballesteros J, Fernández Palop JI, Hernández MÁ, Morales Crespo R. Influence of the positive ion temperature in cold plasma diagnosis. Appl Phys Lett [Internet]. 2006 Sep 4;89(10):101501. Available from: http://aip.scitation.org/doi/10.1063/1.2345252

49. Godyak V, Piejak RB. Abnormally low electron energy and heating-mode transition in a low-pressure argon rf discharge at 13.56 MHz. Phys Rev Lett [Internet]. 1990 Oct 4;65(8):996–9. Available from: https://link.aps.org/doi/10.1103/PhysRevLett.65.996

50. Godyak V. Measuring EEDF in gas plasma discharges. In: Plasma-Surface Interactions and Processing of Materials [Internet]. Dordrecht, The Netherlands: Kluwer Scademic Publishers; 1990. p. 95–134. (E: {Applied} {Sciences}; vol. 176). Available from: https://link.springer.com/chapter/10.1007%2F978-94-009-1946-4_4

51. Godyak V, Alexandrovich BM. Langmuir paradox revisited. Plasma Sources Sci Technol [Internet]. 2015 Aug 20;24(5):052001. Available from: http://stacks.iop.org/0963-0252/24/i=5/a=052001?key=crossref.dfba4edfd27b59bad1928635bc228239

52. Chen FF. Introduction to Plasma Physics. New York and London: Plenum Press; 1974.

53. Loureiro J, Amorim J. Kinetics and Spectroscopy of Low Temperature Plasmas [Internet]. Cham: Springer International Publishing; 2016. (Graduate Texts in Physics). Available from: http://link.springer.com/10.1007/978-3-319-09253-9

54. Huang K. Statistical Mechanics. 2nd Editio. John Wiley & Sons; 1987.

55. Cercignani C. The Boltzmann Equation and Its Applications [Internet]. 1st Editio. John F, Mardsen JE, Sirovich L, editors. New York, NY: Springer New York; 1988. 466 p. (Applied Mathematical Sciences; vol. 67). Available from: http://link.springer.com/10.1007/978-1-4612-1039-9

56. Fernández Palop JI, Ballesteros J, Hernández MÁ, Morales Crespo R, Borrego del Pino S. A simplified model joining the sheath and the plasma in electronegative plasmas. Czechoslov J Phys [Internet]. 2004;54(2):225–238. Available from: http://link.springer.com/article/10.1023/B:CJOP.0000014404.80357.d3

57. Spitzer L. Physics of fully ionized gases. 2nd Editio. New York and London: Interscience Publisher; 1957. 111 p.

58. Lieberman MA, Lichtenberg AJ. Principles of Plasma Discharges and Materials Processing [Internet]. Hoboken, NJ, USA: John Wiley & Sons, Inc.; 2005. Available from: http://doi.wiley.com/10.1002/0471724254

59. Gyergyek T, Kovačič J. Numerical analysis of ion temperature effects to the plasma wall transition using a one-dimensional two-fluid model. I. Finite Debye to ionization length ratio.

Phys Plasmas [Internet]. 2017 Jun 4;24(6):063505. Available from: http://aip.scitation.org/doi/10.1063/1.4984786

60. Gyergyek T, Kovačič J. Numerical analysis of ion temperature effects to the plasma wall transition using a one-dimensional two-fluid model. II. Asymptotic two-scale limit. Phys Plasmas [Internet]. 2017 Jun 4;24(6):063506. Available from: http://aip.scitation.org/doi/10.1063/1.4984787

61. Kuhn S, Riemann K-U, Jelić N, Tskhakaya DD, Tskhakaya D, Stanojević M. Link between fluid and kinetic parameters near the plasma boundary. Phys Plasmas [Internet]. 2006 Jan 4;13(1):013503. Available from: http://aip.scitation.org/doi/10.1063/1.2161181

62. Phelps A V. Cross Sections and Swarm Coefficients for Nitrogen Ions and Neutrals in N2 and Argon Ions and Neutrals in Ar for Energies from 0.1 eV to 10 keV. J Phys Chem Ref Data. 1991;20(3):557–73.

63. Phelps A V. The application of scattering cross sections to ion flux models in discharge sheaths. J Appl Phys. 1994;76(2):747–53.

64. Brandsen B H. Atomic Collision Theory. First Edit. Benjamin WA, editor. New York: W A Benjamin Inc.; 1970. 457 p.

65. Robertson S. Sheaths in laboratory and space plasmas. Plasma Phys Control Fusion [Internet]. 2013 Sep 1;55(9):093001. Available from: http://stacks.iop.org/0741-3335/55/i=9/a=093001?key=crossref.c40103827dcc428e922b7bc464dbedbd

66. Tskhakaya DD, Kos L, Jelić N. A unified analysis of plasma-sheath transition in the Tonks–Langmuir model with warm ion source. Phys Plasmas [Internet]. 2014 Jul 4;21(7):073503. Available from: http://aip.scitation.org/doi/10.1063/1.4885638

67. Riemann K-U. Plasma-sheath transition in the kinetic Tonks-Langmuir model. Phys Plasmas [Internet]. 2006 Jun 1;13(6):063508. Available from: http://aip.scitation.org/doi/10.1063/1.2209928

68. Godyak V, Meytlis VP, Strauss HR. Tonks-Langmuir problem for a bi-Maxwellian plasma. IEEE Trans Plasma Sci [Internet]. 1995 Oct 4;23(4):728–34. Available from: http://ieeexplore.ieee.org/document/467995/

69. Kos L, Tskhakaya DD, Jelić N. Potential profile near singularity point in kinetic Tonks-Langmuir discharges as a function of the ion sources temperature. Phys Plasmas [Internet]. 2011 May 4;18(5):053507. Available from: http://aip.scitation.org/doi/10.1063/1.3587112

70. Limpaecher R, Mackenzie KR. Magnetic Multipole Containment of Large Uniform Collisionless Quiescent Plasmas. Rev Sci Instrum. 1973;44:726–31.

71. Wong AY, Mamas DL, Arnush D. Negative ion plasmas. Phys Fluids. 1975;18:1489–93.

72. McGrayne SB, Kashy E. Encyclopaedia Britannica: Electricity [Internet]. Encyclopædia Britannica. 2020 [cited 2020 May 25]. Available from: https://www.britannica.com/science/electricity

73. Oliphant MLE. The Action of Metastable Atoms of Helium on a Metal Surface . Proc Phys

Soc Sect A. 1929;124(793):228–42.

74. Cenian A, Rachubinski H, Chernukho A, Dudeck M. Plasma-wall interactions in DC discharges and sheath of Langmuir probes. Eur Phys J Spec Top [Internet]. 2013 Oct 23;222(9):2143–56. Available from: http://link.springer.com/10.1140/epjst/e2013-01991-y

75. Gyergyek T, Kovačič J, Čerček M. Potential formation in front of an electron emitting electrode immersed in a plasma that contains a monoenergetic electron beam. Phys Plasmas [Internet]. 2010 Aug 4;17(8):083504. Available from: http://aip.scitation.org/doi/10.1063/1.3467500

76. Allen JE. The plasma–sheath boundary: its history and Langmuir's definition of the sheath edge. Plasma Sources Sci Technol [Internet]. 2009 Feb 1;18(1):014004. Available from: http://stacks.iop.org/0963-0252/18/i=1/a=014004?key=crossref.b5f93f3f6faebdeac633052805b0e5b2

77. Riemann K-U. Plasma and sheath. Plasma Sources Sci Technol [Internet]. 2009 Feb 1;18(1):014006. Available from: http://stacks.iop.org/0963-0252/18/i=1/a=014006?key=crossref.cf2126356a9859589751fd7910a745d3

78. Cuyt AAM, Petersen VB, Verdonk B, Waadeland H, Jones WB. Handbook of Continued Fractions for Special Functions. Handbook of Continued Fractions for Special Functions. Springer Netherlands; 2008.

79. Kostov KG, Machida M, Prysiazhnyi V, Honda RY. Transfer of a cold atmospheric pressure plasma jet through a long flexible plastic tube. Plasma Sources Sci Technol [Internet]. 2015 Apr 7;24(2):025038. Available from: http://stacks.iop.org/0963-0252/24/i=2/a=025038?key=crossref.5b495ebcabf35d43ebfaf7489e939ab2

80. Shintani H, Sakudo A, Burke P, McDonnell G. Gas plasma sterilization of microorganisms and mechanisms of action. Exp Ther Med [Internet]. 2010 Oct 4;1(5):731–8. Available from: https://www.spandidos-publications.com/10.3892/etm.2010.136

81. Amemiya H. Plasmas with negative ions-probe measurements and charge equilibrium. J Phys D Appl Phys. 1990 Aug 14;23(8):999–1014.

82. Amemiya H, Annaratone BM, Allen JE. The collection of positive ions by spherical and cylindrical probes in an electronegative plasma. Plasma Sources Sci Technol [Internet]. 1999 Feb 1;8(1):179–90. Available from: http://stacks.iop.org/0963-0252/8/i=1/a=020?key=crossref.cb2fac8e30a7f88cbb26bb2fe2db06a8

83. Bredin J, Chabert P, Aanesland A. Langmuir probe analysis in electronegative plasmas. Phys Plasmas [Internet]. 2014 Dec 4;21(12):123502. Available from: http://aip.scitation.org/doi/10.1063/1.4903328

84. Franklin RN. Electronegative plasmas why are they so different? Plasma Sources Sci Technol [Internet]. 2002 Aug 1;11(3A):A31–7. Available from: http://stacks.iop.org/0963-0252/11/i=3A/a=304?key=crossref.9adb45bae74350587ea5fa5de722c70c

85. Bryant P, Dyson A, Allen JE. Langmuir probe measurements of weakly collisional electropositive RF discharge plasmas. J Phys D Appl Phys [Internet]. 2001 May

21;34(10):1491–8. Available from: http://stacks.iop.org/0022-3727/34/i=10/a=309?key=crossref.dbf479c808d8090de3f59f93f69a788a

86. Demidov VI, Koepke ME, Raitses Y. Magnetically insulated baffled probe for real-time monitoring of equilibrium and fluctuating values of space potentials, electron and ion temperatures, and densities. Rev Sci Instrum [Internet]. 2010 Oct;81(10):10E129. Available from: http://dx.doi.org/10.1063/1.3490022

87. Birdsall CK, Langdon AB. Plasma physics via computer simulation. Plasma Physics via Computer Simulation. 2004.

88. Voloshin D, Kovalev A, Mankelevich Y, Proshina O, Rakhimova T, Vasilieva A. Evaluation of plasma density in RF CCP discharges from ion current to Langmuir probe: experiment and numerical simulation. Eur Phys J D [Internet]. 2015 Jan 21;69(1):23. Available from: http://link.springer.com/10.1140/epjd/e2014-50313-2

89. Iza F, Lee JK. Particle-in-cell simulations of planar and cylindrical Langmuir probes: Floating potential and ion saturation current. J Vac Sci Technol A Vacuum, Surfaces, Film [Internet]. 2006 Jul 27;24(4):1366–72. Available from: http://avs.scitation.org/doi/10.1116/1.2187991

90. Taccogna F, Longo S, Capitelli M. PIC Model of the Ion Collection by a Langmuir Probe. Contrib to Plasma Phys [Internet]. 2004 Nov 1;44(7–8):594–600. Available from: http://doi.wiley.com/10.1002/ctpp.200410087

91. Taccogna F, Longo S, Capitelli M. A particle-in-cell/Monte Carlo model of the Ar + ion collection in He gas by a cylindrical Langmuir probe in the transition regime. Eur Phys J Appl Phys [Internet]. 2003 Apr 25;22(1):29–39. Available from: http://www.epjap.org/10.1051/epjap:2003015

92. Taccogna F, Longo S, Capitelli M. Ion-Neutral Collision Effects in Langmuir Probe Theory. Contrib to Plasma Phys [Internet]. 2008 Jul 1;48(5–7):509–14. Available from: http://doi.wiley.com/10.1002/ctpp.200810082

93. Cenian A, Chernukho A, Bogaerts A, Gijbels R, Leys C. Particle-in-cell Monte Carlo modeling of Langmuir probes in an Ar plasma. J Appl Phys [Internet]. 2005 Jun 15;97(12):123310. Available from: http://aip.scitation.org/doi/10.1063/1.1938275

94. Sternovsky Z, Robertson S, Lampe M. Ion collection by cylindrical probes in weakly collisional plasmas: Theory and experiment. J Appl Phys [Internet]. 2003 Aug 1;94(3):1374–81. Available from: http://aip.scitation.org/doi/10.1063/1.1587889

95. Trunec D, Španěl P, Smith D. The Influence of Ion – Neutral Collisions in the Plasma Sheath on the Ion Current to an Electrostatic Probe: Monte Carlo Simulation. Contrib to Plasma Phys [Internet]. 1995 Oct 1;35(3):203–12. Available from: http://doi.wiley.com/10.1002/ctpp.2150350304

96. Trunec D, Španěl P, Smith D. Monte Carlo Simulations of the Influence of Ion-Neutral Collisions on the Ion Currents Collected by Electrostatic Probes. Contrib to Plasma Phys [Internet]. 2002 Jan 1;42(1):91–8. Available from: http://doi.wiley.com/10.1002/1521-3986%28200201%2942%3A1%3C91%3A%3AAID-CTPP91%3E3.0.CO%3B2-5

97. Bellan PM. Fundamentals of plasma physics. Vol. 9780521821, Fundamentals of Plasma Physics. 2006.

98. Maiorov SA, Petrov OF, Fortov VE. Calculation of resonant charge exchange cross-sections of ions Rubidium, Cesium, Mercury and noble gases. In: 34th EPS Conf on Plasma Physics. 2007. p. P-2.115.

99. Chen FF. Industrial applications of low-temperature plasma physics. Phys Plasmas. 1995;2(6):2164–75.

100. Weltmann KD. Future trends in plasma science. Plasma Process Polym. 2019;16(1):1890001.

101. Shashurin A, Li J, Zhuang T, Keidar M, Beilis II. Application of electrostatic Langmuir probe to atmospheric arc plasmas producing nanostructures. Phys Plasmas. 2011;18(7):1–8.

102. Bogaerts A, Neyts E, Gijbels R, van der Mullen J. Gas discharge plasmas and their applications. Spectrochim Acta Part B At Spectrosc [Internet]. 2002 Apr;57(4):609–58. Available from: https://linkinghub.elsevier.com/retrieve/pii/S0584854701004062

103. Valentini H-B. Removal of singularities in the hydrodynamic description of plasmas including space-charge effects, several species of ions and non-vanishing ion temperature. J Phys D Appl Phys [Internet]. 1988 Feb 14 [cited 2016 Dec 2];21(2):311–21. Available from: http://stacks.iop.org/0022-3727/21/i=2/a=011?key=crossref.2856921a650b2bc405445de069d1d626

104. Bryant P. Theory of cylindrical Langmuir probes in weakly ionized, non-thermal, stationary and moderately collisional plasmas. Plasma Sources Sci Technol [Internet]. 2009 Feb 1;18(1):014013. Available from: http://stacks.iop.org/0963-0252/18/i=1/a=014013?key=crossref.1b103acb96b6f46ff94ea31f799b70c7

105. Franklin RN, Ockendon JR. Asymptotic matching of plasma and sheath in an active low pressure discharge. J Plasma Phys [Internet]. 1970 May 13;4(2):371–85. Available from: https://www.cambridge.org/core/product/identifier/S0022377800005067/type/journal_article

106. Almeida NA, Benilov MS. Physics of the intermediate layer between a plasma and a collisionless sheath and mathematical meaning of the Bohm criterion. Phys Plasmas [Internet]. 2012 Jul 4;19(7):073514. Available from: http://aip.scitation.org/doi/10.1063/1.4737080